6. MODEL DISCUSSION

This section describes the site response ground motion model and the stochastic point-source ground motion model employed to develop earthquake ground motion inputs for the Yucca Mountain Project. The ground motion results using of these models are also described. The site response ground motion model is used to model the effect of site materials (tuff and soil) on ground motion propagating through them. The model is used within an overall approach that provides site-specific ground motions that are consistent with the AFE (hazard level) of the control motion that are input to the model. Hazard-consistent preclosure design ground motion inputs (response spectra and time histories) are required for two sites at the repository: at the depth of the waste emplacement drifts in the RB and on the surface at the SFA. In addition, hazard-consistent strain-compatible soil properties are required for the SFA.

The site response ground motion model is also used to determine the level of ground motion required to produce shear strains in the tuff at Yucca Mountain that would result in pervasive damage to the rock. The lack of observed damage allows an inference on the level of ground motion that Yucca Mountain has not experienced in 12.8 million years. This information provides part of the characterization of extreme (low frequency of occurrence, high-amplitude) ground motions at Yucca Mountain.

The stochastic point-source ground motion model is used for two purposes. First, it is used as an alternate approach to the shear-strain approach to characterizing extreme ground motions at Yucca Mountain. The model is used in conjunction with an assessment of the upper range distribution of stress drops associated with earthquakes in the Yucca Mountain vicinity to characterize the upper range of extreme ground motion that is credible for the site. Results of this evaluation, combined with the reasonable upper limit determined from the lack of observed pervasive damage to the rock at Yucca Mountain, are used to modify (condition) the PSHA reference rock outcrop ground motions that form the basis for developing site-specific ground motion inputs (Section 6.1.1 and Appendix A).

Second, the stochastic point-source model is used to evaluate the ratio between vertical and horizontal ground motion at Yucca Mountain. Results of the modeling are combined with available empirical observations to develop V/H ratios as a function of spectral response oscillator period. As described in Sections 6.5.2.2.2 and 6.5.3.2.2, the V/H ratios are used to develop vertical ground motions based on results for horizontal ground motion.

This section begins with an overview of approaches to develop site-specific ground motions that incorporate site response such that the hazard level of the site-specific ground motions are consistent with those of the control motion upon which they are based (Section 6.1). Next the RVT-based equivalent-linear site response model is summarized (Section 6.2). This model is described in more detail in BSC (2004 [DIRS 170027], Section 6.1). Section 6.3 describes the stochastic point-source ground motion model. This is followed by a discussion of the development of inputs to be used in the site response ground motion model and the point-source ground motion model (Section 6.4). Finally, Section 6.5 describes the modeling and analyses to produce ground motion inputs. That section presents the approach for conditioning the PSHA reference rock outcrop ground motions to reflect new information on extreme ground motions at Yucca Mountain, the approach for incorporating site response into hazard-consistent site-specific

ground motions, the approach for developing vertical ground motions on the basis of the results for horizontal ground motion, and the resulting ground motions for the SFA and the RB.

6.1 OVERVIEW OF APPROACH TO DEVELOP EARTHQUAKE GROUND MOTION INPUT

The overall approach to develop earthquake ground motion input consists of the following elements (Figure 6.1-1):

- Use of new information that has been developed since the PSHA to condition reference rock outcrop hazard to extreme earthquakes. Two approaches are used. One establishes a level of ground motion that has not been experienced at Yucca Mountain. The second estimates the ground motion associated with a distribution of extreme stress drops (also referred to as stress parameters) for a stochastic point-source ground motion model.

- Site-response modeling to determine how the conditioned reference rock outcrop ground motion is modified by propagation through the site materials. The random-vibration-theory-based equivalent-linear model is used. A one-dimensional velocity profile and dynamic material properties, based on geotechnical data and other information, represent the site materials. Deaggregation of the ground motion hazard forms the basis for selecting response spectra that serve as control motions input into the site-response model. Both epistemic and aleatory variability (uncertainty and randomness) in material properties are taken into account.

- Incorporation of site response into horizontal-component ground motion hazard while maintaining the AFE of the conditioned reference rock outcrop motion. Approach 3 of NUREG/CR-6728 (McGuire et al. 2001 [DIRS 157510], Section 6.1) is implemented using a full integration method. Both epistemic and aleatory variabilities in site dynamic material properties were incorporated to obtain results that have an AFE consistent with that of the input control motion. Site-specific hazard curves comprise the output of the analysis.

- Development of vertical-component ground motion hazard curves using appropriate vertical-to-horizontal (V/H) ratios. V/H ratios are determined based on available empirical and ground motion simulation results.

- Site-specific horizontal and vertical hazard curves were developed for AFEs down to 10^{-8}.

- For AFEs of 1×10^{-3}, 5×10^{-4}, and 1×10^{-4}, 5%-damped design spectra, time histories that match the design spectra, scaling of the 5%-damped design spectra to other damping values, and strain-compatible soil properties were calculated.

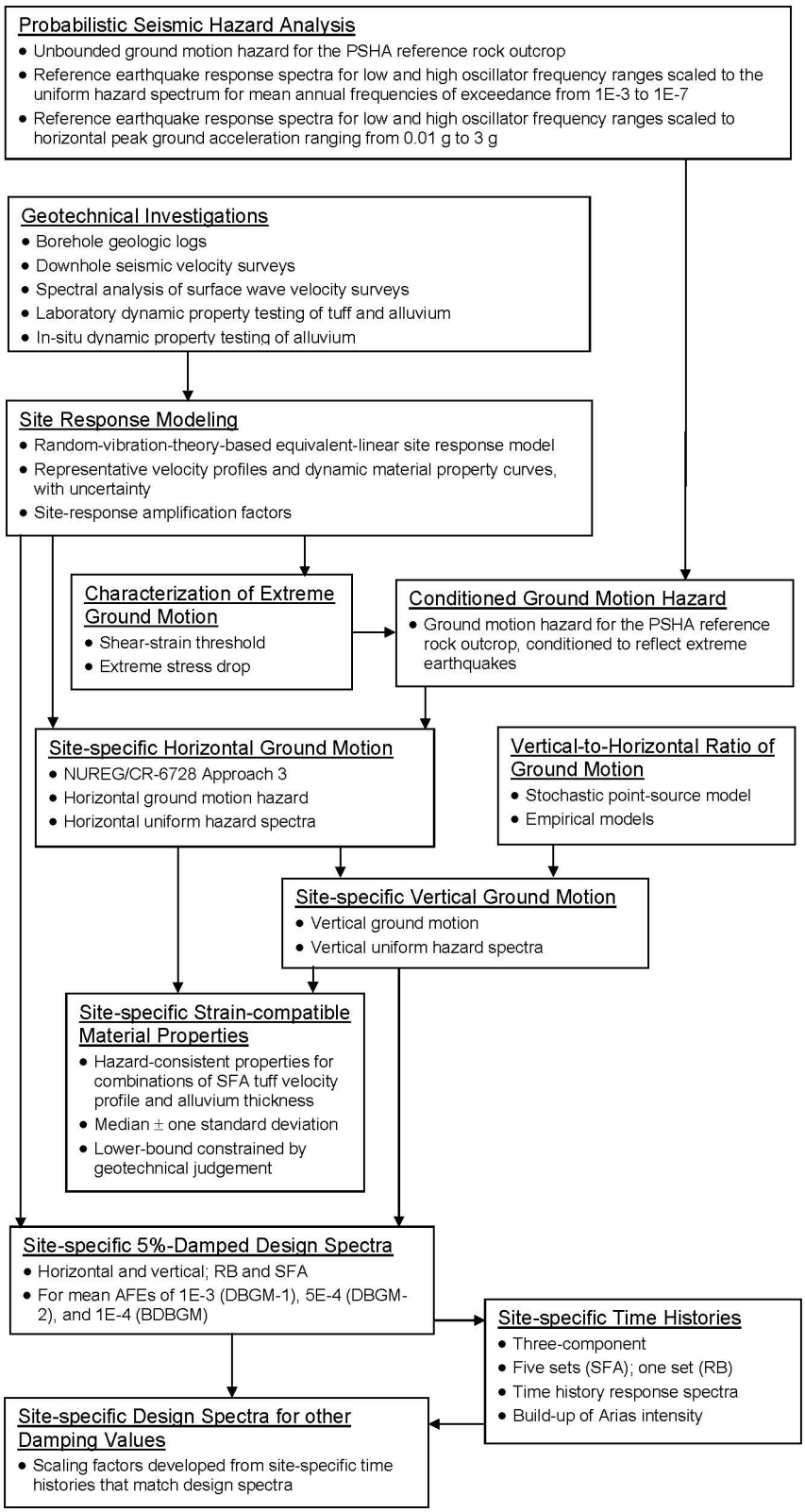

Figure 6.1-1 Flow Diagram for Developing Earthquake Ground Motion Inputs

6.1.1 Conditioning of Reference Rock Outcrop Hazard to Reflect Extreme Earthquakes

A PSHA for Yucca Mountain (BSC 2004 [DIRS 168030]) determined the annual frequency with which various values of ground motion would be exceeded for a hypothetical reference rock outcrop with defined "hard-rock" material properties. As part of that analysis, an expert elicitation process was used to characterize seismic sources and ground motion attenuation relationships for the Yucca Mountain vicinity. The ground motion experts developed interpretations of median ground motion, its standard deviation, and the uncertainties in both. Aleatory variability in ground motion was characterized using untruncated lognormal distributions. As a result of the large epistemic uncertainty in estimates of median motions as well as untruncated aleatory variabilities about median estimates, at low probabilities (AFE < 10^{-4} to 10^{-5}), the corresponding ground motions naturally increased to values generally considered not credible for the site and source conditions. This is not an uncommon occurrence as any PSHA, at low enough AFEs, will result in mean or median motions that are not considered credible. In particular, for soil sites, low probability soil motions can easily exceed the soil's capacity to transmit the motions based on a deterministic analysis, using a realistic suite of dynamic material properties.

While is easy to focus on the level of motions as being credible or not credible, the issue is actually with the probability estimated for the motions at very low AFEs. The real question is not whether the expected motions are credible but rather what probability should be more appropriately associated with the very high ground motions (recall in a hazard analysis, ground motion is the independent variable and the analysis provides estimates of frequency of exceedance, conditional on a level of motion).

To address this issue, an initial analysis (BSC 2005 [DIRS 170137]) made use of geological observations in underground excavations at Yucca Mountain, laboratory rock testing, numerical simulations of rock mass deformation, and site response modeling to estimate a level of peak horizontal particle velocity (PGV) which had not been exceeded in 12.8 million years. This nonexceedance observation over 10^{7} yrs was used to condition the repository level PGV hazard curve to an AFE of 10^{-8}. While accommodating epistemic variability (uncertainty) in levels of shear strains not observed at Yucca Mountain, the initial approach did not directly accommodate the aleatory variability associated with site-specific dynamic material properties, implicit in estimates of PGV conditional on a shear strain value. Additionally, the initial approach concentrated solely on site observations, neglecting the implications on earthquake source processes to produce strong ground motions with sufficient amplitude to induce permanent deformation (fracturing) of the rock mass.

To further characterize low AFEs at Yucca Mountain, the present study used both the site nonexceedance observations, while incorporating aleatory variability in dynamic material properties, as well as an assessment (probability distribution) of extreme source processes (Appendix A). In addition, base-case dynamic material properties were updated based on additional geotechnical investigations (Section 6.4.2) as well as engineering judgment (Section 6.4.4). In the current extreme event conditioning, revised reference hard rock outcrop horizontal hazard curves were developed for all structural frequencies considered in the original PSHA (CRWMS M&O 1998 [DIRS 103731]), as well as horizontal- and vertical-component PGV.

The conditioned reference rock outcrop hazard curves were then used to develop hazard-consistent horizontal and vertical motions for the RB as well as the SFA.

For the extreme event conditioning of the earthquake source, the simple point-source model was used to provide estimates of hard rock ground motions, conditional on the dominant magnitude and distance, for distributions of extreme stress drops. As expected, when both site and source extreme event conditioning is applied, source conditioning controls the estimates of AFEs as it requires extreme stress drops, at the upper range of the distribution, to develop motions sufficient to induce fractures within the stiff tuff units.

6.1.2 Overview of Approach to Incorporate Site Response while Maintaining Hazard Level

In general there are two distinct phases in developing fully probabilistic site-specific design motion. In the first phase, transfer functions are developed which transform, through a model or models, reference horizontal (5%-damped response spectra) or motions appropriate for the site conditions of the PSHA to site-specific horizontal motions. These transfer functions are often referred to as amplification factors. The transfer functions are intended to model the differences in motions between those of the reference site and motions expected for the local site conditions, conditional on the same input or control motion (e.g., earthquake magnitude and distance). For horizontal motions, the RVT-based equivalent-linear vertically-propagating shear-wave model is used to evaluate the effects of both the reference site condition and local site conditions on input motions. Control or input motions are based on PSHA results by scaling the spectra of the low- and high-frequency reference earthquakes (RE), based on deaggregation of the Yucca Mountain ground motion hazard, to produce a suite of reference site peak acceleration values ranging from linear response at 0.01g to highly nonlinear response at 10.00g (to cover AFEs from 10^{-2} to below 10^{-8}). The two REs (spectra) are used to accommodate any dependence of nonlinear site response on magnitude (control motion spectral shape).

The other component of the transfer functions are V/H ratios (5%-damped response spectra), which are used to develop or transform the site-specific horizontal motions into site-specific vertical motions. The vertical motions are modeled as incident inclined compression and vertically polarized shear-waves (P-SV) using a point-source model. To completely cancel source or control motion effects, corresponding horizontal-component waves are modeled as vertically-propagating shear-waves with a point source model as well. A linear analysis is performed for the vertical component, based on observations and modeling of vertical motions recorded at both rock and soil sites (EPRI 1993 [DIRS 103319]). For the horizontal-component analyses, the RVT equivalent-linear approach is used, consistent with the development of the horizontal amplification factors. To accommodate potential magnitude effects on nonlinear site response, V/H ratios are computed for **M** 5, 6, and 7 at the same suite of reference site peak acceleration values, 0.01 to 10.00g. The horizontal and vertical site response models have been described and validated in BSC (2004[DIRS 170027], Sections 6 and 7).

To augment the site-specific V/H ratios, appropriate empirical western North America V/H ratios were included to accommodate model epistemic variability or model uncertainty. Because the model for the vertical motions is less accurate than that for the horizontal motions, based on validation exercises, less reliance is placed on the analytical V/H ratios. Full weight for the

empirical V/H ratios is not warranted as few strong motion sites in western North America reflect site conditions similar to the very stiff local alluvium and tuff units. Additionally, for application to the repository, empirical V/H ratios do not exist for at-depth motions.

Subsequent to the development of the transfer functions, amplification factors and V/H ratios, the horizontal ground motion hazard is computed by integrating the amplification factors with the conditioned reference rock outcrop hazard curves. This integration is carried out over the entire reference rock outcrop hazard curve, reflecting peak accelerations ranging from values less than 0.1g to values exceeding 5g at very low AFEs. This fully probabilistic approach then accommodates contributions to the site-specific hazard at a given AFEs from the reference rock outcrop hazard at all AFEs, properly weighted by their respective probabilities. The result is a site-specific ground motion hazard that preserves the AFE of the reference rock outcrop hazard, an essential component of performance-based design.

To develop corresponding vertical motion hazard, the V/H ratios are integrated with the site-specific horizontal hazard curves, following the same approach. This process then results in site-specific vertical motion hazard at the same AFE as the horizontal motion hazard.

Site-response modeling is described in Sections 6.5.2 and 6.5.3. Development of inputs to the model is presented in Section 6.4. The model itself is summarized in Section 6.2.

6.1.3 Approach to Develop Fully Probabilistic Site-Specific Ground Motion Hazard

In calculating the probabilistic site-specific ground motions at Yucca Mountain, the RB and SFA ground motions must be hazard consistent, i.e., the AFE of the tuff and soil UHS should be the same as the reference rock outcrop UHS. In NUREG/CR-6728 (McGuire et al. 2001 [DIRS 157510]), several approaches are recommended to incorporate site response to produce soil motions consistent with the rock outcrop hazard. In this study, ground motions are computed on soil at the SFA and for a tuff interface for the waste emplacement area. While the McGuire et al. (2001 [DIRS 157510]) report discusses the approaches in terms of a soil site response, the discussion applies to site response in general. In particular, it applies to the conditions at Yucca Mountain in which site response must be evaluated for tuff and alluvium materials. These approaches also incorporate site-specific aleatory variabilities of material properties into the site-specific motions. McGuire et al. (2001 [DIRS 157510]) identified four basic approaches for incorporating site response in determining the UHS at a specific site. The approaches range from a PSHA using ground motion attenuation relations for the specific site of interest (Approach 4) to scaling the rock UHS on the basis of a site response analysis using a broadband input motion (Approach 1). Conceptually, Approach 4 is an exact approach and other approaches are approximations to it.

The following discussion provides a framework for the rationale for the approach used in this study. McGuire et al (2001 [DIRS 157510]) identify four approaches to develop site-specific design motions or hazard. These four approaches are characterized by increasing accuracy defined as preserving the desired frequency of exceedance in the site-specific hazard or motions (hazard-consistent) as well as accommodating site-specific aleatory and epistemic variabilities. In NUREG/CR-6728 (McGuire et al. 2001 [DIRS 157510], Section 6) the approaches are presented in terms of a soil response, but the approaches can be generalized to any column of

site-specific dynamic material properties that are different than those of the reference site condition for which the PSHA was computed.

Approach 1: This approach is fundamentally deterministic and involves using the outcrop UHS to drive the overlying site-specific soil column(s). By definition it assumes a rock outcrop hazard (UHS) but has no mechanism to conserve the outcrop AFE. For cases where the hazard is dominated by earthquakes with significantly different **M** at low and high (or intermediate) structural frequencies like Yucca Mountain (Section 6.4.1.1), the outcrop UHS may be quite broad, unlike any single earthquake, resulting in unconservative high-frequency site-specific motions (too nonlinear in site response). Even if only a single earthquake is the major contributor at all structural frequencies, variabilities incorporated in the hazard analysis may result in a broad spectrum, again unlike any single earthquake.

Approach 2: This approach is intended to avoid the broad-band control motion of Approach 1 and uses low-and high-frequency (and intermediate if necessary) deterministic spectra computed from the weighted attenuation relations used in the PSHA, scaled to the UHS at the appropriate frequencies (e.g., Regulatory Guide 1.165 1997 [DIRS 119139]). These scaled motions, computed for the modal deaggregation **M** and distance *D* are then used as control motions to develop multiple (typically 2 to 3) mean transfer functions based on randomized soil columns. The mean transfer functions are then enveloped with the resulting transfer function applied to the outcrop UHS. This method was termed Approach 2A in NUREG/CR-6728 (McGuire et al. 2001 [DIRS 157510]). The use of mean (rather than median) transfer functions followed by enveloping is an empirical procedure to conservatively maintain the outcrop AFE (NUREG/CR-6728 and CR-6769; McGuire et al. 2001 [DIRS 157510], 2002 [DIRS 163799]). Hazard consistency is typically maintained to a mean AFE of about 10^{-4} and may be slightly unconservative at high frequency and for a mean AFE of 10^{-5} and below (NUREG/CR-6769, McGuire et al. 2001 [DIRS 157510]), particularly for highly nonlinear sites.

For cases where there may be a wide magnitude range contributing to the hazard at low or high frequency and (or) the site has highly nonlinear dynamic material properties, low, medium, and high **M,** control-motion spectra may be developed at each frequency of interest. A weighted mean transfer function (e.g., with weights of 0.2, 0.6, 0.2 reflecting 5%, mean, and 95% **M** contributions, respectively) is then developed at each structural frequency of interest. Following Approach 2A, the weighted-mean transfer functions for each frequency of interest are then enveloped with the resultant transfer function applied to the outcrop UHS. This more detailed analysis procedure was termed Approach 2B. Comparisons detailed in McGuire et al. (2001 [DIRS 157510]) indicate that Approach 2B is adequately conservative at AFEs down to 10^{-4} with respect to Approach 4. In BSC (2004 [DIRS 170027], p. 6-232) a case is made that ground motions developed using Approach 2B for the waste emplacement level are also adequately conservative to AFE's as low as 10^{-7} because the site-specific rock motions are dominated by upgoing waves and reflect little nonlinearity.

A potential drawback to Approach 2 is the ambiguity in accommodating site epistemic variability. Because epistemic variability is treated by averaging multiple hazard curves over frequency in a PSHA (as well as in Approach 3), it is clear that simple averaging of transfer functions is not appropriate and is likely unconservative. Enveloping mean transfer functions

reflecting alternate site dynamic models remains the only alternative but may result in overly conservative estimates of motions or significantly lower probability than desired.

Approach 3: This approach is a fully probabilistic analysis procedure which moves the site response, in an approximate way, into the hazard integral. The approach is described by Bazzurro and Cornell (2004 [DIRS 177290]) and NUREG/CR-6769 (McGuire et al. 2002 [DIRS 163799]). In this approach, the hazard at the soil surface, or for a site condition or location which differs from that of the outcrop PSHA (e.g., reference rock outcrop site condition), is computed by integrating the site-specific hazard curve at the bedrock level with the probability distribution of the amplification factors (Lee et al. 1998 [DIRS 182431], 1999 [DIRS 182432]). The soil site-specific amplification is characterized by a suite of frequency-dependent amplification factors that account for nonlinearity in soil response. Approach 3 involves approximations to the hazard integration using suites of transfer functions, or, for vertical motions, V/H ratios, which result in complete site-specific hazard curves at the ground surface for specific ground motion parameters (e.g., spectral accelerations) and a range of frequencies.

It is important to note there are two ways to implement Approach 3. The first is the full integration method whereas the second is to simply modify the attenuation relation ground motion value during the hazard analysis with a suite of transfer functions (Cramer 2003 [DIRS 182407]). Both approaches will tend to double-count site aleatory variability: once in the suite of transfer-function realizations and again in the aleatory variability about each median attenuation relation. The full integration method tends to lessen any potential impacts of the large total site aleatory variability (Bazzuro and Cornell 2004 [DIRS 177290]). Approximate corrections for the large site component of aleatory variability may be made by implementing the approximate technique (below) with C = 0, AF =1, and a negative exponential, where a_{rp} = the soil amplitude and σ is the component of variability that is removed.

For hazard curve slopes of about 3 and sigma (ln) in the typical 0.2 to 0.3 range, the correction (reduction) is about 10%. This correction can be applied to either implementations of Approach 3. Alternatively, in the implementation of Approach 3 wherein attenuation relations are modified one can simply use the median transfer function rather than the full distribution or remove the transfer function sigma from the attenuation relation aleatory variability and use the full distribution. Any of these corrections will approximately avoid potential double-counting of site aleatory variability.

A distinct advantage of Approach 3 is the proper incorporation of site epistemic variability. Multiple hazard curves may be developed reflecting multiple site models (e.g., velocity profiles, G/G_{max} and hysteretic damping curves) which are then averaged over probability to develop mean, median, and fractile estimates. Additionally, vertical hazard curves may also be developed that are consistent with the horizontal by employing distributions of V/H ratios (transfer functions) to the resulting site specific horizontal hazard curves.

Approach 4: This approach entails the use of site-specific attenuation relations which incorporate the site-response characteristics of the site in the PSHA. The relations accommodate site-specific and perhaps region-specific median estimates as well as site/region-specific aleatory variabilities about the median. As a result, potential double-counting site variability with either of the Approach 3 approximations (integration of suites of transfer functions outside the hazard

integral or modifying generic attenuation relations with transfer functions within the hazard integral) is avoided. Approach 4 is considered the most accurate as it is intended to accommodate the appropriate amounts of aleatory variability into site- and region-specific attenuation relations. Epistemic variability is appropriately captured through the use of multiple attenuation relations. Approach 3 is considered to be a fully probabilistic approximation to Approach 4.

6.1.3.1 Full Integration Method for Approach 3

For the work described in this report, the full integration method for Approach 3 is used. The proposed method for computing surface-hazard curves for $Z = S^s_a(f)$ convolves the site-specific rock hazard curves for $X = S^r_a(f)$ with the probability distribution of $= AF(f)$. The soil hazard curve can be calculated using the discretized form of Eq. 6-1 from Bazzurro and Cornell (2004 [DIRS 177290]):

$$G_Z(z) = \sum_{all\ x_j} P\left[Y \geq \frac{z}{x} \middle| x_j \right] px(x_j) = \sum_{all\ x_j} G_{Y|X}\left(\frac{z}{x} \middle| x_j \right) p_X(x_j) \quad \text{(Eq. 6-1)}$$

where $G_Z(z)$ is the hazard curve for $S^s_a(f)$, that is, the annual probability of exceeding level z. On the right-hand side,

$$G_{Y|X}\left(\frac{z}{x} \middle| x \right) = \hat{\Phi}\left(\frac{ln\left[\frac{z}{x}\right] - ln\left[\hat{m}_{Y|X}(x)\right]}{\sigma_{\ln Y|X}} \right) \quad \text{(Eq. 6-2)}$$

where $G_{Y|X}$ is the complementary cumulative distribution function of $Y = AF(f)$, conditional on a rock amplitude x;

$\hat{\Phi} = 1 - \Phi$ is the widely tabulated complementary standard Gaussian cumulative distribution function;

$\hat{m}_{Y|X}$ is the conditional median of Y;

$\sigma_{\ln Y|X}$ is the conditional standard deviation of the natural logarithm of Y; and

$p_X(x_j)$ is the probability that the rock input level is equal to (in the neighborhood of) x_j.

This approach is implemented in the SOILUHSI component of the SOILHAZ SET software item (STN 11234-1.0-00) (Figure 6.1-2).

6.1.3.2 Approximate Method for Approach 3

An approximate method for implementing Approach 3 is described here for completeness, but is not used in these analyses. Eq. 6-3 from Bazzuro and Cornell (2004 [DIRS 177290]) is a closed

form approximation of the integration of the amplification factor over a range of rock amplitudes.

$$z_{rp} = a_{rp}\,\overline{AF_{rp}}\,exp\left(\tfrac{1}{2}\,K\,\sigma\delta^2\,/\left(1-\mathrm{C}\right)\right) \qquad \text{(Eq. 6-3)}$$

where z_{rp} is soil amplitude z associated with return period r_p; a_{rp} is the rock acceleration, a, associated with return period r_p; AF_{rp} is the geometric mean (mean log) amplification factor for the rock motions with return period r_p; k is the log-log slope of the rock hazard curve that is calculated at each ground motion point from the input rock hazard curve; C is the negative of the log-log slope of input amplification factor that is calculated at each structural frequency point from the input amplification factors, AF; and σ_δ is the log standard deviation of the AF, which is read from the input file.

6.1.4 Implementation of Approach 3

In implementing Approach 3 using the full integration method for the work described in this report, the following steps are taken for each site:

- Randomization of base case site-dynamic material properties to produce a suite of velocity profiles as well as G/Gmax and hysteretic damping curves that incorporate site variability.

- Computation of transfer functions (amplification for horizontal motions and V/H ratios for vertical motions) as characterized by a distribution for each set of base case site properties using the RVT-based equivalent-linear site response model.

- Full integration of the conditioned PSHA reference rock outcrop fractile and mean hazard curves with the transfer functions amplification factors to arrive at a distribution of site-specific horizontal and vertical hazard curves.

- Computation of site-specific UHS.

Approach 3 is implemented through a number of computer programs, which are described below (Figure 6.1-1). The computation of the amplification factors is the first phase of the calculations and is similar to what is done in other site-response approaches.

6.1.4.1 RVT-Based Equivalent-Linear Site Response Approach

Essentially there are three elements in the site response approach. The first element involves an RVT-based equivalent-linear site response in which vertically-propagating shear-waves are assumed. RVT is employed in two ways, to provide estimates of peak time domain shear strains as well as in developing response spectra. The computed horizontal motions are used to develop both amplification factors and V/H ratios for suites of reference rock peak acceleration values.

The second element involves computation of vertical motions and assumes incident inclined P-SV waves. The vertical component analyses assume linearity, based on observations as well as modeling recorded vertical motions. Control motions for the vertical and corresponding

horizontal equivalent-linear analyses are provided by the point-source model, using the same suite of source parameters. The point-source is used for both the horizontal and vertical component analyses to ensure a cancellation of source processes in computing the V/H ratio. To provide a suite of transfer functions (V/H ratio) that covers the range in magnitude of the reference rock hazard, site response analyses were done for **M** 5, 6, and 7. For each magnitude, analyses were performed for a suite of 22 reference rock peak acceleration values ranging from 0.01g to 10.00g. This suite of motions was intended to cover the entire range in the reference rock horizontal hazard. Following recommendations in Regulatory Guide 1.165 (1997 [DIRS 119139]), the control motions for the horizontal amplification factors were based on the low- and high-frequency REs, each scaled to the same suite of peak acceleration values. This recommendation in Regulatory Guide 1.165 (1997 [DIRS 119139]) is intended to avoid cases where only a single broad-band spectrum is used as control motions, possibly resulting in unconservative amplification factors at high-frequency. This condition is avoided in the V/H ratio analyses by the use of multiple magnitudes.

The third aspect in the site response approach is the use of empirical western North America V/H ratios. Appropriate empirical V/H ratios are weighted along with the site-specific numerical V/H ratios as the model for the vertical motions has not been as thoroughly validated nor perform as well as the model for the horizontal motions. The use of the two models, analytical and empirical, is treated as epistemic variability with complete hazard curves computed for each model, weighted, and averaged over probability to develop a mean hazard curve. This process then properly incorporates modeling epistemic variability (uncertainty) into fully probabilistic vertical design motions.

In application of the amplification factors during the Approach 3 analyses for horizontal motions, a weighted contribution of the factors developed from the low- and high-frequency RE is used based on the reference rock outcrop hazard deaggregations. For the V/H ratios, since distance is a controlling factor as well as **M**, the ratios are weighted based on distance deaggregations of the reference rock outcrop hazard. As a result the transfer functions, amplification factors as well as V/H ratios, change with AFE.

6.1.4.1.1 Site Aleatory Variability

To accommodate random variations in velocity, depth to reference rock outcrop, modulus reduction, and hysteretic damping values across the site, multiple realizations are developed for dynamic material properties. The profile randomization scheme (EPRI 1993 [DIRS 103319]; BSC 2004 [DIRS 170027]) is based on a variance analysis of measured shear-wave velocity profiles across the site and varies both velocity and layer thickness. The model includes a velocity distribution at depth coupled with a velocity correlation with depth. The depth correlation is intended to eliminate unnatural velocity variations at a given depth that are independent of realizations above and below. Driven by measured velocities, the correlation length (distance) increases with depth with a corresponding decrease in the velocity COV at a given depth. Profiles typically vary less as depth increases and become more uniform, on average.

To accommodate random fluctuations in compression-wave velocity when modeling vertical motions, Poisson ratio is held constant at the base case values and random compression-wave

velocities are then generated based on shear-wave velocity realizations and base-case Poisson ratios. In reality Poisson ratio will vary but is likely correlated with shear-wave velocity. As a result, varying Poisson ratio when properly correlated with shear-wave velocity will likely not result in a greater variation in compression-wave velocity than assumed here. Additionally, variation in compression-wave velocity has a much smaller effect on motions than shear-wave velocity as the wavelengths typically are 2 to 5 times greater. A correlated shear- and compression-wave profile randomization scheme is desirable but not yet available.

To capture random variations in modulus reduction and damping curves, values are randomized assuming a log-normal distribution, consistent with shear-wave velocity and material damping. Based on random variations in laboratory dynamic testing for soils of the same type or classification (EPRI 1993 [DIRS 103319]) a σ_{ln} of 0.15 and 0.3 is used for G/G_{max} and hysteretic damping, respectively. These standard deviations are taken at a cyclic shear-strain of 0.03%, where the G/G_{max} curves typically show significant reduction. Suites of curves are generated by sampling the distribution, applying the random perturbation to the base-case (initial) curve at 0.03% shear strain, and preserving the shape of the base case curve to generate an entire random curve. Bounds are placed at $\pm 2\sigma$ over the entire strain range to prevent nonphysical excursions. Shear-wave damping is separately (independently) randomized following the same procedure.

The randomization code can accommodate coupling or correlation of any degree (-1 to 1) between modulus reduction and hysteric damping, which is expected to occur between mean or base-case curves reflecting different material type curves. However, for random variations within the same material type the correlation is likely low; that is, a randomly linear curve is not necessarily associated with a randomly low damping. Additionally, because modulus reduction is far more significant than material damping in site response (Silva 1992 [DIRS 183482]), the issue is not considered significant.

Specific computer codes and analysis flow is discussed in the following sections.

6.1.4.1.2 Horizontal Motions

To compute the ground motions at the ground surface or within the repository, the results of the PSHA are modified using a site-response model. In this case, the model is the RVT-based equivalent linear model contained in the computer program RASCALS (Section 6.2; Figure 6.1-1). Inputs to RASCALS are as follows:

- Location of input and output motions within the site profile.
- Input (control) motions characterized by earthquake power spectra.
- Incidence angles of input motion.
- A representation of the rock and soil at the site, consisting of homogeneous layers with specified thickness, seismic velocity, and density.
- A representation of the dynamic material properties of the rock and soil at the site, consisting of strain-dependent shear modulus and damping curves for each layer.

Control motions (power spectral density) must be calculated for input into the site response analysis that are representative of the earthquake magnitude and distance dominating the hazard at the desired level of ground motion. The basis for the control motions are the magnitude and distances specified by the hazard deaggregation. Control motions may be specified by a response spectrum, which is then followed by an RVT spectral match to generate a power spectral density or a point-source model. This is then input to the site column as an outcrop motion at the control point. The appropriate control response spectrum should be based on the rock attenuation relations used in developing the rock outcrop UHS (e.g., Regulatory Guide 1.165 1997 [DIRS 119139]). Evaluation of site-response using the equivalent-linear site response model is based on convolution of appropriate control motions through randomized velocity profiles combined with randomized G/Gmax and hysteretic damping curves. The randomized profiles and curves are generated from base case velocity and nonlinear dynamic properties. The convolutions yield transfer functions for 5%-damped response spectra and peak particle velocity.

For the computation of spectra for a site with uncertain properties and exhibiting a degree of lateral random variability, the uncertainty and variability (randomness) need to be incorporated in the site response analysis. To incorporate the uncertainty (epistemic variability), best-estimate base case velocity profiles representing alternate means are developed. To represent random variability, the base case profiles are used to stochastically simulate 60 V_S profiles using the computer program RANPAR (Figure 6.1-2). Additionally, strain-dependent shear modulus and hysteretic damping are also randomized about best-estimate base cases. The simulations attempt to capture the variability in the soil or rock parameters and layer thickness.

Input control motions at each location were computed using RASCALS for each set of 60 velocity profiles and dynamic property curves (Figure 6.1-2). RASCALS was used for horizontal spectra using normally-incident and inclined SH-waves. For each control motion, the transfer functions, ratios of 5%-damped response spectra, were computed using SMRATIO (Figure 6.1-2) to produce the amplification factors. The mean (log) and standard deviation of the transfer functions were then computed using LOGNORM. The amplification factors include the effects of the inherent aleatory variability (randomness) of the site properties about each base case and any possible effects of magnitude of the control motions. Epistemic uncertainty is captured in consideration of alternate base case (mean) profiles and properties.

The conditioned reference rock outcrop hazard curves (Section 6.5.1) and the amplification factors derived for each site were used in SOILUHSI to calculate site-specific hazard curves. The details of this full integration method were described in Section 6.1.1.1.

The epistemic uncertainty in seismic hazard is typically represented by a set of weighted hazard curves. Using these sets of curves as discrete probability distributions, they can be sorted by the frequency of exceedance at each ground-motion level and summed into a cumulative probability mass function. When the cumulative probability mass function for a particular exceedance frequency equals or exceeds fractile y, then the exceedance frequency represents the y^{th} fractile. The weighted-mean hazard curve is the weighted average of the exceedance frequency values. This approach is a standard practice in PSHA. These procedures are contained in the computer program FRACTILE, which was used to produce the final site-specific hazard curves.

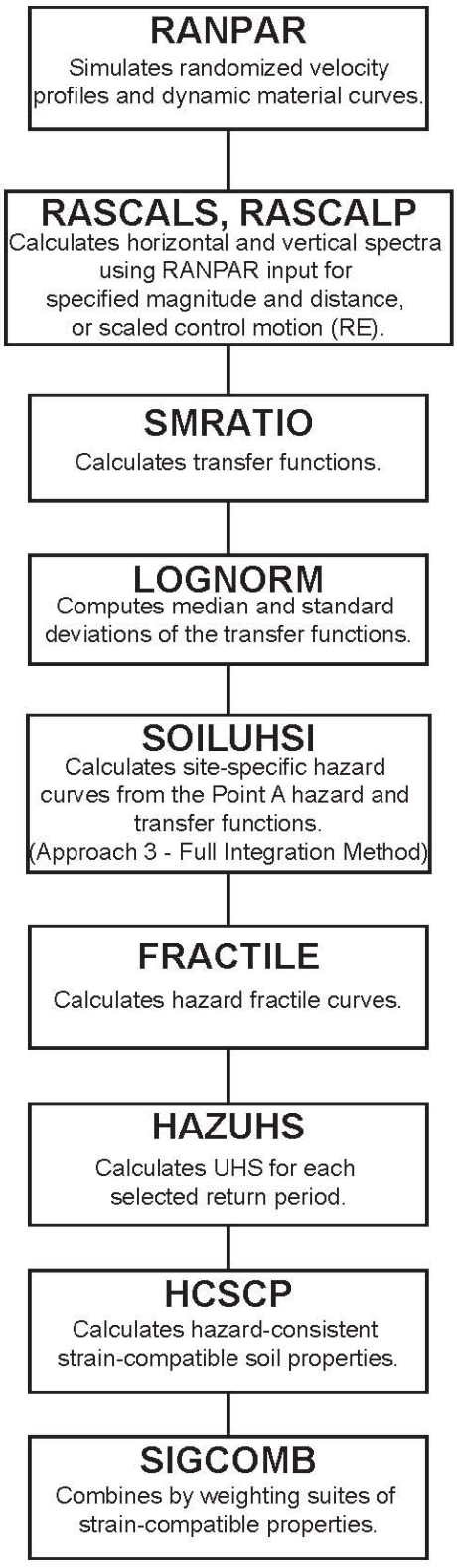

Figure 6.1-2 Flow Diagram of Computer Programs Used in Site Response Analysis

6.1.4.1.3 Vertical Motions

The point-source stochastic model as employed in the computer code RASCALP was used to compute site-specific V/H ratios (Sections 6.5.2.1.2 and 6.5.3.1). To model vertical motions, incident inclined P-SV waves are modeled from the source to the site using the plane-wave propagators of Silva (1976 [DIRS 103326]) assuming a shear-wave point-source spectrum (Silva 1997 [DIRS 163747]). The angle of incidence at the top of the layer containing the source is computed by two-point ray tracing through the crust and site-specific profile. To model site response, the near-surface V_P and V_S profiles described in Section 6.4.2 are placed on top of the Yucca Mountain crustal structure (Section 6.3), the incident P-SV wavefield is propagated to the surface, and the vertical (or radial) motions are computed.

For typical crustal structures without strong near-surface V_P gradients and at close distances, the predominant motion on the vertical component is principally due to the SV wavefield. In a soil column (particularly deep profiles), however, because there is usually a large V_P gradient (larger for P-waves than for S-waves as Poisson's ratio generally decreases with depth), the vertical component is usually controlled by the compressional wavefield at short period. The separation of rock and soil sites in terms of predominant wavefields in the vertical component depends on specific velocity profiles (site-specific as well as the underlying rock and crustal profile), source depth and mechanism through their effect on incidence angles, as well as the depth of the water table.

In the current implementation of the equivalent-linear approach to estimate V/H response spectral ratios, the horizontal component analyses are performed for vertically-propagating shear waves using the RVT methodology (RASCALS). To compute the vertical motions, a linear analysis is performed for incident inclined P-SV waves using low-strain, V_P and V_S derived from the velocity profiles using RASCALP (Silva et al. 1996 [DIRS 110474]). The P-wave damping is assumed to be equal to the low strain S-wave damping (Johnson and Silva 1981 [DIRS 110447]). The horizontal component and vertical component analyses are assumed to be independent.

The approximations of linear analysis for the vertical component and uncoupled vertical and horizontal components have been validated in two ways. Fully nonlinear modeling using a 3D soil model showed that the assumption of largely independent horizontal and vertical motions for loading levels up to about 0.5g (soil surface, horizontal component) for moderately stiff profiles was appropriate (EPRI 1993 [DIRS 103319]). Additionally, validation exercises with recorded motions were conducted at over 50 sites which recorded the 1989 **M** 6.9 Loma Prieta and 1992 **M** 6.7 Northridge earthquakes. These validations showed the overall bias and variability for vertical motions was acceptably low for engineering applications but was higher than that for horizontal motions (EPRI 1993 [DIRS 103319]; Silva 1997 [DIRS 163747]). An indirect validation was also performed by comparing V/H ratios from western United States (WUS) empirical attenuation relations with model predictions over a wide range in loading conditions (Silva 1997 [DIRS 163747]). The empirical results showed a favorable comparison with the model with the latter conservative in predictions at high frequency, particularly at soil sites and at high loading levels. For engineering design applications, this reflects a conservative and therefore acceptable bias. In the V/H comparisons with empirical relations, the model also showed a small underprediction at low frequency ($\leq$ 1 Hz) and at large distance ($\geq$ 20 km). To

accommodate this potential unconservatism, a lower bound of 0.4 is used, based on WUS empirical attenuation relations.

To model the site-specific V/H ratios, the same **M**, stress drops, and suite of distances are used as in developing horizontal transfer functions. For the vertical analyses, a total kappa value of 0.01 sec, half that of the horizontal, was used. This factor of 50% is based on observations of kappa at strong motion sites (Anderson and Hough 1984 [DIRS 128813]), validation exercises (EPRI 1993 [DIRS 103319]), and the observation that the peak in the vertical spectral acceleration (5% damped) for WUS rock and soil sites is generally near 10 to 12 Hz compared to the horizontal motion peak which occurs at about 5 Hz, conditional on **M** 6.5 at a distance of about 10 to 30 km. This difference of about two in peak frequency is directly attributable to differences in kappa of about two.

Empirical WUS V/H ratios were included in the development of vertical motions in addition to site-specific point-source simulations. The use of WUS empirical V/H ratios implicitly assumes similarity in shear- and compression-wave profiles as well as nonlinear dynamic material properties between soft rock and deep firm soils in WUS and site-specific columns. While this may not be the case for the average WUS deep firm soil (Silva 1997 [DIRS 163747]), the range in site conditions sampled by the WUS empirical generic rock and soil relations likely accommodates the local stiff alluvium soils and underlying tuff units. Additionally, because the model for vertical motions is not as thoroughly validated as the model for horizontal motions (EPRI 1993 [DIRS 103319]; Silva 1997 [DIRS 163747]), inclusion of empirical models is warranted. The additional epistemic variability introduced by inclusion of both analytical and empirical models also appropriately reflects the difficulty and lack of industry consensus on developing (modeling) site-specific vertical motions (EPRI 1993 [DIRS 103319]). In the implementation of Approach 3 to develop vertical hazard curves, the epistemic variability is properly accommodated in the mean vertical UHS, reflecting a weighted average over vertical hazard curves computed for each model. The vertical UHS then maintain the desired hazard levels, consistent with the horizontal design response spectra and UHS. Equal weights were given to the empirical and analytical models.

The empirical relations that specified both horizontal and vertical components included those of Abrahamson and Silva (1997 [DIRS 104205]) and Campbell and Bozorgnia (2003 [DIRS 183814]). For the Abrahamson and Silva (1997 [DIRS 104205]) relation, an update that includes a normal faulting factor (Abrahamson and Becker 1997 [DIRS 166530]) was implemented. The relations were equally weighted in the analysis. The vertical hazard curves were calculated by applying V/H ratios also using SOILUHSI. In applying the V/H ratios, the aleatory variability, σ_{ln}, was set to 0.2 to accommodate the slightly larger variability in the vertical components compared to the average horizontal component (Abrahamson and Silva 1997 [DIRS 104205]). This process properly incorporates the variabilities (epistemic and aleatory) in the V/H ratios and results in horizontal and vertical hazard as well as UHS with the desired AFEs across structural frequency for both horizontal and vertical components.

6.1.5. Development of Ground Motion Inputs

HAZUHS was used to calculate the UHS for each selected return period based on the suite of hazard curves from FRACTILE (Figure 6.1-2). Based on the UHS, design spectra and time histories are calculated as described in Section 6.5.

Finally, HCSCP computes hazard-consistent strain compatible properties for a given hazard curve. For each base case of dynamic material properties HCSCP, at the hazard level (ground motion value) of interest, compiles strain-compatible properties computed from the site response analyses. Program SIGCOMP then combines the suites of hazard-consistent strain-compatible properties using the same weights as those used in developing the hazard curves. Similarly, based on the desired AFE, the strain compatible properties, computed with the low- and high-frequency RE, are also weighted and combined using the reference rock outcrop deaggregation. As expected, strain-compatible properties vary somewhat with structural frequency. This is due to the varying contributions of low- and high-frequency control motions (RE) and the impacts on nonlinear site response. It should be noted, although unpleasant, this is a natural and expected consequence of ground motion hazard being dominated by different earthquakes sources at differing structural as well as exceedance frequencies. To maintain consistency with the decision to develop single design spectra, rather than distinct high- and low-frequency design spectra, the strain compatible properties computed at 100 Hz (peak acceleration) and at 1 Hz were averaged to produce a single suite of hazard consistent strain compatible dynamic material properties. The hazard-consistent and strain-compatible properties represent median and $\pm$ 1σ estimates for levels of design motions at the desired AFE. The standard deviation reflects both aleatory variability due to random variations in dynamic material properties as well as epistemic variability or uncertainty in base case parameters. The median and σ estimates then reflect the site-specific uncertainty and randomness incorporated in the design motions, consistent with the levels of motion at the desired AFE.

6.2 SITE RESPONSE MODEL

To compute the ground motion inputs for preclosure analyses, the results of the PSHA (i.e., the motions at Point A) are modified using a site response model. In the analyses performed to date (BSC 2004 [DIRS 170027]) and in this study, a RVT-based equivalent-linear site response model was used.

6.2.1 Model Description

The computational formulation that has been most widely employed to evaluate 1D site response assumes vertically-propagating plane S-waves. Departures of soil response from a linear constitutive relation are treated in an approximate manner through the use of the equivalent-linear formulation .

The equivalent-linear formulation, in its present form, was introduced by Idriss and Seed (1968 [DIRS 163520]). It is a particular application of the general equivalent-linear theory developed by Iwan (1967 [DIRS 110379]). Basically, the approach is to approximate a second-order nonlinear equation, over a limited range of its variables, by a linear equation. Formally this is done in such a way that the average of the difference between the two systems is minimized. This was done in an ad-hoc manner for ground motion response modeling by defining an effective strain that is assumed to exist for the duration of the excitation. This value is typically taken as 65% of the peak time-domain strain calculated at the midpoint of each layer, using a linear analysis. Shear modulus reduction and hysteretic damping curves are then used to define new parameters for each layer based on the effective strain computations. The linear response calculation is repeated, new effective strains evaluated, and iterations continue until the changes in parameters are below an established tolerance level. Generally a few iterations are sufficient to achieve a strain-compatible linear solution.

This stepwise analysis approach was formalized into a 1D, vertically propagating S-wave code called SHAKE (Schnabel et al. 1972 [DIRS 103323]). Subsequently, this code has become the most widely used and validated analysis package for 1D site response calculations.

The advantages of the equivalent-linear formulation are that parameterization of complex nonlinear soil models is avoided and the mathematical simplicity of a linear analysis is preserved. (Limitations are discussed in Section 6.2.5.) A truly nonlinear approach requires the specification of the shapes of hysteresis curves and their cyclic dependencies through an increased number of material parameters. In the equivalent-linear methodology the soil data are utilized directly and, because at each iteration the problem is linear and the material properties are frequency independent, the damping is rate independent and hysteresis loops close.

Careful validation exercises between equivalent-linear and fully nonlinear formulations using recorded motions (peak horizontal acceleration) from 0.05 to 0.5 g showed little difference in results (BSC 2004 [DIRS 170027]). Both formulations compared favorably to recorded motions suggesting both the adequacies of the vertically propagating S-wave model and the approximate equivalent-linear formulation. While the assumptions of vertically propagating S-waves and equivalent-linear soil response represent approximations to actual conditions, their combination has achieved demonstrated success in modeling observations of site effects and represent a

stable, mature, and reliable means of estimating the effects of site conditions on strong ground motions (Schnabel et al. 1972 [DIRS 103323]; EPRI 1988 [DIRS 107489]; Schneider et al. 1993 [DIRS 110467]; EPRI 1993 [DIRS 103320], Appendix 6.B).

A consequence of the equivalent-linear formulation is the preservation of the superposition principle. For linear systems this principle permits, among other things, spectral decomposition and frequency-domain solutions such as the propagator matrix solution scheme (Haskell 1960 [DIRS 163513], Schnabel et al. 1972 [DIRS 103323], Silva 1976 [DIRS 103326]) for efficient frequency-domain solutions of the wave equation. The superposition principle then permits a spectral recomposition of the wavefields (sum over frequencies) through an inverse Fourier or Laplace transform. A nonsubtle result of this is that the deconvolution process, that of propagating the control motion down rather than up, results in a unique solution (EPRI 1988 [DIRS 107489], Section 3). That is, for a given motion at the surface, within an equivalent-linear framework there is only one input motion (solution). In reality, of course, if the soils are behaving in a nonlinear fashion and have degraded, many different input motions at the base of the soil could have resulted in a similar surface response.

Both the RASCALS code (including RASCALP, the P-wave version of the code), which has been implemented in this study, and the SHAKE code represent an implementation of the equivalent-linear formulation of Seed and Idriss (1969 [DIRS 163655]) applied to 1D site response analyses. The RASCALS code is an RVT-based equivalent-linear approach, which propagates an outcrop (control motion) power spectral density through a 1D soil column. RVT is used to predict peak time domain values of shear strain based upon the shear-strain power spectrum. In this approach, the control motion power spectrum is propagated through the 1D rock/soil profile using the plane-wave propagators of Silva (1976 [DIRS 103326]). Both P-SV (vertically polarized S-wave) and SH (horizontally polarized S-wave) waves are included in the analysis and have specified angles of incidence.

6.2.2 Uncertainties

The mathematical formulation used in the site response model is exact in its computation of motions for a given set of input parameters. Accuracy of results in the context of how well the model captures observed effects of site conditions on strong ground motions are assessed in the model validation (BSC 2004 [DIRS 170027]). Limitations and appropriateness of the model are discussed in Section 6.2.5. The uncertainties of the input into the site response model are discussed in Section 6.4.2.

6.2.3 Description of Input

Inputs to the model, as implemented in the software codes RASCALS and RASCALP, are as follows:

- Location of input and output motions within the site profile.
- Input (control) motions characterized by earthquake response spectra and corresponding power spectra.

- Incidence angles of input motion.
- A representation of the rock and soil at the site, consisting of homogeneous layers with specified thickness, seismic velocity, and density.
- A representation of the dynamic material properties of the rock and soil at the site, consisting of strain-dependent shear modulus and damping for each layer.

Section 6.4 describes the development of specific values for these inputs. Use of these inputs in subsequent modeling and analyses is described in Section 6.5.

6.2.4 Use of Output

Preclosure seismic ground motion inputs are developed for two locations: the rock interface at the depth of the waste emplacement drifts (RB) and the SFA. Acceleration response spectra are developed for both horizontal and vertical components and for hazard mean annual exceedance rates appropriate for preclosure analysis (e.g., $5x10^{-4}$). In addition, time histories (2 horizontal and 1 vertical components) consistent with the spectra are calculated as well as 3D dynamic strains and curvatures, peak ground acceleration, and peak particle velocity as functions of depth between the surface and the waste repository level. Strain-compatible soil properties are also estimated at the SFA.

6.2.5 Limitations

The two fundamental simplifications of the RVT site response model used in these analyses, plane horizontal layers (1D) and equivalent-linear approximation to nonlinear dynamic material response, are its two limitations. For conditions under which lateral variations in dynamic material properties control strong motions, the 1D model may not be appropriate. Generally these conditions involve deep basins with sources located outside of the basins (large source-to-site distances), and at low frequencies (≤ 0.5 Hz) (Campbell 1981 [DIRS 102191], Joyner 2000 [DIRS 164134], Boore 2001 [DIRS 163993]). For these cases, surface waves may dominate the low frequencies, resulting in long duration wavetrains. Experience has shown that conventional site response analyses assuming vertically-propagating S-waves accommodates much of the amplification due to surface waves. Seed et al. (1988 [DIRS 163924]) were successful in modeling ground motions from the 1985 moment magnitude (**M**) 7.9 Mexico City earthquake using a simple 1D model. Additional analyses by Chávez-García et al. (1995 [DIRS 164971]) indicate that the 1985 ground motions were dominated by surface waves. The data collected from the geotechnical investigations to date (BSC 2002 [DIRS 157829]) do not indicate significant 2D or 3D velocity variations at the SFA or the RB. The 1D limitation is not considered an issue of concern for Yucca Mountain because the conditions there are not conducive to the generation of surface waves. Also the site response analyses are performed to develop appropriate spectral levels and not durations.

The limitation involving the equivalent-linear approximation is generally cast in the form of acceptable levels of cyclic shear strain. In assessing the ability of the equivalent-linear approximation to appropriately accommodate the effects of material nonlinearity on peak acceleration, peak particle velocity, and peak oscillator response (5%-damped response spectra),

maximum cyclic shear strains are considered the key indicator. Current validations of the equivalent-linear approximation have successfully modeled response spectra computed from motions recorded at soil sites, which have experienced large enough shear strains, mean peak of 1.00%, to fail (liquefy) (Section 7; Silva et al. 1999 [DIRS 164081]).

6.3 POINT-SOURCE STOCHASTIC GROUND MOTION MODEL

The following is a description of the stochastic point-source ground motion model used in these analyses. This description has been extracted from Silva et al. (1996 [DIRS 110474]).

6.3.1 Model Description

The stochastic ground motion model as implemented in this study had its inception with the early observation by Hanks (1979 [DIRS 182045]) that RMS (root mean square) accelerations at close distances could be interpreted as band-limited, finite duration white noise with a source spectrum consistent with the omega-square model of Aki (1967 [DIRS 182349]), Brune (1970 [DIRS 103315], 1971 [DIRS 131516]). This early point-source model was later extended to estimate peak accelerations by applying random vibration theory (RVT) to relate peak time domain values to RMS accelerations (Hanks and McGuire 1981 [DIRS 163510]). Hanks and McGuire (1981 [DIRS 163510]) further validated the model with existing strong motion data (moment magnitude [**M**] ≥ 4) over the distance range of about 10 to 100 km. Their results showed that the simple point-source model, using a Fourier amplitude spectrum which is constant between the earthquake source corner frequency (Brune 1970 [DIRS 103315], 1971 [DIRS 131516]) and a high-frequency cutoff due to propagation path/site damping, predicted peak acceleration values to within 50% or less of recorded ground. This is a remarkably close agreement since typical empirical relations have a standard deviation on peak acceleration of about 0.5 (natural log).

The two corner frequencies (source and path/site) give rise to the band-limited characterization of the model with the strong motion or faulting duration defined as the inverse of the magnitude-dependent source corner frequency. The only free parameters in the Hanks and McGuire (1981 [DIRS 163510]) model are the two corner frequencies and distance (1/R geometrical attenuation). Due to the assumed constant Fourier acceleration spectrum, the model can easily be integrated for the a_{RMS}:

$$a_{RMS} = 0.85 \frac{(2\pi)^2}{106} \frac{\Delta\sigma}{\rho R} \sqrt{\frac{f_{max}}{f_O}} \qquad \text{(Eq. 6-4)}$$

where $\Delta\sigma$ is stress drop, ρ is density, R is hypocentral distance, f_0 is the source corner frequency, and f_{max} is a maximum frequency.

Assuming the acceleration time history is white Gaussian noise, the RVT estimate of peak acceleration is given by

$$a_{max} = a_{RMS} \sqrt{2 ln\left(\frac{2 f_{max}}{f_O}\right)} \qquad \text{(Eq. 6-5)}$$

The source corner frequency (f_0) is determined by the magnitude using Brune scaling and is the low frequency limit, while the high frequency limit, f_{max}, is taken as the highest frequency passed through the recording instrument. The stress drop $\Delta\sigma$ is constant and for this first model, a value of 100 bars provided the best fit to the RMS and peak value data.

The model for a_{RMS} (Eq. 6-4) is the simplest possible physically correct expression for ground motions. This remarkably simple analytical expression has correctly predicted the magnitude and distance dependencies of peak ground accelerations and showed that high frequency strong ground motion increases with magnitude only because the faulting duration increases. Larger earthquakes have larger high frequency motions not because of any fundamental difference in source processes but simply because they last longer. This is a direct result of the stochastic assumption, the longer the source radiates, the higher the probability of observing larger motions.

The extension of this simple point-source model to response spectral ordinates as well as peak particle velocity resulted from the work of Boore (1983 [DIRS 103317]) and Boore and Joyner (1984 [DIRS 163174]). This work (Boore 1983 [DIRS 103317]) also validated the model over a wide magnitude range ($0.4 \leq \mathbf{M} \leq 7.7$) and wide frequency range (up to 400 Hz).

Methods for the generation of complete time histories using the point-source model was presented in Boore (1983 [DIRS 103317]) and by Silva and Lee (1987 [DIRS 103325]). The latter work also presented an implementation of the model to developing spectrum compatible time histories. Later, the model was extended to include crustal amplification effects (Boore 1986 [DIRS 103318], Silva and Lee 1987 [DIRS 103325]), and validated with strong motion data and at long periods using amplitude and dominant period data recorded by the World Wide Standardized Seismographic Network for magnitudes up to **M** 9.5 (Boore 1986 [DIRS 103318]). More recent extension of the point-source model includes an RVT equivalent-linear site response as well as accommodating crustal wave propagation (Ou and Herrmann 1990 [DIRS 170648]).

The conventional stochastic ground motion model uses an ω-square source model (Brune 1970 [DIRS 103315], 1971 [DIRS 131516]) with a single corner frequency and a constant stress drop (Boore 1983 [DIRS 103317], Atkinson 1984 [DIRS 174445]). RVT is used to relate RMS (values to peak values of acceleration (Boore 1983 [DIRS 103317]), and oscillator response (Boore and Joyner 1984 [DIRS 163174], Silva and Lee 1987 [DIRS 103325]) computed from the power spectra to expected peak time domain values (Boore 1983 [DIRS 103317]).

The shape of the acceleration spectral density, $a(f)$, is given by

$$a(f) = \mathrm{C} \frac{\mathrm{f}^2}{1 + \left(\frac{\mathrm{f}}{\mathrm{f_C}}\right)^2} \frac{\mathrm{M_O}}{R} P(f) A(f) e^{-\frac{\pi \mathrm{f R}}{\beta_O Q(\mathrm{f})}} \qquad \text{(Eq. 6-6)}$$

where

$$\mathrm{C} = \left(\frac{1}{\rho_O \beta_O{}^3}\right) \cdot (2) \cdot (0.55) \cdot \left(\frac{1}{\sqrt{2}}\right) \cdot \pi$$

M_0 = seismic moment in dynes/cm

R = hypocentral distance in km

β_o = shear-wave velocity at the source in km/sec

ρ_0 = density at the source in g/cm^3

Q(f) = frequency dependent quality factor (crustal damping),

A(*f*) = amplification,

P(f) = high-frequency truncation filter,

f_C = source corner frequency in Hz.

C is a constant which contains source region density (ρ_0) and shear-wave velocity terms and accounts for the free-surface effect (factor of 2), the source radiation pattern averaged over a sphere (0.55) (Boore 1986 [DIRS 103318]), and the partition of energy into two horizontal components ($1/\sqrt{2}$).

Source scaling is provided by specifying two independent parameters, the seismic moment (M_0) and the high-frequency stress parameter or stress drop ($\Delta\sigma$). The seismic moment is related to magnitude through the definition of **M** by the relation

$\log M_0 = 1.5\ \mathbf{M} + 16.05$ (Hanks and Kanamori 1979 [DIRS 106061]) (Eq. 6-7)

The stress drop ($\Delta\sigma$) relates to the corner frequency f_C to M_0 through the relation

$f_C = \beta\ (\Delta\sigma/8.44\ M_0)^{1/3}$ (Brune 1970 [DIRS 103315], 1971 [DIRS 131516]) (Eq. 6-8)

The stress drop is sometimes referred to as the stress parameter (Boore 1983 [DIRS 103317]) since it directly scales the Fourier amplitude spectrum for frequencies above the corner frequency (Silva 1991 [DIRS 163656], Silva and Darragh 1995 [DIRS 105398]). High (> 1 Hz) frequency model predictions are then very sensitive to this parameter (Silva 1991 [DIRS 163656]), and the interpretation of it being a stress drop or simply a scaling parameter depends upon how well real earthquake sources (on average) obey the omega-square scaling and how well they are fit by the single-corner-frequency model. The parameter is a physical parameter if the model is considered to generally work well and its values have physical interpretations in source processes. Otherwise, it simply is a high frequency scaling factor.

The spectral shape of the single-corner-frequency ω-square source model is then described by the two free parameters M_0 and $\Delta\sigma$. The corner frequency increases with the shear-wave velocity and with increasing stress drop, both of which may be region dependent.

The amplification accounts for the increase in wave amplitude as seismic energy travels through lower-velocity crustal materials from the source to the surface. The amplification depends on average crustal and near-surface shear-wave velocity and density.

The P(f) filter is an attempt to model the observation that acceleration spectral density appears to fall off rapidly beyond some region-dependent maximum frequency. This observed phenomenon truncates the high-frequency portion of the spectrum and is responsible for the band-limited

nature of the stochastic model. The band limits being the source corner frequency at low frequency and the high-frequency spectral attenuation. This spectral fall-off has been attributed to near-site attenuation (Hanks 1982 [DIRS 182046], Anderson and Hough 1984 [DIRS 128813]) or to source processes (Papageorgiou and Aki 1983 [DIRS 182047]) or perhaps to both effects. In the Anderson and Hough (1984 [DIRS 128813]) attenuation model, adopted here, the form of the P(f) filter is taken as

$$P(f) = e^{-\pi\kappa(r)f} \qquad \text{(Eq. 6-9)}$$

Kappa (r) ($\kappa(r)$ in Eq. 6-9) is a site- and distance-dependent parameter that represents the effect of intrinsic attenuation upon the wavefield as it propagates through the crust from source to receiver. $\kappa(r)$ depends on epicentral distance (r) and on both the shear-wave velocity (β_R) and quality factor (Q_S) averaged over a depth of H beneath the site (Hough and Anderson 1988 [DIRS 164686]).

At zero epicentral distance kappa (κ) is given by

$$\kappa = \frac{H}{\overline{\beta_R}\,\overline{Q_S}} \qquad \text{(Eq. 6-10)}$$

The bar in Eq. 6-10 represents an average of these quantities over a depth H. The value of kappa at zero epicentral distance is attributed to attenuation in the very shallow crust directly below the site (Hough and Anderson 1988 [DIRS 164686], Silva and Darragh 1995 [DIRS 105398]). The intrinsic attenuation along this part of the path is not thought to be frequency-dependent and is modeled as a frequency-independent, but site-dependent, constant value of kappa (Hough and Anderson 1988 [DIRS 164686], Rovelli et al. 1988 [DIRS 182048]). This zero epicentral distance kappa is the model implemented in this study. The crustal path attenuation from the source to just below the site is modeled with the frequency-dependent quality factors Q(f).

The Fourier amplitude spectrum, $a(f)$, given by Eq. 6-6 represents the stochastic ground motion model employing a Brune source spectrum that is characterized by a single corner frequency. It is appropriate for a point-source and models direct shear-waves in a homogeneous half-space (with effects of a velocity gradient through the $A(f)$ filter, Eq. 6-6). For horizontal motions, vertically-propagating shear-waves are assumed. Validations using incident inclined SH-waves with raytracing to find appropriate incidence angles leaving the source showed little reduction in uncertainty. For vertical motions P/SV propagators are used coupled with raytracing to model incident inclined plane waves (EPRI 1993 [DIRS 103319]).

Eq. 6-6 represents a ground motion model that accommodates source and wave propagation physics as well as propagation path and site effects with an attractive simplicity. The model is appropriate to an engineering characterization of ground motion since it captures the general features of strong ground motion in terms of peak acceleration and spectral composition with a minimum of free parameters (Boore 1983 [DIRS 103317], McGuire et al. 1984 [DIRS 166349], Boore 1986 [DIRS 103318], Silva and Green 1989 [DIRS 182433], Darragh et al. 1989 [DIRS 184399], Schneider et al. 1993 [DIRS 110467]). An additional important aspect of the stochastic model employing a simple source description is that the region-dependent parameters can be evaluated by observations of small local or regional earthquakes. Region-specific seismic hazard

evaluations can then be made for areas with sparse strong motion data with relatively simple spectral analyses of weak motion (Silva 1993 [DIRS 170696]).

In order to compute peak time-domain values, i.e., peak acceleration and oscillator response, RVT is used to relate RMS computations to peak value estimates. Boore (1983 [DIRS 103317]) and Boore and Joyner (1984 [DIRS 163174]) describe an excellent development of the RVT methodology as applied to the stochastic ground motion model. The procedure, in general, involves computing the RMS value by integrating the power spectrum from zero frequency to the Nyquist frequency and applying Parsevall's relation. Extreme value theory is then used to estimate the expected ratio of the peak value to the RMS value of a specified duration of the stochastic time history. The duration is generally taken as the inverse of the corner frequency (Boore 1983 [DIRS 103317]).

Factors that effect strong ground motions such as surface topography, finite and propagating seismic sources, laterally varying near-surface velocity and Q gradients, and random inhomogeneities along the propagation path are not included in the model. While some or all of these factors are generally present in any observation of ground motion and may exert controlling influences in some cases, the simple and elegant stochastic point-source model appears to be robust in predicting median or average properties of ground motion (Boore 1983 [DIRS 103317], 1986 [DIRS 103318]; Schneider et al. 1993 [DIRS 110467]; Silva 1993 [DIRS 170696]). For this reason it represents a powerful predictive and interpretative tool for engineering characterization of strong ground motion.

6.3.2 Uncertainties

The mathematical formulation used in the stochastic point-source ground motion model is exact in its computation of motions for a given set of input parameters. Accuracy of results in the context of how well the model simulates observed strong ground motions are assessed in the model validation (Section 7). The uncertainties of the input into the stochastic model are discussed in Section 6.2. The uncertainties of the RVT-equivalent linear model were described in BSC (2004 [DIRS 170027]).

6.3.3 Consideration of Alternative Conceptual Models

Numerous numerical ground motion models have been developed in the past 25 years including a finite-fault version of the stochastic ground motion model (Silva et al. 1996 [DIRS 110474]). Most of these alternative models simulate a finite fault. For example, in the Yucca Mountain PSHA (CRWMS M&O 1998a [DIRS 103731]), three finite-fault ground motion models were used: (1) the composite source model of Zeng and Anderson; (2) the stochastic model of Silva; and (3) the empirical Green's function technique of Somerville. These three models were deemed the best available models by the Group Motion experts to use in their development of site-specific attenuation relationships.

The stochastic point-source model was used in these analyses because of its simplicity, which was highly suitable for its application in this study and because it is probably the most validated ground motion model available (Silva et al. 1996 [DIRS 110474]). The model has been used extensively worldwide in ground motion prediction. In a sense, most ground motion models are

fundamentally similar, well founded in seismic source and wave propagation physics and importantly they are all approximate. The single essential element in selecting a model is to incorporate the appropriate degree of rigor through extensive validation exercises. Hence because of the latter as described in Section 7, the stochastic point-source model was used in these analyses.

6.3.4 Description of Input

Inputs to the model as implemented in the software code RASCALS include:

- Moment magnitude of the earthquake to be modeled
- Distance between the point-source and the site
- Depth of the point-source
- Stress drop of the point-source ($\Delta\sigma$)
- Crustal attenuation as expressed by the frequency-dependent $Q(f) = Q_o f^{\eta}$
- Kappa of the site
- Crustal model that describes the propagation path

6.3.5 Assumptions, Idealizations, and Simplifications

The stochastic nature of the point-source model is simply the assumption made about the character of ground motion time histories that permits stable estimates of peak parameters (e.g., acceleration, velocity, strain, stress, oscillator response) to be made without computing detailed time histories (Hanks and McGuire 1981 [DIRS 163510]; Boore 1983 [DIRS 103317]). The model uses RVT to relate a time domain peak value to the time history root mean square (RMS) value (Boore 1983 [DIRS 103317]).

An important assumption is that the process is normally distributed random noise and stationary (its statistics do not change with time) over its duration. A visual examination of any time history quickly reveals that this is clearly not the case: time histories (acceleration, velocity, stress, strain, oscillator) start, build up, and then diminish with time. However, during the critical strong-motion part of the shaking, the assumption is accurate enough to permit the approach to work well, as numerous comparisons with recorded motions and both qualitative and quantitative validations have shown (Hanks and McGuire 1981 [DIRS 163510]; Boore 1983 [DIRS 103317], 1986 [DIRS 103318]; Boore and Atkinson 1987 [DIRS 182044]; Silva and Darragh 1995 [DIRS 105398]).

6.3.6 Initial and/or Boundary Conditions

There are no initial and/or boundary conditions in the stochastic point-source ground motion model.

6.3.7 Mathematical Formulation

The mathematical formulation was described in Section 6.3.1.

6.3.8 Model Testing, Sensitivities, and Calibration Activities

Testing, sensitivities, and calibration of the stochastic point-source model are described in Section 7.

6.3.9 Use of Output

The stochastic point-source ground motion model is used to evaluate V/H ground motion ratios for Yucca Mountain (Section 6.5.2) and to corroborate a bound to ground motion at Yucca Mountain in the context of ground motion expected from a scenario earthquake in the vicinity of the site (Section 6.5.1 and Appendix A).

6.3.10 Limitations

Factors that effect strong ground motions such as surface topography, finite and propagating seismic sources, laterally varying near-surface velocity and Q gradients, and random inhomogeneities along the propagation path are not included in the stochastic point-source model. While some or all of these factors are generally present in any observation of ground motion and may exert controlling influences in some cases, the simple stochastic point-source model appears to be robust in predicting median or average properties of ground motion (Boore 1983 [DIRS 103317], Schneider et al. 1993 [DIRS 110467], Silva 1993 [DIRS 170696]).

Comparisons of point-source simulations to empirical model spectra at large distances for **M** 6.5 and **M** 7.5 have shown the point-source model to underpredict ground motions at intermediate frequencies (about 0.3 to 3.0 Hz) (Silva et al. 1996 [DIRS 110474]). The underprediction is significant at distances exceeding about 100 km and for $\mathbf{M} \geq 6.5$ with a significant portion likely due to a magnitude independent geometrical attenuation incorporated in the point-source model. Finite-fault simulations reduced the underprediction by 50%, supporting the magnitude dependent attenuation rate being due to source finiteness and suggesting that the remaining 50% may be due to wave propagation effects in crossing crustal structure boundaries (Silva et al. 1996 [DIRS 110474]).

These observations are not viewed as limitations in terms of the applications of the stochastic ground motion in this study because the applicable range of use is well within distances of 100 km and in the frequency range above 1 Hz.

6.4 MODEL INPUTS

A goal of approaches to model ground motion numerically (including site response models) is a quantitative assessment of prediction variability (Silva et al. 1996 [DIRS 110474], Section 5.1). A desirable approach to achieving this goal is in a manner that lends itself to characterizing the variability associated with model results. For a ground motion model, variability in results is due to a combination of modeling variability and parametric variability. Modeling variability is a measure of how well the model works (how accurately it predicts ground motions) when specific parameter values are known. Modeling variability is determined through validation exercises in which model predictions are compared to recorded motions. This variability can be due to source, path, and site factors for which the model does not account (e.g., linear site response does not completely accommodate nonlinear effects). Parametric variability results from a viable range of values for model parameters (e.g., soil profile, normalized shear modulus, and damping curves). It is the sensitivity of a model to a viable range of values for model parameters. The total variability, modeling plus parametric, represents the variance associated with the ground motion estimation and, because it is expressed as fractile levels, is as important as median estimates.

Both the *modeling* and *parametric* variabilities may have components of randomness (aleatory variability) and uncertainty (epistemic uncertainty). The following summarizes the four components of total variability in the context of ground motion estimates (Silva et al. 1996 [DIRS 110474], Table 5.1). Uncertainty is that portion of both modeling and parametric variability that, in principle, can be reduced as additional information (knowledge) becomes available, whereas randomness represents the intrinsic or irreducible component of variability for a given model or suite of parameters. The uncertainty component reflects a lack of knowledge and may be reduced as more data are analyzed. In the context of the PSHA, uncertainty is characterized by weighted alternatives in logic trees. Randomness (aleatory variability) is integrated in the hazard calculation. The terminology shown below is followed in this report.

Contributions to Total Variability in Ground Motion Models

	Modeling Variability	**Parametric Variability**
Uncertainty *(also Epistemic Uncertainty)*	Modeling Uncertainty: Variability in estimated motions resulting from particular model assumptions, simplifications and/or fixed parameter values. *Can be reduced by adjusting or "calibrating" model to better fit observed earthquake response.*	Parametric Uncertainty: Variability in estimated motions resulting from incomplete data needed to characterize parameters. *Can be reduced by collection of additional information, which better constrains parameters.*
	Modeling Variability	**Parametric Variability**
Randomness *(also Aleatory Variability)*	Modeling Randomness: Variability in estimated motions resulting from discrepancies between model and actual complex physical processes. *Cannot be reduced for a given model form.*	Parametric Randomness: Variability in estimated motions resulting from inherent randomness of parameters values. *Cannot be reduced a priori* by collection of additional information.*

Source: Silva et al. (1996 [DIRS 110474], Table 5.1)

NOTE: *Some parameters (e.g., source characteristics) may be well defined after an earthquake.

In conventional deterministic geotechnical engineering practice, the lack of reliable and unambiguous test results may represent an unacceptable condition in developing design motions as it would likely result in highly conservative design. However, with a fully probabilistic approach, uncertainty in dynamic material properties may be easily and properly treated in a manner that correctly accommodates parametric uncertainty (epistemic uncertainty) in the development of site-specific design motions. The significant issue then becomes a development of alternative cases that fully accommodate the expected range in mean *in-situ* properties. As an extreme, site-specific design motions can be developed without any site characterization whatsoever. As long as a full range of site conditions is accommodated as epistemic uncertainty through a suite of base-cases, the resulting site hazard will correctly reflect the site uncertainty in the level of motions for a given exceedance probability (as well as the ratio of the mean to median hazard). Increased knowledge through site characterization would then typically reduce the hazard, provided a single suite of base case properties given low weight initially and which produce high motions are not found to dominate across the site.

Site parametric epistemic uncertainty is treated in precisely the same manner as other components of uncertainty in the PSHA such as earthquake source parameters and expected ground motion conditional on magnitude and distance (attenuation relation). Simply stated, to produce estimates of mean hazard, a reasonable and defensible range in alternative models and accompanying weights must be developed to characterize uncertainties in source, path, and site parameters. For each component of parametric uncertainty, corresponding hazard curves are developed, weighted, and averaged over frequency to produce estimates of mean hazard. This

process then properly accommodates all components of parametric uncertainty in a consistent manner resulting in site-specific hazard at desired exceedance frequencies.

Inputs into the site response model consist of control motion response spectra, small-strain velocities, densities, and nonlinear dynamic material properties. Inputs into the stochastic point-source model include earthquake source, path, and site parameters including magnitude, distance, source depth, stress drop, crustal attenuation Q(f), and site attenuation (kappa). This section describes the development of these inputs and how the input uncertainties are characterized.

6.4.1 Control Motion Response Spectra

Response spectra forming the control motion for site response modeling are based on the results of a PSHA for Yucca Mountain (CRWMS M&O 1998 [DIRS 103731]). The PSHA employed a formal expert elicitation process involving 18 seismic source characterization experts and 7 ground motion experts. The probabilistic methodology allows the frequency of earthquake occurrences to be incorporated, and allows uncertainties and randomness to be quantified in a consistent manner in the final hazard results. The methodology is described in detail in *Methodology to Assess Fault Displacement and Vibratory Ground Motion Hazards at Yucca Mountain* (YMP 1997 [DIRS 100522]).

In the PSHA Project, the hazard was specified at a defined hard-rock free-field site condition termed the reference rock outcrop (Point A, Figure 1-1) (CRWMS M&O 1998 [DIRS 103731], Sections 5.3.1.2 and 5.7.1). Rock properties for the reference rock outcrop were those that available data indicated existed at a nominal 300-m depth, the approximate depth of the repository waste emplacement horizon. The V_S at the reference rock outcrop was estimated to be 1900 m/sec (6200 ft/sec). This value was derived from a Yucca Mountain velocity profile with the top 300 m removed (Schneider et al. 1996 [DIRS 103270], Section 5). Based on recent site-specific data, the depth at which the velocity conditions of the reference rock outcrop are achieved was revised (Sections 6.4.2.3 and 6.4.2.4).

In defining conditions for the PSHA reference rock outcrop, site attenuation (damping) was also prescribed. By defining the reference rock outcrop, detailed geotechnical site information could be incorporated through analyses using the site response model. In particular, response of the tuff as well as soil materials could be incorporated into the analyses as site characterization results became available.

Because site response calculations include damping, to avoid double counting, surface measurements of site attenuation had to be adjusted to remove the effects of damping in the upper 300 m. This was accomplished by defining a value of the site attenuation parameter, kappa, for the reference rock outcrop. Kappa for surface sites in the vicinity of Yucca Mountain was determined to be 0.022 sec based on data given in Su et al. (1996 [DIRS 100087], Table 4). For the PSHA, a value of 0.02 sec was adopted to represent site attenuation as measured at the surface (CRWMS M&O 1998 [DIRS 103731], Section 5.3.1.2). To correct this value to one appropriate for the reference rock outcrop, damping in tuff was measured in the laboratory (Stokoe et al. 1998 [DIRS 107635]). Low-strain damping in the top 300 m was found to correspond to a kappa of 0.0014 sec (CRWMS M&O 1998 [DIRS 103731], Section 5.3.1.2).

Therefore, the surface kappa value of 0.02 sec was reduced by 0.0014 sec to give a kappa at the reference rock outcrop of 0.0186 sec. The precision of the reference rock outcrop value of kappa is an artifact of the calculation that was made; it is not meant to imply that kappa is known with that precision.

Control motion response spectra to be used as input to site-response modeling are based on results of the PSHA. Representative hazard results from the PSHA are shown in Figures 6.4.1-1 through 6.4.1-4. In BSC (2004 [DIRS 170027], Section 6.2.2.3) UHS are determined from the PSHA results for mean AFEs of 10^{-3}, 5×10^{-4}, 10^{-4}, 10^{-5}, 10^{-6}, and 10^{-7}. Because the UHS are broad-band response spectra, reflecting contributions to ground motion hazard from earthquakes with a range of magnitudes and distances, reference earthquake response spectra were developed to represent the UHS in applying site-response results (BSC 2004 [DIRS 170027], Section 6.2.2.4). For each AFE, two reference earthquakes, characterized by a modal magnitude (M*) and modal distance (R*), were determined. One was based on deaggregation of the seismic hazard for spectral response at 1 Hz and 2 Hz (Figures 6.4.1-5 through 6.4.1-10) and the other on deaggregation of the seismic hazard for spectral response at 5 Hz and 10 Hz (Figures 6.4.1-11 through 6.4.1-16). Response spectra for the reference earthquakes for a given AFE were scaled to match the UHS in the appropriate frequency range (i.e., 1 to 2 Hz or 5 to 10 Hz). Those results, which form the basis for inputs to the site-response modeling documented in this report, are summarized in Table 6.4-1. Data tracking numbers (DTNs) for the reference earthquake data are summarized in Table 6.4-2.

Table 6.4-1. Summary of Deaggregation Results and Reference Earthquakes

10^{-3} AFE

	M*	R*	RE Magnitude and Distance	Horizontal Scale Factor	Vertical Scale Factor
5-10 Hz	5.15	8.75	**M** 6.3, 5 km	0.572	0.543
1–2 Hz 1-2 Hz Regional Sources 1-2 Hz Local Sources	7.35 7.35 5.85	51.25 51.25 3.75	**M** 6.9, 52 km	3.830	4.880

Source: BSC (2004 [DIRS 170027], Table 6.2-4), DTN: MO0211REDES103.000 [DIRS 170424]

5×10^{-4} AFE

	M*	R*	RE Magnitude and Distance	Horizontal Scale Factor	Vertical Scale Factor
5-10 Hz	5.15	8.75	**M** 6.3, 5 km	0.843	0.812
1–2 Hz 1-2 Hz Regional Sources	7.35 7.35	51.25 51.25	**M** 7.0, 51 km	4.820	5.361

Source: BSC (2004 [DIRS 170027], Table 6.2-4), DTN: MO0208UNHZ5X10.000 [DIRS 163722]

10^{-4} AFE

	M*	R*	RE Magnitude and Distance	Horizontal Scale Factor	Vertical Scale Factor
5-10 Hz	6.2	3.75	**M** 6.3, 5 km	1.835	1.855
1–2 Hz 1-2 Hz Regional Sources	7.7 7.7	51.3 51.3	**M** 7.7, 52 km	5.613	6.824

Source: BSC (2004 [DIRS 170027], Table 6.2-4), DTN: MO0211DERES104.000 [DIRS 170423]

10^{-5} AFE

	M*	R*	RE Magnitude and Distance	Horizontal Scale Factor	Vertical Scale Factor
5-10 Hz	6.25	3.75	**M** 6.4, 4 km	4.261	4.624
1–2 Hz	6.25	3.75	**M** 7.7, 51 km	13.735	15.531
1-2 Hz Regional Sources	7.35	51.25			

Source: BSC (2004 [DIRS 170027], Table 6.2-4), DTN: MO0308UNHAZ105.000 [DIRS 170425]

10^{-6} AFE

	M*	R*	RE Magnitude and Distance	Horizontal Scale Factor	Vertical Scale Factor
5-10 Hz	6.15	1.25	**M** 6.5, 1 km	8.030	8.675
1–2 Hz	6.65	1.25	**M** 7.7, 51 km	30.600	47.640
1-2 Hz Regional Sources	7.65	51.25			

Source: BSC (2004 [DIRS 170027], Table 6.2-4), DTN: MO0206UNHAZ106.001 [DIRS 163723]

10^{-7} AFE

	M*	R*	RE Magnitude and Distance	Horizontal Scale Factor	Vertical Scale Factor
5-10 Hz	6.15	1.25	**M** 6.5, 1 km	16.843	18.583
1–2 Hz	6.65	1.25	**M** 7.7, 51 km	64.225	72.809
1-2 Hz Regional Sources	7.65	51.25			

Source: BSC (2004 [DIRS 170027], Table 6.2-4), DTN: MO0209UNHAZ107.000 [DIRS 163724]

Table 6.4-2. Summary of Data Tracking Numbers for REs

Description	DTN
REs for AFE of 10^{-3}	MO0211REDES103.000 [DIRS 170424]
REs for AFE of $5x10^{-4}$	MO0208UNHZ5X10.000 [DIRS 163722]
REs for AFE of 10^{-4}	MO0211DERES104.000 [DIRS 170423]
REs for AFE of 10^{-5}	MO0308UNHAZ105.000 [DIRS 170425]
REs for AFE of 10^{-6}	MO0206UNHAZ106.001 [DIRS 163723]
REs for AFE of 10^{-7}	MO0209UNHAZ107.000 [DIRS 163724]

In BSC (2004 [DIRS 170027]) development of REs was one step in the process to implement Approach 2B of NUREG/CR-6728 (McGuire et al. 2001 [DIRS 157510], Section 6.1). The two REs for each AFE, based on deaggregation of response spectral acceleration for a high oscillator frequency range and a low oscillator frequency range, provided a deterministic representation of the probabilistic UHS.

For the analyses described in this report, Approach 3 of NUREG/CR-6728 (McGuire et al. 2001 [DIRS 157510], Section 6.1) is being implemented (Section 6.1). In developing a suite of site-response amplification factors for use in integrating over ground motion, site-response modeling is carried out for a range of ground motion levels (PGA from 0.01 to 10 g) rather than a sequence

of AFEs (10^{-3}, 5×10^{-4}, 10^{-4}, 10^{-5}, 10^{-6}, and 10^{-7}). Control motion input to the site response model, however, still makes use of the REs. The control motion response spectrum for each level of ground motion is determined by scaling an appropriate RE response spectrum to the PGA level of interest (BSC 2004 [DIRS 170027]). The appropriate RE for each ground motion level is chosen by comparing the PGA level of interest to the PGA level of the RE spectrum. Since the spectral shapes of the RE change little with AFE, a minimum suite of RE was selected that adequately span the range of expected Point A motions. Table 6.4-3 summarizes the use of REs. Figure 6.4.1-17 shows representative control motion response spectra used as input for site-response modeling to develop the suite of amplification factors for the range of ground motion considered.

Table 6.4-3. REs Used to Scale Response Spectra to Determine Control Motion for Site-Response Modeling

PGA Level (g)	Low-Frequency (1-2 Hz) RE / PSHA AFE	High-Frequency (5-10 Hz) RE / PSHA AFE
0.010	M 7.0 at 51 km / 5×10^{-4}	M 6.3 at 5 km / 10^{-3}, 5×10^{-4}, 10^{-4}
0.050	M 7.0 at 51 km / 5×10^{-4}	M 6.3 at 5 km / 10^{-3}, 5×10^{-4}, 10^{-4}
0.10	M 7.0 at 51 km / 5×10^{-4}	M 6.3 at 5 km / 10^{-3}, 5×10^{-4}, 10^{-4}
0.20	M 7.0 at 51 km / 5×10^{-4}	M 6.3 at 5 km / 10^{-3}, 5×10^{-4}, 10^{-4}
0.30	M 7.7 at 52 km / 10^{-4}	M 6.3 at 5 km / 10^{-3}, 5×10^{-4}, 10^{-4}
0.40	M 7.7 at 52 km / 10^{-4}	M 6.3 at 5 km / 10^{-3}, 5×10^{-4}, 10^{-4}
0.50	M 7.7 at 52 km / 10^{-4}	M 6.3 at 5 km / 10^{-3}, 5×10^{-4}, 10^{-4}
0.75	M 7.7 at 51 km / 10^{-5}, 10^{-6}, 10^{-7}	M 6.3 at 5 km / 10^{-3}, 5×10^{-4}, 10^{-4}
1.00	M 7.7 at 51 km / 10^{-5}, 10^{-6}, 10^{-7}	M 6.3 at 5 km / 10^{-3}, 5×10^{-4}, 10^{-4}
1.25	M 7.7 at 51 km / 10^{-5}, 10^{-6}, 10^{-7}	M 6.4 at 4 km / 10^{-5}
1.50	M 7.7 at 51 km / 10^{-5}, 10^{-6}, 10^{-7}	M 6.4 at 4 km / 10^{-5}
1.75	M 7.7 at 51 km / 10^{-5}, 10^{-6}, 10^{-7}	M 6.4 at 4 km / 10^{-5}
2.00	M 7.7 at 51 km / 10^{-5}, 10^{-6}, 10^{-7}	M 6.4 at 4 km / 10^{-5}
2.50	M 7.7 at 51 km / 10^{-5}, 10^{-6}, 10^{-7}	M 6.5 at 1 km / 10^{-6}, 10^{-7}
3.00	M 7.7 at 51 km / 10^{-5}, 10^{-6}, 10^{-7}	M 6.5 at 1 km / 10^{-6}, 10^{-7}
4.00	M 7.7 at 51 km / 10^{-5}, 10^{-6}, 10^{-7}	M 6.5 at 1 km / 10^{-6}, 10^{-7}
5.00	M 7.7 at 51 km / 10^{-5}, 10^{-6}, 10^{-7}	M 6.5 at 1 km / 10^{-6}, 10^{-7}
6.00	M 7.7 at 51 km / 10^{-5}, 10^{-6}, 10^{-7}	M 6.5 at 1 km / 10^{-6}, 10^{-7}
7.00	M 7.7 at 51 km / 10^{-5}, 10^{-6}, 10^{-7}	M 6.5 at 1 km / 10^{-6}, 10^{-7}
8.00	M 7.7 at 51 km / 10^{-5}, 10^{-6}, 10^{-7}	M 6.5 at 1 km / 10^{-6}, 10^{-7}
9.00	M 7.7 at 51 km / 10^{-5}, 10^{-6}, 10^{-7}	M 6.5 at 1 km / 10^{-6}, 10^{-7}
10.00	M 7.7 at 51 km / 10^{-5}, 10^{-6}, 10^{-7}	M 6.5 at 1 km / 10^{-6}, 10^{-7}

Note: In cases for which more than one AFE is listed for a magnitude and distance combination, the reference earthquake response spectrum shape is identical for each AFE, but the scaling factor, to match the reference earthquake response spectrum to the UHS in the oscillator frequency range of interest for the AFE, differs (BSC 2004 [DIRS 170027], Section 6.2.2.4).

6.4.2 Development of Seismic Velocity Profiles

Major inputs into the site response model are the V_S and V_P profiles for the RB and the SFA. The goal is to develop velocity profiles that appropriately represent the uncertainty and variability in velocities for the RB and SFA. Profiles are developed keeping in mind that, in terms of final ground motions, the RB and SFA are each treated as a single site. That is, a single set of site-specific ground motion hazard curves and related ground motion inputs are developed for each site. To the extent that different base case velocity profiles characterize different portions of each site, site response calculations are made using each base case profile and the results are enveloped. In the case in which there is epistemic uncertainty in a given base case velocity profile, alternative interpretations are used in site response calculations and the associated hazard curve results are combined in a weighted average based on the assessed degree to which each interpretation is supported by the available data. Aleatory variability (randomness) in velocity profiles is also incorporated into the site response calculations. Each base case profile forms the basis for developing a suite of 60 randomized profiles that are used in site response calculations.

The velocity profiles are developed on the basis of available velocity data and an understanding of the geologic framework of the sites. Velocity data for the site were acquired using a range of techniques: spectral-analysis-of-surface-waves (SASW), downhole seismic velocity surveys, suspension logging surveys, sonic velocity logging, and vertical seismic profiling (VSP). Borehole-based techniques provide information on velocities in the immediate vicinity of the borehole. SASW surveys complement the borehole-based measurements and provide information on the average velocity along the length of the survey line. SASW surveys were also carried out in the subsurface within the ESF and the ECRB cross-drift. Geologic data are used to provide insights on the areas or zones in which various representative velocity profiles apply.

For the SFA, base case velocity profiles for alluvium and tuffs of the Timber Mountain and Paintbrush Groups are based on a combination of surface-based SASW, downhole seismic, and suspension logging data. For the RB, surface-based SASW data form the basis for developing profiles for the tuffs of the Paintbrush Group. For both the SFA and RB, sonic logging data provide the technical basis for an assumption of V_S values for the Calico Hills Formation and the Prow Pass Tuff (Section 5.1). VSP data, downhole velocity data from shallow (< 200 ft) boreholes on the RB, and subsurface-based SASW data are used to compare to and corroborate the developed base case profiles, but are not relied on directly. Final profiles for site response modeling are developed by combining, as appropriate, the component profiles for alluvium, the tuffs of the Timber Mountain and Paintbrush Groups, and the assumed V_S values for the Calico Hills Formation and Prow Pass Tuff. P-wave velocity (V_P) profiles are determined from the V_S profiles based on an analysis of Poisson's ratio.

In the following sections, first the available geologic and velocity data are described. Then the development of base case velocity profiles for the SFA and the RB is presented. Velocity profiles developed for ground motion calculations completed in 2004 (BSC 2004 [DIRS 170027]) are also summarized.

In the development of base case velocity profiles, a lognormal distribution of velocities was adopted and arithmetic mean velocities were calculated using the formula (exp [mean log + $\sigma^2/2$)]). In this report, we refer to the "arithmetic mean" as the "mean." (Because velocities are lognormally distributed, the geometric mean or median velocity profile should have been used in place of the arithmetic mean. Sensitivity calculations were performed to assess the impact on the design ground motions using both mean and median base case velocity profiles and the differences (< 5%) were judged to be insignificant.)

6.4.2.1 Geology of RB and SFA

Yucca Mountain and the SFA lie within the central southern part of Nevada within the Great Basin, which is part of the Basin and Range structural/physiographic province. Pre-Tertiary rocks, consisting of a thick sequence of Proterozoic and Paleozoic sedimentary rocks, underlie approximately 1,000 to 3,000 m of Miocene volcanic rock in the Yucca Mountain area (BSC 2002 [DIRS 157829], Section 6.6.1).

Units of the Paintbrush and Timber Mountain groups are included in the Miocene volcanic sequence exposed at Yucca Mountain. The Claim Canyon caldera and environs, located approximately 6 km north of the study area, is the source of the 12.7 to 12.8 million-year old pyroclastic rock and lava comprising the Paintbrush Group. Four formations of pyroclastic-flow and pyroclastic-fall deposits with interbedded lavas, dipping 5 to 10° to the east, form a homoclinal sequence included in the Paintbrush Group. Two of these formations, the Topopah Spring Tuff and Tiva Canyon Tuff, are voluminous, densely welded ignimbrites, grading upward from rhyolite to quartz latite composition (BSC 2002 [DIRS 157829], Section 6.6.1).

The crest of Yucca Mountain, located about 2 miles to the west, is at an average elevation of about 4,900 feet. Near the site of the SFA, relief is approximately 250 feet, ranging from about elevation 3,850 feet at the crest of Exile Hill, to the west, to about elevation 3,600 feet at the center of Midway Valley, to the east (BSC 2002 [DIRS 157829], Section 6.6.1).

The SFA is situated in Midway Valley along the east side of Exile Hill. Exile Hill is bounded on its west side by the Bow Ridge fault and on its east side by the Exile Hill fault. Exile Hill consists of Tiva Canyon Tuff that is surrounded and partially covered by Quaternary alluvium/colluvium. The upper Tertiary and Quaternary sediments (identified by the symbol Qac) that fill Midway Valley consist mostly of alluvial deposits (fluvial and colluvial sediments) and some thin eolian deposits. Over most of the SFA the alluvium is covered by an artificial fill known as the North Portal pad or by the adjacent muck piles. The North Portal pad is a man-made fill constructed on the Midway Valley alluvium to support tunneling of the ESF. (BSC 2002 [DIRS 157829], Section 6.6.1).

Based on the drilling data, an interpretation of subsurface geologic conditions has been developed for the SFA (BSC 2002 [DIRS 157829], Section 6.6.2). The interpretation presumes that the thicknesses of lithostratigraphic units remain relatively constant across the SFA, and that a northeast-striking, southeast-dipping volcanic sequence has been structurally disrupted by several northerly-trending, high-angle, primarily normal, faults. These faults are depicted as cutting the entire volcanic bedrock sequence, but not disrupting the overlying alluvium. The lack

of disruption of the alluvium is supported by a top of rock profile developed from drilling that indicates a relatively even bedrock/alluvium contact.

The alluvium varies in thickness from zero on the western edge of the SFA along the base of Exile Hill to about 200 feet on its eastern margin (SNL 2008 [DIRS 183779], Figure 6.2-4). Alluvial materials in the SFA consist of interbedded caliche-cemented and non-cemented, poorly sorted gravel with some fines, cobbles and boulders.

Under the alluvium are welded and nonwelded volcanic rock units of the Timber Mountain and Paintbrush groups (BSC 2002 [DIRS 157829]), Section 6.6.2). Figure 6.4.2-1 provides a lithostratigraphic column for relevant units of these groups. Nonwelded units beneath the site include the pre-Rainier Mesa Tuff bedded tuffs (Tmbt1) of the Timber Mountain Group, and the Tuff unit "x" (Tpki) and pre-Tuff unit "x" bedded tuffs (Tpbt5) of the Paintbrush Group. Beneath these nonwelded units is the Tiva Canyon Tuff, which is generally densely welded. The Tiva Canyon Tuff has been divided into two members; the crystal-rich member (Tpcr) and the crystal-poor member (Tpcp). These members are further divided into zones, for example, the Tiva Canyon Tuff crystal-rich nonlithophysal zone of the Tiva Canyon Tuff (Tpcrn) (Buesch et al. 1996 [DIRS 100106]). To simplify the distinction between the welded and nonwelded Tiva Canyon Tuff and the post-Tiva Canyon Tuff bedded tuffs, the vitric and lithophysal zones (Tpcrv and Tpcrl) of the crystal-rich member of the Tiva Canyon Tuff have been included with the crystal-rich nonlithophysal zone (Tpcrn) in this report.

The most prominent structural feature in the SFA is a north-northwest-trending, east-northeast-dipping normal fault that cuts across the SFA, near boreholes RF#14 and RF#29 (BSC 2002 [DIRS 157829], Section 6.6.2). This fault is informally referred to in this report as the "Exile Hill fault splay." The largest displacement observed on the Exile Hill fault splay lies between boreholes RF#22 and RF#24 where there is approximately 300 feet of down-to-the-northeast separation, dropping the nonwelded pre-Rainier Mesa Tuff bedded tuffs (Tmbt1) on the northeast against the densely welded Tiva Canyon Tuff on the southwest. This relatively substantial vertical displacement along the Exile Hill fault splay has, in effect, subdivided the SFA into two distinct areas. Southwest of this fault, the top of the welded Tiva Canyon Tuff is relatively near the surface, ranging from zero to a maximum of about 190 feet below natural grade. In contrast, on the northeast side of the Exile Hill fault splay, the top of the Tiva Canyon Tuff ranges from about 250 to 480 feet below natural grade. A substantially greater thickness of the post-Tiva Canyon Tuff nonwelded bedded tuffs (Tptb5, Tpki, Tmbt1, and Tmr) occurs beneath the alluvium on the northeast side of the Exile Hill fault splay relative to the southwest side. The offset diminishes to the southeast along the strike of the fault, with 65 feet of down-to-the-east separation near borehole RF#14.

6.4.2.2 Summary of 2000 to 2001 Data

This section provides an overview of geotechnical and geologic site investigations carried out in 2000 and 2001. Details of the geotechnical investigations and the collected velocity data are presented in reports (BSC 2002 [DIRS 157829], 2004 [DIRS 170027]). Table 6.4-4 summarizes the data sets that were used in the 2004 analyses (BSC 2004 [DIRS 170027]). The scope and techniques used in these investigations are summarized in Section 6.2 of BSC (2004 [DIRS 170027]).

Table 6.4-4. 2000 to 2001 Input Data for Development of Seismic Velocity Profiles

Input Data	Data Source	Data Tracking Number
Velocity Seismic Profile Results from Boreholes NRG-6, WT-2, RF-4, RF-7/7A, SD-12, G-2 & G-4	Majer et al. (1996 [DIRS 104685], Section IV)	LB0306VSP95DAT.001
Downhole Velocity Measurements at the WHB Site (V_S and V_P Profiles from boreholes RF#13, 14, 15, 16, 17, 18, 19, 20, 21, 22, 23, 24, 25, 26, 28, & 29)	BSC (2002 [DIRS 157829], Section 6.2.5)	MO0111DVDWHBSC.001
Downhole Velocity Measurements at the WHB Site (V_S and V_P Profiles from boreholes RF#13 & 17)	BSC (2002 [DIRS 157829], Section 6.2.5)	MO0110DVDBOREH.000
Downhole Velocity Measurements from the Top of Yucca Mountain (V_S and V_P Profiles from boreholes UZ-N66, UZ-N94, UZ-N71, UZ-N75, UZ-N64, UZ-N27, & UZ-N46)	BSC (2002 [DIRS 157829], Section 6.4.3)	MO0202DVDWHBSC.002
SASW V_S Data from the WHB Site (Surveys SASW-1 through -9, SASW-11 through -31, SASW-33, SASW-10+37, SASW-32+35, and SASW-34+36)	BSC (2002 [DIRS 157829], Section 6.2.7)	MO0110SASWWHBS.000
SASW V_S Data from the Top of Yucca Mountain (2000) (Surveys SASW CYM-1 through CYM-7)	BSC (2002 [DIRS 157829], Section 6.4.2)	MO0203SEPSASWD.000
SASW V_S Data from the Top of Yucca Mountain (2001) (Surveys D-1 through D-12 and S-1 through S-12)	BSC (2002 [DIRS 157829], Section 6.4.2)	MO0110SASWVDYM.000
SASW V_S Data from Rock Sites on Yucca Mountain and in the ESF (Surveys R-1 through R-3 and T-1 through T-5)	BSC (2002 [DIRS 157829], Sections 6.3.2 and 6.4.2)	MO0206SASWROCK.000
Borehole Suspension V_S and V_P Data at the WHB Site	BSC (2002 [DIRS 157829], Section 6.2.6)	MO0204SEPBSWHB.001
Borehole Suspension V_S and V_P Data for RF#13 at the WHB Site	CRWMS M&O (1999 [DIRS 109209], Section 4.4, Appendix O)	MO0204SEISDWHB.001
Geotechnical Borehole Logs from RF#13, 14, 15, 16, 17, 18, 19, 20, 21, 22, 23, 24, 25, 26, 28 & 29	BSC (2002 [DIRS 157829], Sections 6.2.2, 6.2.3, and 6.6.2)	GS030783114233.001

Data that were acquired in 2000 and 2001 within the WHB area (a subset of the current SFA) that were used in the current analysis consist of:

- Geologic data from 15 boreholes designated as UE-25 RF#14 through UE-25 RF#26, UE-25 RF#28, and UE-25 RF#29 (Figure 6.4.2-2).
- V_S and V_P profiles from downhole seismic surveys in boreholes RF#13 through RF#26, RF#28, and RF#29.
- V_S and V_P profiles from suspension seismic surveys in boreholes RF#13 through RF#26, RF#28, and RF#29.

- V_S profiles from SASW surveys SASW-1 to SASW-37. Six of these surveys were combined resulting in three profiles (SASW 10+37, SASW 32+35 and SASW 34+36).

Data that were acquired in 2000 and 2001 for the RB and used in the current analysis consist of:

- SASW surveys CYM-1 to CYM-7, S-1 to S-12 and D-1 to D-11.

The velocity data from the downhole seismic surveys using existing boreholes UZ-N27, UZ-N33, UZ-N46, UZ-N64, UZ-N66, UZ-N71, UZ-N75, and UZ-N94 were not used in the current analysis since these measurements were too shallow and were not considered to impact the base case velocity profile developed for the RB.

VSP data collected in 1995 in existing boreholes near the waste emplacement area footprint (Majer et al. 1996 [DIRS 104685], Section IV) were also evaluated and are discussed in (BSC 2004 [DIRS 170027], Section 6.2.3.2.5).

6.4.2.3 Summary of 2004 Base Case Models

Two base case V_S and V_P profiles required for input into the site-response model were developed for the RB. For the SFA, a single base case tuff and base case alluvium profile were developed. The development of these models is described in detail in BSC (2004 [DIRS 170027], Section 6.2.3).

To accommodate the epistemic uncertainty in tuff V_S data, two base case profiles were developed for the RB (Figure 6.4.2-3). One profile was based on results of the SASW and downhole seismic surveys on and near the RB. The second profile was based on results of the VSP surveys obtained in boreholes at the edge of or slightly outside of the RB. The two data sets had little spatial overlap and appeared to indicate significantly different results.

V_P profiles for RB tuff were calculated from the V_S profiles and Poisson's ratio (ν). Poisson's ratio was determined using data from RB boreholes in which P-wave and S-wave quality was sufficient. To calculate base case #1 and #2 V_P profiles from the respective V_S profiles, ν was taken to decrease linearly from 0.33 (V_P/V_S = 1.99) at the surface to 0.30 (V_P/V_S = 1.87) at a depth of 250 ft and to maintain a constant value of 0.30 at depths below 250 ft.

Velocity profiles for the SFA were based on downhole, suspension, and SASW results from the surveys carried out in the WHB area (Figure 6.4.2-2). Data were restricted to data obtained southwest of the Exile Hill fault splay.

For the SFA, epistemic uncertainty was less than for the RB. More data are available and the area to be represented by the profiles was smaller. Thus, a single SFA base case profile was developed for each of the two materials that are present: tuff (Figure 6.4.2-4) and alluvium (Figure 6.4.2-5). The base case profile was computed by calculating a geometric mean of the median SASW, downhole, and suspension profiles. (The suspension profiles were not used for the alluvium base case (BSC 2004 [DIRS 170027]).)

Similar to the SFA base case V_S profile, the base case V_P profile for tuff was computed from the downhole and suspension data. The base case profile is the geometric mean of the two median

profiles. As was the case for the V_S profile, it was only appropriate for the area southwest of the Exile Hill fault splay.

The base case V_S profile for the alluvium was developed by calculating a geometric mean of the median downhole and SASW profiles southwest of the Exile Hill fault splay. The suspension data were not used because of the unreliability of some of the shallower data. The SFA base case profile does not include velocities from the fill (tunnel muck), which was excluded from the SASW and downhole data by estimating its depth from the borehole logs.

The only available V_P data for the alluvium were the downhole data. SASW does not yield a direct measurement of V_P and the suspension data were not considered reliable. To maintain consistency with the alluvium V_S base case model, which was based on both downhole and SASW data, the base case V_P profile was calculated by multiplying the discretized base case V_S profile by smoothed depth-varying V_P/V_S ratios for the alluvium from the downhole data south of the fault.

All base case velocity profiles were the result of smoothing by eye the actual mean profiles from the velocity data.

6.4.2.4 New Data

The following describes additional data not available for the 2004 analyses that were considered in the current analyses. These data are summarized in Table 6.4-5.

Table 6.4-5. 2004-2005 Input Data for Development of Seismic Velocity Profiles

Input Data	Data Source	Data Tracking Number
Surface Spectral Analysis of Surface Waves (SASW) Theoretical Dispersion Curves and Vs Profiles For FY04 and FY05 For YMP (Surveys NPF-1, NPF-2+14, NPF-3+9, NPF-10, NPF-12, NPF-16 to NPF-28, AP-1, AP-3, AP-5 to AP-8, YM-1 to YM-6, YM-8, YM-10, YM-12 to YM-26)	SNL (2008 [DIRS 183779], Sections 6.2 and 6.3)	MO0609SASWSTDC.003 [DIRS 182125]
Underground Spectral Analysis of Surface Waves (SASW) Theoretical Dispersion Curves and Vs Profiles for FY05 for YMP	SNL (2008 [DIRS 183779], Section 6.4)	MO0609SASWUTDC.004 [DIRS 183295],

In developing velocity profiles for the current study, data that were available when the velocity profile analyses were being carried out were used. These data are a subset of the data associated with the DTNs listed in Table 6.4-5 and described in SNL (2008 [DIRS 183779], Section 6). Uncertainties incorporated into the site-response analyses are consistent with the available data that were used, as is appropriate for the development of probabilistic ground motions. Additional data that became available after the velocity profile analyses or that becomes available in the future can be used to reduce the incorporated uncertainties. "Preliminary and unqualified" data that were used were verified as unchanged once the data status was upgraded to "qualified" following completion of reviews.

6.4.2.4.1 2004 to 2005 Data at the SFA

A review of the 2000-2001 V_S profiles developed from the three techniques, namely downhole, suspension logging, and SASW, for the then WHB area indicated that the majority of the V_S surveys were carried out in the region shown as Southwest of the Exile Hill Fault Splay in Figure 6.4.2-2. The only data available for the area Northeast of the Fault were 6 SASW profiles (SASW-3, SASW-15, SASW-16, SASW-19, SASW-30, and SASW34+36) and the downhole and suspension data from four boreholes (RF#17, RF#19, RF#22 and RF#29). The displacement of about 200 to 300 ft (BSC 2004 [DIRS 170027]) across the fault suggested that the velocity structure may be different across the fault and that was indicated by the limited velocity data north of the fault compared to the data south of the fault. In addition, the locations of some of the waste handling facilities at the SFA have changed since the last phase of analysis, extending to the northeast beyond the area characterized in 2000-2001. Finally, the earlier surveys at the SFA were performed to a maximum depth of only 500 to 600 ft and thus the velocity structure of the units below the Tiva Canyon Tuff at the SFA was uncertain particularly northeast of the fault. To enhance the previous geotechnical characterization, additional field investigations were carried out for the SFA in 2004-2005 (SNL 2008 [DIRS 183779]).

The 2004 to 2005 field investigation program was developed to enhance the understanding of the subsurface characteristics of the area where important-to-safety buildings are to be located on either side of the Exile Hill Fault Splay. Figure 6.4.2-2 shows the locations of the 2004 to 2005 SASW surveys at the SFA. A total of 25 SASW surveys were performed at 20 locations across the SFA area (also referred to as the North Portal Facility area or NPF sites) to a maximum depth of about 1350 ft (SNL 2008 [DIRS 183779]). Table 6.4-6 summarizes the 25 SASW measurements performed at the SFA. Multiple SASW measurements at a given location were averaged and used in the analysis. In addition, four of these (NPF-2&14 and NPF-3&9) were combined resulting in 18 SASW measurements that were used in the development of the base case V_S profile at the SFA. The V_S profiles developed from each of these measurements are shown in Appendix C. The profiles are included with data having DTN MO0609SASWSTDC.003 [DIRS 182125].

Table 6.4-6. 2004 SASW Survey at the SFA

SASW ID	Coordinates of Center of Array		Depth of Interpreted Velocity Profile (feet)
	Northing	Easting	
NPF 1-T1	765841.68	570276.72	40
NPF 1-T2	765869.34	570306.99	40
NPF 2-T1	764713.07	571088.25	1093
NPF 3-T1	765768.96	571088.43	925
NPF 9-T1	764820.52	571356.81	925
NPF 10-T1	766199.33	571480.13	1272
NPF 12-T1	766634.56	572265.22	1097
NPF 14-T1	763803.30	570926.16	1093
NPF 16-T1	763119.37	571053.01	533
NPF 17-T1	761413.40*	571625.12*	1183
NPF 17-T2	762128.56	571470.26	487

SASW ID	Coordinates of Center of Array		Depth of Interpreted Velocity Profile (feet)
	Northing	Easting	
NPF 18-T1	765076.08	571540.98	487
NPF 19-T1	765402.61	571870.58	751
NPF 20-T1	766013.08	571878.85	815
NPF 21-T1	765776.71	571641.02	743
NPF 22-T1	766266.14	571578.25	572
NPF 22-T2	766266.21	571578.01	572
NPF 23-T1	765620.48	571353.85	1347
NPF 23-T2	766109.98	571252.36	1347
NPF 24-T1	765692.92	571690.62	949
NPF 25-T1	766776.42	571880.07	1345
NPF 25-T2	766776.31	571880.03	1345
NPF 26-T1	766264.52	571901.84	575
NPF 27-T1	765993.84	571668.86	635
NPF 28-T1	765793.42	570497.91	424

DTN: MO0701ABSRFLL2.000 [DIRS 182483], MO0609SASWSTDC.003 [DIRS 182125]

Note: * Coordinates not from center of array but one end.

Six SASW surveys were also performed in the area northwest of the Exile Hill. Data from these surveys (A-1, A-3, A-5 through A-8) are not being considered in these analyses as no important-to-safety facilities are currently planned for that area.

6.4.2.4.2 2004 to 2005 Data at the RB

A review of the 2000 to 2001 V_S measurements at the RB indicated that there were areas across the mountain, within or close to the footprint of the emplacement areas, like the ridge in the vicinity of borehole G-2 (Figure 6.4.2-6) where additional information would aid in the development of RB base case V_S profiles. In addition, previous SASW measurements described in BSC (2002 [DIRS 157829]) were interpreted to provide velocity profiles to at most about 750 ft in depth. Thus, additional SASW surveys were carried out in 2004-2005 to enhance the characterization of velocity for the RB.

In 2004-2005, SASW surveys were carried out at a total of 24 sites (YM-1 through 6, YM-8, YM-10, YM-12, YM13, YM14A, YM-14B, YM15 A, YM-15B, YM16 through YM-26) away from the SFA (SNL 2008 [DIRS 183779], Section 6.3). These surveys were carried out to increase the spatial coverage of the RB and to provide data allowing velocity interpretation to greater depths than in 2000-2001. Figure 6.4.2-6 shows the SASW surveys used in this analysis to characterize the RB units above the Calico Hills Formation (Table 6.4-7). At some of these sites, multiple surveys (example YM-1-T1 and YM-1-T2) were performed in different directions resulting in a total of 41 SASW surveys as summarized in Table 6.4-7. The V_S profiles developed from each of these measurements are shown in Appendix C. The profiles are included with data having DTN MO0609SASWSTDC.003 [DIRS 182125].

Table 6.4-7. 2004 SASW Surveys at the RB

SASW ID	Coordinates of Center of Array		Depth of Interpreted Velocity Profile (feet)	Location Description
	Northing	Easting		
YM-1-T1	769721.10	559150.33	1100	Test Location #1 on YMP Crest
YM-1-T2	770331.95	559167.38	1100	2nd Test at location #1 on YMP Crest
YM-2-T1	766539.9	558889.99	1097	Test Location #2 on YMP Crest
YM-2-T2	766539.9	558889.99	1097	2nd test at location #2 on YMP Crest, the same location for 2C used in both tests
YM-3-T1	764181.8	558952.28	1121	Test Location #3 on YMP Crest
YM-3-T2	764181.8	558952.28	1121	2nd test at location #3 on YMP Crest, the same location for 3C used in both tests.
YM-3-T3	NA	NA	1121	3rd test at location #3 on YMP Crest, location 3C not found in the field
YM-4	760814.24	558291.74	970	Test location #4 on YMP Crest
YM-5-T1	775234.27	563327.63	1100	Test location #5 on Bleach Bone Ridge
YM-5-T2	775543.03	563262.85	1100	2nd test at location #5 on Bleach Bone Ridge
YM-6-T1	772769.64	564032.43	456	Test location #6 and 7 on Bleach Bone Ridge, locations combined in one SASW test
YM-6-T2	772859.9	563986.59	456	Test location #6 and 7 on Bleach Bone Ridge, locations combined in one SASW test
YM-8	773300.4418	561191.372	833	Test location #8 and 9 in Tea Cup Wash combined as one SASW test
YM-10-T1	772304.783	561945.671	976	Initial test location #10 in Tea Cup Wash
YM-10-T2	772294.03	561847.16	976	2nd test at location #10 in Tea Cup Wash
YM-12	771537.59	560208.49	743	Test location #12 in Drill Hole Wash
YM-13-T1	769862.81	562025.44	848.7	Test location #13 in Drill Hole Wash
YM-13-T2	770239.01	561377.58	848.7	2nd test at location #13 in Drill Hole Wash
YM-14A-T1	766177.06	565161.78	982	Test location #14A near NRG-6 borehole
YM-14A-T2	767028.79	564644.47	982	2nd test at location #14 near NRG-6.
YM-14B	767741.05	563891.69	982	Test location #14B near NRG-6 borehole
YM-15A-T1	760675.94	564976.81	1353	Test location #15A near UZ-16 borehole. Survey crosses Dune Wash fault; thus data not used.
YM-15A-T2	761463.77	564116.29	1353	2nd test at location #15A. Survey crosses Dune Wash fault; thus data not used.

SASW ID	Coordinates of Center of Array		Depth of Interpreted Velocity Profile (feet)	Location Description
	Northing	Easting		
YM-15B-T1	760363.38	564870.87	1158	Test location #15B near UZ-16 borehole. Survey crosses Dune Wash fault; thus data not used.
YM-15B-T2	760332.06	564784.11	1158	Test location #15B near NRG-6 borehole. Survey crosses Dune Wash fault; thus data not used.
YM-16-T1	760817.03	562941.76	688	Test location #16 near WT-2 borehole
YM-16-T2	760431.89	563900.43	688	2nd test at location #16 near WT-2 borehole
YM-17-T1	778482.06	560529.59	1492	Test location #17 near G-2 borehole on Bleach Bone Ridge
YM-17-T2	778380.46	560610.93	1492	Test location is #17 on Bleach Bone Ridge near G-2
YM-19-T1	757567.9994	558314.688	818	Test location on top of Yucca Mtn on the left road when the road reaches the top of the crest.
YM-19-T2	757568.467	558334.431	818	2nd test at this location on top of Yucca Mtn on the left road when the road reaches the top of the crest.
YM-20-T1	749713.348	574526.059	965	Test location along Fran Ridge, source placed on pad at large block and the SASW line run to the north.
YM-20-T2	748830.778	574516.913	965	2nd test at this location along Fran Ridge with shorter spacings
YM-21-T1	766108.574	564024.99	995	Test location is on the road located in Coyote Wash.
YM-21-T2	766144.384	564220.858	995	2nd test at this location in Coyote Wash using smaller spacings.
YM-22	780202.349	565442.821	777	Test location is near WT-6 and is located along the road
YM-23	767716.937	563178.89	1031	Test location is on the road leading to SD-9
YM-24	N/A*	N/A*	451	N/A. Located away from the RB; data from this site not used.
YM-25	745040.569	573988.356	790	Test location is on the road near WT-3 at the south end of Fran Ridge. Located away from the RB; data from this site not used.

SASW ID	Coordinates of Center of Array		Depth of Interpreted Velocity Profile (feet)	Location Description
	Northing	Easting		
YM-26	747375.376	568949.557	1486	Test location is on the road near WT-17 near Rainer Ridge. Located away from the RB; data from this site not used.

Coordinates: Nevada State Plane, Central Zone, NAD27 Horizontal, NGVD29 Vertical. Units: U.S. Survey Feet

Notes: N/A: Not Available. Although included with data submitted under DTN MO0609SASWSTDC.003 [DIRS 182125], survey YM-18 was considered as scoping in nature and is not intended for use in characterizing site properties (SNL 2008 [DIRS 183779], Table 6.3-1). Thus it is not included in this table, nor the count of surveys carried out.

DTN: MO0701ABSRFLL2.000 [DIRS 182483], MO0609SASWSTDC.003 [DIRS 182125]

Source: Stokoe 2007 [DIRS 183272]

At locations like YM-5, where multiple SASW surveys were performed in different directions, the available V_S surveys were averaged and a single V_S profile was developed for that location.

Three of the 24 SASW surveys, namely YM-24, YM-25 and YM-26, were conducted away from the RB at sites where geologic units beneath the Timber Mountain Group are believed to be closer to the surface. These surveys were not included in the development of the base case V_S profiles for RB units above the Calico Hills Formation (Table 6.4-7). In addition, V_S profiles YM-15A, YM-15B, and YM-16 were surveyed across the Dune Wash fault and therefore were not deemed suitable to be included in the analysis. Thus, the V_S profiles from a total of 18 survey sites were used in the analysis.

In addition, SASW surveys were performed in two different underground tunnel sections, the ECRB (Enhanced Characterization of the RB) Cross Drift and the Exploratory Studies Facility (ESF) (Figure 6.4.2-7) (SNL 2008 [DIRS 183779], Section 6.4). These measurements were performed to provide an independent determination of velocities at depth and to compare with the V_S profiles at tunnel depths determined from surface-based SASW measurements. SASW data from the ESF and ECRB cross-drift are used to corroborate results determined from the surface-based surveys, but are not used as direct input to the profile analyses.

The tunnel crosses through different lithostratigraphic units along its length and therefore the V_S data available for the tunnels correspond to different units. Since the V_S data obtained from surface SASW surveys become sparse at deeper depths corresponding to the Topopah Spring Tuff units, the tunnel measurements of primary interest for this analysis are the ones corresponding to the three Topopah Spring Tuff units listed on Table 6.4-8 and shown on Figure 6.4.2-7. The Topopah Spring Tuff lithostratigraphic units through which the tunnel traverses and the corresponding SASW measurements are also listed on Table 6.4-8.

At the time that the velocity profile analyses were carried out, not all results from the ESF and ECRB cross-drift surveys were available. Thus, only a subset of the data described in SNL (2008 [DIRS 183779], Section 6.4) were considered in this study. Results from the surveys listed in Table 6.4-8 are those used for comparison and corroboration purposes. These results were verified as unchanged following their change in status from “preliminary and unqualified” to “qualified.”

Table 6.4-8. SASW Measurements for the Different Lithostratigraphic Units in the ECRB and ESF Tunnels That Were Used for Comparison with and Corroboration of Velocity Profiles

Lithostratigraphic Units	SASW Measurements
Tptpul	ECRB_4 Profile 1, ECRB_4 Profile 2, ECRB_5, ESF-2, ESF-12, ESF-13
Tptpmn	ECRB_3 Profile 1, ECRB_3 Profile 2, ESF-3, ESF-7, ESF-8 Profile 1, ESF-8 Profile 2, ESF-9 Profile 1, ESF-9 Profile 2, ESF-10, ESF-11
Tptpll	ESF-5, ESF-6, ECRB-1, ECRB-2

DTN: MO0609SASWUTDC.004 [DIRS 183295]; BSC (2004 [DIRS 170029])

6.4.2.4.3 Sonic Velocity Data

As discussed in Section 5.1, sonic velocity data are used as the basis of an assumption that the V_S of the Calico Hills Formation is 5600 ft/sec and of the Prow Pass Tuff is 6000 ft/sec. The top of the Prow Pass Tuff (6000 ft/sec) is taken as equivalent to the PSHA reference rock outcrop which has a defined V_S of 1900 m/sec (6200 ft/sec).

Geophysical logs and core measurements from 40 boreholes at the project site were compiled and published by USGS in 1991 (DTN GS960708312132.002 [DIRS 113584] and GS990908314213.001 [DIRS 150287]). These data include sonic velocity measurements in 16 of the 40 boreholes. Both V_S and V_P measurements were made in 11 of the 16 boreholes while only V_P measurements were made in the remaining 5 of the 16 boreholes. Based on the proximity of the 16 boreholes to the SFA and RB (Figure 6.4.2-3), these 16 boreholes were selected for analysis. A complete listing of these 16 boreholes is given below in Table 6.4-9.

Table 6.4-9. Summary of 16 Boreholes Compiled by USGS

Short Name	Long Name	Total Depth (ft)	V_S Measurement (Yes/No)	V_P measurement (Yes/No)	Included in Current Analysis (Yes/No)
G-1	USW G-1	6000	No	Yes	Yes
G-2	USW G-2	6006	Yes	Yes	Yes
G-3/ GU-3	USW G-3/GU-3	5031/2644	Yes	Yes	Yes
G-4	USW G-4	3003	Yes	Yes	Yes
A-1	UE-25a#1	2501	No	Yes	Yes
B-1H	UE-25b#1	4002	Yes	Yes	Yes
P-1	UE-25p#1	5923	Yes	Yes	Yes
H-1	USW H-1	6000	Yes	Yes	Yes
H-3	USW H-3	4000	Yes	Yes	Yes
H-4	USW H-4	4000	Yes	Yes	Yes
H-5	USW H-5	4000	No	Yes	Yes
H-6	USW H-6	4002	No	Yes	Yes

Short Name	Long Name	Total Depth (ft)	V_S Measurement (Yes/No)	V_P measurement (Yes/No)	Included in Current Analysis (Yes/No)
C-1	UE-25c#1	3000	Yes	Yes	Yes
C-2	UE-25c#2	3000	Yes	Yes	Yes
C-3	UE-25c#3	3000	Yes	Yes	Yes
J-13	J-13	3498	No	Yes	No

DTN: GS960708312132.002 [DIRS 113584] and GS990908314213.001 [DIRS 150287]

Figures 6.4.2-8 through 6.4.2-23 show the V_S profiles obtained from the sonic measurements at each of the 16 boreholes. The plots also show the V_S profile calculated from the measured V_P profile using Poisson's ratio of 0.3 (BSC 2004 [DIRS 170027], Section 6.2.3.3.2). Wherever direct V_S measurements were unavailable, these inferred V_S profiles were used in the analysis. Figures 6.4.2-8 through 6.4.2-23 also show the geologic profile at each of the boreholes obtained from DTN MO0004QGFMPICK.000 [DIRS 152554]. Based on a review of the characteristics of the lithologic units, the pre-Calico Hills Formation bedded tuffs (Tacbt) at the bottom of Calico Hills Formation are grouped with Prow Pass Tuff while the crystal poor vitric units (Tptpv) and the pre-Topopah bedded tuffs (Tpbt1) at the bottom of Topopah Spring Tuff formation are grouped with Calico Hills Formation.

Based on the above, the Vs measurements corresponding to the Calico Hills Formation, Prow Pass Tuff and Bullfrog Tuff were extracted from each of the boreholes and analyzed. Figures 6.4.2-24 through 6.4.2-26 show the V_S profile obtained for each of the units, Calico Hills Formation, Prow Pass Tuff, and Bullfrog Tuff from these 16 boreholes. The profiles have been normalized to the top of each unit so the vertical scale is depth below the top of the unit or in other words the thickness of the unit. Note that there may be certain depths/units in a borehole where no V_S measurements were available. Accordingly, the number of profiles for each unit ranges from 1 to 15 and the number decreases with thickness (Figures 6.4.2-24 to 6.4.2-26). Although the Calico Hills Formation V_S is shown to a thickness of 1060 ft, only one measured profile extends more than a thickness of about 450 ft (Figure 6.4.2-24).

A mean V_S for each unit across boreholes was calculated and used in the analysis (Appendix C, "Average Velocity Deeper Units (Calico Onwards)(Thickness) (with Inferred).xls"). When all available data are considered, except data for borehole J-13, which is removed from the area of interest, a V_S value of 5611 ft/sec is determined for the Calico Hills Formation and 6128 ft/sec for the Prow Pass Tuff. As discussed in Section 5.1, these results form the basis for an assumption of a V_S of 5600 feet/sec for the Calico Hills Formation and a V_S of 6000 feet/sec for the Prow Pass Tuff.

The velocity data from different boreholes across the site were compared to evaluate the spatial variability of the mean V_S values across the site. Little difference in the mean V_S values was observed between the boreholes in the vicinity of the RB and SFA. Therefore, no distinction was made between the V_S values for the deeper units at the RB and SFA. However, the GFM was considered more appropriate to be used for the layer thickness at the RB than the geologic profiles from the boreholes. Therefore, the depths and thickness to the deeper units was based on those obtained from the GFM for all the survey locations for the RB (see Section 6.4.2.6.1, Figure 6.4.2-78) and on the boreholes for the SFA. Accordingly, the mean depths and mean thicknesses shown on Table 6.4-10 were used in the site response analysis.

Table 6.4-10. Depth and Thickness for the Deeper Units at the RB and SFA

Units	Depth to Top of Unit (feet)	Mean Thickness of Unit (feet)	Variation in Depth (feet)
Calico Hills (SFA)	1300	400	± 300
Prow Pass (SFA)	1700	N/A	± 300
Calico Hills (RB)	1100	400	± 300
Prow Pass (RB)	1500	N/A	± 300

6.4.2.5 SFA Velocity Profiles

Based on the velocity data described in Sections 6.4.2.4.1 and 6.4.2.4.3, base case V_S and V_P profiles required for input into the site-response model were developed for the SFA. The following subsections describe their development.

6.4.2.5.1 V_S Base Case Profiles

The velocity profiles obtained from the three techniques described in Section 6.4.2.4.1 at the SFA were reviewed. To evaluate potential differences in the V_S profiles across the SFA, their locations and the geologic logs of the fifteen boreholes were reviewed, which suggested certain patterns in the distribution of V_S profiles across the SFA (Figure 6.4.2-2). Accordingly, the SFA was subdivided into three areas: Northeast, South and Southwest of Exile Hill Fault splay as shown on Figure 6.4.2-2. Based on the geologic logs, an average geologic column for each of the three zones was developed as shown on Figure 6.4.2-27. It can be seen that from northwest to southeast along the Exile Hill fault splay, the lithology transitions from welded tuff on the southwest side and nonwelded on the northeast, then to nonwelded material on both sides. The welded and nonwelded (Tcprn and Tmbt1/Tpki tuff) were separated and this forms the basis for subdividing the SFA into three zones. The geologic columns for each zone (Figure 6.4.2-2) can be defined as follows:

***Northeast of Fault*:** The subsurface is characterized by the presence of bedded tuffs comprised of lithologic units Tmbt1, Tpki, and Tpbt5 between lithologic units Tpcrn and Qal.

South of Fault: The subsurface is characterized by the presence of bedded tuffs Tpki and Tpbt5 between lithologic units Tpcrn and Qal.

***Southwest of Fault*:** The subsurface is characterized by the absence of the bedded tuffs Tpki and Tpbt5. Tpcrn is directly below Qal layer.

The borehole velocity data and the SASW profiles included in each of the three zones are as follows:

Table 6.4-11. Velocity Measurements in the SFA Zones

Northeast of Fault	South of Fault	Southwest of Fault
RF17, RF19, RF22, RF29, SASW-3, SASW-15, SASW-16, SASW-19, SASW-30 (averaged with RF22) , SASW34+36 (averaged with RF17, NPF-3&9, NPF-10, NPF-12, NPF-18, NPF-19, NPF-20, NPF-21, NPF-22, NPF-23, NPF-24, NPF-25, NPF-26, NPF-27	RF13, RF14, RF16, RF18, RF20, RF23, RF26, SASW-1, SASW-4, SASW-14, SASW-20, SASW-21, SASW-22, SASW-29, SASW-32, SASW-33, SASW-35, NPF-2&14, NPF-16, NPF-17	RF15, RF21, RF24, RF25, RF28, SASW-2, SASW-5, SASW-6, SASW-7, SASW-8, SASW-9, SASW-10, SASW-11, SASW-12, SASW-13, SASW-17, SASW-18, SASW-23, SASW-24, SASW-25, SASW-26, SASW-27, SASW-28, SASW-31, NPF-1, NPF-28

Figures 6.4.2-28 to 6.4.2-36 show the V_S profiles included in each of the three zones for each of the three techniques and the mean V_S profile for that zone and that technique. For downhole and suspension techniques, the V_S profile developed at each of the 15 borehole locations is shown. For SASW technique, the V_S profiles corresponding to about 40 SASW profiles developed in 2000-2001 and about 30 V_S profiles developed during 2004-2005 have been shown. Note that only the velocities for tuff units are shown. The alluvium V_S profiles were analyzed separately and are discussed later. It was observed that in the computation of the mean profile, a location bias was being introduced since at some sites, data from more than one technique were available. As an example, at borehole RF#23 measurements from all three techniques (downhole, suspension, SASW-32) are available whereas at borehole RF#20 measurements from two techniques (downhole and suspension) are available. Therefore, to average all the available V_S profiles in a given zone would introduce a bias to sites with more data. To address this issue, during the development of the base case Vs profiles, the velocity profiles from multiple techniques were averaged at a given location. The mean V_S profiles at all the sites within a zone were averaged to obtain a mean V_S profile for a given zone.

Mean V_S profiles (mean of all three techniques) were developed for each of the three zones and are also shown on Figures 6.4.2-28 to 6.4.2-36. Currently, no important-to-safety facilities are planned in the area described as Southwest of Exile Hill Fault splay. Therefore, this area was not analyzed further. Base case profiles were developed only for the zones Northeast and South of the Exile Hill fault splay.

Note that while developing the base case V_S profiles, the velocities corresponding to alluvium and tuff units were evaluated separately. (Velocities corresponding to fill were not considered.) Figure 6.4.2-37 shows the average V_S profile computed for tuff units for the zone Northeast and South of the Exile Hill fault splay using all three measurement techniques. Figure 6.4.2-37 also illustrates that the number of profiles for the region South of Exile Hill fault splay decrease to one profile below a depth of 550 ft. Also, below a depth of 550 ft, is a low-velocity zone. It is likely that this low-velocity zone is not realistic and may be an artifact of the lack of measurements below this depth. To account for the uncertainty in velocities below a depth of 550 ft, two versions of the mean V_S profile developed for the South of Exile Hill fault were used. South of Fault Case A (Figure 6.4.2-38) gives more weight to the SASW data and follows a value of 4800 ft/sec below a depth of 550 ft till it reaches the Calico Hills Formation depth of 1300 ft where the profile velocity changes to 5600 ft/sec. South of Fault Case B (Figure 6.4.2-38) also gives more weight to the SASW data. For this case the profiles follows the mean SASW velocity profile at shallower depths (less than about 400 ft) and extrapolates along the

gradient the V_S values till they reach a V_S of 5600 ft/sec at a depth of 800 ft. From 800 ft to the base of the Calico Hills Formation at 1700 ft, the V_S values remain constant at 5600 ft/sec for South of Fault Case B. The development of a South of Fault Case C, also shown on Figure 6.4.2-38, will be discussed later.

The SASW measurements performed at the SFA far outnumber the downhole and suspension measurements made at the site. A comparison between the mean of the each of the three techniques would not be a fair comparison. In order to compare the three techniques employed at Yucca Mountain, the downhole, suspension and corresponding closest SASW measurement to each borehole were compared. Such a comparison has been performed for Yucca Mountain (Lin 2007 [DIRS 182739]). Since not every borehole had a SASW measurement nearby, only 12 of the boreholes were included in Lin (2007 [DIRS 182739]). The results of Lin (2007 [DIRS 182739]) indicate that, in general, the V_S measurements from the three techniques compare well.

Figure 6.4.2-39 compares the three techniques for the area Northeast of the Fault. Note that the mean profiles based on four downhole, four suspension and 17 SASW measurements are compared. The results for the three techniques are generally consistent, differing by less than about 1000 ft/sec. Thus a single base case velocity profile for tuff is developed for the Northeast of the Fault area. However, for the area South of Exile Hill fault splay, the mean V_S profiles obtained from the available downhole and suspension measurements are significantly higher than those obtained using SASW measurements below about 400 ft (Figure 6.4.2-40). While the means for the different techniques are based on few profiles at this depth, uncertainty in the velocity determined from the different techniques is incorporated into the site response modeling through the development of an additional base case (C) for the South of Exile Hill Fault Splay area. The South of Exile Hill Fault Splay Case C (Figure 6.4.2-38) was developed using the V_S data from downhole and suspension techniques only. As presented earlier, Figure 6.4.2-38 shows the three mean profiles developed for the zone south of Exile Hill Fault Splay: South of Fault Splay Case A, South of Fault Splay Case B and South of Fault Splay Case C. As discussed in Section 6.4.2.4.1, the downhole and suspension data were available only to a depth of about 550 ft. In the absence of data below 550 ft, a V_S value of 6000 ft/sec is used from a depth of 500 ft to the top of the Calico Hills Formation at a depth of 1300 ft and a V_S value of 5600 ft/sec to the top of the Prow Pass Tuff where the velocity increases back to 6000 ft/sec. An alternative profile, South of Fault Splay Case C1, follows the mean profile based on downhole and suspension velocity data to a V_S value of 5600 ft/sec at a depth of 450 ft. This profile maintains that velocity until the top of the Prow Pass Tuff where V_S increase to 6000 ft/sec. Note that South of Fault Splay Case C1 was not included in the base case profiles as it was not deemed to cause a significant change in the hazard obtained from the South of Fault Case C run.

In addition to the above cases, seven sensitivity cases (Table 6.4-12) were run by varying the depth to the Calico Hills by ± 500 ft, the thickness of Calico Hills by ± 200 ft and the velocity of Calico Hills by ± 500 ft/sec.

Whereas different base case velocity profiles were developed for the tuff units for the different zones, a single V_S profile was developed for alluvium as shown on Figure 6.4.2-42. The alluvium post-dates movement on the Exile Hill fault and its splays and so the alluvium should be the same material on either side of the fault. The similar V_S profiles for alluvium across the

fault as shown on Figure 6.4.2-43, supports this conclusion. The thickness of the alluvium, however, varies across the SFA.

An alluvium contour map developed for the SFA (SNL 2008 [DIRS 183779], Figure 6.2-4) was reviewed to determine the range of thicknesses of the alluvium layer in the different zones. The alluvium thickness ranges from 45 to 180 feet northeast of the Exile Hill fault splay and about 5 to 120 feet south of the fault. Accordingly, the analysis was performed for the following alluvium thicknesses

- Northeast of the Fault: 30 ft, 70 ft, 100 ft and 200 ft
- South of the Fault Case A: 30 ft, 70 and 100 ft
- South of the Fault Case B: 30 ft, 70 and 100 ft
- South of the Fault Case C: 30 ft, 70 and 100 ft

Differences in site response due to thickness variation of ± 20 ft are not significant and so mean thicknesses of 30, 70, and 100 ft were used. A value of 200 ft was added to northeast of the fault cases to cover thicknesses up to 180 ft.

The mean V_S profiles developed for alluvium, tuffs of the Timber Mountain and Paintbrush Groups, the Calico Hills Formation and the Prow Pass Tuff were combined for various alluvium thicknesses and different velocity zones across the SFA to obtain the final base case profiles and sensitivity cases shown on Tables 6.4-12 and 6.4-13. The thirteen base cases used in the site response analyses are shown on Figures 6.4.2-44 to 6.4.2-56. For the remaining seven sensitivity runs shown on Table 6.4-12, an alluvium depth of 100 ft was used.

Table 6.4-12. SFA Sensitivity Cases

Sensitivity Case Number	Sensitivity Case Velocity Profile Name()	Alluvial Depth (ft)	Calico Hills Depth (ft), Velocity (ft/sec) and Thickness (ft)	Velocity Data Used for the Development of V_S Profiles for Tuff Overlying the Calico Hills Formation*
1‡	South of the Fault Case A1	100	800, 5600, 400	Downhole, suspension and SASW data south of fault
2‡	South of the Fault Case A2	100	1800, 5600, 400	Downhole, suspension and SASW data south of fault
3‡	South of the Fault Case A3	100	1300, 5600, 600	Downhole, suspension and SASW data south of fault
4‡	South of the Fault Case A4	100	1300, 5600, 200	Downhole, suspension and SASW data south of fault
5‡	South of the Fault Case A5	100	1300, 5100, 400	Downhole, suspension and SASW data south of fault
6‡	South of the Fault Case A6	100	1300, 6100, 400	Downhole, suspension and SASW data south of fault
7†	South of the Fault Case A7	100	1300, 5600, 400	Downhole, suspension and SASW data south of fault

Notes: ‡ Velocity, depth to and thickness of the Calico Hills are each varied in these sensitivity studies (see bold number for item varied).
† Velocity of alluvium is shifted upwards by 5 ft so lowest velocity layer has been removed from the profile.
* As discussed in the text, downhole and suspension data extend to at most about 500 to 550 ft for the South of the Fault area; two SASW profiles extend below this depth to about 1100 ft.

Table 6.4-13. SFA Base Cases

Base Case Number	Base Case Velocity Profile Name	Alluvial Depth (ft)	Calico Hills Depth (ft), Velocity (ft/sec) and Thickness (ft)	Velocity Data Used for the Development of V_S Profiles for Tuff Overlying the Calico Hills Formation*
1	NE Fault	30	1300, 5600, 400	Downhole, suspension and SASW data northeast of fault
2	NE Fault	70	1300, 5600, 400	Downhole, suspension and SASW data northeast of fault
3	NE Fault	100	1300, 5600, 400	Downhole, suspension and SASW data northeast of fault
4	NE Fault	200	1300, 5600, 400	Downhole, suspension and SASW data northeast of fault
5	South of Fault Case A	30	1300, 5600, 400	Downhole, suspension and SASW data south of fault
6	South of Fault Case A	70	1300, 5600, 400	Downhole, suspension and SASW data south of fault
7	South of Fault Case A	100	1300, 5600, 400	Downhole, suspension and SASW data south of fault
8	South of Fault Case B	30	1300, 5600, 400	Downhole, suspension and SASW data south of fault
9	South of Fault Case B	70	1300, 5600, 400	Downhole, suspension and SASW data south of fault
10	South of Fault Case B	100	1300, 5600, 400	Downhole, suspension and SASW data south of fault
11	South of Fault Case C	30	1300, 5600, 400	Downhole and suspension data south of fault
12	South of Fault Case C	70	1300, 5600, 400	Downhole and suspension data south of fault
13	South of Fault Case C	100	1300, 5600, 400	Downhole and suspension data south of fault

Notes:

* As discussed in the text, downhole and suspension data extend to at most about 500 to 550 ft for the South of the Fault area; two SASW profiles extend below this depth to about 1100 ft. For the Northeast of the Fault area, downhole and suspension data extend to at most about 650 ft; 9 SASW profiles extend below this depth with two reaching about 1300 ft

6.4.2.5.2 Poisson's Ratios

The Poisson's ratios for the tuff units were developed for use in calculating V_P profiles based on the base case V_S profiles. For the upper about 600 ft, the downhole and suspension data in the 15 boreholes drilled in the SFA region in 2000 and 2001 were used. These measurements were used to compute the Poisson's ratios for each of the 15 boreholes, which were then averaged (arithmetic mean). Separate Poisson's ratios were computed for the different zones on either side of Exile Hill fault splay. The resulting Poisson's ratio profiles were then smoothed and, based on VSP data, extrapolated to greater depths. The VSP data indicated an almost constant Poisson's ratio with depth (BSC 2004 [DIRS 170027], Figure 6.2-117) (Figures 6.4.2-57 and 6.4.2-58). Another set of Poisson's ratios was also calculated using data from all the 15 boreholes together. This profile was also smoothed and also extrapolated to greater depths

(Figure 6.4.2-59). V_P profiles corresponding to the different V_S profiles were calculated using both sets of Poisson's ratios (different ratios across the Exile Hill fault splay, called version 1, and same ratios across the Exile Hill fault splay, called version 2) (Figures 6.4.2-60 to 6.4.2-62). The difference in the calculated V_P profiles was about 10%, which was not considered significant enough to use different Poisson's ratios for the two zones across the fault. Therefore, the smoothed and extrapolated Poisson's ratios, based on the data from all 15 boreholes, were used for the development of the V_P profiles. For tuff, a Poisson's ratio of 0.29 was used to a depth of 1300 ft.

Below 1300 ft, for the Calico Hills Formation and the Prow Pass Tuff, a Poisson's ratio of 0.25 was used. This value of Poisson's ratio was obtained using the measured V_S and V_P values obtained from the 11 USGS boreholes discussed in Section 6.4.2.4.3. A Poisson's ratio of 0.30 was used in Section 6.4.2.4.3 to calculate inferred sonic V_S profiles from the sonic V_P profiles for depths at which only V_P data were available. These data were used to calculate average V_S for the Calico Hills Formation and Prow Pass Tuff. The value of 0.30 should have been used to calculate the base case V_P profiles for the Calico Hills Formation and Prow Pass Tuff for consistency. The Poisson's ratio of 0.30 is considered more reliable for these units than 0.25 because it is based on the VSP data within the RB. Sensitivity calculations show that the difference in base case V_P profiles has a insignificant difference in the modeled site response.

The Poisson's ratios for alluvium were calculated using the downhole velocity data for the 15 boreholes. This was done because the top 100 feet of the suspension data, which corresponds to the maximum depth of alluvium in the boreholes, were excluded from the study. This is consistent with what was done in the 2004 study (BSC 2004 [DIRS 170027]). Again, based on the same rationale used for development of V_S profiles for alluvium as discussed in Section 6.4.2.4.1, Poisson's ratios for alluvium were calculated using all the 15 boreholes and no distinction was made between the data collected Northeast and South/Southwest of the Exile Hill fault splay. For alluvium, depth-dependent Poisson's ratios as shown on Figure 6.4.2-63 were used.

6.4.2.5.3 V_P Base Case Profiles

The V_P base case profiles were developed from the V_S base case profiles using the Poisson's ratios developed in Section 6.4.2.5.2.

As for the V_S profiles, the average V_P profiles developed for alluvium, tuffs of the Timber Mountain and Paintbrush Groups, the Calico Hills Formation, and the Prow Pass Tuff were combined for various alluvium thicknesses and different velocity zones across the SFA to obtain the final thirteen V_P base case profiles corresponding to the thirteen base case V_S profiles. Note that V_P profiles were not developed for the sensitivity cases shown on Table 6.4-13. The thirteen base case V_P profiles used in the site response analyses are shown on Figures 6.4.2-64 to 6.4.2-76.

6.4.2.6 RB Velocity Profiles

Based on the velocity data described in Sections 6.4.2.2, 6.4.2.4.2, 6.4.2.4.3, and 6.4.2.5.2, base case V_S and V_P profiles required for input into the site-response model were developed for the RB. The following subsections describe their development.

6.4.2.6.1 V_S Base Case Profiles

In order to develop V_S base case profiles for the RB, the 21 velocity profiles from the 2004-2005 data presented in Section 6.4.2.4.2 were used together with the 2000-2001 SASW profiles described in Section 6.4.2.2. Figure 6.4.2-77 shows all the SASW profiles available in the vicinity of the RB collected during the 2000-2001 and 2004-2005 field investigations.

Due to the large variability in the V_S values on Figure 6.4.2-77, the V_S profiles at individual locations were examined to see if there was a spatial component to this. It was observed that the V_S profiles showing higher velocities at depths ranging from about 600 ft to 1000 ft (e.g., YM-8, YM-10, YM-12, YM-13, YM-14A, YM-14B, YM-21, and YM-15B) tend to cluster spatially. We have termed these sites as "stiff" sites. The remaining V_S profiles which do not show this increase were termed the "soft" profiles and the locations where these soft V_S profiles were measured were termed the "soft" sites (see following discussion).

To analyze this observation, the lithostratigraphic structure of the mountain was examined further. Geologic cross-sections at each of the SASW locations obtained from the GFM (DTN MO0012MWDGFM02.002 [DIRS 153777]) were reviewed to evaluate whether they could be grouped based on similarities in the occurrence of the various lithostratigraphic units and their thicknesses. Based on our review, it was concluded that the RB could be subdivided into four zones based on similarities in lithology. Figure 6.4.2-78 shows the average geologic columns for each of the four zones developed based on the output from the GFM.

The four zones and the SASW profiles that are included in each of the four zones are shown on Figure 6.4.2-3 and Table 6.4-14. In addition to the valley sites, which are located in the central stiff zone, the other zones are termed "soft" zones.

Table 6.4-14. Four Velocity Zones Developed For the RB

Zone	SASW Profiles Included
Northern Soft Zone	YM-5, YM-6 and YM-17
Central Soft Zone	YM-1, YM-2, S-7, S-8, S-9, S-10, D-9, D-10, CYM-1 and CYM-3
Southern Soft Zone	YM-3, YM-4, YM-19, S-1, S-2, S-3, S-4, S-5, S-6, S-11, S-12, CYM-5, CYM-6, CYM-7, D-5, D-6, D-7 and D-8.
Central Stiff Zone	YM-8, YM-10, YM-12, YM-13, YM-14A, YM-14B, YM-23, D-1, D-2 and D-3

Figure 6.4.2-79 shows the mean V_S profiles for the three soft zones (northern, central, and southern). The mean profiles were calculated by averaging the V_S profiles for the SASW surveys in each zone. Figure 6.4.2-79 also shows the mean of the three soft zones based on: (1)

computing the mean of each zone and (2) averaging over all SASW velocity profiles. As shown on Figure 6.4.2-79, the two soft zone means are very similar. In order to avoid a bias towards a zone that had more V_S measurements, it was decided to use the mean V_S profile based on the three zone means as the base case V_S profile for the soft zones. To evaluate the sensitivity of the ground motions to the base case velocity profiles, the northern and southern soft zones were used in sensitivity runs (Section 6.5.4.5). To accommodate the variability in tuff V_S data, two base case profiles as shown on Figure 6.4.2-80 were developed for use as input to the site response model as discussed below. One base case represents the soft zones and the second the central stiff zone.

Figures 6.4.2-81 to 6.4.2-83 show the individual SASW profiles that were included in the calculations of the means for each of the three soft zones. Also shown on Figures 6.4.2-81 and 6.4.2-83 for comparison purposes are the V_S profile from VSP measurements at boreholes G-2 and WT-2 (BSC 2004 [DIRS 170027]; Figure 6.4.2-5) within the northern and the southern soft zones, respectively. The comparison indicates that, in general, for the soft zones the VSP measurements yield higher velocity values than the SASW technique.

Figure 6.4.2-84 illustrates the stiff V_S profiles that were included in development of the base case profile for the stiff zone. Note that YM23 is an outlier for the central stiff zone because it resembles a soft profile. The dispersion curve corresponding to YM-23 (SNL 2008 [DIRS 183779], Figures V-65 and V-66) was reviewed and based on the relatively poor fit was downweighted to 50% below a depth of 500 feet and not included in the mean calculations below a depth of 950 feet (when the other velocity profiles from the other measurements drop out). YM-8 was also found to be an outlier for the central stiff zone because of the very large increase in V_S at a depth of about 560 ft (Figure 6.4.2-84). However, the dispersion curve for YM-8 (SNL 2008 [DIRS 183779], Figures V-20 and V-21) was found to be satisfactory and it was retained in the computations. Also shown on Figure 6.4.2-84 for comparison is the V_S profile from VSP measurement at borehole NRG-6 within the central stiff zone. This comparison shows that the VSP-based V_S values are lower than those obtained by the SASW technique for the central stiff zone. The inconsistency between the V_S profiles from the VSP and the SASW techniques for the soft and the stiff zones is currently unexplained. However, as base case velocity profiles for both the soft and stiff zones are included in site response modeling, the uncertainties are accommodated in the final ground motions.

Figures 6.4.2-81 through 6.4.2-83 also show the comparison of the surface-based V_S measurements to the mean V_S values obtained for the specific Topopah Spring Tuff units in the ESF and ECRB cross-drift tunnels (SNL 2008 [DIRS 183779], Section 6.4.5). The SASW measurements described in Table 6.4-15 were separated into hard and soft measurements based on their occurrence in either of the four zones as summarized in Table 6.4-14.

Table 6.4-15. SASW Surveys in the ECRB and ESF Tunnels Used for Comparison to Surface-Based SASW Velocity Profiles

Lithostratigraphic Units	Soft Zones	Central Stiff Zone
Tptpul	ESF-2	ECRB_4-09+10 Profile 1, ECRB_4-09+10 Profile 2, ECRB_5-06+59, ESF-12, ESF-13

Tptpmn	ECRB_3-12+20 Profile 1, ECRB_3-12+20 Profile 2, ESF-3, ESF-7, ESF-8 Profile 1, ESF-8 Profile 2, ESF-9 Profile 1, ESF-9 Profile 2, ESF-10	ESF-11
Tptpll	ESF-5, ESF-6, ECRB-1, ECRB-2	

The tunnel measurements in Tptpmn were found to be consistently higher than the SASW measurements from the surface (Figures 6.4.2-81 to 6.4.2-84). This can be explained on the basis of sampling bias. In the tunnel, an equal number of test locations had been selected in the high fracture and the low fracture zones. However, in the field the volume of high fracture material may be more than the low fracture material. The tunnel measurements for the other two units, Tptpul and Tptpll agree well with the SASW from the surface (Figures 6.4.2-81 to 6.4.2-84).

Figure 6.4.2-85 shows the final base case (#1) used for the soft zones, which is a smoothed version of the mean soft profile for all the 33 soft V_S profiles shown on Figure 6.4.2-79. Note that base case #1 hits the assumed Calico Hills Formation V_S of 5600 ft/sec at a depth of 1300 ft and the Prow Pass Tuff (Point A) velocity of 6000 ft/sec at 1700 ft depth. Base case #2 developed for the central stiff zone is shown on Figure 6.4.2-86. Base case #2 was developed using the mean V_S profile developed for the central stiff zone as shown on Figure 6.4.2-80.

In addition to the two base cases discussed above, three sensitivity cases were developed for the RB. Ultimately these sensitivity cases were not run because base case runs showed that ground motions are not sensitive to the different profiles. The sensitivity case profiles are described here, however, for completeness. As shown earlier on Figure 6.4.2-79, the maximum difference between the mean soft profile for all 33 V_S profiles (base case 1) and each of the mean profiles developed for the northern and the southern soft zones is about 600 ft/sec. To investigate the impact of this difference on site response and ground motion, two sensitivity cases were developed using the mean profile for the northern soft and southern soft zones shown on Figure 6.4.2-79. Figures 6.4.2-87 and 6.4.2-88 show the two sensitivity cases for the soft zones based on the average V_S profile for the northern soft and southern soft zones.

The third sensitivity case was developed for the stiff zone. As shown earlier on Figure 6.4.2-84, the mean V_S profile increases to 6800 ft/sec between 750 ft and 800 ft. At 995 ft depth, there is only one V_S profile, which results in a reduction in the V_S profile. To incorporate the uncertainty in the V_S measurements below this depth, it was decided to develop one sensitivity profile for the central stiff zone in addition to the base case (base case #2) discussed above. As mentioned earlier, the profile with a V_S value of 6800 feet/sec extending all the way from a depth of 995 ft to 1300 ft (Calico Hills Formation depth) was selected as the base case profile for the central stiff zone (#2) and is shown on Figure 6.4.2-86. The V_S profile for the central stiff zone with V_S truncated to 5600 feet/sec below 995 feet to the top of Calico Hills Formation at 1300 ft was selected as a sensitivity case as shown on Figure 6.4.2-89. All the above mentioned base cases and sensitivity cases reach the Calico Hills Formation velocity of 5600 ft/sec at 1100 ft depth and the Prow Pass Tuff (Point A) velocity of 6000 ft/sec at 1500 ft depth.

To summarize, Figures 6.4.2-85 to 6.4.2-89 show the two base cases and the three sensitivity cases developed for the RB. Inspection of the sensitivity cases and their potential effect on site

response resulted in only the RB base case profiles being used in the site response analysis. As shown on these figures, the original mean V_S profiles were smoothed to arrive at the base case or the sensitivity case profiles. Note that these V_S profiles were developed for tuff primarily of the Paintbrush Group and were combined with the assumed Calico Hills Formation and the Prow Pass Tuff velocities as discussed in Section 6.4.2.3.3 at the appropriate depths.

Tables 6.4-16 and 6.4-17 shows the different base case and sensitivity profiles used for the site response analysis of the RB, respectively.

Table 6.4-16. RB Base Case Profiles

Base Case Velocity Profile Name(Base Case Number)	Calico Hills Formation Depth (ft), Velocity (ft/sec) and Thickness (ft)	Velocity Data Used for the Development of V_S Profiles for Tuffs of the Paintbrush Group
Average Soft Zone (#1)	1100, 5600, 400	SASW profiles in all the three soft zones
Central Stiff Zone (#2)	1100, 5600, 400	SASW profiles in the central stiff zone

Table 6.4-17. RB Sensitivity Case Profiles

Sensitivity Case Velocity Profile Name(Sensitivity Case Number)	Material Models Run	Calico Hills Formation Depth (ft), Velocity (ft/sec) and Thickness (ft)	Velocity Data Used for the Development of V_S Profiles for Tuffs of the Paintbrush Group
Northern Soft Zone (#1)	UMT, LMT	1100, 5600, 400	SASW profiles in the northern soft zone
Southern Soft Zone (#2)	UMT, LMT	1100, 5600, 400	SASW profiles in the southern soft zone
Central Stiff Zone (#3)[†]	UMT, LMT	1100, 5600, 400	SASW profiles in the central stiff zone

[†] Tuff velocities truncated to 5600 ft/sec below 995 ft to 1300 ft.

Although the VSP measurements were not included in the base case calculations, a comparison of the base case profiles and the VSP measurements as shown on Figure 6.4.2-90 illustrates that the two are in good agreement given the large spatial variability across the RB. This comparison was performed as an independent verification of the base case V_S profiles used as an input in the site response analysis.

6.4.2.6.2 Vp Base Case Profiles

V_P profiles for the RB tuff were estimated using the Vs profiles described in Section 6.4.2.4.1 and the Poisson's ratios computed for the RB. Previously, Poisson's ratios were taken to decrease linearly from 0.33 at the surface to 0.30 at a depth of 250 ft and held constant at 0.30 at depths below 250 ft (Section 6.2.3.3, BSC 2004 [DIRS 170027]). These Poisson's ratios were also used in the current analysis. However, instead of a linearly decreasing Poisson's ratio in the upper 250 ft of the material, a constant Poisson's ratio on 0.30, was used throughout the tuff

units in the RB. The base case V_P profiles corresponding to the two base case Vs profiles are shown on Figures 6.4.2-91 and 6.4.2-92.

6.4.2.7 Depth to the Reference Rock Outcrop Conditions and Comparison of the 2004 and Current Base Case V_S Profiles

The PSHA reference rock outcrop V_S, which determines the depth of the control motion input to the site response model, was defined as 1900 m/sec (approximately 6000 ft/sec). Based on available data in 2002, the depth at which this velocity was obtained beneath the RB was determined to be 1100 ft (Figure 6.4.2-93; BSC 2004 [DIRS 170027], Figure 6.2-116). At the SFA, available data led to identification of the reference rock outcrop V_S at a depth of 500 ft (Figure 6.4.2-94; BSC 2004 [DIRS 170027], Figure 6.2-119). Recognizing that the depth to the reference rock outcrop V_S varied spatially, for site response modeling it was randomly varied from 700 to 1500 ft for the RB and from 400 to 600 ft for the SFA (BSC 2004 [DIRS 170027], Section 6.2.3.5).

Based on data available in October 2006, the depth at which the reference rock outcrop V_S is obtained has been revised. It is now associated with the Prow Pass Tuff formation. Using the GFM, the upper contact of the Prow Pass Tuff is taken at 1500 ft for RB base case profiles and 1700 ft for the SFA base case profiles (Section 6.4.2.4.3).

The current availability of additional SASW-based velocity profiles that extend to greater depth than those from 2000-2001 and that provide greater spatial coverage of the waste emplacement footprint have reduced uncertainty in characterization of V_S for the repository block. Whereas in BSC (2004 [DIRS 170027], Section 6.2.3) differences in velocity profiles based on SASW and VSP data were treated as epistemic uncertainty, the available data now support an interpretation that the velocity of the RB varies spatially. Thus to develop site-specific ground motions that apply to the entire RB, site response modeling is carried out for two base case profiles and the results are enveloped (Section 6.5.3).

Comparison of the RB base case profiles from BSC (2004 [DIRS 170027], Section 6.2.3.3.1) and those determined in this analysis shows similarities and differences. The base case #1 profiles agree fairly well with each other. Both show a rapid increase in velocity in the upper 50 ft and then a gradual increase to a depth of about 700 ft. From 700 to 1100 ft, the 2004 base case #1 profile used a linear increase in velocity between the velocities interpreted from surface-based SASW measurements at 700 ft to the value determined at about 1100 ft from subsurface-based SASW measurements in the ESF (Figure 6.4.2-93). Sensitivity analyses determined that site response was not sensitive to alternate velocity interpretations over this depth range (BSC 2004 [DIRS 170027], Section 6.2.3.3.1). For this analysis, additional surface-based SASW data allow velocity interpretations to greater depths (Section 6.4.2.4.2) and the base case #1 profile is based on these interpretations. The surface-based measurements are corroborated by subsurface-based measurements covering a wider range of units than in the 2004 study (Section 6.4.2.4.2).

Comparison of base case #2 profiles from BSC (2004 [DIRS 170027], Section 6.2.3.3.1) and this analysis shows significant differences. For the 2004 study, the base case #2 profile was based on VSP data from areas in and near the RB for which SASW data were not available. These data suggested that a profile with higher velocities characterized the RB. Additional SASW data

gathered since 2001 have clarified that the higher velocities do not represent epistemic uncertainty, but rather that different velocity profiles characterize different areas of the RB. The currently available data indicate a moderate rate of increase in velocity from about 1000 ft/sec at the surface to about 7400 ft/sec at a depth of 750 ft. This contrasts with a more gradual increase based on the VSP data in the 2004 study (Figure 6.4.2-93). In the current analysis, the VSP data are not included because SASW data are now available and are considered more reliable.

In 2004, there was a single base case tuff V_S profile for the SFA south of Exile Hill fault splay, which went to a depth of 500 ft because the available data indicated that a V_S of 1900 ft/sec was reached at that depth (BSC 2004 [DIRS 170027], Section 6.2.3.4; Figure 6.4.2-94). In the current analyses, which incorporates additional SASW-based profiles that are interpreted to depths of about 500 to over 1000 ft, there are three base case tuff V_S profiles that represent the epistemic uncertainty in the V_S profile at depths greater than 500 ft and at shallower depths related to differences in the data acquired using different measurement techniques (SASW, downhole, and suspension). The current base case tuff V_S profiles are similar to the 2004 base case profiles at least to a depth of 400 ft with base case C resembling the 2004 base case to 500 ft depth. An additional tuff Vs profile has now also been included in site response modeling to represent the SFA northeast of the Exile Hill fault splay (Figure 6.4.2-94) where important-to-safety facilities are now planned.

6.4.2.8 Correlation Between Velocity and Lithology

As part of the current study, we also evaluated the possible correlation between velocities obtained from the various field investigations and the lithologic units at the site. The various velocity profiles and the idealized geologic columns developed as part of this study were examined and analyzed visually to see any trends that would demonstrate dependence of the velocity values observed in the field to the corresponding lithologic unit. Based on our review, we concluded that correlation between velocity and lithostratigraphic unit can be observed on a location-specific basis but not on an areal-basis. We also observed that the within-unit variation in velocity was at least as much as, if not more than, the between-unit variation. Therefore, assignment of lithologic unit-specific velocity values to the tuff layers underlying the site would be subject to significant uncertainty.

6.4.2.9 Treatment of Uncertainty and Variability in Velocity Profiles

Development of velocity profiles and their use in site response modeling take into account uncertainty and variability. Uncertainty (epistemic uncertainty) results when available knowledge allows multiple interpretations of a mean base case profile. To incorporate this uncertainty, alternative base case profiles are developed and used in site response modeling. The site response results are then used to develop alternative site-specific hazard curves that are combined in a weighted average according to the weight assigned to each alternative profile based on its support in the data.

Two types of variability are included in developing site-specific ground motions: deterministic and random. Deterministic variability also refers to the situation in which base case properties are known to vary spatially in a deterministic manner. Examples at Yucca Mountain are the depth of alluvium at the SFA, the different velocity profiles across the Exile Hill fault splay, and

the "soft" and "stiff" velocity profiles at the RB. Velocity profiles are developed to represent this variability and used in site response modeling. For example, at the SFA velocity profiles with alluvium thickness of 30 ft, 70 ft, and 100 ft are used for the south of Exile Hill fault splay region. For the northeast of Exile Hill fault splay region an additional alluvium thickness of 200 ft is modeled. Because the objective at Yucca Mountain is to determine a single set of ground motions each for the RB and SFA, variability in ground motion results deriving from deterministic variability in velocity profiles is enveloped over, not averaged.

Random variability (aleatory variability) also occurs at Yucca Mountain. Random variability refers to the stochastic variation in velocity across the site that cannot be reduced by additional data collection. Random variability in velocity is accommodated by using the base case V_S profiles, along with information on the observed randomness in velocity at the site, to synthesize a suite of 60 random velocity profiles that have similar overall statistics as the observed data. This is accomplished using the software program RANPAR V2.2 (Software Tracking Number RASCAL SET V1.1 11232-1.1-00) (RASCAL SET 2007 [DIRS 184053]). Corresponding random V_P profiles are determined using the random V_S profiles and the Poisson's ratio as a function of depth associated with the base case velocity profile being used. The randomization process involves velocity, layer thickness, and the depth of the profile. For velocity and layer thickness, results of a probabilistic representation of velocity profiles at the site are implemented in RANPAR V2.2. For each base case velocity profile, 60 model runs are performed, one for each random profile, and the geometric mean of the resulting amplification factors are calculated along with its associated sigma.

For repository depth, a uniform distribution varying from 800 to 1400 ft is used. This distribution is based on an analysis of overburden thickness that subtracted the waste emplacement area elevation (BSC 2004 [DIRS 172801]) from the topography (MO0012MWDGFM02.002 [DIRS 153777]) using EarthVision 5.1 (EarthVision 2000 [DIRS 167994]). This range also reflects uncertainty in the depth at which reference rock conditions (i.e., S-wave velocity of about 1900 m/sec) are obtained. For the SFA the overall depth of the profile is varied from 1000 to 1600 ft to reflect uncertainty in the depth of reference rock conditions. A uniform distribution is again used.

6.4.2.10 Probabilistic Velocity Correlation Approach

In incorporating aleatory variability in site response modeling, probabilistically-based velocity correlation approach was used to generate 60 random synthetic velocity profiles, which in turn were used as inputs for the site response model. These synthetic profiles are statistically similar to the observed profiles. The development of this probabilistic representation of velocity profiles for the RB and SFA is described in BSC (2004 [DIRS 170027], Section 6.2.3.6) and implemented in the RASCAL SET (STN 11232-1.0-00 [DIRS 182468], STN 11232-1.1-00 [DIRS 184053]) module RANPAR. This representation considers both the variability among profiles in each area and the variability in velocity with depth within a given profile.

The velocity correlation approach consists of three elements. The first element consists of a probabilistic description of velocity layer thicknesses for the ensemble of profiles. The second element is the median velocity profile. Although each profile consists of discrete constant-velocity layers, the median profile is smooth as if the layer boundaries are randomly located.

The third element is a probabilistic description of the deviations of the velocity at the mid-point of each layer from the median and its correlation with the velocity in the layer above. The standard deviations associated with the median profiles are taken as similar to those of the 2004 values. Details of these formulations are described in BSC (2004 [DIRS 170027], Section 6.2.3.6). (As stated, the probabilistic approach requires use of a median velocity profile. In these analyses, arithmetic mean velocity profiles were developed. The impact on the site response calculations was evaluated to assess the difference between using median versus mean velocity profiles. The impact was less than 5% and deemed not significant.)

Tables 6.4-18 and 6.4-19 list the correlation parameters for V_S and layer thickness, respectively, for both the RB and the SFA. The top seven entries in these tables indicate the values of the logarithmic σ at various control depths. Subsequent entries indicate the values of the parameters that control the correlation coefficient ρ and the rate of layer boundaries

The analysis of velocities also estimates median velocity profiles for both locations, but these values are not used in the development of amplification factors. These median velocity profiles, however, are compared to the base case profile to assure an unbiased statistical sampling of velocity profiles is used in the analysis.

Table 6.4-18. Parameters of the Probabilistic Representation of Velocity Profiles for the RB

Quantity	Value	Units
σ (0 m)	0.364	None
σ (10 m)	0.364	None
σ (60 m)	0.198	None
σ (100 m)	0.198	None
σ (101 m)	0.198	None
σ (102 m)	0.198	None
σ (366 m)	0.198	None
ρ_0	0.8	None
Δ	6	M
ρ_{200}	0.6	None
h_0	0.01	M
b	0.3	None
c_1	1.051	M
c_2	0.9601	None
c_3	1.0999	m^{c2-1}
h_c	0.001	M

Quantity	Value	Units
COV(τ)	0.79	None

Source: DTN: MO0208VCPRBWHB.000 [DIRS 163801]

Table 6.4-19. Parameters of the Probabilistic Representation of Velocity Profiles for the SFA

Quantity	Value	Units
σ(0 m)	0.331	None
σ(5 m)	0.331	None
σ(10 m)	0.181	None
σ(10.01 m)	0.181	None
σ(10.02 m)	0.181	None
σ(10.02 m)	0.181	None
σ(366 m)	0.181	None
ρ_0	0.95	None
Δ	6	m^{c2-1}
ρ_{200}	0.6	None
h_0	0.01	M
b	0.15	None
c_1	1.051	M
c_2	0.9601	None
c_3	1.0999	m^{c2-1}
h_c	0.001	M
COV(τ)	0.62	None

Source: DTN: MO0208VCPRBWHB.000 [DIRS 163801]

Examples of the randomized profiles, in this case, for the V_S base case #1 profile for the RB and the V_S base case #2 (northeast of the Exile Hill fault splay, 30 ft of alluvium) profile for the SFA are shown on Figures 6.4.2-95 and 6.4.2-96, respectively.

6.4.3 Densities

Densities are required input in the site response modeling but the resulting ground motions have a negligible sensitivity to the parameter since they vary little throughout the profiles. Assumed densities for alluvium, tuff of the Timber Mountain and Paintbrush Canyon Groups, and tuff of the Calico Hills Formation and Prow Pass Tuff are presented and discussed in Section 5.6. Values used are 1.8 g/cm^3 (112 pcf), 2.2 g/cm^3 (137 pcf), 2.4 g/cm^3 (150 pcf), respectively.

6.4.4 Characterization of Nonlinear Dynamic Material Properties

The development of nonlinear dynamic material properties for input into the site response analyses is presented in this section. Shear modulus reduction and damping curves are required for each horizontal layer represented in the site profile. The curves were developed for both tuff (Section 6.4.4.2) and alluvium (Section 6.4.4.3) by the Project Team, experts in ground motion analyses and geotechnical engineering. As described in BSC (2004 [DIRS 170027], Section 6.2.4), the curves were developed by the Project Team based on the available laboratory test data and relevant current research on similar materials as described below.

To represent epistemic uncertainty, alternate mean G/G_{max} and hysteretic damping curves were developed for both the desert alluvium and tuff units. Because neither the tuff nor desert alluvium can be sampled and tested in a manner which unambiguously reflects *in-situ* conditions, multiple base cases were considered necessary to adequately characterize the large epistemic uncertainty in nonlinear dynamic material properties. For the alluvium, which consists primarily of poorly sorted gravels and cobbles with highly variable degrees of cementation, sampling and testing of undisturbed samples are problematic. Results of such testing are currently unavailable. Similarly with the tuff units, because large-scale fracture systems as well as voids (lithophysae) are present to varying degrees throughout the units, obtaining and testing samples of sufficient size to accommodate the fracture systems is extremely difficult. Additionally, and more importantly, testing under *in-situ* confinement levels, and with the proper combined static and dynamic stress states, is not possible with currently available equipment.

The following sections document the development of the G/G_{max} and hysteretic damping curves for both alluvium and tuff. The curves were originally developed in 2004 (BSC 2004 [DIRS 170024], Section 6.2.4) and are updated for the current analysis. The update involves both alluvium and tuff curves and includes accommodating effects of confining pressure. The adjustment is based on comparing more typical materials (soft rock and soils) amenable to laboratory dynamic testing with the curves for more typical material confirmed through modeling recorded motions (Silva et al. 1996 [DIRS 110474]). Because the earlier development of ground motion inputs (BSC 2004 [DIRS 170027]) involved enveloping motions over site epistemic uncertainty, as a semi-deterministic conservative approach (Approach 2B) was used (BSC 2004 [DIRS 170024], Section 6.3.1.1), accommodation of confining pressure effects on the tuff curves would not have increased final motions. This is the case as the LMT curves, which would have the largest impact of potential confining pressure effects, control the low frequency envelope, likely resulting in lower motions. The UMT curves are quite linear and would have confining pressure effects only at greater depths, beyond about 500 ft, where the shear-wave velocities are those of firm rock (at or above 5000 ft/sec). However, in the development of design motions, which are intended to be hazard consistent and preserve the

exceedance frequencies of the reference rock hazard (Section 6.4.1), site epistemic uncertainty must be accommodated with relative weights over hazard curves computed for each base-case suite of properties. As a result, a more accurate representation of nonlinear dynamic material strain dependencies, including potential depth dependencies, is required to avoid unintentional bias in the resulting hazard. Fundamentally, a fully probabilistic seismic hazard analysis compared to a deterministic analysis necessitates more rigor in assessing all factors which contribute to strong ground motions: source, path, and site effects.

Further updates to the alluvium curves reflect trends observed in recent dynamic testing on cemented sands. Development of the original suite of curves (BSC 2004 [DIRS 170024], Section 6.2.4) and the recent updates are discussed in the following sections. As previously discussed, to achieve hazard consistent motions, hazard curves developed for each component of site epistemic uncertainty are given weights based on engineering judgment, which reflect relative confidence of expected *in-situ* behavior. Relative weights are discussed in Section 6.4.5.

6.4.4.1 Inputs for Development of Nonlinear Dynamic Material Properties

Development of shear modulus reduction and material damping curves is based in part on dynamic laboratory testing of tuff and alluvium taken from boreholes at the SFA and the North Portal area of the ESF. The dynamic testing consisted mainly of resonant column and torsional shear testing of specimens. This testing is described in BSC (2002 [DIRS 157829], Sections 6.2.10, 6.3.3, and 6.5.3). Two series of tests were performed. In 1999, dynamic laboratory testing was performed on six intact tuff specimens and four reconstituted alluvium specimens from RF#13. In 2000, dynamic laboratory testing was performed on 18 intact tuff specimens from RF#14, RF#15, RF#16, and RF#17, five intact tuff specimens from the North Portal area, and one reconstituted alluvial specimen from RF#17. Table 6.4-21 lists the tuff and alluvium specimens tested in 1999 and 2000.

Table 6.4-21. Input Data for Development of Nonlinear Dynamic Material Properties Curves

Specimen ID	Borehole No. or Collection Location	Specimen Depth* (ft)	Lithostratigraphic Unit	DTN
Tuff Samples				
UTA-11-E	RF#13	138.3	Tpki	MO9905LABDYNRS.000 [DIRS 103792]
UTA-11-B	RF#13	141.5	Tpki	MO9905LABDYNRS.000 [DIRS 103792]
UTA-11-F	RF#13	142.0	Tpki	MO9905LABDYNRS.000 [DIRS 103792]
UTA-11-I	RF#13	254.6	Tpcpmn	MO9905LABDYNRS.000 [DIRS 103792]
UTA-11-G	RF#13	255.5	Tpcpmn	MO9905LABDYNRS.000 [DIRS 103792]
UTA-11-H	RF#13	257.3	Tpcpmn	MO9905LABDYNRS.000 [DIRS 103792]
UTA-23-C	RF#14	361.0	Tpcpul	MO0203DHRSSWHB.001 [DIRS 158082]
UTA-23-D	RF#14	397.0	Tpcpmn	MO0203DHRSSWHB.001 [DIRS 158082]
UTA-23-G	RF#15	192.5	Tpcpul	MO0203DHRSSWHB.001 [DIRS 158082]
UTA-23-T	RF#15	192.5	Tpcpul	MO0203DHRSSWHB.001 [DIRS 158082]

Specimen ID	Borehole No. or Collection Location	Specimen Depth* (ft)	Lithostratigraphic Unit	DTN
UTA-23-H	RF#15	322.0	Tpcpln	MO0203DHRSSWHB.001 [DIRS 158082]
UTA-23-J	RF#17	575.6	Tpcpul	MO0203DHRSSWHB.001 [DIRS 158082]
UTA-20-B	RF#16	189.5	Tpcrn	MO0203DHRSSWHB.001 [DIRS 158082]
UTA-20-C	RF#16	235.5	Tpcpul	MO0203DHRSSWHB.001 [DIRS 158082]
UTA-23-B	RF#14	241.5	Tpcrn	MO0203DHRSSWHB.001 [DIRS 158082]
UTA-23-R	RF#14	241.5	Tpcrn	MO0203DHRSSWHB.001 [DIRS 158082]
UTA-23-E	RF#15	27.3	Tpcrn	MO0203DHRSSWHB.001 [DIRS 158082]
UTA-23-F	RF#15	88.7	Tpcpul	MO0203DHRSSWHB.001 [DIRS 158082]
UTA-23-S	RF#15	88.7	Tpcpul	MO0203DHRSSWHB.001 [DIRS 158082]
UTA-20-A	RF#16	126.8	Tpki	MO0203DHRSSWHB.001 [DIRS 158082]
UTA-23-Q	RF#16	126.8	Tpki	MO0203DHRSSWHB.001 [DIRS 158082]
UTA-20-D	RF#16	80.5	Tpki	MO0203DHRSSWHB.001 [DIRS 158082]
UTA-23-A	RF#14	104.5	Tpki	MO0203DHRSSWHB.001 [DIRS 158082]
UTA-23-I	RF#17	400.2	Tpcrn	MO0203DHRSSWHB.001 [DIRS 158082]
UTA-20-F	ESF	4.5	Tpki	MO0203DHRSSWHB.001 [DIRS 158082]
UTA-20-G	ESF	6.5	Tpki	MO0203DHRSSWHB.001 [DIRS 158082]
UTA-20-I	ESF	Not measured	Tpcrv	MO0203DHRSSWHB.001 [DIRS 158082]
UTA-20-J	ESF	Not measured	Tmbt1	MO0203DHRSSWHB.001 [DIRS 158082]
UTA-20-L	ESF	Not measured	Tpki	MO0203DHRSSWHB.001 [DIRS 158082]
Alluvium Samples				
UTA-11-C	RF#13	57.3	Qal	MO9905LABDYNRS.000 [DIRS 103792]
UTA-11-A	RF#13	57.5	Qal	MO9905LABDYNRS.000 [DIRS 103792]
UTA-11-J	RF#13	66.9	Qal	MO9905LABDYNRS.000 [DIRS 103792]
UTA-11-D	RF#13	67.0	Qal	MO9905LABDYNRS.000 [DIRS 103792]
UTA-23-X	RF#17	59.0	Qal	MO0203DHRSSWHB.001 [DIRS 158082]

NOTE: *Depth is measured from the top of the boreholes. For samples from the ESF, depth is horizontal distance from the tunnel wall.

Corroborative Data–Laboratory dynamic testing was conducted in 1998 on 10 intact tuff specimens recovered from three boreholes (SD-9, SD-12, and NRG-7/7a) on Yucca Mountain (Stokoe et al. 1998 [DIRS 107635]). These data do not form direct input to the development of nonlinear dynamic material properties curves, but rather are corroborative information. At the time dynamic material property curves were developed for site response modeling described in this report, these dynamic test results were the only ones available for specimens within the RB and are used only to corroborate the applicability to the RB of curves developed for tuff based on specimen test results from the SFA. Table 6.4-22 lists the specimens tested in 1998.

Table 6.4-22. Corroborative Data for Development of Nonlinear Dynamic Material Properties Curves for Tuff

Specimen ID	Borehole No.	Specimen Depth (ft)	Material Type
UTA-2-A	USW NRG-7/7A	43	Welded Tuff (Tpc_un)
UTA-2-B	USW SD-12	92	Welded Tuff (Tpc_un)
UTA-2-C	USW NRG-7/7A	86	Unwelded Tuff (Tpcpv1)
UTA-2-D	USW NRG-7/7A	94	Unwelded Tuff (Tpcpv1)
UTA-2-E	USW NRG-7/7A	136	Unwelded Tuff (Tpy)
UTA-2-F	USW SD-9	79	Unwelded Tuff (Tpcpv1)
UTA-2-H	USW SD-9	79	Unwelded Tuff (Tpcpv1)
UTA-2-K	USW NRG-7/7A	78	Unwelded Tuff (Tpcpv2)
UTA-2-L	USW SD-12	135	Welded Tuff (Tpc_un)
UTA-2-M	USW NRG-7/7A	44	Welded Tuff (Tpc_un)

Source: Stokoe et al. (1998 [DIRS 107635], Table 1) and DTN MO0004QGFMPICK.000 [DIRS 152554] (for material type lithostratigraphic unit)

Subsequent to the site response modeling described in this report additional data on the nonlinear properties of tuffs at Yucca Mountain became available (SNL 2008 [DIRS 183779]). SNL (2008 [DIRS 183779]) extends the results from BSC (2002 [DIRS 157829]) and Stokoe et al. (1998 [DIRS 107635]) to provide results for a wider range of lithologic units, including those underlying the Tiva Canyon Tuff within the RB. Taking into account the limitations of laboratory testing relative to in situ conditions (SNL 2008 [DIRS 183779], Section 7.2.4), the results of SNL (2008 [DIRS 183779], Section 6.5) are consistent with the dynamic property curves used here for site response modeling.

Other Information–EPRI (1993 [DIRS 103320], Section 7.A.5) developed a simple hyperbolic model of nonlinear shear stress-shear strain behavior for use in equivalent-linear site response analyses. A simple model of soil behavior under simple shear loading conditions can be constructed by representing the shape of the shear stress-shear strain relationship with a hyperbola that has an initial slope equal to G_{max}, the shear modulus at small strains, and is asymptotic to τ_{max}, the shear strength (EPRI 1993 [DIRS 103320], Appendix 7, p. 7.A-17). The ratio of τ_{max} to G_{max}, defined as the reference strain, γ_r, is useful both in expressing the stress-strain relationship in mathematical form and as a measure of the relative values of τ_{max} and G_{max}. Soils with larger values of γ_r have greater shear strengths relative to their small strain modulus and show more elastic (linear) stress-strain behavior than soils with smaller values of γ_r. Thus gravelly soils have low reference strain values and more plastic clays have high values (EPRI 1993 [DIRS 103320], Appendix 7, p. 7.A-17). The hyperbolic shape used in the EPRI (1993 [DIRS 103320]) generalized curves provides a good fit to laboratory data on the variation of the secant, or equivalent-linear shear modulus, with shear strain up to cyclic shear strains of 0.1 to 1.0 percent (EPRI 1993 [DIRS 103320], Appendix 7, p. 7.A-28).

The work presented in EPRI (1993 [DIRS 103320], Section 7.A.5) forms part of the basis for the development of the shear modulus reduction and damping curves. As discussed in Sections 6.4.4.2 and 6.4.4.3, the EPRI (1993 [DIRS 103320], Section 7.A.5) work is used to guide the

extrapolation of the curves beyond the range in strain as well as confining pressure of available test results. In other words, EPRI curve shapes are used as a general guide as they are based on laboratory test data for traditional soils (sands, silts, clays) and they have been validated through extensive modeling of recorded motions (Silva et al. 1996 [DIRS 110474]).

Laboratory dynamic testing data used as direct input to an analysis of dynamic material properties for tuff are associated with DTNs MO9905LABDYNRS.000 [DIRS 103792] and MO0203DHRSSWHB.001 [DIRS 158082].

Laboratory dynamic and static testing data used as direct input to an analysis of dynamic material properties for alluvium are associated with DTNs MO9905LABDYNRS.000 [DIRS 103792], MO0203DHRSSWHB.001 [DIRS 158082], GS020483114233.004 [DIRS 158242], and GS020783114233.005 [DIRS 159542].

6.4.4.2 Tuff Normalized Shear Modulus Reduction and Material Damping Curves

The tested tuff samples represent a range of lithostratigraphic units and rock characteristics. Samples from units Tpki, Tpcrn, Tpcpul, Tpcpmn, Tpcpln, Tmbt1, and Tpcrv were tested. The distribution of these materials in the SFA is presented in BSC (2002 [DIRS 157829], Section 6.6). As shown on Figure 6.4.2-1, the repository host horizon consists of the lower units of the Topopah Spring Tuff. Dynamic laboratory test data were not available for the Topopah Spring Tuff nor some of the overlying bedded tuff units at the time the dynamic curves were developed for initiating site response calculations. Units for which dynamic laboratory test data are available from SFA borehole samples are noted on Figure 6.4.4-1. Data from ESF samples show similar behavior except for two samples (UTA-20-I [Tpcrv] and UTA-20-L [Tpki]) that are believed to have been disturbed by the tunnel boring process (BSC 2002 [DIRS 157829], Section 6.3.3.2).

To assess the potential differences in nonlinear dynamic material properties between tuff stratigraphic units, several correlation analyses were performed: shear-wave velocity, degree of welding, and dry unit weight. For a qualitative comparison of curves between tested stratigraphic units, based on results from SFA borehole samples, Figure 6.4.4-1 shows general similarity between units. The between unit variability (potential difference in mean curves or epistemic uncertainty) appears to be less than the within unit variability (aleatory variability or randomness). The possible exception may be Tuff x, perhaps showing somewhat more nonlinear behavior than the other units at strains above 0.02%. The Tuff x unit is nonwelded, suggesting potential differences in nonlinear dynamic material properties between welded and nonwelded tuff, as well as a dependence on shear-wave velocity.

To determine whether the degree of welding has a significant influence on the nonlinear dynamic behavior of the tuff, laboratory dynamic test results for samples from the SFA boreholes also were divided into two groups, welded and nonwelded. Laboratory test results for welded and nonwelded tuff specimens are shown on Figures 6.4.4-2 and 6.4.4-3, respectively. These data indicate no consistent difference in modulus reduction and material damping relationships between the two groups. Results from ESF samples show similar trends (BSC 2002 [DIRS 157829], Figures 155 and 156).

Dynamic testing results for tuff samples from SFA boreholes were also examined with respect to dry unit weight (γ_{dry}). A plot of dry unit weight (γ_{dry}) versus low-strain V_S (Figure 6.4.4-4), indicates a trend of increasing low-strain V_S with increasing γ_{dry} for the tuff specimens. As a result, three groups were identified on the basis of dry unit weight: Group 1 specimens have 147 pcf > γ_{dry} > 133 pcf; Group 2 specimens have 132 pcf > γ_{dry} > 117 pcf; and Group 3 specimens have 94 pcf > γ_{dry} > 78 pcf. Dynamic testing results from these three groups are shown on Figures 6.4.4-5 and 6.4.4-6. Although there is significant variability between specimens in the same group, there is significant overlap among the groups. Thus, the trends in G/G_{max} and damping in these three groups also do not warrant developing separate mean curves for each unit weight group.

These results show that correlations between nonlinear dynamic material properties and lithostratigraphic unit, degree of welding, or dry unit weight are not strongly supported. Note also that sensitivity analyses indicate that differences in tuff dynamic properties have a minor effect on computed ground motions, especially compared to the effect of alluvium dynamic properties (Sections 6.5.2.4.3 and 6.5.3.5.2). Therefore, dynamic properties were developed for all tuff units as a whole.

Although laboratory test results provide information on the dynamic properties of tuff samples at Yucca Mountain, uncertainties exist with respect to how well the test results represent *in-situ* conditions. The relatively small intact specimens do not contain the fractures, voids, and planes of weaknesses that are present in the field. In fact, to facilitate testing, samples are preferentially selected from unfractured, competent materials. As a result, laboratory G/G_{max} curves tend to be more linear than field behavior and hysteretic damping values tend to be lower than field behavior. This bias is shown on Figure 6.4.4-7 by comparing the values of V_S measured in the field and in the laboratory for samples from SFA boreholes. In every case, the laboratory value exceeds any value of V_S measured seismically in the field at the specimen depth. (The higher the V_S the more linear behavior.) In addition, smaller laboratory specimens (~1 inch diameter) cored from larger laboratory specimens (~2 inch diameter) generally exhibit slightly higher values of V_S as shown on Figure 6.4.4-8. Hence, sample disturbance and/or specimen size seem to have a small but measurable effect on the intact specimens. On the other hand, samples are subject to disturbance associated with their collection and, thus, may exhibit more nonlinear behavior than *in-situ* unfractured rock. As an example, there is a suggestion, based on Figures 6.4.4-2 and 6.4.4-3, that nonwelded tuff units may behave somewhat more nonlinearly at high loading levels than welded tuff. These potential differences may also be related to sampling and testing issues, having a stronger effect on nonwelded units. Uncertainty related to both of these potential sampling effects, disturbance and exclusion of fractures and large voids due to sample size limitations, must be accommodated in developing dynamic material property curves.

To accommodate the resulting uncertainty in appropriate mean shear modulus reduction and hysteretic damping curves to be used for the tuff, two sets of mean normalized shear modulus reduction and damping curves were developed in BSC (2004 [DIRS 170027], Section 6.2.4). One set of curves represents the case in which *in-situ* conditions consist of unfractured rock. The second set is developed to represent *in-situ* conditions that reflect fracturing and heterogeneity, the effects of which are not captured in laboratory testing.

For the first case, referred to as the "upper mean tuff (UMT) curves," the normalized shear modulus reduction curve is developed by visually fitting a generic, cohesionless soil curve (EPRI 1993 [DIRS 103320], Appendix 7.A-5) (for shape) through the most linear tuff data (Figure 6.4.4-9). The EPRI (1993 [DIRS 103320]) shape was fit to the most linear data rather than through an average of the data because the samples may exhibit disturbance effects and to account for the possibility of unfractured tuff units. Both factors would tend to result in G/G_{max} and hysteretic damping curves resulting from testing that are somewhat more nonlinear than *in-situ* properties. For shearing strains above about 0.1 percent, the EPRI (1993 [DIRS 103320]) most linear (500 to 1000 ft) shape forms the entire basis for the curve, as data are unavailable for these higher shearing strain levels due to the stiffness of the samples (Figure 6.4.4-9). For the material damping curve, the corresponding (500 to 1000 ft) EPRI (1993 [DIRS 103320]) damping curve shape was used at the same strains as the G/G_{max} shape fit. The damping curve is constrained to have a small-strain material damping value of 0.5 percent for consistency with the overall site damping (kappa) (0.02 sec) at the surface of Yucca Mountain.

For the second case, termed the "lower mean tuff (LMT) curves," the normalized shear modulus reduction curve is developed by first visually fitting the generic, cohesionless soil curve shape (EPRI 1993 [DIRS 103320]) through the middle of the laboratory testing data. Next, the reference strain for the EPRI (1993 [DIRS 103320]) curve is adjusted downward by a factor of four based on the ratio of G_{max} in the field and laboratory (determined from V_S) to account for *in-situ* fracturing and heterogeneity. This adjustment represents the affect of voids and fracture systems on nonlinear dynamic material properties directly through reference strain and directly proportional to the differences (laboratory verses field) in shear moduli. As for the UMT curve, the shape of the EPRI (1993 [DIRS 103320]) generic curve provides the primary basis for the normalized shear modulus reduction curve at shearing strains greater than 0.1 percent. The resulting curve corresponds to the EPRI (1993 [DIRS 103320]) 21-50 ft curve for cohesionless soil and is similar to the soft (fractured) rock curves developed through modeling response spectra computed from empirical WNA rock attenuation relations (Silva et al. 1996 [DIRS 110474], Section 6.2.3.2). For material damping, the corresponding curve from EPRI (1993 [DIRS 103320]) is used. As was the case for the UMT curves, a small-strain material damping of 0.5 percent was used to constrain the damping curve at small strains (Figure 6.4.4-9).

In the tuff curves developed in 2004 (BSC 2004 [DIRS 170024], Section 6.2.4), no accommodation was made for the potential effects of confining pressure (depth) on the curves. The effects of confining pressure on shear modulus reduction and hysteretic damping curves were expected to be small, particularly for the upper mean tuff curves. More importantly, the 2004 analysis used a semi-deterministic approach (McGuire et al. 2001 [DIRS 157510], Approach 2b) to develop ground motion inputs in which motions reflecting site epistemic variability were enveloped. With this enveloping approach, more nonlinear curves controlled the low frequencies while the more linear curves controlled high frequencies. In a fully probabilistic approach, to achieve desired exceedance probabilities in design and performance assessment spectra, site epistemic variability is treated in a manner analogous to earthquake source uncertainty, with weighted hypotheses. With a fully probabilistic approach, compared to a deterministic approach, in order to achieve unbiased results, more rigor is demanded in characterizing all components of epistemic variability, including those associated with earthquake source characterization. In view of the increased rigor, anticipated effects of confining pressure have been included as an update to the original suite of tuff curves. For the

UMT curves, expected to have a very moderate effect of confining pressure, the reference strain was increased 30% for depths of 500 ft and below (Figure 6.4.4-10). This roughly corresponds to an EPRI "step" or increase in reference strain for a factor of two increase in depth. The "step" size is generally considered to reflect a significant difference in computed motions, depending on loading level and initial stiffness. The LMT curves, which are significantly more nonlinear than the UMT curves, as they were intended to accommodate nonlinearity due to movement along existing_fracture systems, may be expected to have a more pronounced effect of confining pressure due to increased friction along the fractures. As a result the EPRI soil "steps" were adopted with the depth adjustments taken on the LMT curves and applied for the depth intervals as shown on Figure 6.4.4-10. Comparisons between the curves used in BSC (2004 [DIRS 170027], Section 6.2) and the updated curves used here are also shown in Figure 6.4.4-10. Damping curves reach a maximum of 15 percent in accordance with guidance from NUREG-0800, Section 3.7.2 (NRC 2007 [DIRS 180932]).

Data used as direct input in developing the nonlinear dynamic material property curves for tuff come from the SFA. The available RB data for Tiva Canyon Tuff and Yucca Mountain Tuff samples from boreholes SD-9, SD-12, and NRG-7/7a (Stokoe et al. 1998 [DIRS 107635]) is unqualified, but fall within the range of the data from the SFA, as shown on Figure 6.4.4-11. Qualified data from the RB were unavailable at the time that calculations were carried out. However, such data have recently become available (SNL 2008 [DIRS 183779]) and corroborate the curves developed. Based on the range displayed by the two mean curves (UMT, LMT), the comparison of available data from the RB (Stokoe et al. 1998 [DIRS 107635]), as well as the aleatory variability of the laboratory test data as a whole (Figures 6.4.4-9 and 6.4.4-11), application of the dynamic material property curves to the entire Yucca Mountain site appropriately captures the uncertainty in dynamic material properties.

The developed tuff curves for normalized shear modulus reduction and material damping, as a function of shearing strain, are associated with DTN MO0403SDIAWHBC.003 [DIRS 170434].

6.4.4.3 Alluvium Normalized Shear Modulus Reduction and Material Damping Curves

Laboratory dynamic tests were performed on five reconstituted alluvium specimens recovered from boreholes in the SFA. Alluvial materials in the SFA consist of interbedded caliche-cemented and non-cemented, poorly sorted gravel with some fines, cobbles and boulders. The depth to groundwater is approximately 1270 ft, and the water content in the alluvium is estimated at less than 5 percent. The nature of the alluvium (highly-cemented to poorly-cemented) and the presence of cobbles and boulders did not allow for intact samples of the alluvium to be taken from the boreholes or test pits before the summer of 2007, although several methods were attempted. Consequently, disturbed samples were reconstituted in the laboratory to create test specimens. Sample reconstitution, including destruction of cementation present in the field, likely has a significant effect on the measured dynamic properties in the laboratory. Figure 6.4.4-12 shows the measured laboratory specimen V_S compared to field measurements for one of the reconstituted alluvial samples. The comparison shows that contrary to the intact tuff specimens where the laboratory values of V_S were greater than the field values, the reconstituted alluvial specimen is not as "good" as the *in-situ* material and hence likely exhibits more nonlinearity and more damping than the *in-situ* material. In other words, ratios of shear-wave velocity (laboratory/field) may serve as an indication of sampling effects, in this case a

combination of disturbance as well as scalping and reconstitution impacted the laboratory value of V_S.

In addition to the breaking of cementation bonds, the reconstituted specimens have a different grain size distribution and coefficient of uniformity than the alluvium in the field due to specimen retrieval techniques and scalping. Gradation curves from bag samples taken from four test pits are shown on Figure 6.4.4-13. Note that these samples consisted of material from the 20-inch sand cone density tests and do not contain boulders. Limitations on the test specimen sizes due to testing equipment constraints required that the alluvium be scalped on the ½-inch sieve. The removal of the larger particles reduces the average particle size and decreases the coefficient of uniformity of the test specimen relative to the field.

Five testing related factors were considered when developing the G/G_{max} curves for alluvium based on the laboratory test specimens:

1. Destruction of cementation
2. Decrease in coefficient of uniformity
3. Variation of confining pressure in the field
4. Variation of density in the field
5. Increase in mean particle size

The largest influences on the normalized shear modulus curve are due to the cementation destroyed during sampling and the change in gradation. Cementation in the field, which is not preserved in the test specimens, can cause the field behavior to be more or less nonlinear than exhibited by the test specimens, depending on the degree of field cementation and loading level. There has been little research performed on the factors affecting the range in behavior but one important factor seems to be the amount of cementation. For instance, in a weakly cemented granular soil if moderate strains cause the *in-situ* cementation to break, the naturally cemented sand can be more nonlinear than the same sand with the cementation removed as illustrated in Figure 6.4.4-14 (Stokoe and Valle 2003 [DIRS 164689]). However, if cementation is strong enough to be maintained during seismic loading, the field behavior can be more linear than the reconstituted test specimens. Research on sand artificially cemented with varying amounts of cement indicates that with the addition of some initial cementation, the specimen behaves in a more nonlinear manner. However, at some level of increased cementation, the specimen becomes more linear as cementation is strong enough to be maintained during shear loading (Figure 6.4.4-15). Degree of cementation of the alluvium across the site is unknown and difficult to characterize. However, data from the literature on cemented sands also shows that cement content as low as 0.5% can cause a significant increase in the low-strain shear-wave velocity (Figure 6.4.4-16). The laboratory measured low-strain shear-wave velocity of the reconstituted alluvium was 925 ft/sec, while the field measurements from downhole, suspension, and SASW averaged 2300 ft/sec (Figure 6.4.4-12), resulting in a field-to-laboratory ratio of approximately 2.5. Data suggest that the field to laboratory ratio of 2.5 in low-strain shear-wave velocity may be due to the loss of a low level of cementation (< 2%) in the reconstituted laboratory samples (Van Hoff 1993 [DIRS 163890]). At this low level of cementation implied, the normalized shear modulus curve is likely to be more nonlinear than the uncemented sand (Figure 6.4.4-14). The normalized shear modulus curves in the artificially cemented sands did not become more linear

(relative to the uncemented sand) again until the cement content reached 8%, at which time the ratio of low-strain shear-wave velocities was more than seven (much higher than the ratio observed for site data). See Figure 6.4.4-16.

Factor #2 above is the larger coefficient of uniformity, C_u. A larger coefficient for the *in-situ* material relative to the laboratory specimens will cause the field behavior to be more nonlinear than the test specimens. Figure 6.4.4-17 illustrates the effect of variation of C_u on normalized shear modulus and material damping ratio for dense granular materials. In general, the normalized shear modulus curve becomes more nonlinear and the material damping ratio increases (at a given shearing strain) as C_u increases. This same trend holds for very loose to loose to medium-dense granular materials (Menq 2003 [DIRS 164681], page 252). The variations of confining pressure and density in the field (alluvium thickness varies from 0 to 200 ft across the site), factors #3 and #4, are considered to play a less significant role on the dynamic material properties, relative to the other factors (Van Hoff 1993 [DIRS 163890], Figures 7.4 and 7.5). Increase in mean particle size of the field relative to the test specimen, factor #5, will cause the shear modulus to increase, but has little impact on the shape of the curve (i.e., the normalized curve).

Ratios of laboratory to *in-situ* shear moduli, a factor of about 0.25 (Figure 6.4.4-12) suggest *in-situ* nonlinearity should be significantly less than that shown by laboratory test results (Figure 6.4.4-17). However, due to the scalping and loss of cementation, unambiguous adjustment of the reference strain associated with the laboratory test results was not possible. The development of two sets of mean shear modulus reduction and hysteretic damping curves, based primarily on anticipated effects of cementation loss and scalping on test results is considered to adequately accommodate uncertainty in the properties of the alluvium. This uncertainty in mean properties is large, as it is intended to acknowledge the lack of experience of the geotechnical community in the dynamic response of these generally stiff, dry, and cemented soils, particularly at high loading levels.

The lower mean alluvium (LMA) G/G_{max} curve (upper hysteretic damping curve, Figure 6.4.4-18), represents the case in which cementation in the field breaks under ground-motion-producing strains (BSC 2004 [DIRS 170027], Section 6.2.4). The curve was developed taking into account the difference between reconstituted, scalped specimens, and field conditions. A generic, cohesionless soil EPRI (1993 [DIRS 103320], Appendix 7) curve was visually fit through the middle of the data, then adjusted downward (more nonlinear) to represent the cementation breaking during shearing. The correction factor implied in the literature (Van Hoff 1993 [DIRS 163890]) is large (Figure 6.4.4-15) and suggests a curve more nonlinear than used to date for sands or gravels (e.g., Rollins et al. 1998 [DIRS 165570]). Therefore, the middle of the gravel range (EPRI 1993 [DIRS 103320], Figure 7.A-3) was used to characterize the lower mean alluvium curves. In contrast to the curves for tuff, significant nonlinear behavior is evident for shearing strains reached during testing. Thus, for alluvium there is less reliance on the shape of the generic cohensionless soil curve (EPRI 1993 [DIRS 103320], Appendix 7) in defining the site-specific normalized shear modulus reduction curve at high strains.

A second curve, termed the upper mean alluvium (UMA) G/G_{max} curve was developed to accommodate highly cemented alluvium for the case in which cementation remains largely intact throughout the entire range in loading level (BSC 2004 [DIRS 170027], Section 6.2.4). As such,

the G/G_{max} curve is expected to behave in a more linear manner than the LMA, which represents the case in which cementation breaks down under seismic loading and larger grain size particles, gravels and cobbles, control nonlinearity. To develop this more linear curve, an EPRI curve shape was adjusted to generally accommodate the more linear test results (Figure 6.4.4-18). The resulting set of curves generally corresponds to the EPRI (1993 [DIRS 103320], Figure 7.A-18) 250-500 ft cohesionless soil curves and is considered to adequately reflect the state of knowledge for the potential effects of cementation and particle size distribution on nonlinear dynamic material properties.

As with the tuff curves, the initial alluvium curves were developed (BSC 2004 [DIRS 170027], Section 6.2.4) independent of confining pressure effects as their inclusion would not have materially impacted the deterministic enveloping process over site epistemic uncertainty. To accommodate potential effects of confining pressure (depth) as well as recent published (Camacho-Padron 2006 [DIRS 184677]) testing on cemented materials, the initial depth independent LMA curve was adjusted to be more nonlinear, reflecting a reference strain of 0.01% (G/G_{max} value of 0.5) from the initial reference strain of about 0.015%, a 50% change. It should be noted that the reference strain as used in the study is defined as was done by Darendeli (2000 [DIRS 183318]) using a modified hyperbolic model. Because recent test results on cemented sands show a weaker dependence on confining pressure than uncemented cohesionless materials (Camacho-Padron 2006 [DIRS 184677]), the updated curves were taken to be appropriate for the top 50 ft (Figure 6.4.4-19). Depth adjustments consisting of one-half EPRI "step," were then taken for the 50 to 100 ft depth interval and again for 100 to 200 ft, the deepest alluvium encountered across the site (Figure 6.4.4-19).

The alluvium curves developed for normalized shear modulus reduction and material damping, as a function of shearing strain, are associated with DTN MO0708DYNPRP07.000 [DIRS 182579].

6.4.4.4 Treatment of Uncertainties and Randomness of Dynamic Material Properties

Uncertainty in the variation of normalized shear modulus and damping as a function of shearing strain is represented through the use of multiple base-case or mean curves. For tuff and alluvium, two sets of curves are provided for each to represent the epistemic uncertainty in dynamic material properties. The curves, which are intended to represent *in-situ* conditions, are based on dynamic testing of site samples, analog sample testing, and engineering judgment. At shear strains higher than about 0.1%, the curves extend beyond the range of available site-specific laboratory data and are based on analog testing, analog modeling, and engineering judgment.

The curves developed for tuff and alluvium are not intended to represent bounds but rather mean or expected behavior, considering the potential effects of fracture systems on tuff and both cementation and particle size on alluvium. Random variations throughout the SFA and RB are expected to result in curves that vary above or below the expected mean behavior. To accommodate expected randomness (aleatory variability) in strain-dependent shear modulus and damping, the curves are independently randomized about the base case values. Random curves are generated by sampling a transformed normal distribution (lognormal), computing the change in normalized shear modulus reduction or percent damping at $3x10^{-2}$ percent shear strain, and

applying this factor at all strains. The random perturbation factor is reduced or tapered near the ends of the strain range to preserve the general shape of the mean curves (EPRI 1993 [DIRS 103320], Appendix 7). The bounds are taken as plus and minus two sigma. For the log-normal distribution, sigma (ln) is taken as 0.15 for modulus reduction and 0.30 for hysteretic damping. The distribution is empirical, based on examining series of laboratory dynamic test results on materials comprising the same geologic unit or material type (EPRI 1993 [DIRS 103320]). The variability is taken to reflect within unit randomness vertically as well as laterally across the site. Following NUREG-0800, Section 3.7.1 (NRC 2007 [DIRS 180931]) the maximum damping ratio allowed is 15 percent.

6.4.5 Parameter Interpretation Weights

In an effort to achieve design and performance motions (UHS's) at desired exceedance probabilities, hazard curves were developed for each set of mean (base case) site properties using Approach 3 (Section 6.1.3). The suite of base case site properties accommodates the range in possibilities expected for *in-situ* dynamic material behavior, reflecting the current state-of-knowledge or uncertainty in mean profiles as well as the nonlinear G/G_{max} and hysteretic damping curves. Final hazard curves were developed by applying relative weights to hazard curves computed for each case reflecting site parametric epistemic uncertainty. The weights accommodate expert judgment regarding expected in-situ behavior. It is important to distinguish between site parametric epistemic uncertainty (lack of knowledge regarding mean properties) and deterministic or known spatial variability across the SFA as well as within the RB. Deterministic (known and predictable) site variability includes depth of alluvium (to tuff), differences in mean velocity profiles north-east and south of the Exile Hill fault splay, and the presence of relatively soft and stiff zones within the RB. These predictable differences are documented in Sections 6.4.2 and 6.4.4 and resulted in suites of distinct base-case properties. To develop single sets of design motions appropriate for the entire SFA and RB respectively, hazard curves computed for each case of spatial variability were enveloped. This process, as an alternative to developing areas or zones with corresponding suites of design/performance spectra, is fundamentally conservative and results in SFA and RB design/performance spectra that likely reflect lower probability (more conservative) than desired, depending on location, depth of alluvium, and structural frequency. Sections 6.5.2.4 and 6.5.3.4 discuss parametric sensitivities that include comparisons of several components of spatial variability which have been enveloped (hazard) in developing SFA-wide and RB-wide design and performance motions. Examination of these comparisons reveals likely degrees of conservatism implied by the engineering decision regarding single verses multiple, spatially variable, design/performance spectra.

For each component of spatial variability, epistemic variability in dynamic material properties exists and was characterized through development of multiple base-cases (Section 6.4.2 and 6.4.4). These cases include two sets of nonlinear G/G_{max} and hysteretic damping curves for alluvium and tuff as well as alternative velocity profiles A, B, and C for the SFA area south of the Exile Hill fault splay and reflect current state-of-knowledge regarding likely *in-situ* behavior. For the alternative base cases, hazard curves were developed using NUREG/CR-6728 Approach 3 (McGuire et al. 2001 [DIRS 157510]). Relative weights were then applied to achieve design/performance motions at desired exceedance frequencies for each component of spatial variability: RB soft and stiff zones and SFA south and northeast areas as well as mean depth of alluvium. The relative weights capture expert judgment regarding expected *in-situ* behavior in

the absence of unambiguous site information. It should be emphasized this is typically the case at all sites as complete and totally unambiguous site data, laboratory or geophysical, is rarely, if ever, available. This uncertainty is completely analogous to earthquake source characterization where irreducible uncertainties (epistemic variability) exist regarding earthquake location, mechanism, recurrence, and expected ground motion conditional on magnitude, distance, and mechanism.

Considering any site, uncertainties are always reducible in principle through additional tests. However, the reality typically encountered is that some ambiguity (uncertainty) remains due to issues related to sampling and testing as well as velocity surveys (e.g., borehole coupling and/or collapse and for SASW, decreasing resolution at depth). The fundamental issue is not whether a site is thoroughly characterized, but whether it has been sufficiently characterized to develop cases that accommodate a reasonable range in expected *in-situ* behavior. Since it is impossible to eliminate site parametric uncertainty, the issue is whether or not sufficient testing has been performed to reasonably characterize the remaining or residual uncertainty and whether or not it is appropriately reflected in multiple base-cases and associated weights. Additionally, the site parametric uncertainty must be coupled with an analysis method that properly accommodates site parametric uncertainty into estimates of design/performance motions.

6.4.5.1 Weights for Velocity Profiles

Due to the epistemic uncertainty in the velocity structure south of the Exile Hill fault splay, three base case V_S and V_P profiles were developed (Sections 6.4.2.5.1 and 6.4.2.5.3). These base case profiles were weighted as shown in Table 6.4-23. Model A was given slight preference over Models B and C because it follows the trend of V_S data to the depth of the Calico Hills Formation. Recall Model B follows the gradient of the velocities above 550 ft depth to the depth at which a V_S of 5600 ft/sec is obtained. Then this profile maintains a V_S of 5600 ft/sec until the depth at which the Calico Hill Formation is reached (Section 6.4.2.5.1). Model C, which was based on the downhole and suspension velocity data only, addressed the epistemic uncertainty in the V_S profiles between these data and the SASW data (the latter give lower velocities; Section 6.4.2.5.1). It was assigned the lowest weight of 0.21 because it was believed that the SASW velocity data were more reliable since they sample more globally velocity structure at the wavelengths of engineering relevance.

Table 6.4-23. Base Case Weights

Case Weight	
Velocity Profiles	
South Model	Weight
A	0.47
B	0.32
C	0.21
	Total 1.00
Nonlinear Shear Modulus and Hysteretic Damping Curves	
Model	Weight
Upper Mean Alluvium (UMA)	0.55

Lower Mean Alluvium (LMA)	0.45
	Total 1.00
Upper Mean Tuff (UMT)	0.70
Lower Mean Tuff (LMT)	0.30
	Total 1.00

6.4.5.2 Weights for Nonlinear Shear Modulus Reduction and Damping Curves

Relative weights applied to hazard curves computed from analyses using the alternative sets of modulus reduction and hysteretic damping curves are listed in Table 6.4-23. For the alluvium, the lack of test results for undisturbed samples and the limited relevant data in the literature, result in considerable uncertainty regarding expected *in-situ* behavior (Section 6.4.4). Based on available test results as well as a careful examination of analogue materials (cemented sands and effects of scalping on gravelly materials), the UMA and LMA curves are considered to reflect *in-situ* behavior in a nearly equal manner. The UMA curves were given slightly more weight than the LMA curves (0.55 versus 0.45) because it is somewhat more likely the cementation would remain relatively in tact during cyclic loading (Table 6.4-23). It should be noted that development of a weighted set of curves and analyses for a single "mean set" would not produce desired exceedance probabilities, as this approach, although greatly reducing the number of analyses, would not accommodate epistemic uncertainty. The resulting motions would likely be unconservative (higher probability than desired). Increasing the aleatory variability during the randomization of the curves to accommodate the epistemic uncertainty would preserve the probability in the mean hazard, but neglect its contribution should median estimates and fractiles be desired.

For the tuff curves, it was felt the likely impact of fracture systems and lithophysae on the nonlinear dynamic material properties would be small and not a controlling factor. To examine this possibility, modulus reduction and hysteretic damping curves were developed based on numerical modeling of the tuff units both at and above the repository emplacement level (Appendix B). The numerical model does not include matrix nonlinearity (sampled in the testing of small specimens) but accommodates the influence of lithophysae and slip (friction) along fractures as well as yielding of intact rock mass through plastic deformation. The modeling results suggest that the presence of existing fractures under *in-situ* confining pressures has little effect and significant nonlinearity begins only when cyclic shear strains are large enough to cause plastic deformation and large displacements across fractures. For strains below about 0.1% to 0.2%, little nonlinearity was predicted with the numerical model results similar to the UMT curves. For strains beyond this range, the modulus reduction curve decreases more steeply than that of the UMT curve, approaching the LMT curve. At these higher shear strains, the material is reaching threshold shear strains (geologically observable; BSC 2005 [DIRS 170137]) and incipient failure, as evidenced in the tuff samples tested. This is not considered an issue as strains approaching material failure are not reached in the tuff with the reference rock control motions conditioned for both extreme strains as well as extreme source processes (Appendix A).

The results of the numerical modeling (Appendix B) along with the judgment that the effects of large-scale fractures would be small prompted the dominant weight on the UMT curves (0.7

versus 0.3, Table 6.4-23). The retention of some weight on the LMT curves (0.3) reflects residual uncertainty recognizing the UDEC model is not typically used for this application.

6.4.6 Adequacy of Site-Response Model Inputs

Seismic and geotechnical data that form inputs to the RVT-based equivalent-linear site-response model are adequate to develop ground motions for preclosure and postclosure analyses. For control motion inputs, the results of the Yucca Mountain PSHA, conditioned by recent evaluations of the level of extreme ground motion that is consistent with the geologic setting, are used (Section 6.4.1). These results incorporate epistemic uncertainty and aleatory variability in the characterization of seismic sources and ground motion attenuation relationships for the Yucca Mountain vicinity, as determined through a formal expert elicitation process (Section 6.4.1). As part of the PSHA, the experts considered an extensive database of geologic, geophysical, tectonic, and seismic information pertinent to the Yucca Mountain site. Control motion inputs to site-response modeling also incorporate uncertainty in the level of extreme ground motion that Yucca Mountain can experience.

Seismic velocity profiles are determined on the basis of seismic data collected in boreholes and through SASW surveys at the surface and within the ESF and ECRB cross-drift (Section 6.4.2). Through this combination of borehole and SASW data, and using knowledge of the subsurface geology at the site, the velocity characteristics are adequately determined. While not used as direct basis for velocity profiles, laboratory determinations of velocity differ from the *in-situ* data in expected ways and corroborate the profiles of *in-situ* velocity (Figure 6.4.4-7; Section 6.4.4.2).

Uncertainty and variability in velocity characteristics at Yucca Mountain are appropriately accounted for in site-response modeling through the use of multiple velocity profiles, as appropriate. Results from different profiles representing epistemic uncertainty are weighted according to judgments on the degree to which they are supported by the data. Results from different profiles representing spatial variability for the RB and SFA are enveloped to provide ground motions that apply to the entire RB and entire SFA, respectively. For example, for the SFA, the developed ground motions incorporate uncertainty and variability across the entire area, not just beneath any individual important-to-safety structure. Aleatory (random) variability in velocity is also incorporated in the development of site-specific ground motion through site response modeling that employs a suite of randomized velocity profiles determined from a given mean base case profile.

Dynamic material property curves are determined on the basis of laboratory testing of site materials, consideration of results in the literature for other materials, and judgment on how those data relate to *in-situ* conditions at Yucca Mountain (Section 6.4.4). Consideration of this technical basis indicates that there is epistemic uncertainty in the characterization of dynamic properties for tuff and alluvium. Because of this uncertainty, multiple sets of curves for the variation of normalized shear modulus and material damping as a function of shearing strain are incorporated into the site-response modeling. Site-response modeling also incorporates aleatory variability in dynamic properties to provide ground motions appropriate for the entire site of interest. Uncertainty and variability in dynamic properties are appropriately incorporated into site-response modeling and the development of site-specific ground motions.

Thus, inputs to site-response modeling have an adequate technical basis.

6.4.7 Point-Source Input Parameters

As described in Section 6.3, input parameters required for implementing the stochastic point-source ground motion model include magnitude, point-source distance and depth, stress drop, crustal attenuation as parameterized by a frequency-dependent quality factor, Q(f), and site attenuation as parameterized by kappa. The point-source model was used in computing PGA values at the reference rock outcrop as a function of stress drop to aid in conditioning of the extreme ground motions (Section 6.5.1) and in the computation of the V/H ratios (Section 6.5.2.1.2).

Table 6.4-24 lists the input parameters used in conditioning the extreme ground motions. Three magnitudes, **M** 6.0, 6.5, and 6.75 were modeled, which covers the range of possible earthquake scenarios considered for the local seismic sources, i.e., local faults and background earthquakes (CRWMS M&O 1998 [DIRS 103731], Section 7). These magnitudes are also consistent with the modal magnitudes for 5-10 Hz discussed in Section 6.4.1. The horizontal point-source distance was fixed at 1 km. The source depth was fixed at 8 km, which is a typical mean value for earthquakes in the Basin and Range Province that includes the Yucca Mountain region (Wong et al. 2004 [DIRS 170544]). The range of stress drops considered was 150, 400, and 1100 bars. This range was developed by considering available data on stress drops relevant to the geologic setting of Yucca Mountain and consulting with a team of experts in engineering ground motions (Sections 5.4 and 6.5.1).

Table 6.4-24. Point-Source Input Parameters for Computing Extreme Ground Motions

Parameter	Values
Magnitude (**M**)	6.0 and 6.5
Distance (km)	1.0
Source Depth (km)	8
Stress Drops (bars)	150, 400, and 1100
Crustal Attenuation	
Q_0	250
η	0.4
Kappa (sec)	0.02

Frequency-dependent crustal attenuation as expressed by $Q(f) = Q_0 f^{\eta}$ where Q_0 is 250 and η is 0.4 was adopted from the recommended values used in the scenario ground motion modeling study preformed for the Yucca Mountain Project in 1996 (Schneider et al. 1996 [DIRS 103270]). Finally, the value for kappa was adopted from Su et al. (1996 [DIRS 100087]), which was used as the basis to adjust to the reference rock outcrop value of 0.0186 sec in the PSHA (CRWMS M&O 1998a [DIRS 103731]). A velocity profile is also a required input into the point-source model. A Yucca Mountain crustal profile was developed as part of the 1996 scenario ground motion modeling study and this profile was also used in the point-source modeling (Schneider et al. 1996 [DIRS 103270], Table 5-2).

The point-source parameters used for computing the V/H ratios are listed in Table 6.4-25. Magnitude values of **M** 5.0, 6.0, and 7.0 were modeled. The stress drop was held at 50 bars, an average western U.S. stress drop (Atkinson and Silva 1997 [DIRS 163171]). The rate of crustal attenuation, crustal profile, and kappa were the same as discussed above. A total 19 source depth-distance pairs were used to model the range of PGAs from 0.01 to 10.0 g.

Table 6.4-25. Point-Source Input Parameters for Computing V/H Ratios

Parameter	Values
Magnitude (**M**)	5.0, 6.0, and 7.0
Stress Drops (bars)	50
Crustal Attenuation	
Q_0	250
η	0.4
Kappa (sec)	0.02

6.5 MODELING, ANALYSES, AND RESULTS

The overall approach, methodology, modeling, and analyses performed to develop ground motion inputs for the SFA and RB are described in the following subsections. Results are presented in terms of site-specific hazard curves and UHS. In addition, design response spectra, time histories, and, for the SFA, hazard-consistent strain-compatible material properties, are provided for AFEs of 10^{-3} and $5x10^{-4}$. Also, for an AFE of 10^{-4}, a similar set of beyond-design-basis ground motion inputs are developed.

6.5.1 Conditioning of Probabilistically-Derived Ground Motions at Yucca Mountain

This section describes the incorporation of limiting distributions on source and site properties to condition probabilistically derived ground motions. Two methods are used to condition the Yucca Mountain hazard curves based on physical principals. One approach uses geologic observations at repository depths to constrain ground motions that have occurred in the last 12.8 million years. The other approach assesses the distribution of an earthquake source parameter (stress drop) to characterize extreme ground motion that can occur at Yucca Mountain. The first approach is updated from BSC (2005 [DIRS 170137]) using more recent site properties and a refined methodology (Appendix A). The second approach is described in detail in Appendix A.

A PSHA for Yucca Mountain (BSC 2004 [DIRS 168030]) determined the annual frequency for which ground motion would be exceeded for a hypothetical reference rock outcrop with defined "hard-rock" material properties. As part of that study, a formal expert elicitation process was used to characterize seismic sources and ground motion attenuation relationships for the Yucca Mountain vicinity. The ground motion experts developed interpretations of median ground motion, its standard deviation, and the uncertainties in both. Aleatory variability in ground motion was characterized using untruncated lognormal distributions. Consequently, as lower and lower annual AFEs are considered, the corresponding values of ground motion increase without bound. The issue of whether physical principals limit ground motions at Yucca Mountain was not addressed during the PSHA.

Subsequent to the PSHA, scientists have questioned whether the extreme ground motions determined for low AFEs can be physically realized at Yucca Mountain (Corradini 2003 [DIRS 171191]; Reiter 2004 [DIRS 170694], Bommer et al. 2004 [DIRS 184601]). For AFEs of less than about 10^{-6}, the dominant hazard contributions are from **M** 6 to 6.5 earthquakes within a few kilometers of the site (Section 6.4.1, Appendix A). The primary contributions are from the Paintbrush Canyon-Stagecoach Road and Solitario Canyon faults (BSC 2004 [DIRS 168030], Section 6.5.4); faults characterized as left-lateral strike-slip or normal mechanism, dipping moderately to the west. The hazard deaggregation for AFEs of about 10^{-7} and less indicate that a majority of the hazard is contributed from exceedance of the 95th percentile of the attenuation relationships. These levels of motion are far in excess of historic earthquake recordings.

These large probabilistically-derived ground motions occur because of the large expert uncertainty in the median attenuation models for the Yucca Mountain site and the unbounded aleatory variability in the attenuation models. They are of interest because of the performance assessment criteria in 10 CFR 63 (Appendix A, Section A1). Rock-site attenuation relationships incorporate untruncated log-normal distributions and this aleatory variability results in increasing

and unbounded ground motions for decreasing AFEs. Thus, the probabilistically-based ground motions can potentially become unphysical.

Several approaches have been proposed to limit these probabilistically-derived ground motions. These approaches include numerical simulations to estimate the upper limit of peak ground velocity (PGV) (Andrews et al. 2007 [DIRS 184818]), ground motion implications of precariously balanced rocks in the vicinity of Yucca Mountain (Anderson et al. 2007 [DIRS 184472), the use of observed extreme ground motions (Huyse et al. 2007 [DIRS 184355]), observations of unbroken rock at repository level (BSC 2005 [DIRS 170137]), and limits on distribution of extreme stress drop used in the stochastic ground motion model (Appendix A). The approach used here is to employ both the observational site constraints (lack of pervasive seismic-related fractures at repository level) and source constraints (based on an assessed extreme stress drop distribution) to condition the PSHA results.

In BSC 2005 [DIRS 170137], geologic observations in underground excavations at Yucca Mountain together with results of laboratory rock testing supplemented by numerical simulations of rock deformation and ground motion site response modeling were used to establish a level of horizontal PGV that has not been experienced at Yucca Mountain. This result provides a distribution on the upper limit of extreme ground motion that has occurred at Yucca Mountain during the past 12.8 million years. The present study updates the BSC (2005 [DIRS 170137]) analysis and implements a second approach that estimates the ground motions associated with an assessed distribution of extreme stress drops. The previous analysis is updated based on additional site-response modeling that uses revised site material properties and a refined hazard-consistent approach to develop site response (Appendix A, Section A2.2). The hazard-consistent approach incorporates aleatory variability in the site properties and the approach is extended to ground motion measures other than PGV. In addition, constraints on ground motion at the repository waste emplacement level are transformed to constraints on ground motion at the PSHA reference rock outcrop.

The second approach uses a point-source stochastic ground motion model (Section 6.3) to determine ground motions for earthquakes controlling Yucca Mountain postclosure ground motions (Appendix A, Section A3). An assumed distribution of extreme stress drop for the model, which controls the high-frequency level of ground motion, is based on available data and interpretations, and is informed by interactions with experts that took place in a series of workshops in which the issue was discussed (Appendix A-Section A3.2.1.3, Section 5.4).

Both approaches are used to condition the mean PSHA ground motion hazard curves; however, constraints from the second approach (i.e., a distribution on extreme stress drop for the point-source stochastic ground motion model) control the conditioned hazard curve. This result is not unexpected as the previous approach only provides information on the maximum ground motion that has not been experienced at Yucca Mountain. The level of ground motion that is possible can be less than that upper limit of unobserved ground motion based on other physical constraints (e.g., a limit on extreme stress drop).

In the following sections, first the description of the update to the approach based on the shear-strain threshold for damage to lithophysal tuff is presented. Second, the new approach based on

a distribution of extreme stress drop is presented. Finally, the use of both approaches jointly to condition the existing PSHA ground motion hazard curves is discussed.

6.5.1.1 Ground Motion Constraints Based on Geologic Conditions at the Repository Waste Emplacement Level

This approach uses geologic observations at the repository level to develop a limiting distribution on shear-strains experienced at Yucca Mountain (BSC 2005 [DIRS 170137]). In this approach, laboratory rock mechanics data, corroborated by numerical modeling, were used to derive the shear-strain levels required to initiate stress-induced failure of the weaker lithophysal zones. Because these seismic-related failures in the lithophysal units are not observed, it is concluded that the derived threshold shear strains have not occurred since deposition of the Topopah Spring Tuff 12.8 M years ago. BSC (2005 [DIRS 170137]) developed a distribution for shear strain threshold and, using a site response model, developed the corresponding distribution of PGV. The site response model incorporates uncertainty and variability in modeling the lithophysal unit and uncertainties in the geotechnical model for the site. Consequently, distributions are developed for both the shear strain threshold and PGV that are consistent with the site response model. With distributions developed for PGV, BSC (2005 [DIRS 170137]) developed operators in the form of complementary cumulative distribution functions (CCDFs) that were applied to an unbounded hazard curve for the repository waste emplacement level to develop a conditioned hazard curve consistent with geologic observations. The distribution on shear strain threshold of BSC (2005 [DIRS 170137]) is incorporated, in a modified form, in the analysis developed here (Appendix A, Sections A2.2 and A4.5.2).

Although the fundamental assessment that a shear-strain threshold has not been exceeded within the Topopah Spring lithophysal units remains the same, other aspects of the approach are generalized, refined, and updated in its current implementation (Appendix A, Section A2.2 and A4.5.2). First, the approach is generalized to deal with ground motion measures other than horizontal PGV. Response spectral acceleration at 0.3, 0.5, 1, 2, 5, 10, 20 Hz and PGA are now addressed. Second, the approach is modified to use the inferred shear-strain threshold at the repository waste emplacement level to determine the level of ground motion not experienced at the reference rock outcrop, rather than at the waste emplacement level. This allows the approach to be used in analyzing conditioned ground motions at the SFA as well as the RB. Third, implementation of the conditioning is refined to include variability in shear strain levels and integration over the entire hazard curve. Finally, the site-response component of the approach is updated to incorporate additional geotechnical data on RB material properties (Sections 6.4.2 and 6.4.4). As a result of these changes, the strain-based CCDF hazard operators of BSC (2005 [DIRS 170137]) have been revised.

6.5.1.2 Ground Motions Based on Assessment of Extreme Earthquake Stress Drops

As a supplement to the characterization of extreme ground motion at Yucca Mountain based on the physical properties of the tuff units at the site (BSC 2005 [170137]), a second approach is developed that considers physical constraints at the earthquake source (Appendix A3). To implement this approach, a stochastic point-source ground motion model (Section 6.3) is used. The high-frequency source constraint is derived from an assessment on the distribution of extreme stress drop (Section 5.4, Appendix A, Section A.3.2.1.3) that is used in the point-source

model using a single-corner-frequency source representation (Boore 1983 [DIRS 103317]; Atkinson 1984 [DIRS 166350]). Extreme stress drops are defined as stress drops that result in ground motions far in excess of those observed from historical strong motion records. The motivation for this approach is, in part, the observation that ground motion prediction for an earthquake on a nearby fault using the point-source model requires a stress drop in excess of 2000 bars to produce the approximately 11 g PGA value associated with a mean AFE of 10^{-8} (Appendix A4.4). While not statistically sufficient to establish the value of an extreme stress drop, twenty years of modeling earthquakes using the point-source model together with the single-corner source model indicate that a 2000-bar stress drop is in excess of those values inferred from modeling earthquakes worldwide ranging from **M** -3 to 8 (Appendix A).

To address the issue of extreme probabilistic ground motions at low AFEs, the DOE convened a series of workshops to address the possibility of limits on extreme stress drop. A group of four internationally recognized experts in engineering seismology and geophysics participated in the workshops and discussed methods to characterize extreme stress drops for the Yucca Mountain vicinity (Appendix A3.2.1). The experts developed individual assessments of the distribution for extreme stress drop as part of the workshop process. Available data, interpretations, and judgment, informed by discussions that took place during the workshops, serve as the technical basis for the assumed extreme stress drop distribution used in the analysis (Section 5.4, Appendix A, Section A3.2.1.3).

The assumed distribution on extreme stress drop was used in the point-source model to develop distributions on PGA at the reference rock outcrop that were used as operators to condition PGA hazard. The conditioned PGA hazard was then used to scale UHS from the PSHA (BSC 2004 [DIRS 168030]). Scaled-UHS were used to preserve the spectral shape that resulted from the PSHA process. Preservation of this shape is desirable as it is a key output of the PSHA and represents the interpretations developed through the expert elicitation process employed to develop inputs to the PSHA.

The stress drop is determined from the corner frequency of earthquake spectra (Eq.-6.8):

$$f_c = \beta\left(\frac{\Delta\sigma}{8.44 M_0}\right)^{1/3}$$

Where f_c is the corner frequency in hertz, β is the shear wave velocity in km/sec, $\Delta\sigma$ is the stress drop in dynes/cm^2, and M_0 is the seismic moment in dyne-cm.

Once a distribution on extreme stress drop was established, the point-source model (Section 6.3) was used together with the geotechnical model of Yucca Mountain to determine distributions of extreme PGA at the reference rock outcrop.

6.5.1.3 Reference Rock Outcrop Conditioned Hazard

Shear-strain-threshold-conditioned ground motion hazard for the reference rock outcrop using the methodology described in Appendix A (Section A4.5.2) is illustrated in Figures 6.5.1-1, 6.5.1-2, and 6.5.1-3 for PGV, PGA and 1-Hz SA, respectively. The figures also show the effect of different values of shear-strain sigma on the conditioned hazard. For an APE of 10^{-8}, the

shear-strain-threshold-conditioned PGV hazard is reduced from about 1200 cm/sec to about 1100 cm/sec or about 10%. This reduction is substantially less than the reduction observed in BSC (2005 [DIRS 170137]) owing to the modified approach, updated site-specific properties, and consequent reduction in predicted repository emplacement level shear-strains (Appendix A, Section A4.5.2).

Extreme-stress-drop-conditioned hazard for the reference rock outcrop (Appendix A, Section A4.5.1) is illustrated in Figures 6.5.1-4, 6.5.1-5, and 6.5.1-6 for PGV, PGA and 1-Hz SA, respectively. The figures also show the effect of different values of ground motion sigma on the conditioned hazard. For mean PGVs less than about 60 cm/sec (AFEs greater than about $8x10^{-5}$), the conditioned hazard is identical to the unconditioned hazard, consistent with the operator approach taken in Appendix A. For PGVs greater than about 60 cm/sec (AFEs less than about $8x10^{-5}$), the conditioned and unconditioned hazard increasingly diverge with increasing ground motion. For increasing PGV, the slope of the conditioned hazard increases continuously relative to the slope of the unconditioned hazard resulting in a decrease in mean PGV from about 1200 cm/sec to 480 cm/sec at an AFE of 10^{-8} (60% reduction in PGV). Note that at an AFE of 10^{-8} the mean hazard is still increasing and has not reached a maximum, suggesting that the breadth of the uncertainty in extreme stress drop will result in increasing hazard at even lower AFEs.

The results demonstrate that the assessed extreme stress drop distribution has a significant effect on the unconstrained hazard for AFEs less than about 10^{-4} to 10^{-5}. Variability in predicted reference rock outcrop ground motions using the point-source model is significant ($\sigma \sim 0.7$) if distributions are used for all model input parameters, however, for the range of sigma illustrated in Figures 6.5.1-4, 6.5.1-5, and 6.5.1-6, the effects of ground motion sigma have a relatively weak impact on the conditioned hazard. At an AFE of 10^{-8}, the effect of sigma variability on the conditioned hazard is less than about 5% on ground motion (Figures 6.5.1-4, 6.5.1-5, and 6.5.1-6). To avoid double-counting variability that is already included in the PSHA reference rock outcrop hazard, ground motion variability is constrained to 0.15 for this analysis (Appendix A, Sections A4.3 and A4.4).

Conditioned hazard using combined shear-strain-threshold and extreme-stress-drop approaches is illustrated in Figures 6.5.1-7, 6.5.1-8, and 6.5.1-9 for PGV, PGA and 1-Hz respectively. The shear-strain-threshold-conditioning has a marginal impact on the unconditioned hazard as compared to the extreme-stress-drop method.

6.5.1.4 Reference Rock Outcrop Conditioned Uniform Hazard Spectra

The reference rock outcrop horizontal UHS based on the extreme-stress-drop- and shear-strain-threshold-conditioned hazard for periods of 0.01, 0.05, 0.1, 0.2, 0.5, 1.0, 2.0, and 3.3 sec (100, 20, 10, 5, 2, 1, 0.5, 0.3 Hz) are illustrated in Figures 6.5.1-10 through 6.5.1-15 for AFEs of 10^{-3}, 10^{-4}, 10^{-5}, 10^{-6}, 10^{-7} and 10^{-8}, respectively. For AFEs of 10^{-3} and 10^{-4}, spanning the range of AFEs used for design analyses (DBGM-1, DBGM-2, and BDBGM) (Figures 6.5.1-10 and 6.5.1-11), the UHS using conditioned and unconditioned hazard are approximately equal. For the decreasing AFEs of 10^{-5}, 10^{-6}, 10^{-7}, and 10^{-8} (Figures 6.5.1-12 through 6.5.1-15), UHS using the conditioned hazard is increasingly lower than the unconditioned UHS.

6.5.2 SFA Preclosure Ground Motions

This section describes the results of the modeling and analyses to develop seismic hazard curves and design parameters with AFEs of 10^{-3}, $5x10^{-4}$, and 10^{-4} for the SFA. These parameters are used for preclosure design analyses of SFA facilities, as appropriate. For both the SFA and RB, design parameters with an AFEs of 10^{-3} and $5x10^{-4}$ correspond to design basis ground motion levels (DBGM) 1 and 2, respectively, as described in *Preclosure Seismic Design and Performance Assessment Methodology for a Geologic Repository at Yucca Mountain Topical Report* (DOE 2007 [DIRS 181572], Section 3). Design parameters with an AFE of 10^{-4} correspond to beyond design basis ground motions (BDBGM). These ground motions are not used for design, but rather to assess seismic fragilities of important to safety structures. Throughout this report, the DBGM-1, DBGM-2, and BDBGM results will be referred to collectively as "design" ground motions, spectra, and time histories. However, it should be remembered that the BDBGM results are not used for design per se. At each AFE, modeling and analyses result in horizontal and vertical 5%-damped seismic design response spectra and expected horizontal PGVs. Design spectra at other dampings are also calculated. In addition, strain-compatible properties and design time histories are developed.

6.5.2.1 SFA Transfer Functions

As previously discussed (Section 6.1.2), the first phase in developing site-specific ground motions consists of determining transfer functions. Transfer functions include both amplification factors for horizontal motions and V/H ratios. Amplification factors reflect the ratio between the site-specific 5%-damped response spectrum determined from site-response modeling and the 5%-damped response spectrum of the control motion input representing ground motion at the PSHA reference rock outcrop. V/H ratios reflect the ratio between vertical and horizontal 5%-damped response spectra; both determined using a combined stochastic point-source model and site-response model. Both types of transfer functions are ultimately integrated with appropriate hazard curves to determine probabilistic site-specific ground motions.

6.5.2.1.1 Development of Amplification Factors

For the amplification factors, RE spectra computed from the PSHA attenuation relations and scaled to PGA values ranging from 0.01g to 10.00g were used as control motions in site-response modeling (Table 6.4-3, Section 6.4.1). Following Regulatory Guide 1.165 (1997 [DIRS 119139]), both 1-to-2-Hz and 5-to-10-Hz RE spectra were used. . This approach is intended to produce amplification factors appropriate for specific earthquakes (magnitude and distance combinations) dominating the hazard at low- and high-structural frequency, as well as reflecting site- and region-specific spectral shapes. The levels of motion are intended to provide amplification factors appropriate for the ground motion levels observed in the reference rock outcrop hazard curves, conditioned or unconditioned, for AFEs ranging from 10^{-2} to below 10^{-8}.

The amplification factor is determined by taking the ratio between the site-specific 5%-damped response spectrum, calculated using the site-response model, and the corresponding control motion input spectrum. Amplification factors for PGV are computed in a similar fashion. Amplification factors are developed for the various combinations of velocity profile, dynamic material property curves, and alluvium thickness representing epistemic uncertainty and

deterministic variability across the SFA. For each combination, aleatory variability is incorporated in the amplification factors by carrying out site-response modeling for 60 randomized velocity profiles and sets of dynamic material property curves, based on the corresponding base-cases, and then averaging the resulting amplification factors. Details of amplification factor development are presented in Appendix D (Calculations: SFA Site A Control Motion (RVT)).

To accommodate potential differences in amplification factors due to the spectral shape of the control motions (i.e., those based on 1-to-2-Hz RE spectra and 5-to-10-Hz RE spectra), the PSHA deaggregation is used to develop weights for the factors as a function of both structural frequency and AFE. These weights are used in integrating the amplification factors with the reference rock outcrop hazard curves to obtain probabilistic site-specific hazard curves. For each ground motion measure, weights are assessed such that either the amplification factors associated with the 1-to-2-Hz control motion or the 5-to-10-Hz control motion are used. The scaled 1-to-2-Hz RE spectra represent large (**M** > about 7) earthquakes at a distance of about 50 km, while the 5-to-10-Hz scaled RE spectra represent moderate to large (5 < **M** < 7) earthquakes within 5 km of the site (Table 6.4-1). Hazard deaggregation for the 5-to-10-Hz range of spectral acceleration shows that larger earthquakes within 15 km of the site dominate the hazard for AFEs from 10^{-3} to 10^{-7} (Figures 6.4.1-5 to 6.4.1-10). Thus, for high frequency spectral acceleration (5 to 20 Hz) and PGA, the amplification factors associated with the 5-to-10-Hz RE control motions are used. At low frequency spectral acceleration (1 to 2 Hz), hazard deaggregation (Figures 6.4.1-11 to 6.4.1-16) shows that larger nearby events dominate the hazard at AFEs of 10^{-5} and less, but that large distant earthquakes are also important at higher AFEs. Thus, for 1-Hz and 2-Hz spectral acceleration, weights for lower AFEs (10^{-5} to 10^{-8} for 1-Hz spectral acceleration and 10^{-4} to 10^{-8} for 2-Hz spectral acceleration, respectively) use amplification factors associated with the 5-to-10-Hz RE control motions. At higher AFEs, the amplification factors associated with the 1-to-2-Hz RE control motions are used. PGV is treated the same as 1-Hz spectral acceleration. For lower frequency spectral acceleration (0.3 and 0.5 Hz), amplification factors associated with the 1-to-2-Hz RE control motions are used for all AFEs. Table 6.5-1 lists the amplification factor weights for the various combinations of AFE and ground motion measure. Because the two suites of factors based on the two RE structural frequency ranges do not differ dramatically and vary smoothly with loading level (i.e., reference rock outcrop peak acceleration), the weights in Table 6.5-1 adequately accommodate the deaggregation results.

An example of the amplification factors, computed with the scaled 1-to-2-Hz RE spectra, is shown in Figures 6.5.2-1a-d with the full suite documented in Appendix D. The base-case shown in Figures 6.5.2-1a-d is the South of Fault profile A with 100 ft of alluvium and with the most linear combination of dynamic material property curves: upper mean alluvium and upper mean tuff. The maximum amplification is about two with nonlinearity becoming evident at loading levels above 0.5g. For comparison, Figures 6.5.2-2a-d shows the same site conditions but using the scaled 5-to-10-Hz RE spectra as control motions. For this base-case, the results are nearly the same as using the scaled 1-to-2-Hz RE spectra (Figures 6.5.2-1a-d).

For completeness, Figures 6.5.2-3a-d shows amplification factors computed for the same base-case profile and material properties but using the stochastic point-source model for an **M** 7 earthquake to generate control motions. Regional and site values are used for point-source model input parameters (Table 6.5-2, Section 6.4.7). The point-source model is used to compute

site-specific V/H ratios that, when combined with results from WUS empirical attenuation relations, are integrated with the site-specific horizontal hazard curves to obtain vertical hazard curves (Section 6.5.2.1.2). Comparison of amplification factors associated with scaled RE spectra control motions (Figures 6.5.2-1 and 6.5.2-2) to those associated with the point-source model control motions (Figure 6.5.2-3) shows nonlinearity induced by the point-source model control motions is generally similar to that induced by the RE control motions.

Table 6.5-1. Amplification Factor Weights

F(Hz)	AFE	Amplification Factor Weights	
		1-to-2-Hz RE Control Motion	5-to-10-Hz RE Control Motion
0.3	10^{-3} to 10^{-8}	1.0	0.0
0.5	10^{-3} to 10^{-8}	1.0	0.0
1.0	10^{-3} to 10^{-4}	1.0	0.0
	10^{-5} to 10^{-8}	0.0	1.0
2.0	10^{-3}	1.0	0.0
	10^{-4} to 10^{-8}	0.0	1.0
5.0	10^{-3} to 10^{-8}	0.0	1.0
10.0	10^{-3} to 10^{-8}	0.0	1.0
20.0	10^{-3} to 10^{-8}	0.0	1.0
100.0 (PGA)	10^{-3} to 10^{-8}	0.0	1.0
PGV	10^{-3} to 10^{-4}	1.0	0.0
	10^{-4} to 10^{-8}	0.0	1.0

Source: Appendix D

Table 6.5-2. Point Source Parameters

Stress Drop, $\Delta\sigma$ = 50 bars, Q(f) = 250 $f^{0.4}$, κ = 0.0186 sec Crustal Model			
Thickness (km)	Vs (km/sec)	Vp (km/sec)	Density, ρ (cgs)
0.152	1.829	3.167	2.4
0.152	1.981	3.529	2.4
0.505	2.042	3.638	2.4
1.5	2.9	5.0	2.5
2.2	3.4	5.8	2.7
10.7	3.5	6.2	2.78
16.0	3.8	6.5	2.9
	4.6	7.8	3.3

Source: Section 6.4.7

Table 6.5-3. Magnitudes, Distances, and Depths Used in the Point-Source Model to Achieve Target Horizontal PGA Values

Target Horizontal PGA (g)	M 5, 6, 7 Distance (km)			M 5, 6, 7 Depth (km)		
0.01	37	70.00	142.0	8	8	8
0.05	10.40	24.35	44.0	8	8	8
0.10	0.0	12.40	26.0	7.20	8	8
0.20	0.0	1.80	12.86	3.90	8	8
0.30	0.0	0.0	7.05	2.65	5.50	8
0.40	0.0	0.0	2.28	2.00	4.25	8
0.50	0.0	0.0	0.0	1.60	3.43	6.73
0.75	0.0	0.0	0.0	1.087	2.30	4.60
1.00	0.0	0.0	0.0	0.817	1.81	3.48
1.25	0.0	0.0	0.0	0.650	1.40	2.74
1.50	0.0	0.0	0.0	0.544	1.17	2.27
1.75	0.0	0.0	0.0	0.472	0.98	1.94
2.00	0.0	0.0	0.0	0.418	0.85	1.64
2.50	0.0	0.0	0.0	0.331	0.66	1.24
3.00	0.0	0.0	0.0	0.264	0.52	0.96
4.00	0.0	0.0	0.0	0.197	0.356	0.686
5.00	0.0	0.0	0.0	0.146	0.258	0.510
6.00	0.0	0.0	0.0	0.103	0.197	0.391
7.00	0.0	0.0	0.0	0.081	0.157	0.320
8.00	0.0	0.0	0.0	0.065	0.131	0.260
9.00	0.0	0.0	0.0	0.054	0.112	0.220
10.00	0.0	0.0	0.0	0.045	0.091	0.176

Source: Appendix D

6.5.2.1.2 V/H Ratios

Site-specific vertical hazard curves are determined using site-specific horizontal hazard curves and V/H spectral ratios. Two sources of information are used to develop the V/H ratios (Section 6.1.2). One source is empirical ground motion attenuation relations for the western U.S. (WUS). The second source is V/H ratios determined analytically through use of the stochastic point-source model coupled with the site-response model. V/H ratios based on each source of information are given equal weight in developing site-specific vertical hazard curves for the SFA. This section describes how these sources of information are used and combined.

The only empirical relations that provide horizontal and vertical components for both rock and soil site conditions are those of Abrahamson and Silva (1997 [DIRS 104205]) and Campbell and Bozorgnia (2003 [DIRS 183814]). Both relations are used to evaluate V/H ratios for Yucca Mountain; results for each are given equal weight. For the Abrahamson and Silva (1997 [DIRS 104205]) relation, an update that includes a normal faulting factor (Abrahamson and Becker 1997 [DIRS 166530]) is used. Because the alluvium at Yucca Mountain is quite stiff, results for

both rock (soft) and soil (deep firm) conditions were considered. Results for the two material classes are weighted based on the average shear-wave velocity in the upper 30 m (V_{S30}). Comparison of the V_{S30} associated with the rock and soil classes used in deriving the empirical relations to corresponding velocities for the SFA led to the judgment that weights of 0.8 (rock) and 0.2 (soil) are appropriate. Both empirical relations also provide predictions of ground motion for hanging wall and foot wall sites. Because the SFA is in the foot wall of the Bow Ridge fault and the hanging wall of the Paintbrush Canyon fault, results for both conditions are considered. Based on seismic source characterization (recurrence relation, maximum magnitude) for these two faults during the PSHA the Paintbrush Canyon fault has a stronger contribution to overall ground motion hazard (CRWMS M&O 1998 [DIRS 103731], Section 7). Therefore, weights of 0.75 (hanging wall) and 0.25 (foot wall) are adopted.

In addition to empirical information on V/H ratios for the WUS, modeling using the stochastic point-source model combined with the site-response model is also used to provide information to develop site-specific V/H ratios. For this second approach, first the point-source model is run using inputs that are appropriate for the Yucca Mountain vicinity (Table 6.5-2, Section 6.4.7). The model is run for three **M** values (5, 6, 7) and for each magnitude the distance and depth of the point-source are adjusted to produce a target PGA at the PSHA reference rock outcrop. The same suite of target PGA values, ranging from 0.1g to 10g, as was used in developing amplification factors is used for development of V/H ratios. Results of this exercise are summarized in Table 6.5-3.

The second phase of the approach consists of using the output of the first phase as control motions to the site-response model. The site-response model is run in a similar fashion as in computing amplification factors, except that 30 randomizations of velocity profile and dynamic property curves are used instead of 60 to incorporate aleatory variability. Given the approximations and binning to be implemented later in the approach, this reduced number of randomizations was judged to be adequate. Both horizontal and vertical response spectra for the SFA are determined in this approach using identical seismic source inputs. Site-specific response spectra for the SFA, for each of the 52 combinations of alluvium depth, velocity profile, and dynamic material property curves (Table 6.4-12, Section 6.4.4) and for each of the control motion inputs, are the output of this phase of the approach (Appendix D – Calculations/SFA Stochastic Point Source).

In computing V/H ratios using the empirical relations, incorrect values for a coefficient in both the relation of Abrahamson and Silva (1997 [DIRS 104205]) and of Campbell and Bozorgnia (2003 [DIRS 183814]) were used. For Abrahamson and Silva (1997 [DIRS 104205]) use of the incorrect coefficient values affects V/H ratios for periods greater than about 0.2 sec. From 0.2 to about 1 sec, the computed ratio is up to 20% higher using the incorrect values. For periods greater than 1 sec, the computed ratio is up to 40% lower. For the Campbell and Bozorgnia (2003 [DIRS 183814]) relation, use of the incorrect coefficient values affects the V/H ratio at periods less than about 0.8 sec and results in ratios that are 1% to 10% too low. The impact of these individual differences is reduced because different period ranges are affected for each relation and the results of the two empirical relations are combined. The impact is further reduced because the results based on the empirical approach are combined with results based on stochastic point-source ground motion modeling. Taken together, the use of the incorrect coefficients leads to an insignificant impact on the final V/H ratios. Note that the use of

incorrect coefficients only affects vertical ground motion for the SFA; because there are no empirical relations for at-depth motions, only the point-source modeling approach is used to determine vertical motions for the repository waste emplacement level.

As an example of the empirical V/H ratios, Figures 6.5.2-4 and 6.5.2-5 show results for Campbell and Bozorgnia (2003 [DIRS 183814]) computed for **M** 6 at rock (soft) and soil (deep firm) sites, respectively, for a suite of distances. Similarly Figure 6.5.2-6 shows an example of site-specific results computed for the South of Fault velocity profile A, 100 ft alluvium, and upper mean alluvium and tuff dynamic property curves, also for **M** 6. Similar trends are seen in the empirical and site-specific V/H ratios with the analytical ratios showing a peak at higher frequency than the empirical V/H ratios. Note that the apparent jump in V/H ratio from near distances (<2 km) to far distances (> 12 km) reflects the approach of incident angles to critical values at close distances (Figure 6.5.2-6). For the analytical results, distances range from 70 km (0.01g, horizontal motion) to 0 km (0.3g, horizontal motion), which adequately accommodates the hazard deaggregations in distance. The ratios range from about 0.3 to 0.5 at low frequency ($\leq$ 5 Hz) to about 1.3 near the peak at 40 Hz. As the verticals are run linearly, the increase in the ratio as loading level increases (source distance decreases) is due to reduced motions in the horizontal but also due to a decrease in incidence angle for the P-SV wavefield, dominated by compression-waves at high frequency.

As previously discussed, the model predictions of V/H ratios may be slightly unconservative at low-frequency and conservative at high frequency. While it is important to include site-specific effects on the vertical hazard, potential model deficiencies are mitigated with inclusion of empirical V/H ratios computed from WNA generic rock and soil site attenuation relations. Additionally a lower bound of 0.4 is placed on all V/H ratios based on examination of the full suite of **M**, *D*, and site conditions for which empirical relations are currently available.

Distance bins (e.g., Figures 6.5.2-5 and 6.5.2-6) differ between the empirical and analytical V/H ratios because the empirical ratios use a generic suite of distances while the analytical V/H ratios are region specific. Since the ratios vary slowly with distance, the differences in distances are not considered significant.

It is important to note that the site-specific and generic V/H ratios peak at very different frequencies (40 Hz and about 12 Hz respectively) with the site-specific having a much higher peak at high loading levels. Use of an empirical V/H ratio alone would underestimate the vertical hazard at high frequency, provided the model predictions are reasonably accurate.

In assigning the V/H ratios in the Approach 3 analysis, the source **M** and *D* changes significantly as probability changes. To accommodate the deaggregation in integrating the horizontal hazard with the distributions of V/H ratios, the **M** and *D* selection followed that listed in Table 6.5-4. Since the V/H ratios vary slowly with distance, only a smooth approximation to the hazard deaggregation is necessary. To adequately capture the change in **M** and *D* with AFE, only four distance bins were required: 1, 3, 8, and 31 km for the empirical and 2, 10, and 44 km for the analytical V/H ratios (Table 6.5-4). Empirical ratios use a generic suite of distances while the distances for the analytical V/H ratios are region specific.

The site-specific V/H ratios are weighted equally with the empirical ratios (Table 6.5-5). Since the empirical relations include hanging wall site locations, both hanging wall and not hanging wall V/H ratios were included with weights of 0.75 and 0.25 respectively, based on the local source characterization. The weights are summarized in Table 6.5-5.

Table 6.5-4. V/H **M** and *D* Ranges

F(Hz)	AFE	M	*D*	
			Empirical	Model
0.3	10^{-3} to 10^{-8}	7	31	44
0.5	10^{-3} to 10^{-8}	7	31	44
1.0	10^{-3} to 10^{-4}	7	31	44
	10^{-5}	6	3	2
	10^{-6} to 10^{-8}	6	1	2
2.0	10^{-3}	7	31	44
	10^{-4} to 10^{-6}	6	3	2
	10^{-7} to 10^{-8}	6	1	2
5.0	10^{-3}	5	8	10
	10^{-4} to 10^{-5}	6	3	2
	10^{-6} to 10^{-8}	6	1	2
10.0	10^{-3}	5	8	10
	10^{-4} to 10^{-5}	6	3	2
	10^{-6} to 10^{-8}	6	1	2
20.0	10^{-3}	5	8	10
	10^{-4} to 10^{-5}	6	3	2
	10^{-6} to 10^{-7}	6	1	2
100.0(PGA)	10^{-3}	5	8	10
	10^{-4} to 10^{-5}	6	3	2
	10^{-6} to 10^{-8}	6	1	2
PGV				

Table 6.5-5. V/H Ratio Weights

Case	Weight
Empirical	0.5
Model	0.5
Empirical	
Abrahamson and Silva	0.5
Hanging Wall	0.75
Not Hanging Wall	0.25
Campbell and Bozorgnia	0.5
Hanging Wall	0.75
Not Hanging Wall	0.25

Note: For the repository block only analytical (model) V/H ratios are available.

6.5.2.2 SFA Hazard Curves

Hazard curves were calculated for the SFA for horizontal and vertical ground motions. Inputs to the site response and point-source models for the SFA preclosure ground motions and hazard curves are summarized in Table 6.5-6.

Table 6.5-6. Model Inputs for Development of SFA Preclosure Ground Motions

Model Input	Source
RE horizontal response spectra for each AFE (1-2 Hz and 5-10 Hz)	Section 6.4.1.1; REs have DTN MO0211REDES103.000 [DIRS 170424]; DTN MO0208UNHZ5X10.000 [DIRS 163722]; DTN MO0211DERES104.000 [DIRS 170423]; DTN MO0308UNHAZ105.000 [DIRS 170425]; MO0206UNHAZ106.001 [DIRS 163723]; and DTN MO0209UNHAZ107.000 [DIRS 163724].
60 randomized velocity profiles for 13 cases; see Table 6.5-7.	Section 6.4.2.4
60 randomized sets of shear modulus reduction and damping curves for each of the 13 tuff and alluvium base case curves (four combinations). Each combination is run for each of the 52 modeling cases.	Section 6.4.4
Densities for tuff and alluvium	Section 5.6
Point-source parameters	Section 6.4.5

Software programs used to calculate the hazard curves are listed in Sections 6.1.4 and 6.1.5. Their use is further discussed in Appendix D.

As discussed in Section 6.4.2.4, four base case velocity profiles for the SFA were developed (Table 6.5-7). The depth of alluvium in the SFA thickens from zero at the base of Exile Hill to about 200 ft at the eastern boundary. Thus depending on the foundation design and layout of the SFA structures, the thickness of alluvium varies significantly.

Ground motion inputs are developed to provide a set of ground motions applicable to the entire SFA. To accommodate the effect of the varying thickness of alluvium, site-response modeling was carried out for multiple values of alluvium thickness. For the area represented by the Northeast of the Fault tuff velocity profile, alluvium thickness values of 30, 70, 100, and 200 ft were used. For the area represented by the South of the Fault tuff velocity profiles, thickness values of 30, 70, and 100 ft were used. The thickness values span the range found under important to safety facilities for the areas represented by the various tuff velocity profiles (SNL 2008 [DIRS 183779], Section 6.2.2.2, Figure 6.2-4). The result of these variations is a total of 13 profiles (Table 6.5-7).

Table 6.5-7. Initial SFA Base Case Velocity Profiles

1.	30 ft of alluvium over tuff, Northeast of the Fault
2.	70 ft of alluvium over tuff, Northeast of the Fault
3.	100 ft of alluvium over tuff, Northeast of the Fault
4.	200 ft of alluvium over tuff, Northeast of the Fault
5.	30 ft of alluvium over tuff, South of the Fault (South Case A)
6.	70 ft of alluvium over tuff, South of the Fault (South Case A)
7.	100 ft of alluvium over tuff, South of the Fault (South Case A)
8.	30 ft of alluvium over tuff, South of the Fault (South Case B)
9.	70 ft of alluvium over tuff, South of the Fault (South Case B)
10.	100 ft of alluvium over tuff, South of the Fault (South Case B)
11.	30 ft of alluvium over tuff, South of the Fault (South Case C)
12.	70 ft of alluvium over tuff, South of the Fault (South Case C)
13.	100 ft of alluvium over tuff, South of the Fault (South Case C)

Source: Table 6.4-12, DTN MO0708BCSSWVGB.001 [DIRS 184464]

In development of the SFA hazard curves, for each alluvium thickness, separate sets of hazard curves were developed for cases A, B, and C of the South of Fault tuff velocity profile (cases 5 to 13 above). These separate sets of hazard curves were then combined using the weights determined for the South of Fault tuff velocity profile cases (Section 6.4.5.1) to give a single set of hazard curves for each thickness of alluvium for the South of Fault area (Table 6.5-8, cases 5 through 7). For the Northeast of the Fault area, hazard curves were determined for each of the four values of alluvium thickness that were modeled (Table 6.5-8, cases 1 through 4).

Table 6.5-8. Cases Shown in Figures 6.5.2-7 to 6.5.2-27

Case	Description
1.	30 ft of alluvium over tuff, Northeast of the Fault
2.	70 ft of alluvium over tuff, Northeast of the Fault
3.	100 ft of alluvium over tuff, Northeast of the Fault
4.	200 ft of alluvium over tuff, Northeast of the Fault
5.	30 ft of alluvium over tuff, South of the Fault
6.	70 ft of alluvium over tuff, South of the Fault
7.	100 ft of alluvium over tuff, South of the Fault

Source: Not applicable

Mean horizontal and vertical hazard curves are plotted in Figures 6.5.2-7 to 6.5.2-27 for the seven combinations of alluvium and tuff for the SFA at PGA, 0.2, and 1.0 sec SA. The vertical seismic hazard curves are calculated using V/H ratios (Section 6.5.2.1.2). The data for these plots are contained in Appendix D.

The seven combinations of alluvium and tuff hazard curves are then combined to make two sets of curves, one for Northeast of the Fault and one for South of the Fault. The hazard curves for the four combinations of alluvium depth for Northeast of the Fault (cases 1 to 4 in Table 6.5-8) are enveloped. Similarly, hazard curves for the three combinations for South of the Fault (cases 5 to 7 in Table 6.5-8) are enveloped. Mean horizontal and vertical hazard curves are plotted in Figures 6.5.2-28 to 6.5.2-33 for the Northeast of the fault and South the fault velocity profiles, for PGA, 0.2, and 1.0 sec SA. The data for these plots are located in Appendix D.

Finally, these two sets of hazard curves were enveloped to produce one set of curves for the entire SFA. Mean horizontal and vertical seismic hazard curves for the SFA and PGA, 0.05, 0.1, 0.2, 0.5, 1.0, 2.0, and 3.3 sec SA are provided in Figures 6.5.2-34 to 6.5.2-41. The data for these plots are identified by DTN: MO0801HCUHSSFA.001 [DIRS 184802]. The mean horizontal PGV hazard curve for the SFA is shown in Figure 6.5.2-42. The data for this plot is also identified by DTN: MO0801HCUHSSFA.001 [DIRS 184802].

Details for the modeling and analyses described in this section are provided in Appendix D.

6.5.2.3 SFA Horizontal and Vertical Design Spectra

Horizontal and vertical UHS for the SFA are calculated from the hazard curves using the program HAZUHS. UHS are determined for AFEs of 10^{-3}, $5x10^{-4}$, 10^{-4}, 10^{-5}, $2x10^{-6}$, 10^{-6}, and 10^{-7} (Figures 6.5.2-43 to 6.5.2-49). The UHS are for 5%-damping. The UHS have been submitted to the TDMS and are identified by DTN MO0801HCUHSSFA.001 [DIRS 184802].

In computing UHS, hazard curve data for 3.3 sec SA were inadvertently used as if they represented hazard results for 3.0 sec SA. Thus, for periods greater than 2.0 sec, the SA amplitude is lower (has a higher AFE) than appropriate for the nominal UHS AFE. The applicability of the UHS for periods greater than 2 sec is, therefore, limited. Because design response spectra are based on the UHS, and design time histories are spectrally matched to the design response spectra, these outputs are similarly limited. Users of these outputs need to take into account this limitation when assessing their adequacy for a given intended purpose.

As the AFE decreases, the V/H ratio generally increases at short-periods. For AFEs of 10^{-4} and smaller, this results in the vertical UHS exceeding slightly the horizontal UHS at short periods (about 0.02 to 0.1 sec). This trend is consistent with the hazard deaggregation that shows large nearby events dominate the hazard at AFEs less than about 10^{-4}. For nearby events, short-period vertical motions are observed to exceed horizontal motions.

Details for the analyses described in this section are provided in Appendix D (Calculations/ SFA Horizontal SOILUHSI/HAZUHS).

6.5.2.3.1 5%-Damped Design Spectra

The mean horizontal and vertical UHS form the basis for the horizontal and vertical design spectra, respectively. For the horizontal design spectra, the corresponding UHS is taken and extrapolated to a response spectral period of 10 seconds based on a linear trend in log(period) and log(SA) at 2 and 3.3 sec. Each of these spectra is then digitized and interpolated to 298 points. Following an analysis to determine design spectra for damping values other than 5% (Section 6.5.2.3.2), all design response spectra are interpolated to 28 points and submitted to the TDMS. For the vertical design spectra, the process is the same except that the vertical UHS were smoothed slightly at their peaks during the step to extend them to a response spectral period of 10 seconds. The horizontal and vertical SFA design spectra are shown on Figures 6.5.2-50 to 6.5.2-57. The SFA seismic design spectral values (5%-damped) are listed in Tables 6.5-11 to 6.5-13. They are also identified by DTNs MO0706DSDR1E3A.000 [DIRS 181423], MO0706DSDR5E4A.001 [DIRS 181422], and MO0706DSDR1E4A.001 [DIRS 181421] for AFEs of 10^{-3}, $5x10^{-4}$, and 10^{-4}, respectively.

Details for the analyses described in this section are provided in Appendix D.

6.5.2.3.2 Development of Scaling Coefficients

In addition to 5%-damped seismic design spectra, SFA spectra at other damping values were calculated for the AFEs of 10^{-3}, $5x10^{-4}$ and 10^{-4}. Spectral ratios and damping coefficients as described below were computed and used to develop the suite of damped spectra. This methodology of estimating damped spectra at spectral damping ratios other than 5% is based on the approach developed by Idriss (1993). This approach provides two sets of relationships, one for damping ratios less than 5% and the other for damping ratios greater than 5%, which can be used to obtain the spectral ratios for a given damping value. Eq. 6-11 and Eq. 6-12 represent the model for damping less than or equal to 5% and damping greater than 5%, respectively. The 5%-damped spectral value when multiplied by this spectral ratio yields the spectral value at that damping ratio.

Spectral Ratio (f,D) = a1 - b1 LN(D) (f is frequency, D is damping and D <= 5%) (Eq. 6-11)

Spectral Ratio (f,D) = a2 - b2 LN(D) (f is frequency, D is damping and D > 5%) (Eq. 6-12)

Response spectra at damping values of 0.5%, 1%, 2%, 3%, 5%, 7%, 10%, 15% and 20% were generated using the computer program SPCTLRv1.0. This program uses an acceleration time history provided to it and generates response spectra at the damping value specified by the user. Spectra were generated using the five sets of spectrally-matched seismic design time histories (two horizontal and one vertical component) for each AFE (Section 6.5.2.5). Therefore, for each AFE there were 90 horizontal (5 sets x 2 components x 9 damping values) and 45 vertical (5 sets x 1 component x 9 damping values) response spectra that were generated. Each of these spectra had spectral acceleration values, computed in units of g, at 298 frequency points. The reason for using the design time histories was to ensure that the damped spectra were consistent with the hazard-consistent design spectra to which the time histories were matched.

For each response spectrum developed as described above, a ratio was calculated between the spectral acceleration value of that spectrum and the corresponding value for the corresponding

5%-damped spectrum. This ratio is termed the "data ratio" to differentiate it from the "smoothed ratio" described below. For each of the nine damping values listed above, the lognormal mean of the corresponding 30 horizontal (5 sets x 2 horizontal components x 3 return periods) and 15 vertical (5 sets x 1 vertical component x 3 return periods) ratios was computed. The calculations are shown on Excel files HORIZONTAL.xls and VERTICAL.xls included in Appendix D.

For each of the nine damping values, a best-fit curve was fit through the average data ratios using the trendline option in Excel. A sample curve is shown in Figure 6.5.4-58. The equation of this trendline was used to calculate smoothed spectral ratios at 28 frequency points. These 28 frequency points are considered to be a representative sample of the 298 frequency points at which the original spectra were developed.

Next, the smoothed spectral ratios computed above were divided into two groups, one for damping less than 5% and the other for damping greater than 5%. For each group, at each of the 28 frequency points, another best-fit line was fit through the set of smoothed spectral ratios computed above and the corresponding damping values to get an equation similar in form to Eq. 6-11 or Eq. 6-12. This equation was used to obtain the coefficients a1, b1, a2 and b2 that are site-specific and therefore used to obtain the site-specific damped spectra for the project.

Figure 6.5.4-59 shows an example of the best-fit line for smoothed spectral ratio versus damping for the horizontal component, damping less than 5%, and a structural frequency of 10Hz. The values of the coefficients a1 and b1 as obtained from the equation are 1.8744 and 0.6036, respectively.

Tables 6.5-9 and 6.5-10 show the site-specific coefficients developed for the horizontal and the vertical cases using the above procedure. Damping scaling for frequencies above 70 Hz was insignificant and neglected.

Table 6.5-9. Horizontal Coefficients

Structural Frequency (Hz)	a1	b1	a2	b2
0.1	1.0661	0.0237	1.2355	0.1371
0.2	1.2802	0.1348	1.4137	0.2576
0.298	1.3803	0.1927	1.4723	0.2982
0.404	1.4500	0.2384	1.5012	0.3191
0.498	1.4956	0.2667	1.5144	0.3292
0.6	1.5346	0.2938	1.5222	0.3356
0.706	1.5677	0.3176	1.5263	0.3395
0.793	1.5907	0.3346	1.5279	0.3415
0.89	1.6133	0.3517	1.5284	0.3427
1	1.6353	0.3688	1.5279	0.3434
2.01	1.7560	0.4689	1.5087	0.3369
2.98	1.8121	0.5201	1.4886	0.3271
4.04	1.8461	0.5539	1.4700	0.3173
4.98	1.8638	0.5734	1.4555	0.3093

Structural Frequency (Hz)	a1	b1	a2	b2
5.99	1.8746	0.5873	1.4417	0.3014
7.05	1.8797	0.5963	1.4288	0.2938
8.11	1.8805	0.6013	1.4171	0.2867
9.11	1.8782	0.6034	1.4070	0.2804
10	1.8744	0.6036	1.3985	0.2751
20	1.8400	0.5518	1.3236	0.2243
30.5	1.6513	0.4693	1.2691	0.1844
40.4	1.6100	0.3727	1.2193	0.1465
49.8	1.3910	0.2862	1.1797	0.1156
59.9	1.2636	0.1943	1.1403	0.0845
70.5	1.1358	0.1012	1.1023	0.0542
81.1	1.0000	0.0000	1.0000	0.0000
91.1	1.0000	0.0000	1.0000	0.0000
100	1.0000	0.0000	1.0000	0.0000

Source: Appendix D

Table 6.5-10 Vertical Coefficients

Structural Frequency (Hz)	a1	b1	a2	b2
0.1	1.0598	0.0169	1.1902	0.1112
0.2	1.2607	0.1267	1.3747	0.2335
0.298	1.3620	0.1867	1.4330	0.2747
0.404	1.4356	0.2331	1.4618	0.2963
0.498	1.4852	0.2658	1.4756	0.3074
0.6	1.5283	0.2952	1.4844	0.3151
0.706	1.5654	0.3213	1.4900	0.3205
0.793	1.5915	0.3400	1.4929	0.3236
0.89	1.6172	0.3588	1.4951	0.3262
1	1.6425	0.3777	1.4966	0.3284
2.01	1.7831	0.4890	1.4961	0.3341
2.98	1.8496	0.5467	1.4907	0.3333
4.04	1.8906	0.5850	1.4845	0.3306
4.98	1.9124	0.6074	1.4787	0.3276
5.99	1.9264	0.6236	1.4723	0.3239
7.05	1.9339	0.6345	1.4655	0.3198
8.11	1.9363	0.6410	1.4586	0.3155
9.11	1.9352	0.6442	1.4520	0.3112
10	1.9322	0.6451	1.4460	0.3073
20	1.8344	0.5965	1.3745	0.2601
30.5	1.7057	0.5132	1.3042	0.2137
40.4	1.5621	0.4145	1.2298	0.1649

Structural Frequency (Hz)	a1	b1	a2	b2
49.8	1.4363	0.3257	1.1652	0.1228
59.9	1.3044	0.2311	1.0975	0.0788
70.5	1.1723	0.1352	1.0293	0.0348
81.1	1.0000	0.0000	1.0000	0.0000
91.1	1.0000	0.0000	1.0000	0.0000
100	1.0000	0.0000	1.0000	0.0000

Source: Appendix D

These coefficients were used to compute the spectral ratios for different damping values using Eq. 6-11 and Eq. 6-12. These ratios are termed the "model ratios." These model ratios were multiplied with the 5% target spectra to obtain the "model spectra" at damping other than 5%.

6.5.2.3.3 Design Spectra at Other Dampings

Design spectra for damping values of 0.5, 1, 2, 3, 7, 10, 15, and 20% are determined for the SFA by developing scaling factors to adjust the 5%-damped spectra. As described in Section 6.5.2.3.2, to develop site-specific scaling factors, time histories that are spectrally matched to the 5%-damped design spectrum are used to determine response spectra at other damping values. These time histories are developed by adjusting recorded accelerograms that have magnitude and distance characteristics consistent with those shown by seismic hazard deaggregation to control the hazard at the site for a given AFE (Section 6.5.2.5). By using time histories that are spectrally matched to the 5%-damped design spectra, employment of the resulting scaling factors leads to response spectra at other damping values that are consistent with the time histories for design analyses.

Using the scaling factors described in Section 6.5.2.3.2, both horizontal and vertical design response spectra at 10^{-3}, $5x10^{-4}$, and 10^{-4} AFE were computed for additional damping values of 0.5, 1.0, 2.0, 3.0, 7.0, 10.0, 15.0, and 20.0% (Figures 6.5.2-60 to 6.5.2-65). These additional design spectra are consistent with the design time histories because the scaling factors were developed using those site-specific time histories. Note also that the time histories were developed to have phase and duration characteristics similar to those earthquakes that are the dominant contributors to hazard at the site (Section 6.5.4.3). The calculations are documented in Microsoft Excel ® workbooks HORIZONTAL.xls and VERTICAL.xls (Appendix D).

6.5.2.3.4 Comparison With 2004 SFA Unconditioned Design Spectra

Also shown on Figures 6.5.2-50 to 6.5.2-55 are the horizontal and vertical design spectra calculated in 2004 (BSC 2004 [DIRS 170027]). The velocity data forming the basis for profiles used in site-response modeling supporting these earlier results were collected from the area southwest of the Exile Hill splay fault. Also, the 2004 spectra were developed using Approach 2B from NUREG/CR-6728 (McGuire et al. 2001 [DIRS 157510], Section 6.1), rather than Approach 3, and the site-response control motions were not conditioned to reflect updated characterization of extreme ground motion at Yucca Mountain. At AFEs of 10^{-3} and $5x10^{-4}$, the supplemental SFA horizontal design spectra are lower at short periods (< about 0.1 sec), comparable at intermediate periods (about 0.1 to 1 sec), and slightly higher at longer periods (>

about 1 sec) (Figures 6.5.2-50 and 6.5.2-51). At 10^{-4} AFE, the supplemental horizontal design spectrum is lower at all periods except in the range of about 1.5 to 2.5 sec for which it is negligibly higher (Figure 6.5.2-52). In a similar fashion, the supplemental vertical design spectra at AFEs of 10^{-3} and $5x10^{-4}$ are lower than the 2004 spectrum at short periods (< 0.2 to 0.3 sec) and long periods (> 2 sec) and higher at periods between about 0.3 and 2 sec (Figures 6.5.2-53 and 6.5.2-54). At 10^{-4} AFE, the supplemental vertical design spectrum is significantly lower than the 2004 spectrum at short periods (Figure 6.5.2-55). The difference at PGA is more than a factor of two. In Figures 6.5.2-56 and 6.5.2-57, the SFA damped horizontal and vertical design spectra are summarized.

Table 6.5-11. Summary of SFA Seismic Design Spectra (5%-Damped) in g's at 10^{-3} AFE

Period (sec)	Horizontal Motion (Spectral Acceleration, g)	Vertical Motion (Spectral Acceleration, g)
0.010 (PGA)	0.33	0.22
0.050	0.59	0.50
0.10	0.82	0.54
0.20	0.80	0.43
0.50	0.55	0.30
1.0	0.29	0.16
2.0	0.14	0.074
3.3	0.057	0.027

Source: DTN: MO0706DSDR1E3A.000 [DIRS 181423]

Table 6.5-12. Summary of SFA Seismic Design Spectra (5%-Damped) in g's at $5x10^{-4}$ AFE

Period (sec)	Horizontal Motion (Spectral Acceleration, g)	Vertical Motion (Spectral Acceleration, g)
0.010 (PGA)	0.45	0.32
0.050	0.83	0.77
0.10	1.2	0.085
0.20	1.1	0.64
0.50	0.80	0.43
1.0	0.44	0.23
2.0	0.19	0.11
3.3	0.086	0.044

Source: DTN: MO0706DSDR5E4A.000 [DIRS 181422]

Table 6.5-13. Summary of SFA Seismic Design Spectra (5%-Damped) in g's at 10^{-4} AFE

Period (sec)	Horizontal Motion (Spectral Acceleration, g)	Vertical Motion (Spectral Acceleration, g)
0.010 (PGA)	0.91	0.72
0.050	1.6	1.8
0.10	2.4	2.2
0.20	2.3	1.5
0.50	1.6	0.92

Period (sec)	Horizontal Motion (Spectral Acceleration, g)	Vertical Motion (Spectral Acceleration, g)
1.0	0.96	0.51
2.0	0.46	0.25
3.3	0.18	0.092

Source: DTN: MO0706DSDR1E4A.000 [DIRS 181421]

6.5.2.4 SFA Parameter Sensitivities

To clearly illustrate the impacts of site parameters on the SFA design motions, a suite of sensitivity analyses was conducted. The analyses included isolating the effects of: 1) depth of alluvium (30, 70, 100, and 200 ft) to tuff; 2) base case velocity profiles (Northeast of Fault; South of Fault cases A, B, C); 3) modulus reduction and hysteretic damping curves; and 4) depth and V_S of the Calico Hills Formation, the unit above the assumed reference rock outcrop (top of Prow Pass).

6.5.2.4.1 Effects of Alluvium Depth

The Northeast of Fault profile (Section 6.4.2.5), which spans the largest range in mean depths to tuff (30 to 200 ft), is used to illustrate the effects of alluvium depth on the UHS at AFEs of 10^{-3}, $5x10^{-4}$, 10^{-4}, 10^{-5}, and 10^{-6}. The hazard estimates include the weighting over G/G_{max} and hysteretic damping curves (Section 6.4.5) to isolate the potential impacts of alluvium depth on design ground motion in a manner consistent with the development of the final design motions. Figures 6.5.2-66 to 6.5.2-70, beginning with the highest AFE (10^{-3}; Figure 6.5.2-66), shows the expected trends. The shallow alluvium (30 ft depth) is associated with the highest motions at high-frequency, crossing over near 5 Hz where the shallowest depth to alluvium results in the lowest motions. For the deepest alluvium considered for the north-east profile (200 ft), the converse is the case with the deep alluvium producing the highest motions at low-frequency (Figure 6.5.2-66). Finally, at very low frequency, expected motions for all depths become similar. At low-frequency the wavelengths are sufficiently long, coupled with the relatively low loading level resulting in little profile softening, such that the low frequency energy does not "see" the upper 200 ft of the profile.

At the lower probabilities, the same trends continue but with larger differences as motions increase (AFE decreases). At very low exceedance probability (e.g., 10^{-6}; Figure 6.5.2-70), the differences at low-frequency persist to the lowest frequency at which the reference rock hazard was computed (0.3 Hz, Section 6.4.1). At high loading levels the deeper alluvium has softened sufficiently, shortening the wavelength such that motion near 0.3 Hz is sensitive to the upper 30 to 200 ft of the profile. At 10^{-6} AFE, the expected peak accelerations on alluvium range from about 2 to 3 g, reflecting extremely high loading levels (Figure 6.5.2-70). It is important to emphasize the likely counterintuitive result of a fully probabilistic site-specific hazard analysis (e.g., Approaches 3 and/or 4) for very low AFEs; the resulting UHS can result in motions, which exceeds the soil's capacity to transmit such a high level of motion. This is necessarily the case and is due to the aleatory (and perhaps epistemic) variability accommodated in fully probabilistic site-specific dynamic material properties. The same issue would apply to a PSHA conducted using empirical soil attenuation relations (e.g., western North America, Abrahamson and Shedlock 1997 [DIRS 164486]). At low AFEs, the resulting UHS will easily exceed the capacity

of a generic soil (e.g., Los Angeles basin, Silva et al. 1999 [DIRS 164081]) to transmit the motions, based on deterministic analyses. Clearly, for fragility analyses, which consider AFEs at or below about 10^{-5}, depending on the local soil conditions, guidelines would be appropriate in establishing extreme soil motions or a probability plateau below which the motions remain constant (hazard curves become vertical).

6.5.2.4.2 Effects of Base Case Profile

The four base case profiles (Northeast of Fault and South of Fault A, B, and C; Section 6.4.2.5) reflect both average or mean differences in velocities due to deterministic spatial variability, northeast and south of the Exile Hill fault splay, as well as epistemic uncertainty in the mean profile for the area south of the fault splay. The three south profiles (A, B, and C) are intended to capture the range in interpretations (principally extrapolations) due to the limited amount of geophysical data as well as depth of investigation available for the area south of the fault splay. Figures 6.5.2-71 to 6.5.2-75 compare the estimates of mean UHS computed for the four profiles at AFEs of 10^{-3} to 10^{-6}. To be consistent with the final design spectra, each profile UHS reflects weighted mean hazard curves for the four combinations of modulus reduction and hysteretic damping curves as well as enveloped hazard curves over alluvium depths. For the lowest motions, 10^{-3} AFE, Figure 6.5.2-71 shows little difference between the profiles for frequencies above about 3 to 4 Hz and the Northeast of Fault profile exceeding the South of Fault profiles by about 5% to 10% at lower frequencies. Part of the effect at lower frequencies is related to inclusion of site response for 200 ft of alluvium for the Northeast of Fault profile (Section 6.5.2.4.1). This trend generally persists throughout the suite of hazard levels showing small to moderate differences over the entire frequency range, 0.3 Hz to 100 Hz (Figures 6.5.2-71 to 6.5.2-75). Final design motions, to be applicable to the entire SFA are taken as envelopes of the Northeast of Fault UHS and the weighted (over profiles A, B, and C) mean South of Fault UHS.

6.5.2.4.3 Effects of Nonlinear Dynamic Material Properties

To accommodate epistemic uncertainty in G/G_{max} and hysteretic damping curves in both the alluvium as well as tuff, two base case curves were developed for each material (Section 6.4.4). Because laboratory dynamic testing cannot replicate *in situ* conditions due to both sampling issues as well as limitations of available test devices (e.g., sample size, confining pressure, test configuration), multiple mean curves reflect reasonable and justifiable uncertainty in high strain behavior for the alluvium and tuff units above the Calico Hills Formation (Section 6.4.4). The mean curves for alluvium (UMA and LMA) and tuff (UMT and LMT) result in four possible combinations of alluvium and tuff. The designation, "upper" and "lower", taken for convenience, refers to the modulus reduction curves with "upper" being significantly more linear (i.e., less modulus reduction) at a given strain level than the lower mean tuff or alluvium, respectively. Because the respective curves are not considered equally probable (i.e., they do not have an equal likelihood of reflecting the true state of in situ material properties), weights were applied in developing the design spectra (Section 6.4.4.3). As in the earlier comparisons, to illustrate the effects of the G/G_{max} and hysteretic damping curves on design motions, envelopes over alluvium depths were taken as well as weights over south profiles A, B, and C (Section 6.4.5.1). Finally, as in the design motions, envelopes were taken over hazard computed for the northeast and south (weighted) profiles.

Figures 6.5.2-76 to 6.5.2-80 compare estimates of UHS for the SFA (Northeast of Fault and South of Fault combined) over all four combinations of the tuff and alluvium modulus reduction and damping curves at AFEs of 10^{-3} to 10^{-6}. As expected, the more linear curves generally result in larger high-frequency ground motion and smaller low-frequency motion. At lower probabilities ($\leq 10^{-4}$) the differences become quite large reflecting a range of about two at high frequency ($\geq$ 10 Hz) (Figures 6.5.2-78 to 6.5.2-80). Clearly, for the SFA, as for many sites, the most significant uncertainty in developing estimates of design motions lies in the nonlinear dynamic properties. This is particularly the case at high-frequency and at high loading levels.

6.5.2.4.4 Effects of Calico Hills Formation Properties

The Calico Hills Formation lies immediately above the reference rock outcrop or the control point, which was taken as the top of the Prow Pass Tuff (Section 6.4.2.7). For the base-case velocity profiles, the Calico Hills Formation has a mean or base-case depth of 1,300 ft, thickness of 400 ft, and V_S of 5,600 ft/sec. For the South of Fault profile A, the highest weighted South fo Fault profile, the Calico Hills Formation represents a significant increase in V_S, about 4,800 to 5,600 ft/sec, an increase of about 20%. For the Calico Hills Formation sensitivity analysis, the alluvium depth of 100 ft and the G/G_{max} and hysteretic damping curve combination of UMT and LMA were selected. The alluvium depth of 100 ft reflects a reasonable average over much of South of Fault area (Section 6.4.2.5). Also, the combination of modulus reduction and hysteretic damping curves for alluvium and tuff were selected to allow the most energy into the alluvium (UMT curves) while providing the most nonlinear alluvium response (LMA curves). This combination was intended to maximize the potential effects of the underlying Calico Hills Formation on the response of the alluvium, the major controlling factor in developing estimates of design motions.

To illustrate the sensitivity of the Calico Hills Formation on surface motions, UHS's have been computed for perturbations on depth to the top of the unit (1,300 ft $\pm$ 500 ft), thickness (400 ft $\pm$ 200 ft), and V_S (5,600 ft/sec $\pm$ 500 ft/sec) (Figures 6.5.2-81 to 6.5.2-85). These ranges are intended to conservatively encompass the ranges in epistemic uncertainty in mean Calico Hills Formation wave propagation properties (Section 6.4.2). Figures 6.5.2-81 to 6.5.2-85 compare the UHS (AFEs of 10^{-3}, $5x10^{-4}$, 10^{-4}, 10^{-5}, 10^{-6}, and 10^{-7}) computed for the Calico Hills Formation property permutations with base-case values. Not unexpectedly, the impacts of Calico Hills Formation wave propagation properties are quite small, a range of about 5 to 10%, at the high to moderate AFEs (e.g., 10^{-3} and 10^{-4}). At very low AFEs (10^{-5} and 10^{-6}) and at intermediate frequencies ($\approx$ 2 to 10 Hz), the range increases to about 10 to 15%. In general, the sensitivity to Calico Hills Formation wave propagation properties is considered quite small over a wide range in structural frequency as well as loading levels.

6.5.2.5 SFA Design Time Histories

In this section, the development of supplemental time histories for preclosure analyses is presented. Five sets of three-component time histories were developed for the SFA at 10^{-3}, $5x10^{-4}$, and 10^{-4} AFE resulting in a total of 15 sets. Each set of time histories is developed to closely match the design spectrum at the appropriate AFE. This approach is consistent with how the time histories are to be used in design analyses.

To develop each set of time histories, strong ground motion recordings from past earthquakes are used as input in the spectral matching process to provide time histories with phase and duration characteristics of observed ground motion. The seed strong ground motion recordings are chosen from the NUREG/CR-6728 (McGuire et al. 2001 [DIRS 157510], Appendix B) analysis time history database (Table 6.5-14). Acceleration plots of the seed time histories used to match the design spectra at 10^{-3} and $5x10^{-4}$ AFE are shown in Figures 6.5.2-86 to 6.5.2-90. Corresponding seed plots used to match the beyond design basis spectra at 10^{-4} AFE are shown in Figures 6.5.2-91 to 6.5.2-95.

The seed time histories are chosen based on the deaggregated hazard at Yucca Mountain, as described in Section 6.4.1.1. Assignment of a horizontal component as H1 or H2 follows the assignment in the NUREG/CR-6728 (McGuire et al. 2001 [DIRS 157510], Appendix B) time history database.

Design time histories described in this report follow applicable recommendations in NUREG/CR-6728 (McGuire et al. 2001 [DIRS 157510], Section 5.3) as outlined below:

- The artificial accelerogram should achieve approximately a mean-based fit to the target spectrum. The average ratio of the spectral acceleration calculated from the accelerogram to the target, calculated frequency by frequency, is only slightly greater than one to ensure there are no significant gaps and the result is not biased high with respect to the target.

- Records should have a sufficiently small frequency increment and sufficiently high maximum frequency (or alternatively time increment and maximum duration). The total duration of the record can be increased by zero packing to satisfy these frequency requirements. It is recommended that records have a maximum frequency increment of 0.05 Hz with a Nyquist frequency of at least 50 Hz or a time increment of at most 0.01 sec for a total duration of 20 sec. We used a time increment at 0.005 for all cases.

- Spectral accelerations at 5 percent damping should be computed at a minimum of 100 points per frequency decade, uniformly spaced over the log frequency scale from 0.1 Hz to 50 Hz or the Nyquist frequency. The computed 5%-damped response spectrum of the accelerogram (if one artificial motion is used for analysis) or the average of all accelerograms (if a suite of motions is used for analysis) should not fall more than 10 percent below the target spectrum at any one frequency point. No more than 9 adjacent spectral points may be allowed to fall below the target spectrum at any frequency. This corresponds to a moving frequency window of ± 10 percent centered on the frequency.

- The computed 5%-damped response spectrum of the artificial ground motion (if one motion is used for analysis) or the average of the 5%-damped response spectra (if a suite of motions is used for analysis) should not exceed the target spectrum by more than 30 percent in the frequency range between 0.2 Hz and 50 Hz.

- The upper limit for the zero-lag cross-correlation coefficient between any two design ground motions (acceleration time histories) should be 0.3.

These criteria ensure that no gaps in the power spectral density or Fourier amplitude spectrum will occur over a significant frequency range.

Table 6.5-14. Summary of Input Strong Ground Motion Recordings

	Earthquake	Date	Magnitude (M)	Station	Distance (km	PGA (g)			PGV (cm/sec)			Used as Input Time Histories for:
						H1	H2	V	H1	H2	V	
1	Whittier Narrows, CA	10/1/87	6.0	Calabasas-N. Las Virgenes Road (see note)	53.3	0.119	0.075	0.086	2.8	1.5	2.7	Preclosure time histories for the SFA at 10^{-3} and $5x10^{-4}$ AFEs.
2	Whittier Narrows, CA	10/1/87	6.0	Pasadena Blvd. – CIT Calif Blvd.	15.5	0.177	0.271	0.171	8.1	15.4	7.0	Preclosure time histories for the SFA at 10^{-3} and $5x10^{-4}$ AFEs.
3	Cape Mendocino	4/25/92	7.1	Shelter Cove	33.8	0.648	0.585	0.182	8.9	9.2	3.9	Preclosure time histories for the SFA at 10^{-4} AFE.
4	Landers, CA	6/28/92	7.3	Silent Valley – Poppet Flat	51.7	0.153	0.138	0.134	4.5	5.2	5.4	Preclosure time histories for the SFA at 10^{-4} AFE.
5	Landers, CA	6/2/92	7.3	Twenty Nine Palms	42.2	0.207	0.180	0.125	5.4	4.6	4.8	Preclosure time histories for the SFA at 10^{-4} AFE.
6	Northridge, CA	1/17/94	6.7	Rancho Cucamonga-Deer Canyon	80.0	0.071	0.051	0.025	4.2	5.9	2.2	Preclosure time histories for the SFA at 10^{-3} and $5x10^{-4}$ AFEs.
7	Northridge, CA	1/17/94	6.7	Wrightwood-Jackson Flat	68.4	0.056	0.037	0.034	10.0	7.0	5.8	Preclosure time histories for the SFA at 10^{-3} and $5x10^{-4}$ AFEs.
8	Chi-Chi, Taiwan	9/20/99	7.6	Tap 036	95.6	0.039	0.03	0.017	6.1	7.6	6.9	Preclosure time histories for the SFA at 10^{-3} and $5x10^{-4}$ AFEs.
9	Koaceli, Turkey	8/17/99	7.4	Iznik	29.7	0.103	0.136	0.083	16.5	28.8	7.7	Preclosure time histories for the SFA at 10^{-4} AFE.
10	Kocaeli, Turkey	8/17/99	7.4	Mecidiyekoy	62.3	0.129	0.132	0.084	5.0	8.9	2.4	Preclosure time histories for the SFA at 10^{-4} AFE.

Source: McGuire et al. (2001 [DIRS 157510], Appendix B, Tables B-1 and B-2)

NOTES: Record #1 has been modified for CEUS conditions (McGuire et al. 2001 [DIRS 157510], Appendix B).

6.5.2.5.1 10^{-3} AFE

For preclosure design at the SFA for an AFE of 10^{-3}, five sets of three-component time histories were developed by spectrally matching to the SFA seismic design spectra following the guidelines outlined above in Section 6.5.2.5. Inputs to this analysis for these motions are summarized below in Table 6.5-15.

Table 6.5-15. Analysis Inputs for Development of Seismic Design Time Histories with an AFE of 10^{-3} for SFA

Analysis Input	Source
Set #1: Strong Ground Motion Recording of 1994 Northridge Earthquake, Wrightwood Jackson Flat	Table 6.5-14, Number 7; NUREG-CR-6728 (McGuire et al. 2001 [DIRS 157510], Appendix B)
Set #2: Strong Ground Motion Recording of 1994 Northridge Earthquake, Rancho Cucamonga Deer Canyon	Table 6.5-14, Number 6; NUREG-CR-6728 (McGuire et al. 2001 [DIRS 157510], Appendix B)
Set #3: Strong Ground Motion Recording of 1987 Whittier Narrows Earthquake, Calabasos–N. Las Virg.	Table 6.5-14, Number 1; NUREG-CR-6728 (McGuire et al. 2001 [DIRS 157510], Appendix B)
Set #4: Strong Ground Motion Recording of 1987 Whittier Narrows Earthquake, Pasadena – California Blvd. CIT	Table 6.5-14, Number 2; NUREG-CR-6728 (McGuire et al. 2001 [DIRS 157510], Appendix B)
Set #5 Strong Ground Motion Recording of 1999 Chi-Chi, Taiwan Earthquake, Tap 036	Table 6.5-14, Number 8; NUREG-CR-6728 (McGuire et al. 2001 [DIRS 157510], Appendix B)
SFA Seismic Design Response Spectra with an AFE of 10^{-3}	Table 6.5-11; seismic design spectra have DTN MO0706DSDR1E3A.000 [DIRS 181423]

Software used in the analysis for this case consists of:

- INTERPOL V. 1.0 (Software Tracking Number 10944-1.0-00) [DIRS 163305]
- RASCAL SET V1.1 – module RASCALS V. 5.5 (Software Tracking Numbers 11232-1.1-00, 11232-1.1-01) [DIRS 184513, DIRS 184053]
- BASE4 V. 4.0 (Software Tracking Number 10940-4.0-00) [DIRS 163293]
- MAXMIN V. 1.0 (Software Tracking Number 10945-1.0-00) [DIRS 163309]
- SPCTLR V. 1.0 (Software Tracking Number 10947-1.0-00) [DIRS 163321]
- POST RASCAL V 1.0 – module SMRATIO V. 1.0 (Software Tracking Number 11231-1.0-00) [DIRS 182467]
- CORBB V. 1.0 (Software Tracking Number 10941-1.0-00) [DIRS 163295]
- DUR V. 1.0 (Software Tracking Number 10942-1.0-00) [DIRS 163303

INTERPOL is used to interpolate the SFA seismic design spectra to several hundred frequencies required for spectral matching. RASCAL SET module RASCALS is used to spectrally match the input strong ground motion recording to the SFA design spectra. The resulting spectrally-

matched acceleration time history is baseline corrected and integrated using BASE4. Outputs from BASE4 are baseline corrected acceleration, velocity, and displacement time histories. MAXMIN is used to calculate the PGA and PGV of the time histories. SPCTLR is used to calculate the 5%-damped response spectra of the time histories. The ratio between the time histories' response spectra and the target spectra are computed using SMRATIO. Cross-correlation statistics between time history components are computed using CORBB. Arias intensity versus duration is computed using DUR. This process is followed for two horizontal components and one vertical component. The data files for this analysis are in Appendix D (CALCULATIONS/SFA Time Histories).

Two of the five input strong ground motions are rock sites: the 1994 Northridge earthquake, Wrightwood Jackson Flat station recording (#7; Table 6.5-14), and the 1994 Northridge earthquake, Rancho Cucamonga Deer Canyon station recording (#6; Table 6.5-14). These records, (**M** 6.7, R 68.4 km and R 80.0 km, respectively) were selected from the M: 6.5, D: 50 – 100 km bin of the NUREG/CR-6728 (McGuire et al. 2001 [DIRS 157510], Appendix B) analysis time history database.

The next two of the five input strong ground motions are the 1987 Whittier Narrows earthquake, Calabasas North Las Virgenes station recording (#1; Table 6.5-14), a rock site, and the 1987 Whittier Narrows earthquake, Pasadena - California Blvd. Station recording (#2, Table 6.5-14), a soil site. These records, (**M** 6.0, R 53.3 km and R 15.5 km, respectively), were selected from the M: 6.0, D: 0 – 50 km and D: 50 – 100 km bins of the NUREG/CR-6728 (McGuire et al. 2001 [DIRS 157510], Appendix B) analysis time history database.

The last of the five input strong motions is a rock site, the 1999 Chi-Chi, Taiwan earthquake, Tap 036 Station recording (#8; Table 6.5-14). This record (**M** 7.6, R 95.6 km was selected from the M: 7.5, D: 50 – 100 km) bin of the NUREG/CR-6728 (McGuire et al. 2001 [DIRS 157510], Appendix B) analysis time history database.

The model magnitude and distance determined from the joint deaggregation of the hazard at 10^{-3} AFE gives a **M** 7.4 event at 51 km in the 1-2 Hz frequency range and a **M** 5.2 event at 9 km in the 5-10 Hz frequency range (Table 6.4-1). Following NUREG/CR-6728 (McGuire et al. 2001 [DIRS 157510], Section 5), when matching to a UHS (one spectrum instead of the two deaggregated reference events), it is recommended that the strong ground motion duration be the longer duration associated with the low-frequency event. Thus, four of the five seed strong motion records are for larger more distant earthquakes; one is from a smaller less distant earthquake.

For 10^{-3} AFE, the spectral match to the design (target) spectra, a corresponding plot of the ratio between the time histories' response spectra and the target spectra, and the resulting acceleration, velocity, and displacement time histories are shown in Figures 6.5.2-96 to 6.5.2-140. These results have been submitted to TDMS and have DTN MO0706TH1E3APE.001 [DIRS 182460].

6.5.2.5.2 $5x10^{-4}$ AFE

For preclosure design at the SFA at $5x10^{-4}$ AFE, five sets of three-component time histories were developed by spectrally matching to the SFA seismic design spectrum following the guidelines

outlined above in Section 6.5.2.5. Inputs to this analysis for these motions are summarized in Table 6.5-16. Because deaggregation of the seismic hazard at $5x10^{-4}$ AFE shows that earthquakes dominating the hazard are similar to those at $1x10^{-3}$ AFE (Table 6.4-1), the input time histories used to match the 10^{-3} AFE seismic design spectra are also used for the time histories with a $5x10^{-4}$ AFE.

Table 6.5-16. Analysis Inputs for Development of SFA Seismic Design Time Histories with an AFE of $5x10^{-4}$

Analysis Input	Source
Set #1: Strong Ground Motion Recording of 1994 Northridge Earthquake, Wrightwood Jackson Flat	Table 6.5-14, Number 7; NUREG-CR-6728 (McGuire et al. 2001 [DIRS 157510], Appendix B)
Set #2: Strong Ground Motion Recording of 1994 Northridge Earthquake, Rancho Cucamonga Deer Canyon	Table 6.5-14, Number 6; NUREG-CR-6728 (McGuire et al. 2001 [DIRS 157510], Appendix B)
Set #3: Strong Ground Motion Recording of 1987 Whittier Narrows Earthquake, Calabasos–N. Las Virg.	Table 6.5-14, Number 1; NUREG-CR-6728 (McGuire et al. 2001 [DIRS 157510], Appendix B)
Set #4: Strong Ground Motion Recording of 1987 Whittier Narrows Earthquake, Pasadena – California Blvd. CIT	Table 6.5-14, Number 2; NUREG-CR-6728 (McGuire et al. 2001 [DIRS 157510], Appendix B)
Set #5 Strong Ground Motion Recording of 1999 Chi-Chi, Taiwan Earthquake, Tap 036	Table 6.5-14, Number 8; NUREG-CR-6728 (McGuire et al. 2001 [DIRS 157510], Appendix B)
SFA Seismic Design Response Spectra with an AFE of 10^{-3}	Table 6.5-12; seismic design spectra have DTN MO0706DSDR5E4A.001 [DIRS 181422],

For $5x10^{-4}$ AFE, the spectral match to the design (target) spectra, a corresponding plot of the ratio between the time histories' response spectra and the target spectra, and the resulting acceleration, velocity, and displacement time histories are shown in Figures 6.5.2-141 to 6.5.2-185. These results have been submitted to TDMS and have DTN MO0706TH5E4APE.001 [DIRS 181961].

6.5.2.5.3 10^{-4} AFE

Five sets of three-component time histories were developed for SFA preclosure design analyses at 10^{-4} AFE by spectrally matching to the SFA seismic design spectra following the guidelines outlined above in Section 6.5.2.5. Inputs to this analysis for these motions are summarized in Table 6.5-17.

Table 6.5-17. Analysis Inputs for Development of SFA Seismic Design Time Histories with an AFE of 10^{-4}

Analysis Input	Source
Set #1: Strong Ground Motion Recording of 1999 Kocaeli, Turkey, Iznik	Table 6.5-14, Number 9; NUREG-CR-6728 (McGuire et al. 2001 [DIRS 157510], Appendix B)
Set #2: Strong Ground Motion Recording of 1992 Landers Earthquake, TwentyNine Palms	Table 6.5-14, Number 5; NUREG-CR-6728 (McGuire et al. 2001 [DIRS 157510], Appendix B)
Set #3: Strong Ground Motion Recording of 1992 Cape Mendecino Earthquake, Shelter Cove	Table 6.5-14, Number 3; NUREG-CR-6728 (McGuire et al. 2001 [DIRS 157510], Appendix B)
Set #4: Strong Ground Motion Recording of 1992	Table 6.5-14, Number 4; NUREG-CR-6728 (McGuire et

Analysis Input	Source
Landers Earthquake, Silent Valley	al. 2001 [DIRS 157510], Appendix B)
Set #5 Strong Ground Motion Recording of 1999 Kocaeli, Turkey, Mecidiyekoy	Table 6.5-14, Number 10; NUREG-CR-6728 (McGuire et al. 2001 [DIRS 157510], Appendix B)
SFA Seismic Design Response Spectra with an AFE of 10^{-3}	Table 6.5-13; seismic design spectra have DTN MO0706DSDR1E4A.001 [DIRS 181421],

The modal magnitude and distance determined from the joint deaggregation of the hazard at 10^{-4} AFE gives an **M** 7.7 event at 51 km in the 1-2 Hz frequency range and an **M** 6.2 event at 4 km in the 5-10 Hz frequency range (Table 6.4-1). Based on these results, five sets of seed strong motion recordings were selected.

Three of the five input strong ground motions are: 1) the 1999 Kocaeli earthquake, Iznik Station recording (#9; Table 6.5-14); 2) the 1992 Landers earthquake, Twenty-Nine Palms Station recording (#5); and 3) the 1992 Cape Mendocino earthquake, Shelter Cove Station recording (#3). These records (**M** 7.4, R 29.7 km, **M** 7.3, R 42.2 km, **M** 7.1, R 33.8 km, respectively) were selected from the M: 7.5, D: 10 – 50 km bin of the NUREG/CR-6728 (McGuire et al. 2001 [DIRS 157510], Appendix B) analysis time history database. These recordings are all on rock.

The last two of the five input strong ground motions are also rock sites: the 1992 Landers earthquake, Silent Valley Station recording (#4; Table 6.5-14), and the 1999 Kocaeli earthquake, Mecidiyekoy Station recording (#10). These records (**M** 7.3, R 51.7 km and **M** 7.4, R 62.3 km, respectively) were selected from the M: 7.5, D: 50 – 100 km bin of the NUREG/CR-6728 (McGuire et al. 2001 [DIRS 157510], Appendix B) analysis time history database.

For 10^{-4} AFE, the spectral match to the design (target) spectra, a corresponding plot of the ratio between the time histories' response spectra and the target spectra, and the resulting acceleration, velocity, and displacement time histories are shown in Figures 6.5.2-186 to 6.5.2-230. These results have been submitted to TDMS and have DTN MO0706TH1E4APE.001 [DIRS 181960].

6.5.2.5.4 Discussion of Limitation

As described in Section 6.5.2.3, there is a limitation associated with the developed time histories because UHS hazard results for 3.3 sec SA were inadvertently taken as results for 3.0 sec SA. For periods greater than 2.0 sec, the design response spectra to which the time histories are spectrally matched are low relative to their nominal AFE. Note, however, that in spectrally matching the target response spectrum, while overall meeting the matching criteria (Section 6.5.2.5), the time history response spectrum typically exceeds the target for some periods and is lower than the target at other periods. Thus, the affect of the limitation derived from the UHS at periods greater than 2.0 sec can vary.

6.5.2.6 SFA Strain-Compatible Properties

As described in Section 6.1, Approach 3 from NUREG/CR-6728 (McGuire et al. 2001 [DIRS 157510], Section 6.1), which is used here to develop the site-specific design motions, is probabilistic. The approach takes as input seismic hazard curves for the PSHA reference rock outcrop that have been conditioned to reflect additional information on extreme ground motion at

Yucca Mountain. Site response, which reflects variability in site dynamic material properties, is incorporated through integration over ground motion to produce site-specific hazard curves. For structural analyses, strain-compatible material properties are desired that are consistent with the probabilistic design motions. To achieve hazard consistency in the strain-compatible properties, they must reflect the hazard level (mean AFE), the amplitude of ground motion, and the epistemic uncertainty and aleatory variability in the site dynamic material properties.

6.5.2.6.1 Approach

To achieve both the desired AFE as well as consistency with the level of motion requires an approach for strain-compatible properties analogous to Approach 3. That is, during the integration of the control motion (reference rock outcrop) hazard curves with the suites of site-response amplification factors (comprising epistemic uncertainty and aleatory variability), corresponding strain-compatible properties need to be accumulated for each layer in the profiles. The strain-compatible properties would then be sorted and analyzed to produce percentile and mean values, reflecting the range in properties that is consistent with the desired AFE. While this approach is conceptually straightforward, some practical as well as theoretical issues complicate implementation. First, because the hazard integration used in developing hazard-consistent site-specific design motions is performed separately for each oscillator period, there are corresponding strain-compatible properties for each oscillator period. The strain-compatible properties may differ for each period as a result of changes in magnitude contribution and corresponding amplification factors. Second, horizontal motions are developed separately from vertical motions. The latter are determined employing suites of V/H ratios applied probabilistically to the horizontal site-specific hazard curves to achieve hazard-consistent vertical motions. A probabilistically rigorous approach to combining properties for the suite of oscillator periods and components of motion is ambiguous.

Given these issues, an approximate approach has been developed that results in strain-compatible properties that are adequate for their intended use in soil-structure interaction and other design analyses. The approach adopts a lognormal distribution for strain-compatible properties, consistent with observed strong ground motion parameters (Abrahamson and Shedlock 1997 [DIRS 164486]), and makes use of the distributions of strain-compatible properties catalogued during development of the suites of amplification factors (Section 6.5.3). The approach is applied to determine strain-compatible properties for the Northeast of Fault and South of Fault velocity profiles in combination with each alluvium thickness modeled (Table 6.5-8). For each case representing epistemic uncertainty, the approach examines the site-specific horizontal or vertical hazard curves and determines the ground motion at the AFE of interest (interpolating logarithmically as necessary). Strain-compatible properties calculated for ground motion levels that bracket the ground motion at the AFE of interest are then used as the basis to compute median and sigma values (over aleatory variability) using logarithmic interpolation. To combine the results for the various cases representing epistemic uncertainty in site-specific properties, the same weights used in developing the site-specific hazard curves are applied to the corresponding strain-compatible properties. The weighted median (mean log) set of strain-compatible properties (for each layer) is given by Eq. 6-13, while the associated variance includes both the aleatory component for each epistemic case as well as the variability of mean properties for each base-case (Eq. 6-14).

The approach approximately accommodates median estimates as well as epistemic uncertainty and aleatory variability in strain-compatible properties that are consistent with the site-specific horizontal and vertical hazard used for design. To examine consistency in strain-compatible properties across oscillator periods, the entire process is performed at PGA (100 Hz) and at 1 Hz. Since amplification factors are typically developed for a range in magnitude reflecting contributions at low (≤ 2 Hz) and high (≥ 2 Hz) frequencies, the consistency check at PGA and 1 Hz covers the typical range in control motions. If the differences in properties at high- and low-frequency are less than 10%, the high-frequency properties are used since this frequency range typically has the greatest impact on soil nonlinearity. If the difference exceeds 10% the properties for the difference frequencies are averaged. This is the situation for Yucca Mountain and thus averaged properties have been determined. Alternatively, two sets of properties could be used to carry out separate structural analyses.

In summary, the properties are interpolated corresponding to the appropriate PGA or 1-sec SA for the AFE of interest (mean hazard) and the results are averaged. The properties are calculated for each case of epistemic uncertainty. Each case has median (μ_i) and σ_i properties. Each case of epistemic uncertainty is then combined by the weighted median properties

$$\overline{\mu_{ln}} = \Sigma \, W_i \mu_{ln_i} \qquad \text{(Eq. 6-13)}$$

in which the weights are the same as those used to combine the hazard curve cases. The weighted variances include site epistemic uncertainty (different medians) in combined properties through

$$\text{Var}\,(ln) = \Sigma \left[W_i \, \sigma_{ln_i}^2 + W_i \left(\mu_{ln_i} - \overline{\mu} \right)^2 \right] \qquad \text{(Eq. 6-14)}$$

In soil-structure interaction analyses, best-estimate, upper-bound, and lower-bound properties are used. For Yucca Mountain, best-estimate properties are taken as the median (mean log) properties. Upper-bound and lower-bound properties are determined by taking the best-estimate plus and minus one standard deviation (sigma ln). Such an approach is recommended in NUREG-0800 (NRC 2007 [DIRS 180932], Standard Review Plan Acceptance Criteria). For Yucca Mountain, use of the sigma(ln) to determine upper- and lower-bounds is modified to impose a minimum sigma(ln) consistent with a coefficient of variation (COV) on shear modulus of 0.5. Use of this constraint is recommended in NUREG-0800 (NRC 2007 [DIRS 180932], Standard Review Plan Acceptance Criteria) for well-investigated sites for which only a single site-response calculation is available. While 60 site-response calculations are carried out for Yucca Mountain for each case representing epistemic uncertainty, this constraint is incorporated for conservatism. The same minimum value of sigma *ln* was also applied in determining the upper and lower bounds for S-wave damping, V_P, and P-wave damping. The minimum value of sigma *ln* consistent with a COV on shear modulus of 0.5 is 0.203.

Finally, the value of the *ln* standard deviation was adjusted to account for an assumed lower-bound strain-compatible V_S of 500 ft/sec (Section 5.5).

6.5.2.6.2 Strain-Compatible Property Results

Strain-compatible soil properties were generated for the seven combinations of alluvium over tuff velocity profiles. The seven combinations are listed in Table 6.5-8. Inputs to the analysis are listed in Table 6.5-6.

Software used in the analysis for the strain-compatible properties consists of:

- RASCAL SET V1.1 – modules RASCALS V. 5.5, RASCALP V 5.5, and SCP V 1.0 (Software Tracking Numbers 11232-1.1-00, 11232-1.1-01) [DIRS 184513, DIRS 184053]

- SOILHAZ SET V 1.0 – module HCSCP V 1.0 (Software Tracking Number 11231-1.0-00) [DIRS 182834]

- SIGCOMB V. 1.1 (Software Tracking Number 11233-1.1-00) [DIRS 182835]

The output from RASCAL SET modules RASCALS and RASCALP is in the form of strain-compatible properties for all combinations of material model and velocity profile for each ground motion level. The RASCAL SET module SCP combines the RASCALS and RASCALP output strain-compatible properties. This results in one set of strain-compatible properties (shear-wave and compression wave velocity and associated damping) for each combination of material model and velocity profile for each ground motion level. SOILHAZ SET module HCSCP uses log-log interpolation to calculate the strain-compatible properties from the SCP output corresponding to an AFE of interest. The result is a set of hazard-consistent strain-compatible properties for each combination of material model and velocity profile at each ground motion level and AFE. The resulting hazard-consistent strain-compatible properties are chosen for the appropriate AFE. SIGCOMB implements Eq. 6-13 and 6-14 to combine results for appropriate material models (UMT-UMA, UMT-LMA, LMT-UMA, LMT-LMA) and velocity profiles (South of the Fault cases A, B, C) for each ground motion level, at each AFE. As described above, two limits are applied to the resulting strain-compatible properties: 1) a geotechnically-based lower limit is assumed for the lower-bound strain-compatible V_S (500 ft/sec) (Section 5.5) and 2) a minimum value of sigma $ln(V_S)$ equal to 0.203 is imposed. This minimum value of sigma is consistent with a coefficient of variation (COV) on shear modulus of 0.5. The same minimum value of sigma *ln* was also applied in determining the upper and lower bounds for S-wave damping, V_P, and P-wave damping. The resulting strain-compatible properties for PGA and 1.0 sec SA are averaged to make one set. The data files for this analysis are in Appendix D (CALCULATIONS/SFA Strain Compatible Properties).

The process is followed for seven combinations of velocity profile and alluvium thickness. For the Northeast of the Fault velocity profile, site response modeling is carried out for four representative alluvium thickness values (30, 70, 100, and 200 ft). For the South of the Fault velocity profile, three alluvium thickness values are used in modeling (30, 70, and 100 ft). Thus, strain-compatible material properties are presented for seven cases shown in Table 6.5-8. Depending on the location and depth of alluvium beneath an important-to-safety building that is to be analyzed, an appropriate set of strain-compatible properties can be selected.

Note that design response spectra for the SFA, and their associated time histories, are not strictly consistent with the material properties. This is because the spectra were developed by

enveloping results for the various tuff base case velocity profiles and values of alluvium thickness. However, because of the enveloping process, the spectra and time histories will be conservative with respect to results for each case individually.

Strain-compatible material properties provided are V_S, S-wave damping, V_P, and P-wave damping. For the velocity and damping properties, the median and upper- and lower-bound iterated values are presented. Information on the associated strain values can be found in the output files in Appendix D (subdirectories of Y06.D\RASCALS\AMPS.02\SIG10G45.ALL).

Results for an AFE of 10^{-3} are presented in Figures 6.5.2-231 through 6.5.2-258. Figures 6.5.2-231 through 6.5.2-246 show the strain-compatible properties for 30, 70, 100, and 200 ft of alluvium over tuff using the Northeast of Fault velocity profile. Figures 6.5.2-247 through 6.5.2-258 show the strain-compatible properties for the 30, 70, and 100 ft of alluvium over tuff using the South of Fault velocity profiles. Results for AFEs of $5x10^{-4}$ and 10^{-4} are presented in Figures 6.5.2-259 to 6.5.2-286 and 6.5.2-287 to 6.5.2-314, respectively. These results have been submitted to the TDMS and have DTNs MO0801SCSPS1E3.003 [DIRS 184685] (10^{-3}), MO0801SCSPS5E4.003 [DIRS 184682] ($5x10^{-4}$), and MO0801SCSPS1E4.003 [DIRS 184683] (10^{-4}). Details of the analyses are contained in Appendix D (CALCULATIONS/SFA Strain Compatible Properties).

6.5.3. RB Preclosure Design Ground Motions

This section describes use of modeling and analyses to develop seismic hazard curves and design parameters with AFEs of 10^{-3}, $5x10^{-4}$, and 10^{-4} for the RB waste emplacement level. These ground motion inputs are used for preclosure safety analyses and design of underground facilities, as appropriate. Site response modeling results in horizontal and vertical hazard curves, UHS, and, at each AFE, 5%-damped seismic design response spectra and expected PGVs. Design time histories are also developed for the three AFEs. Results are also used for comparison with RB waste emplacement level ground motions previously developed using alternate modeling inputs and an alternate analysis approach (BSC 2004 [DIRS 170027], Section 6.3).

6.5.3.1 RB Transfer Functions

Following the same process as described for the SFA, horizontal amplification factors and V/H ratios were computed for the waste emplacement area. As an example of the horizontal transfer functions computed for total (within) motion at the RB, relative to outcrop motions at the reference rock outcrop, Figures 6.5.3-1a-d shows results using the Soft Zone velocity profile and UMT dynamic property curves. The dip (deamplification) in the amplification factors is the expected spectral null due to the cancellation of upgoing and downgoing wavefields. The spectral hole is broadened by the velocity profile randomization process and is further broadened in computing UHS by the enveloping of hazard curves computed for the soft and stiff zones as well as the weighting of hazard from the UMT and LMT dynamic property curves. In developing final design motions, the resulting broad dip in the UHS is filled in by smoothing. Due to undulations of the surface topography, the deamplification is not expected to occur to as great a degree nor at the same frequency throughout the repository. This is a limitation of a simple model, adequately compensated for by conservatively ignoring the spectral null.

Similarly with the SFA, V/H ratios were computed for the RB vertical motions relative to reference rock outcrop horizontal motions. Because empirical relations are not available for at-depth motions, only numerical modeling was used. Figure 6.5.3-2 shows an example of V/H ratios computed for the soft zone velocity profile with UMT dynamic property curves for **M** 6.0. In this case, for vertical motions, the depth node is both a peak near 1 Hz followed by a trough near 2 Hz. Additionally, the high frequency peak near 40 Hz for the SFA (Figure 6.5.2-6) has shifted to about 50 Hz (Figure 6.5.3-2). In terms of RE and point-source magnitude contributions varying with structural and exceedance frequency, the distributions used for the SFA were also used for the RB (Tables 6.5-1, 6.5-3, and 6.5-4).

6.5.3.2 RB Hazard Curves

Hazard curves were calculated for the RB for horizontal and vertical ground motions. Inputs to the site response and point-source models for the RB ground motions and hazard curve are summarized in Table 6.5-18.

Table 6.5-18. Model Inputs for Development of RB Ground Motions

Model Input	Source
RE horizontal response spectra for each AFE (1-2 Hz and 5-10 Hz)	Section 6.4.1.1; REs have DTN MO0211REDES103.000 [DIRS 170424]; DTN MO0208UNHZ5X10.000 [DIRS 163722]; DTN MO0211DERES104.000 [DIRS 170423]; DTN MO0308UNHAZ105.000 [DIRS 170425]; MO0206UNHAZ106.001 [DIRS 163723]; and DTN MO0209UNHAZ107.000 [DIRS 163724].
60 randomized velocity profiles for each of the two RB base case profiles	Section 6.4.2.6; base case velocity profiles have DTN MO0708BCSSWVGB.001 [DIRS 184464]
60 randomized sets of shear modulus reduction and damping curves for each of the two tuff base case curves	Section 6.4.4; base case curves have DTN MO0802DYNPRP07.001 [DIRS 184993]
Tuff density	Section 5.6
Point-source parameters	Section 6.4.5

Software programs used to calculate the hazard curves are listed in Section 6.5.2.5.1. As discussed in Section 6.4.2.6, two base case velocity profiles for the RB, a soft zone and a stiff zone, were used in the site response model calculations.

Mean horizontal and vertical hazard curves are plotted in Figures 6.5.3-3 to 6.5.3-8 for the two base case profiles, soft and stiff sites, for the RB at PGA, 0.2, and 1.0 sec SA. The vertical seismic hazard curves are calculated using V/H ratios (Section 6.5.3.1.2). For the RB only analytical V/H ratio data were used as the empirical results to not apply to at-depth motions. The data for these plots are contained in Appendix D.

In the final step to develop hazard curves for the RB, the hazard curves based on the two velocity profiles are enveloped. Mean horizontal and vertical seismic hazard curves for the RB and PGA, 0.05, 0.1, 0.2, 0.5, 1.0, 2.0, and 3.3 sec SA are provided in Figures 6.5.3-9 to 6.5.3-16. The data for these plots are identified by DTN MO0801HCUHSREB.001 [DIRS 184803] and contained in Appendix D along with details of the analysis.

For horizontal and vertical PGV, the mean, median and fractile (5th, 15th, 85th, and 95th percentiles) hazard curves are also developed by enveloping the hazard curves for the two RB base-case velocity profiles. Plots of these curves are provided in Figures 6.5.3-17a and 6.5.3-18, respectively. The data for these plots are identified by DTN MO0801HCUHSREB.001 [DIRS 184803] and contained in Appendix D along with details of the analysis.

The hazard determined in this study results in lower AFEs for a given level of PGV compared to results of previous studies. Figure 6.5.3-17b compares the current horizontal PGV hazard curve to hazard values determined for AFEs of 10^{-5}, 10^{-6}, and 10^{-7} in BSC (2004 [DIRS 170027], Section 6.3.1.4). It also compares the current PGV hazard curve to the conditioned hazard curve from BSC (2005 [DIRS 170137]). For a PGV of about 100 cm/sec the conditioned AFE from this study is about a factor of 2 less than the conditioned AFE from BSC (2005 [DIRS 170137]) and the unconditioned hazard from BSC (2004 [DIRS 170027]). For a PGV of about 250 cm/sec the conditioned AFE from this study is reduced by a factor of 10 or more relative to the earlier studies.

Based on the resulting RB hazard curves, UHS are determined for AFEs of 10^{-3}, $5x10^{-4}$, 10^{-4}, 10^{-5}, 10^{-6}, 10^{-7}, and 10^{-8} using the program HAZUHS (Section 6.1.6). The RB UHS are plotted in Figures 6.5.3-19 to 6.5.3-25. The UHS are identified by DTN MO0801HCUHSREB.001 [DIRS 184803]. Details of the development of the UHS based on the RB hazard curves are described in Appendix D (CALCULATION/Repository SOILUHSI/HAZUHS and CALCULATION/Repository Vertical SOILUHSI/HAZUHS).

In computing UHS, hazard curve data for 3.3 sec SA were inadvertently used as if they represented hazard results for 3.0 sec SA. Thus, for periods greater than 2.0 sec, the SA amplitude is lower (has a higher AFE) than appropriate for the nominal UHS AFE. The applicability of the UHS for periods greater than 2 sec is, therefore, limited. Because design response spectra are based on the UHS, and design time histories are spectrally matched to the design response spectra, these outputs are similarly limited. Users of these outputs need to take into account this limitation when assessing their adequacy for a given intended purpose.

6.5.3.3 RB 5%-Damped Horizontal and Vertical Design Spectra

Design spectra for AFEs of 10^{-3}, $5x10^{-4}$, and 10^{-4} are based on the corresponding UHS for the RB. For the design spectra, the UHS is smoothed and extrapolated to 10 sec SA. In smoothing, a decrease in SA at 1 Hz for the UHS is eliminated (see Section 6.5.3.5). Extrapolation beyond 3.0 sec is based on the slope between 2 and 3.0 sec. In developing the design spectra, an SA value at 0.02 sec is estimated that results in a divergence from a straight-line log-log interpolation between the UHS values at 0.05 and 0.01 sec. Horizontal and vertical design spectra for the RB with AFEs of 10^{-3}, $5x10^{-4}$, and 10^{-4} are shown in Figures 6.5.3-26 to 6.5.3-28; design spectral acceleration values (5%-damped) are listed in Tables 6.5.3-19 to 6.5.3-21.

Table 6.5-19. Summary of RB Seismic Design Spectra (5%-Damped) in g's at 10^{-3} AFE

Period (sec)	Horizontal Motion (Spectral Acceleration, g)	Vertical Motion (Spectral Acceleration, g)
PGA	0.12	0.07
0.05	0.20	0.13
0.1	0.26	0.14
0.2	0.25	0.14
0.5	0.21	0.13
1.0	0.14	0.11
2.0	0.07	0.04
3.3	0.04	0.02

Source: DTN: MO0707DSRB1E3A.000 [DIRS 183128]

Table 6.5-20. Summary of RB Seismic Design Spectra (5%-Damped) in g's at $5x10^{-4}$ AFE

Period (sec)	Horizontal Motion (Spectral Acceleration, g)	Vertical Motion (Spectral Acceleration, g)
PGA	0.17	0.12
0.05	0.30	0.22
0.1	0.39	0.22
0.2	0.36	0.21
0.5	0.30	0.19
1.0	0.20	0.16
2.0	0.10	0.06
3.3	0.06	0.03

Source: DTN: MO0707DSRB5E4A.000 [DIRS 183130]

Table 6.5-21. Summary of RB Seismic Design Spectra (5%-Damped) in g's at 10^{-4} AFE

Period (sec)	Horizontal Motion (Spectral Acceleration, g)	Vertical Motion (Spectral Acceleration, g)
PGA	0.37	0.32
0.05	0.63	0.61
0.1	0.83	0.56
0.2	0.76	0.49
0.5	0.62	0.40
1.0	0.40	0.32
2.0	0.22	0.12
3.3	0.14	0.07

Source: DTN: MO0707DSRB1E4A.000 [DIRS 183129]

6.5.3.4 Comparison With 2004 RB Unconditioned Design Spectra

Design spectra described in Section 6.5.3.3 for the RB waste emplacement level are compared to design spectra from BSC (2004 [DIRS 170027]) in Figures 6.5.3-29 to 6.5.3-34. Development

of design spectra for the RB in BSC (2004 [DIRS 170027]) differ from those developed here as follows:

- Site-response model inputs were based on geotechnical data described in BSC (2002 [DIRS 157829])
- Site-response model results were used to determine site-specific, hazard-consistent ground motion inputs using Approach 2B of NUREG/CR-6728 (McGuire et al. 2001 [DIRS 157510])
- Control motion inputs to the site-response model were not conditioned to reflect new information on extreme ground motion at Yucca Mountain

The 2004 design spectra exceed the 2007 spectra at most spectral periods and particularly for vertical ground motions. The differences may be attributed to similar factors as for the SFA (Section 6.5.2.3.4).

6.5.3.5 RB Parameter Sensitivities

For the RB, to accommodate spatial variability in the mean velocity profile, two base case profiles were developed: stiff and soft. These profiles were based on geotechnical measurements (Section 6.4.2) and reflect significant differences in mean velocity profiles within zones across Yucca Mountain. The differences are likely due to broad lateral changes in fracture density within the tuff units above the Calico Hills Formation (Section 6.4.2). To illustrate potential differences in repository motions due to the two mean profiles, a full suite of UHS were computed for each profile. In addition, to examine the potential impacts on the RB motions due to the epistemic uncertainty in mean modulus reduction and hysteretic damping curves, the soft profile was selected as it will result in higher strains than the stiff profile, revealing the higher sensitivity to dynamic material properties.

It is important to point out the RB motions are computed at repository depths (mean depth of about 1,000 ft). As such they reflect total or "in-layer" motion and include all upgoing and downgoing wavefields. The at-depth total motions then contain the expected depth nodes or cancellation for wavefields 180^{o} out of phase (EPRI 1988 [DIRS 107489]). This phenomena is expected and can be observed in vertical array recordings (EPRI 1988 [DIRS 107489]). One of the principal reasons for randomizing over depth is to smooth the spectral nodes in a realistic manner, which as the following figures clearly show, occurs near 1 Hz for the two profiles. Because the vertically-propagating shear-wave model (site-response model) represents site materials as horizontal plane layers and may over-predict the degree of motion reduction, the dip in the spectra is smoothed (filled) in developing final motions (Section 6.5.3.3).

6.5.3.5.1 Effects of Profile Stiffness

Figures 6.5.2-35 to 6.5.2-41 compare mean UHS computed for the RB (mean depth of 1,000 ft) using the soft and stiff V_S profiles (Section 6.4.2.6) separately. The AFEs considered range from preclosure design to postclosure performance assessment (e.g., 10^{-3} to 10^{-8}). This range in AFE fully illustrates the effects of dynamic material properties on repository motions as it considers all levels of motions used for design as well as performance assessment.

To illustrate the effect of profile stiffness, each UHS (stiff profile and soft profile) reflects a weighted average (Section 6.4.5) over the two sets of tuff modulus reduction and hysteretic damping curves. This approach is consistent with the manner in which repository design motions were estimated (i.e., envelopes over the weighted UHS computed for the soft and stiff profiles).

Interestingly, for the total motions, Figures 6.5.2-35 to 6.5.2-41 show the soft zone profile controls RB ground motions at all AFEs. The difference in motions computed for the soft and stiff zones increases slowly with increasing levels (decreasing AFEs) and is largest near the spectral node (≈ 1 Hz), which naturally differs in frequency for the two profiles. The difference in frequency is not readily apparent due to the frequency sampling (a factor of 2 near 1 Hz, i.e., 0.5, 1.0, 2.0 Hz). In summary, the soft profile controls the envelope over the entire frequency range and all loading levels.

6.5.3.5.2 Effects of Nonlinear Dynamic Material Properties

The soft zone profile was selected to illustrate the effects of the two tuff G/G_{max} and hysteretic damping curves. The UMT and LMT sets of curves reflect two reasonable interpretations regarding the possible behavior of the fractured tuff at high strains. The UMT set of curves is based on the interpretation that the large-scale fracturing does not control dynamic material nonlinearity until very high strains (matrix-dominated nonlinearity), while the LMT set of curves is based on the interpretation that the large scale fractures control dynamic nonlinearity and their effect initiates at low strains (fracture dominated nonlinearity). As described in Section 6.4.5, the two sets of curves were not considered equally probable with the UMT set receiving most of the weight in developing final RB ground motions.

Figures 6.5.2-42 to 6.5.2-48 compare the UHS estimated for the repository soft zone using the UMT and LMT modulus reduction and hysteretic damping curves. In general, for these at-depth motions, the potential impact of the nonlinear dynamic material properties is quite small across structural frequency as well as loading level.

6.5.3.6 RB Design Time Histories

The approach used to develop time histories for RB preclosure analyses is identical to what was done for the SFA. However, only one set of time histories each was developed for the RB at 10^{-3}, $5x10^{-4}$, and 10^{-4} AFE resulting in a total of three sets. Strong ground motion recordings from past earthquakes are used in the spectral matching process to provide realistic time histories with characteristics of observed ground motion. The seed strong ground motion recordings are chosen from the NUREG/CR-6728 (McGuire et al. 2001 [DIRS 157510], Appendix B) analysis time history database (Table 6.5-22). Acceleration plots of the seed time histories used to match the design spectra at 10^{-3} and $5x10^{-4}$ AFE are shown in Figure 6.5.3-49. Corresponding plots of seed time histories used to match the design spectra at 10^{-4} AFE are shown in Figure 6.5.3-50.

Table 6.5-22. Summary of Input Strong Ground Motion Recordings

	Earthquake	Date	Magnitude (M)	Station	Distance (km	PGA (g)			PGV (cm/sec)			Used as Input Time Histories for:
						H1	H2	V	H1	H2	V	
1	Northridge, CA	1/17/94	6.7	Duarte-Mel Canyon	52.0	0.079	0.028	0.046	3.4	2.4	2.2	Preclosure time histories for the RB at 10^{-3} and $5x10^{-4}$ AFE.
2	Chi Chi, Taiwan	9/20/99	7.6	TCU015	47.3	0.114	0.119	0.068	29.5	49.8	17.2	Preclosure time histories for the RB at 10^{-4} AFE.

Source: McGuire et al. (2001 [DIRS 157510], Appendix B, Tables B-1 and B-2)

The seed time histories are chosen based on the deaggregated hazard at Yucca Mountain, as described in Section 6.4.1. H1 and H2 components were taken as defined in the NUREG/CR-6728 (McGuire et al. 2001 [DIRS 157510], Appendix B) time history database.

6.5.3.6.1 10^{-3} AFE

For RB preclosure design for a AFE of 10^{-3}, one set of three-component time histories were developed by spectrally matching to the RB seismic design spectrum following the guidelines outlined above in Section 6.5.2.5. Inputs to this analysis for these motions are summarized in Table 6.5-23.

Table 6.5-23. Analysis Inputs for Development of Seismic Design Time Histories with a AFE of 10^{-3} for the RB

Analysis Input	Source
Set #1: Strong Ground Motion Recording of 1994 Northridge Earthquake, Duarte-Mel Canyon	Table 6.5-22, Number 1; NUREG-CR-6728 (McGuire et al. 2001 [DIRS 157510], Appendix B)
Seismic Design Response Spectra at RB with an AFE of 10^{-3}	Table 6.5-19; seismic design spectra have DTN MO0707DSRB1E4A.000 [DIRS 183129],

Software items used in the analysis are the same as listed in Section 6.5.4.7.

The input strong motion is a rock site, the 1994 Northridge, CA earthquake, Duarte-Mel Canyon station recording (Number 1 in Table 6.5-22). This record (**M** 6.7, R 52.0 km was selected from the M: 6.5, D: 50 – 100 km bin of the NUREG/CR-6728 (McGuire et al. 2001 [DIRS 157510], Appendix B) analysis time history database.

As previously discussed in Section 6.5.4.7.1, the deaggregation of the hazard at 10^{-3} AFE shows that the hazard is dominated by a **M** 6.9 event at 52 km at the 1-2 Hz frequency range and a **M** 6.3 event at 5 km at the 5-10 Hz frequency range. Following NUREG/CR-6728 (McGuire et al. 2001 [DIRS 157510], Section 5), when matching to UHS (one spectrum instead of the two deaggregated reference event spectra), it is recommended that the strong ground motion duration be the longer duration associated with the low-frequency event. The matching criteria presented in NUREG/CR-6728 (McGuire et al. 2001 [DIRS 157510]) were followed for time history spectral matching.

The spectral matches to the target (design) spectra, plots of the ratios between the spectra of the matched time history and the target spectra, and the spectrally-matched time histories for acceleration, velocity, and displacement for 10^{-3} AFE and horizontal and vertical ground motions are shown in Figures 6.5.3-51 to 6.5.3-59. These results have been submitted to TDMS and have DTN MO0707THRB1E3A.000 [DIRS 183196].

6.5.3.6.2 $5x10^{-4}$ AFE

For RB preclosure design at $5x10^{-4}$ AFE, the same set of three-component seed time histories as used for 10^{-3} AFE were used to spectrally match to the seismic design spectra. Inputs to this analysis for these motions are summarized in Table 6.5-24.

Table 6.5-24. Analysis Inputs for Development of Seismic Design Time Histories with an AFE of $5x10^{-4}$ for the RB

Analysis Input	Source
Set #1: Strong Ground Motion Recording of 1994 Northridge Earthquake, Duarte-Mel Canyon	Table 6.5-22, Number 1; NUREG-CR-6728 (McGuire et al. 2001 [DIRS 157510], Appendix B)
Seismic Design Response Spectra at RB with an AFE of $5x10^{-4}$	Table 6.5-20; seismic design spectra have DTN MO0707DSRB5E4A.000 [DIRS 183130],

The spectral matches to the target (design) spectra, plots of the ratios between the spectra of the matched time history and the target spectra, and the spectrally-matched time histories for acceleration, velocity, and displacement for $5x10^{-4}$ AFE and horizontal and vertical ground motions are shown in Figures 6.5.3-60 to 6.5.3-68 in respective order. These results have been submitted to TDMS and have DTN MO0707THRB5E4A.000 [DIRS 183197].

6.5.3.6.3 10^{-4} AFE

For RB preclosure design at 10^{-4} AFE, one set of three-component time histories was developed by spectrally matching to the RB seismic design spectrum following the guidelines outlined above in Section 6.5.5.3. Inputs to this analysis for these motions are summarized in Table 6.5-25.

Table 6.5-25. Analysis Inputs for Development of Seismic Design Time Histories with an AFE of 10^{-4} for the RB

Analysis Input	Source
Set #1: Strong Ground Motion Recording of 1994 Chi Chi, Taiwan, Station TCU015	Table 6.5-22, Number 2; NUREG-CR-6728 (McGuire et al. 2001 [DIRS 157510], Appendix B)
Seismic Design Response Spectra at RB with an AFE of 10^{-4}	Table 6.5-21; seismic design spectra have DTN MO0707DSRB1E4.000 [DIRS 183129]

The input strong ground motion site is a rock site, the 1999 Chi Chi, Taiwan earthquake, TCU015 station recording (Number 2 in Table 6.5-22). This record, (**M** 7.6, R 47.3 km) was selected from the M: 7.5, D: 0-50 km bin of the NUREG/CR-6728 (McGuire et al. 2001 [DIRS 157510], Appendix B) analysis time history database. It was selected in light of the deaggregation of the hazard at 10^{-4} AFE, which is dominated by a **M** 7.7 event at 52 km at the 1-2 Hz frequency range and a **M** 6.3 event at 5 km at the 5-10 Hz frequency range.

The spectral matches to the target (design) spectra, plots of the ratios between the spectra of the matched time history and the target spectra, and the spectrally-matched time histories for acceleration, velocity, and displacement for 10^{-4} AFE and horizontal and vertical ground motions are shown in Figures 6.5.3-69 to 6.5.3-77. These results have been submitted to TDMS and have DTN MO0707THRB1E4A.000 [DIRS 183200].

6.5.3.7 Comparison with 2004 RB Time Histories

In this section the RB time histories developed for postclosure analyses in BSC (2004 [DIRS 170027], Section 6.3.2.3) are compared to the updated UHS for corresponding AFEs described in this report. In BSC (2004 [DIRS 170027], Section 6.3.2.3) suites of 17 sets of three-component time histories were developed for three AFEs: 10^{-5}, 10^{-6}, and 10^{-7}. For each AFE, seed time histories were selected based on deaggregation of the PSHA results. The H1 component of each seed time history was then scaled according to the horizontal PGV determined from site-response modeling. The other two components were scaled to maintain the inter-component variability of the original seed time history (BSC 2004 [DIRS 170027]), Section 6.3.2.3.1). Control motion inputs to the site-response modeling in BSC (2004 [DIRS 170027]) were not conditioned to reflect new information on extreme ground motion.

Median and ± 1 sigma response spectra for the horizontal time histories developed in BSC (2004 [DIRS 170027], Section 6.3.2.3, Figures 6.3-145, 6.3-133, 6.3-137) are compared to the horizontal UHS developed in this study for the corresponding AFE (Figures 6.5.3-78 through 6.5.3-80). For an AFE of 10^{-5} (Figure 6.5.3-78), the median response spectrum of the horizontal components of the 17 suites of time histories is similar for oscillator frequencies of about 1 to 10 Hz. At lower frequencies, the current results are slightly higher; at higher frequencies the current results are slightly lower. For an AFE of 10^{-6} (Figure 6.5.3-79), the current UHS is significantly lower than the median for the 2004 time histories at all oscillator frequencies above about 0.6 Hz. Above about 3 Hz, the current results are comparable to or lower than the -1 sigma spectrum. For an AFE of 10^{-7} (Figure 6.5.3-80), the current results are significantly lower than the -1 sigma spectrum for oscillator frequencies above about 2 Hz and below the median for the 2004 time histories at all oscillator frequencies.

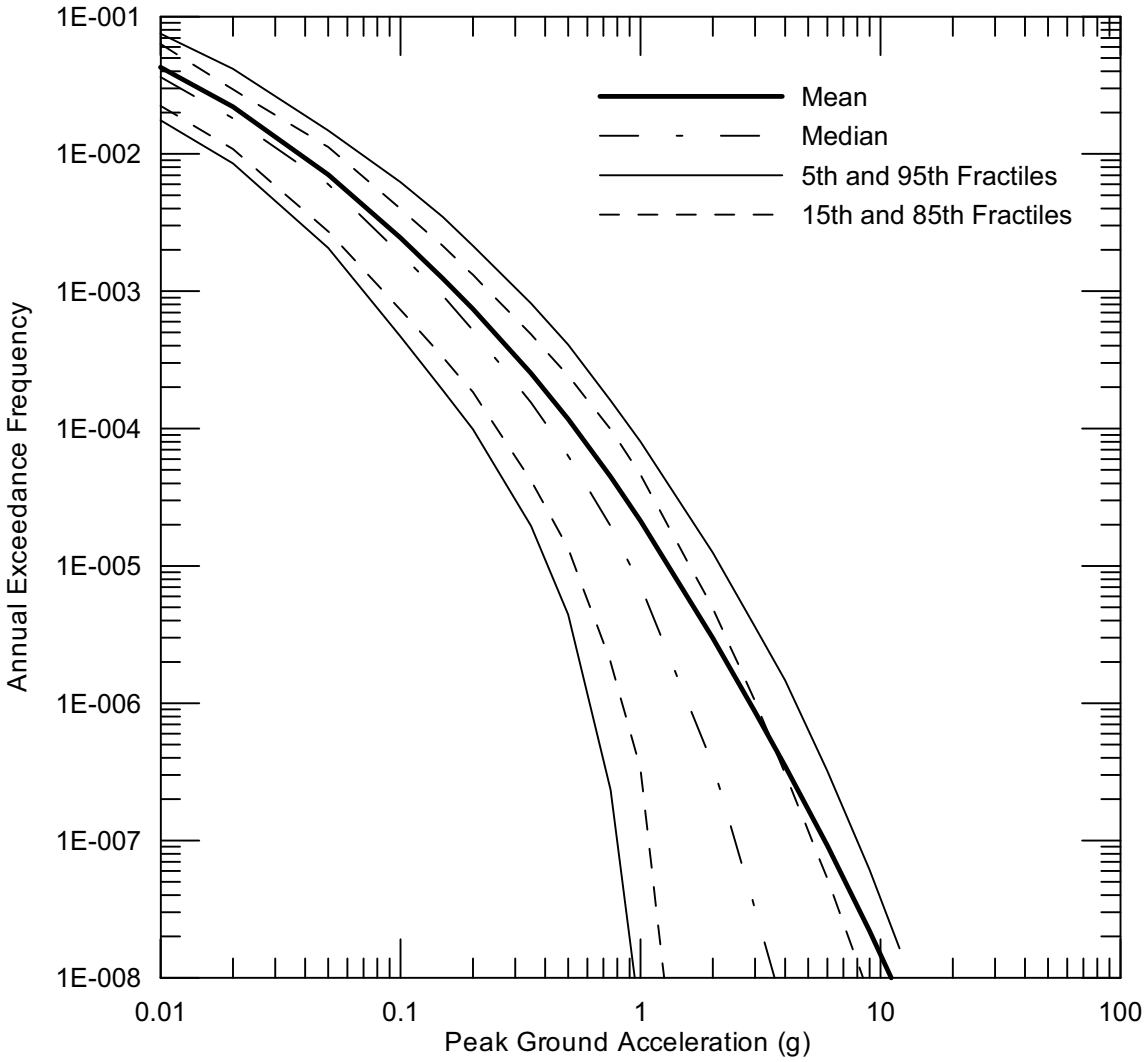

Figure 6.4.1-1. Hazard Curves at Reference Rock Outcrop for Peak Horizontal Spectral Acceleration

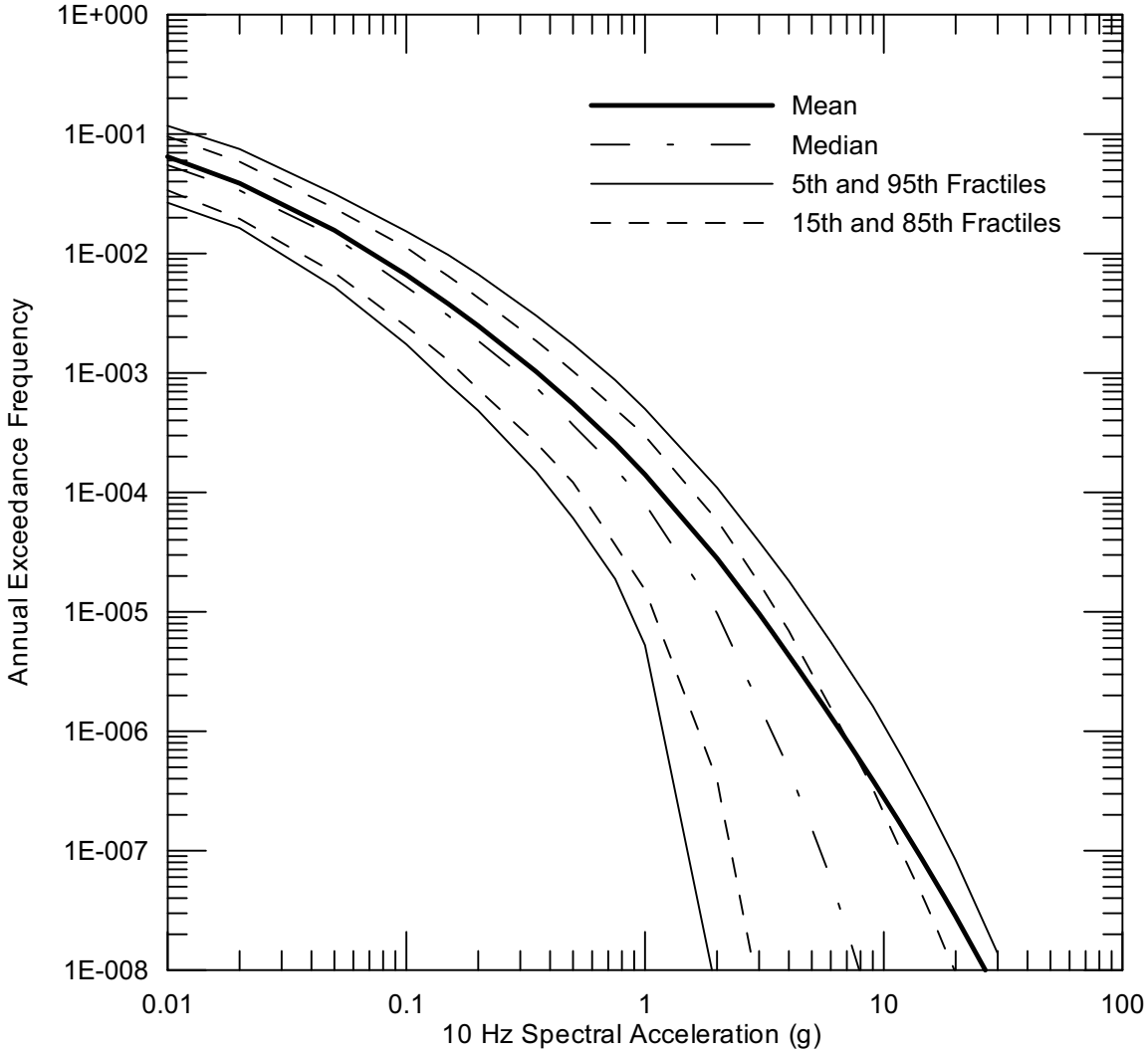

DTN: MO03061E9PSHA1.000 [DIRS 163721]

Figure 6.4.1-2. Hazard Curves at Reference Rock Outcrop for 1 Hz Horizontal Spectral Acceleration

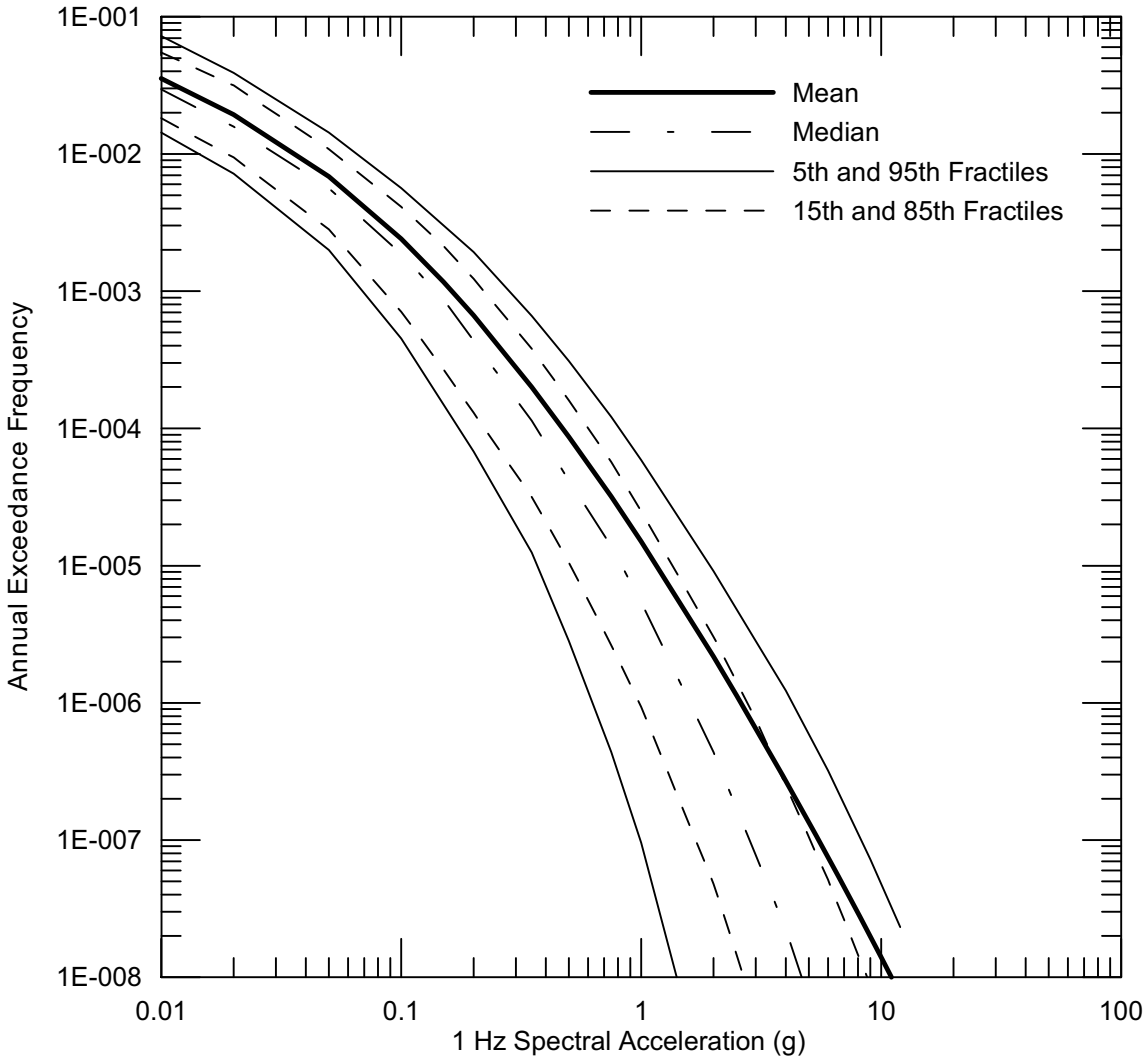

DTN: MO03061E9PSHA1.000 [DIRS 163721]

Figure 6.4.1-3. Hazard Curves at Reference Rock Outcrop for 1 Hz Horizontal Spectral Acceleration

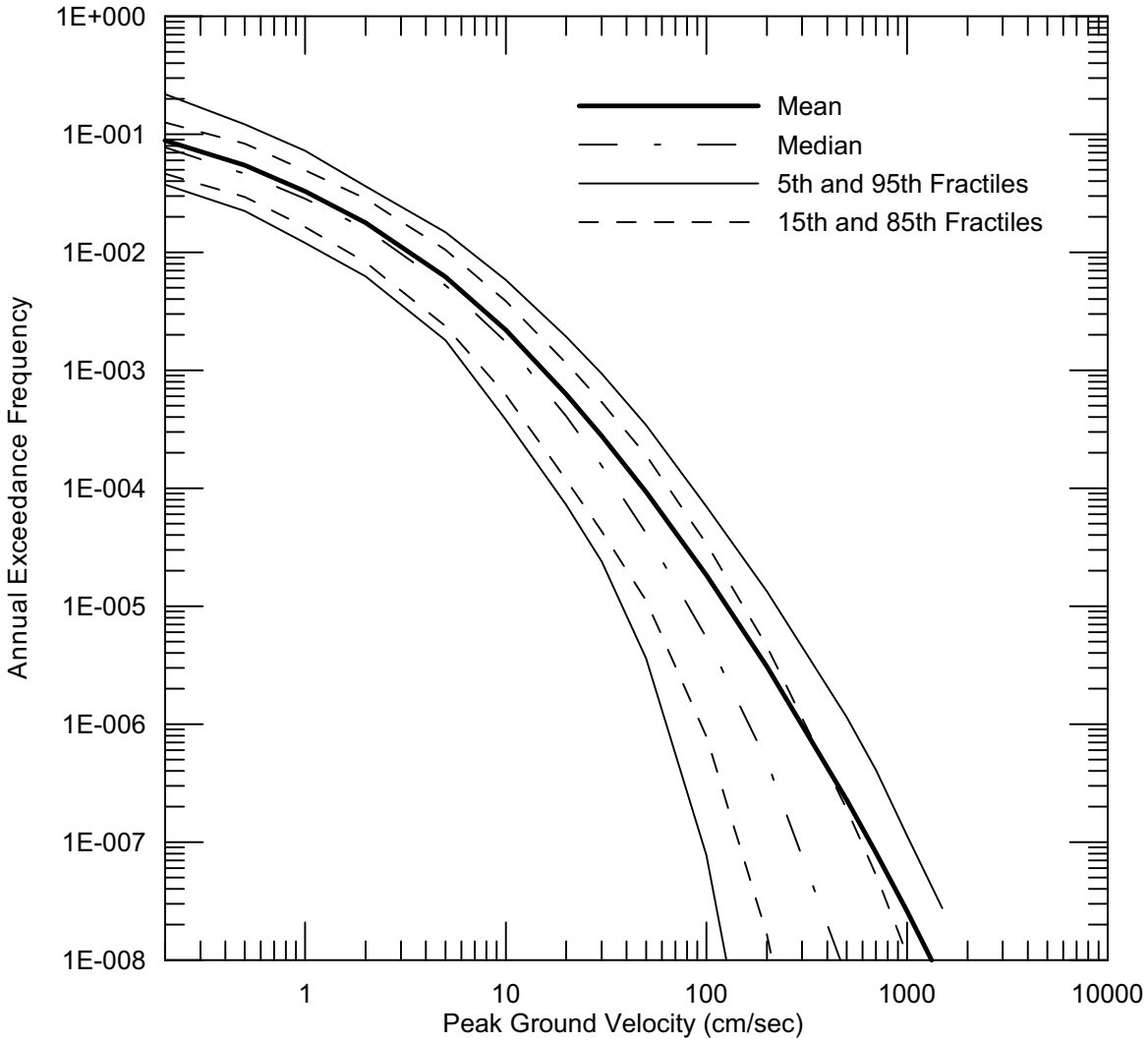

DTN: MO03061E9PSHA1.000 [DIRS 163721]

Figure 6.4.1-4. Hazard Curves at Reference Rock Outcrop for Peak Horizontal Ground Velocity

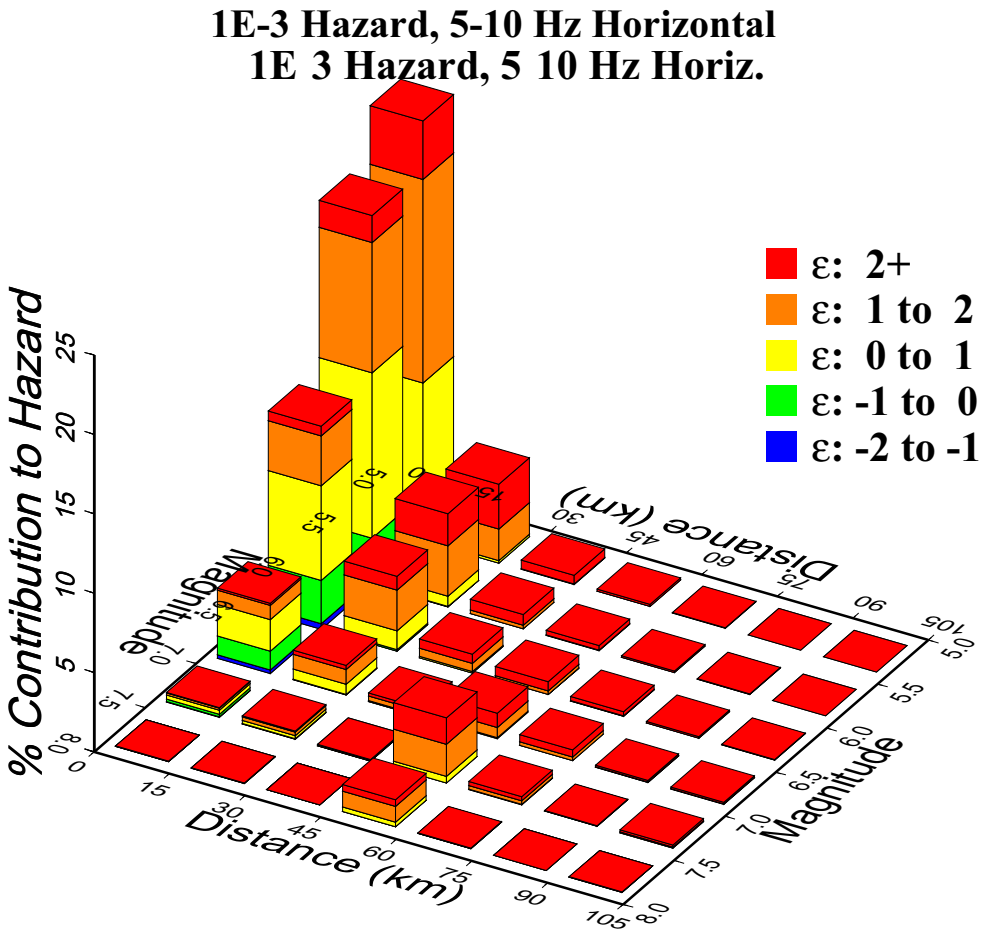

Source: BSC (2004 [DIRS 170027], Figure 6.2-17

Figure 6.4.1-5. Contribution to Mean Hazard by Magnitude, Distance, and Epsilon (ε) for the 5-10 Hz Horizontal Ground Motions, 10^{-3} Annual Exceedance Frequency

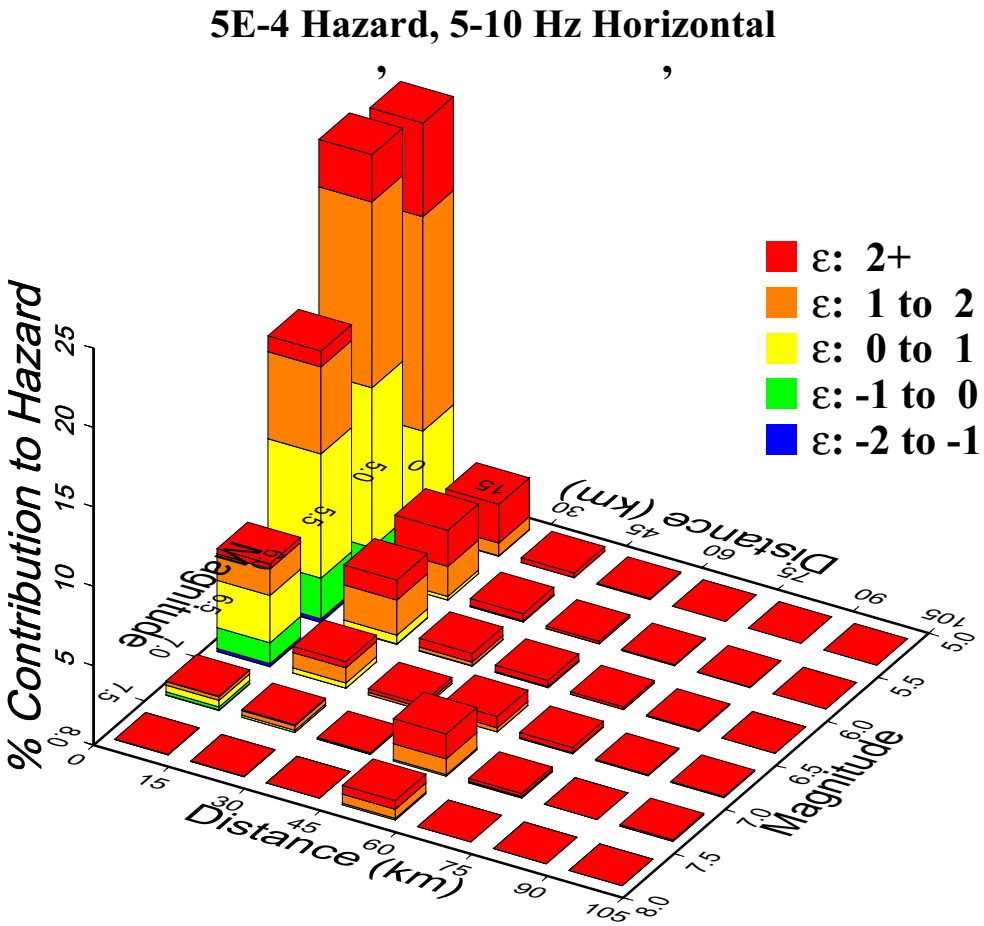

Source: BSC (2004 [DIRS 170027], Figure 6.2-18

Figure 6.4.1-6. Contribution to Mean Hazard by Magnitude, Distance, and Epsilon (ε) for the 5-10 Hz Horizontal Ground Motions, $5x10^{-4}$ Annual Exceedance Frequency

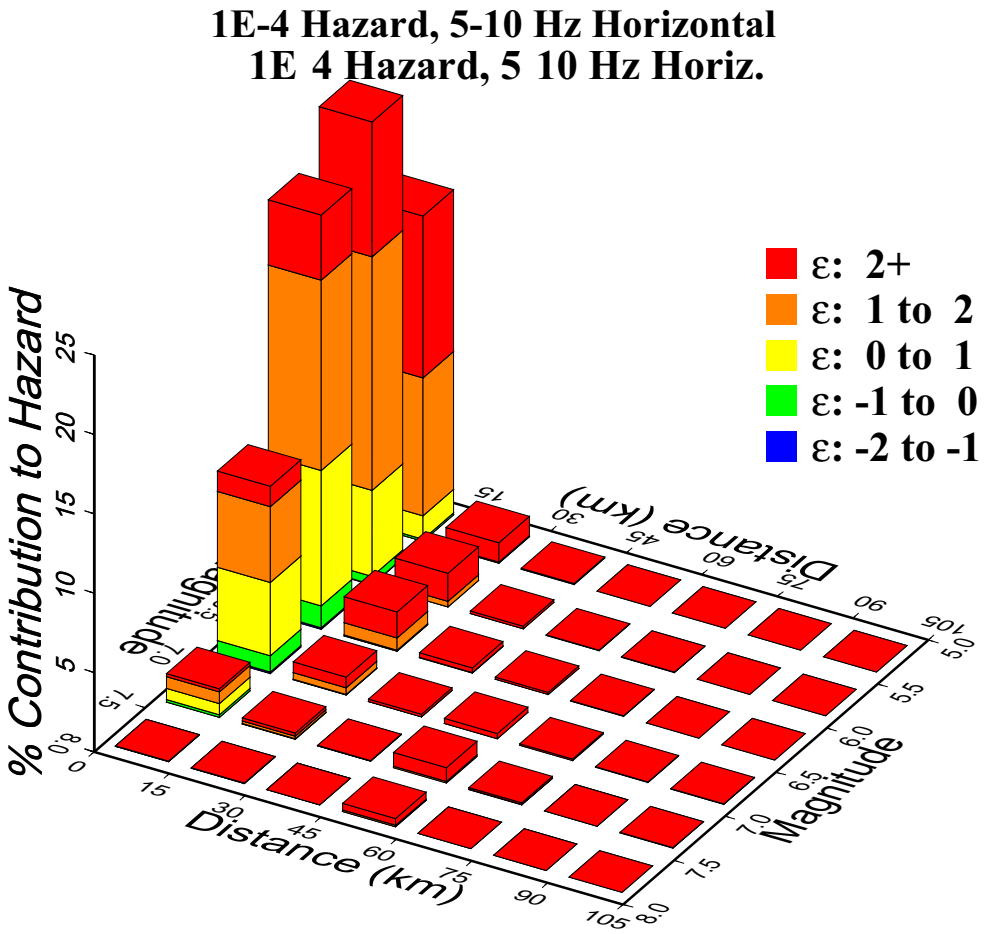

Source: BSC (2004 [DIRS 170027], Figure 6.2-19

Figure 6.4.1-7. Contribution to Mean Hazard by Magnitude, Distance, and Epsilon (ε) for the 5-10 Hz Horizontal Ground Motions, 10^{-4} Annual Exceedance Frequency

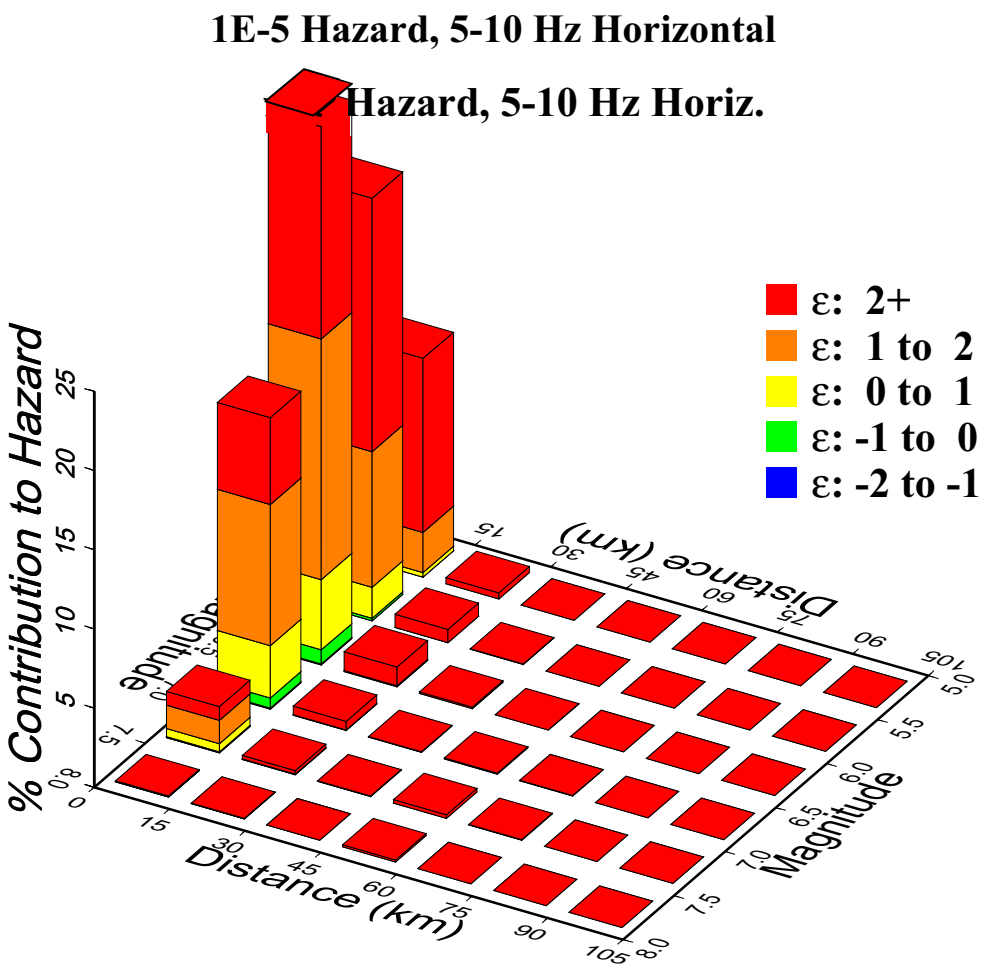

Source: BSC (2004 [DIRS 170027], Figure 6.2-20)

Figure 6.4.1-8. Contribution to Mean Hazard by Magnitude, Distance, and Epsilon (ε) for the 5-10 Hz Horizontal Ground Motions, 10^{-5} Annual Exceedance Frequency

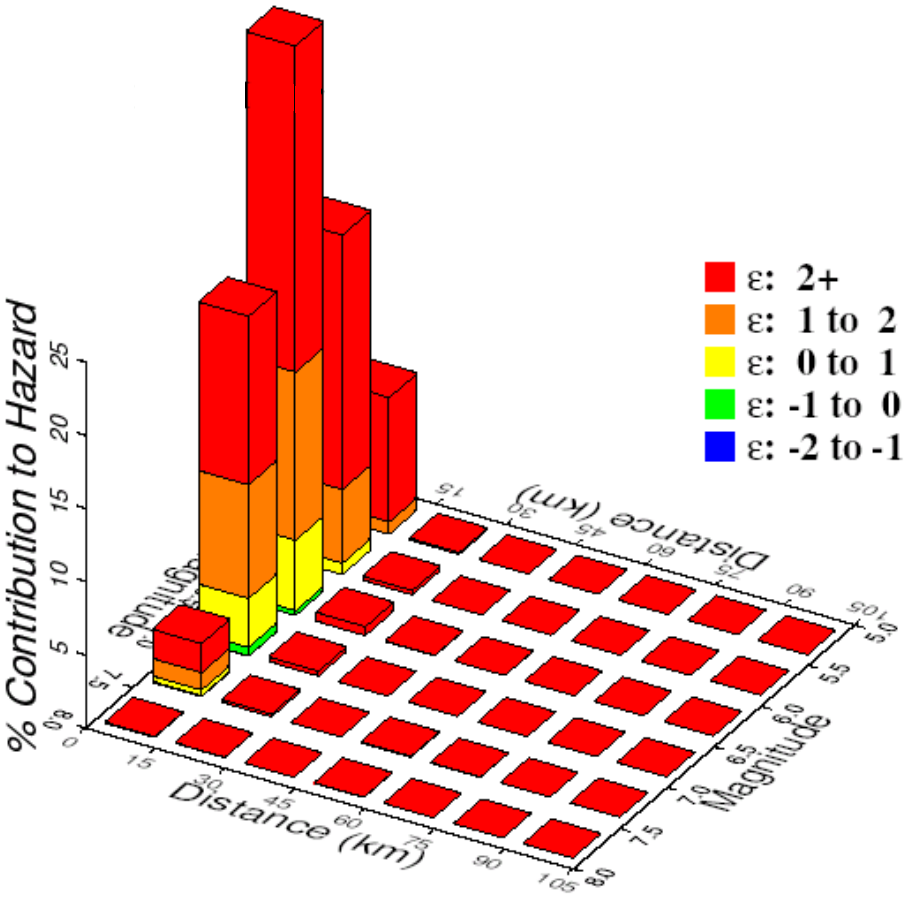

Source: BSC (2004 [DIRS 170027], Figure 6.2-21 ,

Figure 6.4.1-9. Contribution to Mean Hazard by Magnitude, Distance, and Epsilon (ε) for the 5-10 Hz Horizontal Ground Motions, 10^{-6} Annual Exceedance Frequency

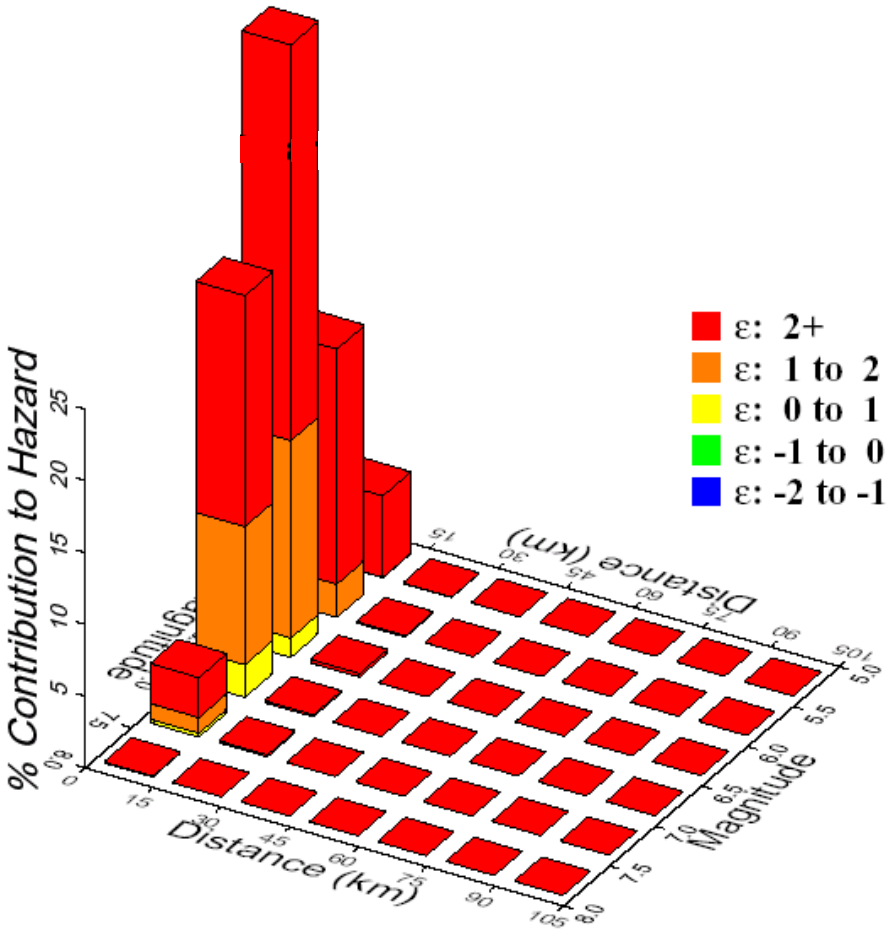

Source: BSC (2004 [DIRS 170027], Figure 6.2-22

Figure 6.4.1-10. Contribution to Mean Hazard by Magnitude, Distance, and Epsilon (ε) for the 5-10 Hz Horizontal Ground Motions, 10^{-7} Annual Exceedance Frequency

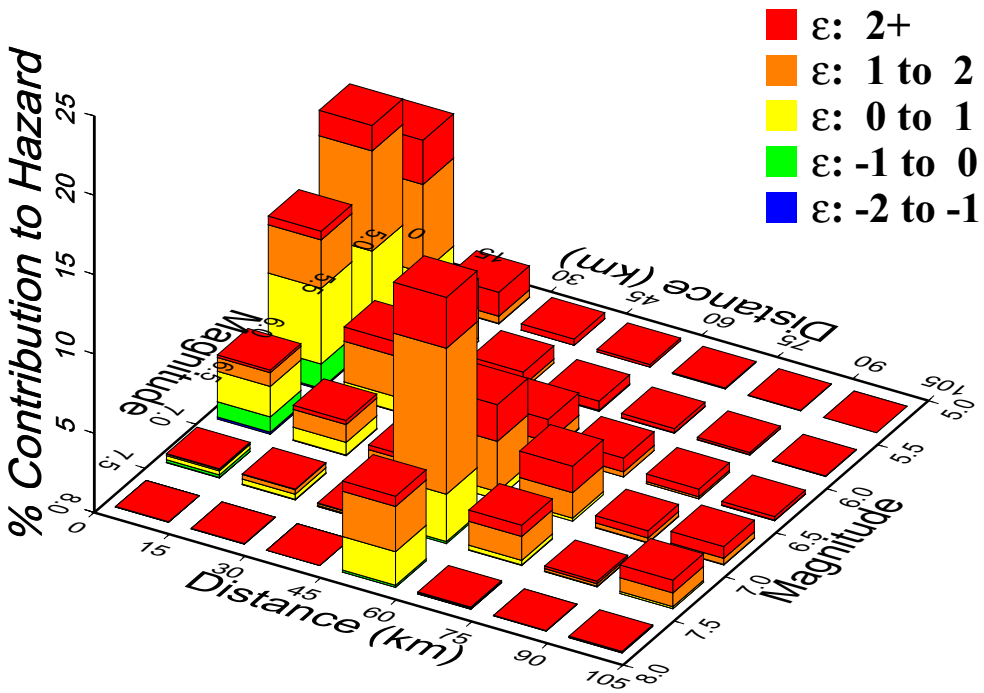

Source: BSC (2004 [DIRS 170027], Figure Figure 6.2-23

Figure 6.4.1-11. Contribution to Mean Hazard by Magnitude, Distance, and Epsilon (ε) for the 1-2 Hz Horizontal Ground Motions, 10^{-3} Annual Exceedance Frequency

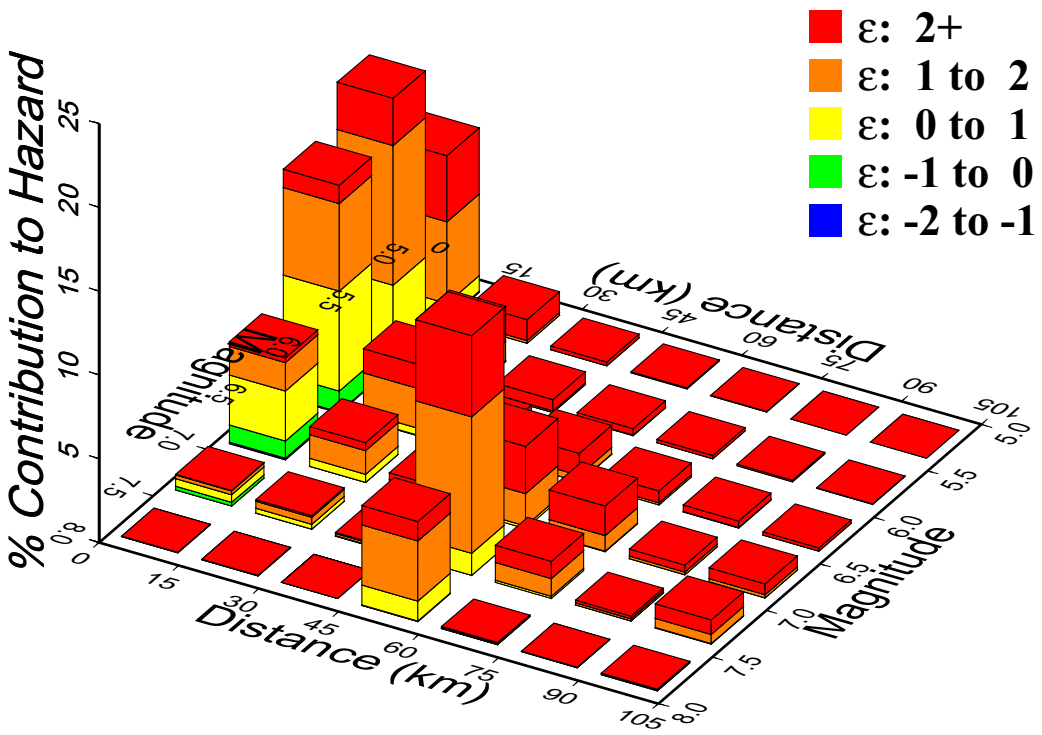

Source: BSC (2004 [DIRS 170027], Figure 6.2-24

Figure 6.4.1-12. Contribution to Mean Hazard by Magnitude, Distance, and Epsilon (ε) for the 1-2 Hz Horizontal Ground Motions, $5x10^{-4}$ Annual Exceedance Frequency

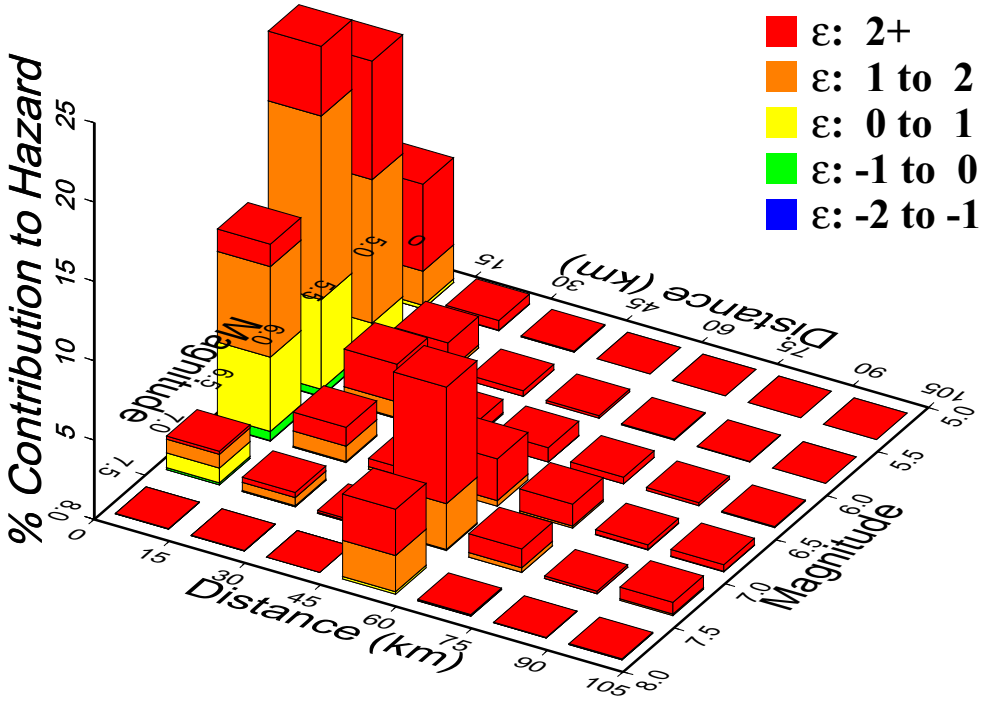

Source: BSC (2004 [DIRS 170027], Figure 6.2-25

Figure 6.4.1-13. Contribution to Mean Hazard by Magnitude, Distance, and Epsilon (ε) for the 1-2 Hz Horizontal Ground Motions, 10^{-4} Annual Exceedance Frequency

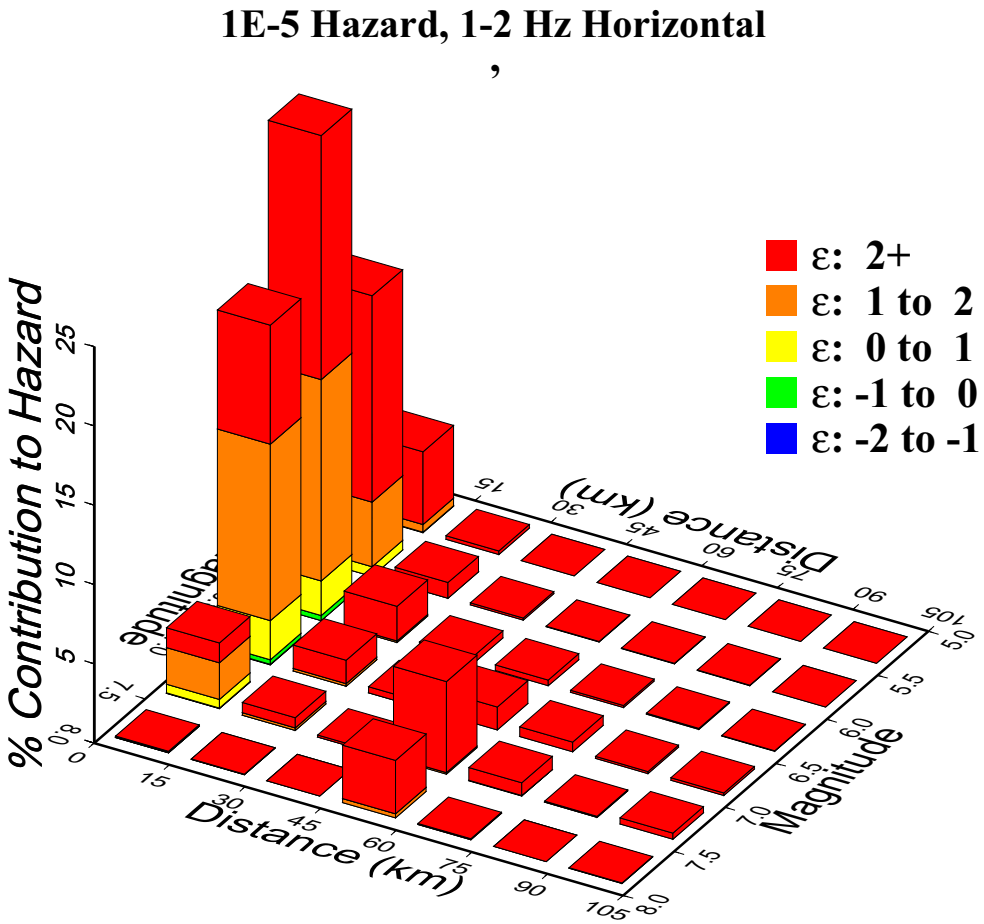

Source: BSC (2004 [DIRS 170027], Figure 6.2-26

Figure 6.4.1-14. Contribution to Mean Hazard by Magnitude, Distance, and Epsilon (ε) for the 1-2 Hz Horizontal Ground Motions, 10^{-5} Annual Exceedance Frequency

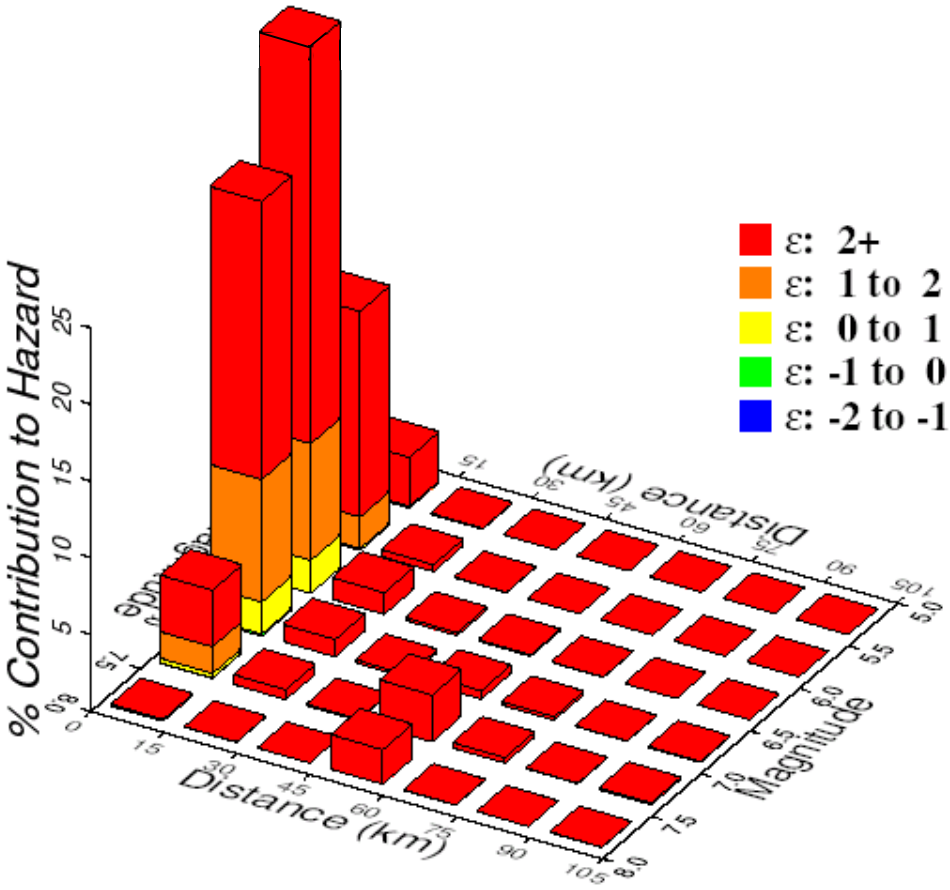

Source: BSC (2004 [DIRS 170027], Figure 6.2-27

Figure 6.4.1-15. Contribution to Mean Hazard by Magnitude, Distance, and Epsilon (ε) for the 1-2 Hz Horizontal Ground Motions, 10^{-6} Annual Exceedance Frequency

1E-7 Hazard, 1-2 Hz Horizontal

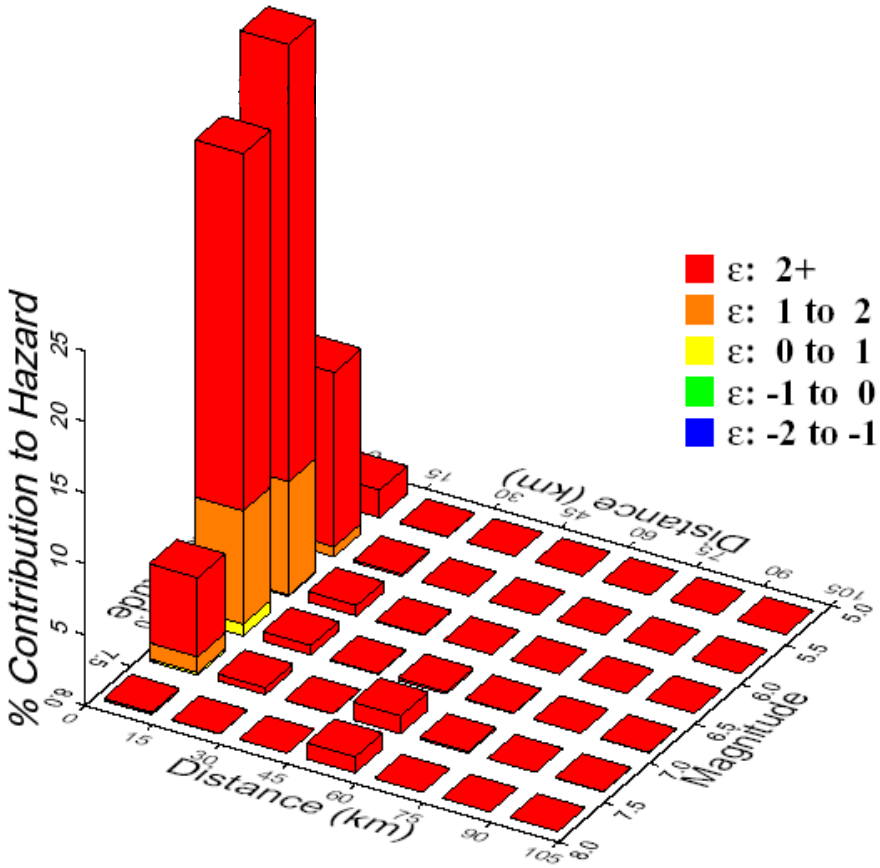

Source: BSC (2004 [DIRS 170027], Figure 6.2-28

Figure 6.4.1-16. Contribution to Mean Hazard by Magnitude, Distance, and Epsilon (ε) for the 1-2 Hz Horizontal Ground Motions, 10^{-7} Annual Exceedance Frequency

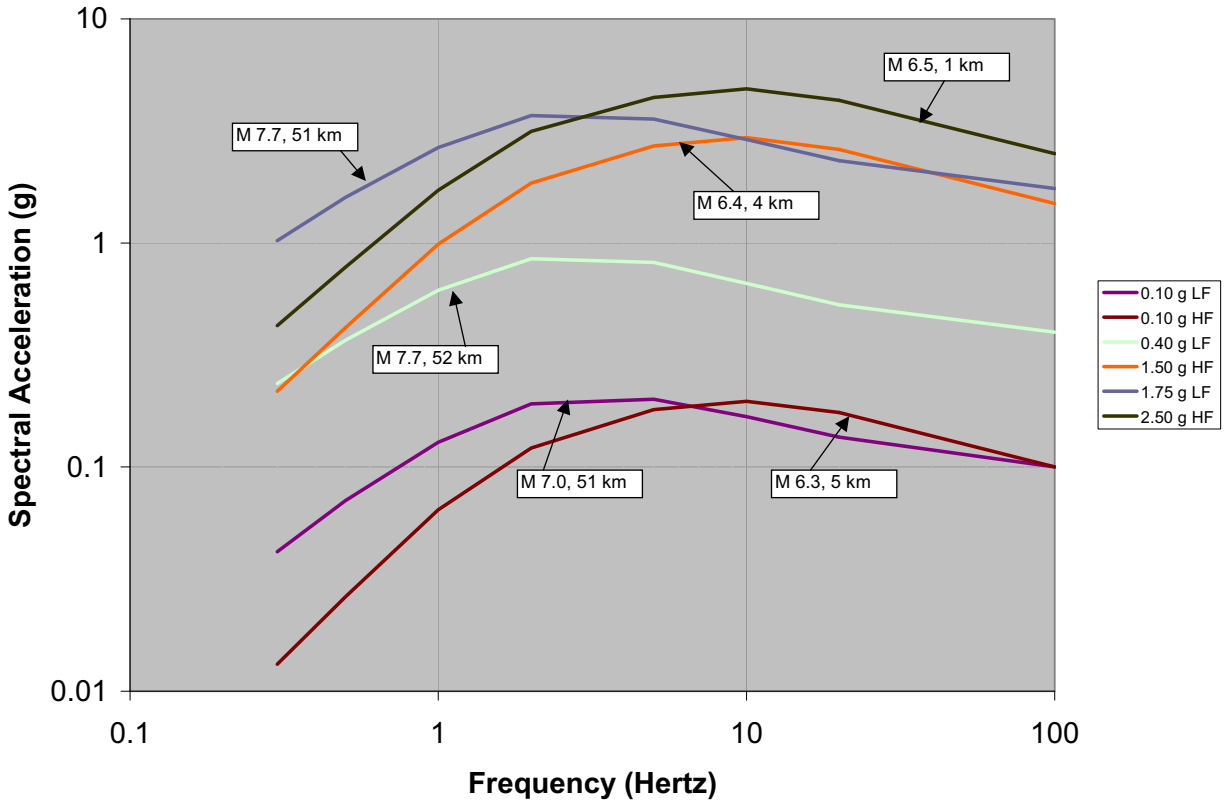

Sources: Appendix D, Table D-1

Notes:

1. Labels indicate the magnitude and distance of the reference earthquake providing the response spectral shape that is scaled to the PGA level of interest
2. LF = low frequency (1 to 2 Hz) response spectrum; HF = high frequency (5 to 10 Hz) response spectrum

Figure 6.4.1-17. Representative Control Motion Response Spectra for Site Response Modeling

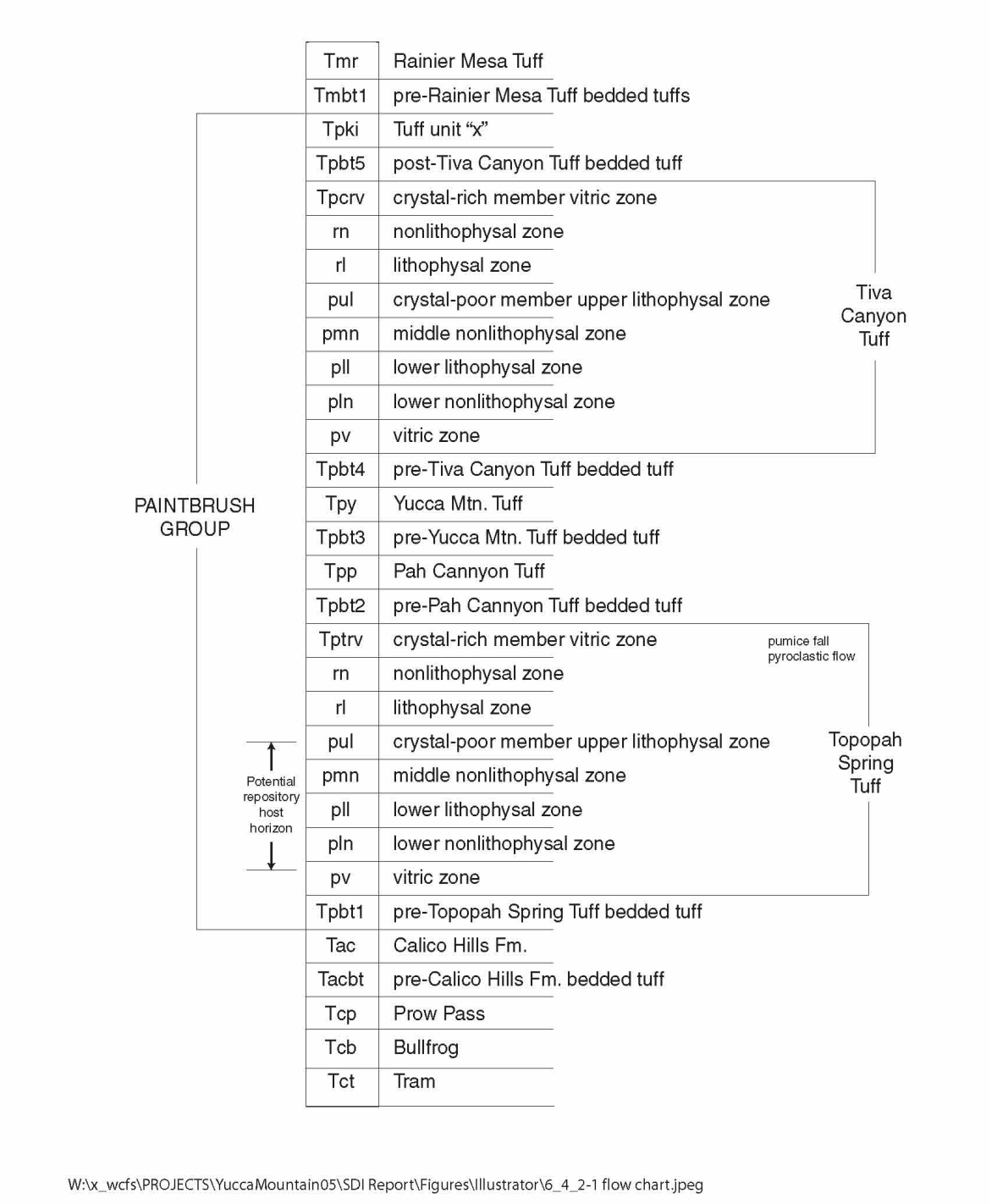

Figure 6.4.2-1. Generalized Lithostratigraphic Column of the Paintbrush Group and Adjacent Units

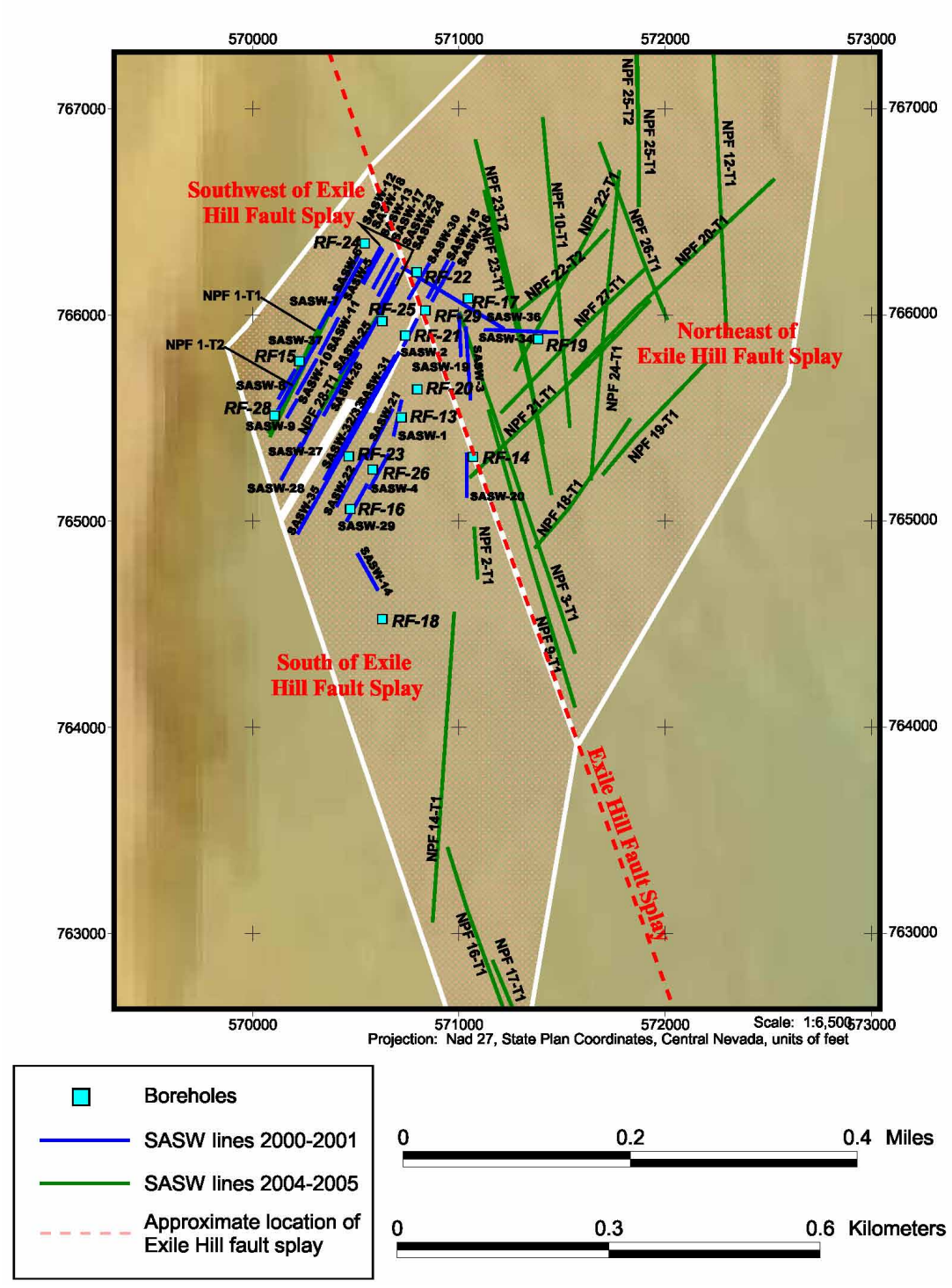

Source: BSC 2004 [DIRS 170027], Figure 6.2-90

MO0701ABSRFLL2.000 [DIRS 182483] AND GS030783114233.001 [DIRS 164561]

Note: The white lines separate three areas of SFA considered in developing velocity profiles.

Figure 6.4.2-2. Map of the SFA, Boreholes With Seismic Surveys, SASW Surveys, and Velocity Zones

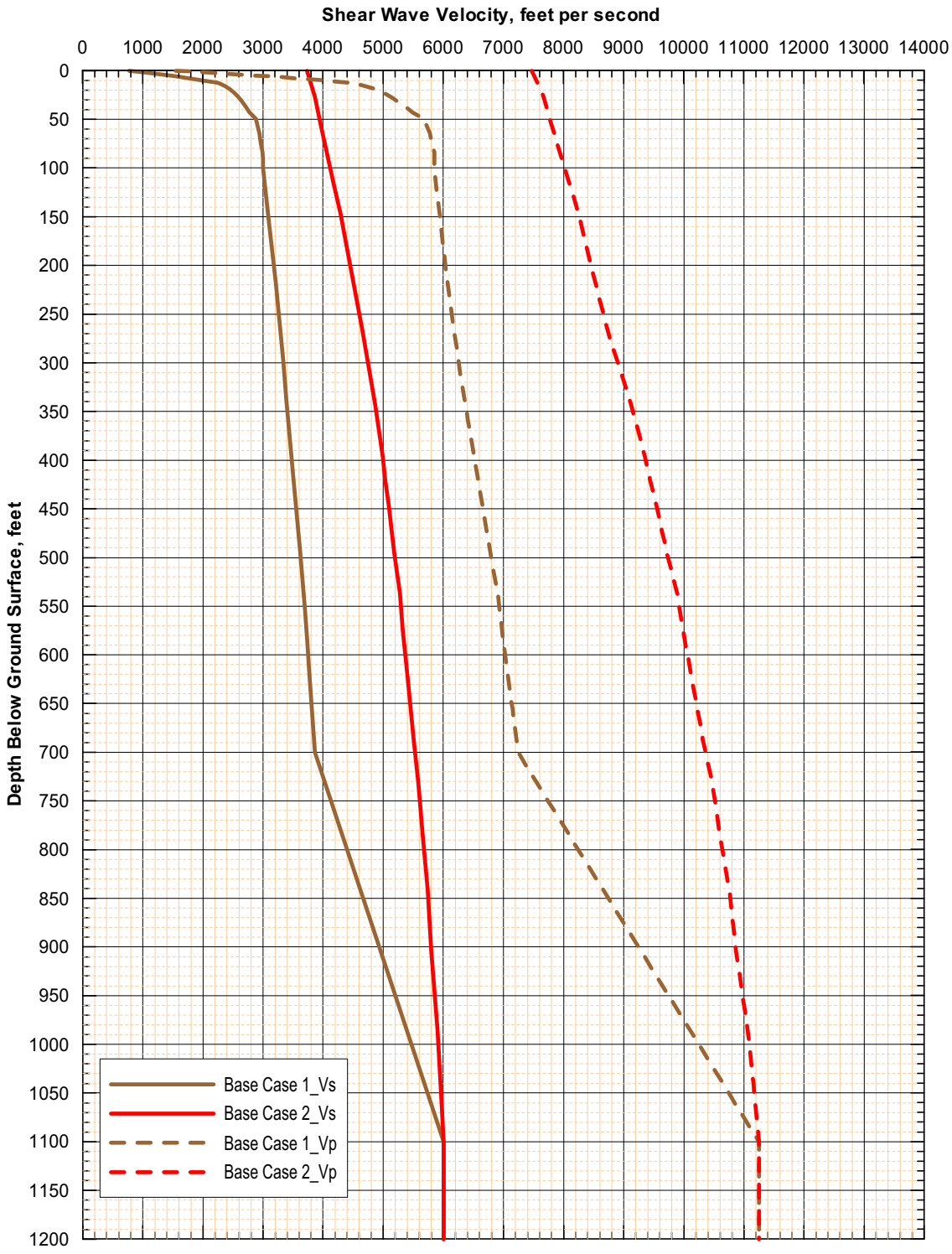

Source: BSC 2004 [DIRS 170027], Figure 6.2-118; Appendix C, Table C-1

Note: V_S profile shown in black; V_P profile shown in blue. Dashed and solid lines represent smoothed and unsmoothed base case profiles.

Figure 6.4.2-3. 2004 Base Case V_S Profiles Developed for the RB

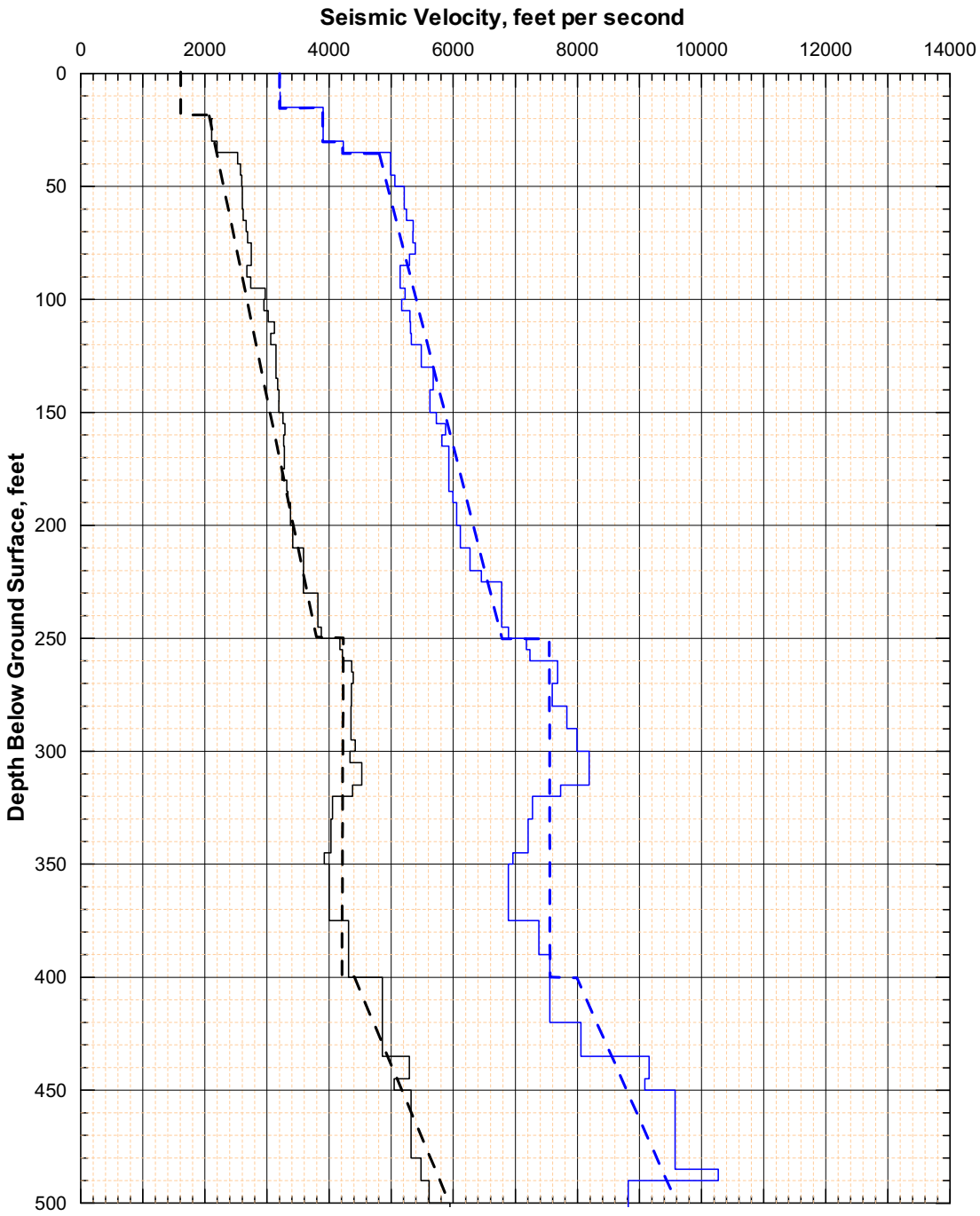

Source: BSC 2004 [DIRS 170027], Figures 6.2-119 and 6.2-120

Note: Vs profile shown in black; Vp profile shown in blue. Solid and dashed lines show unsmoothed and smoothed base case profiles, respectively.

Figure 6.4.2-4. 2004 Base Case V_S and V_P Profiles Developed for Tuff at SFA

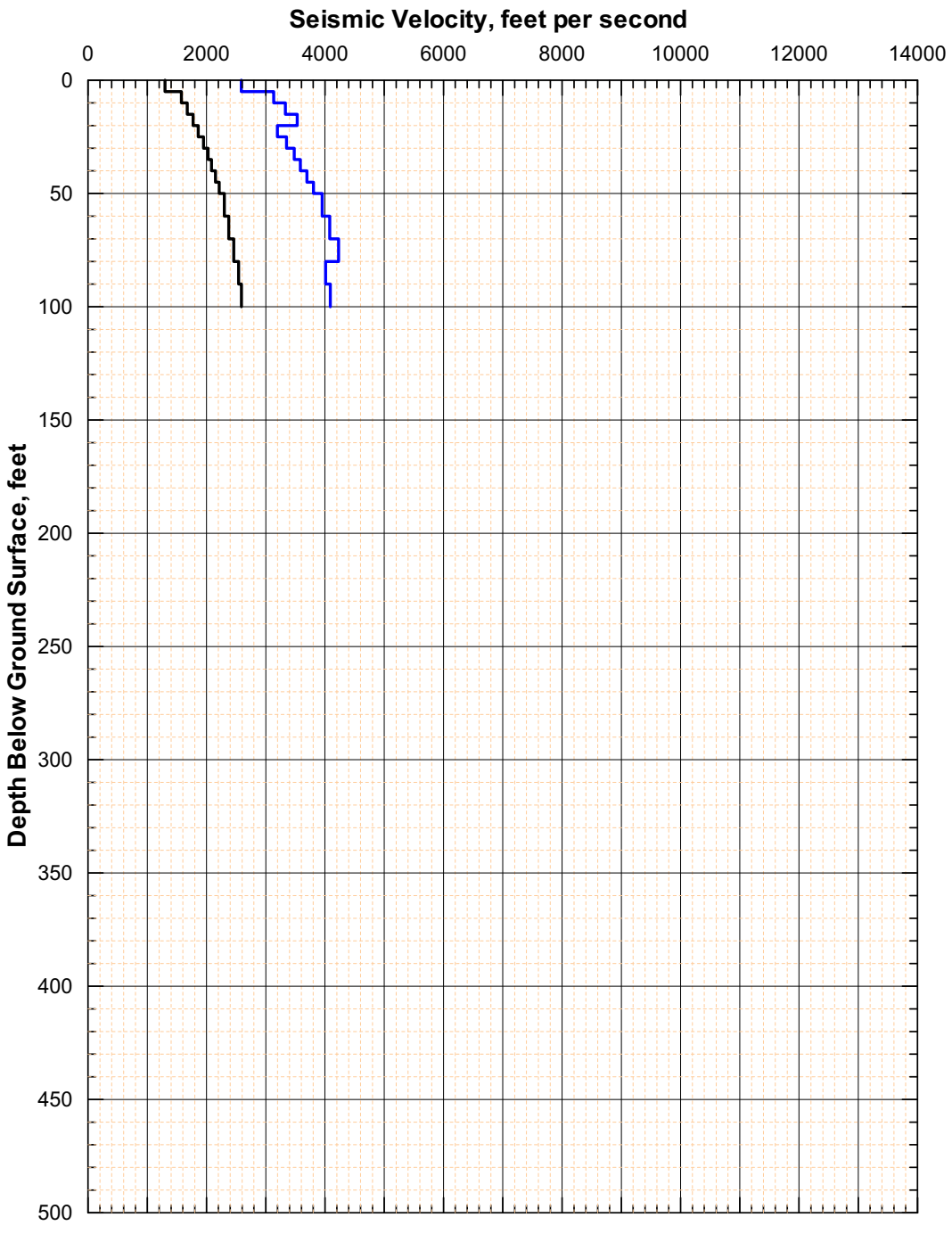

Source: BSC 2004 [DIRS 170027], Figures 6.2-121 and 6.2-122

Figure 6.4.2-5. 2004 Base Case V_S and V_P Profiles Developed for Alluvium at SFA

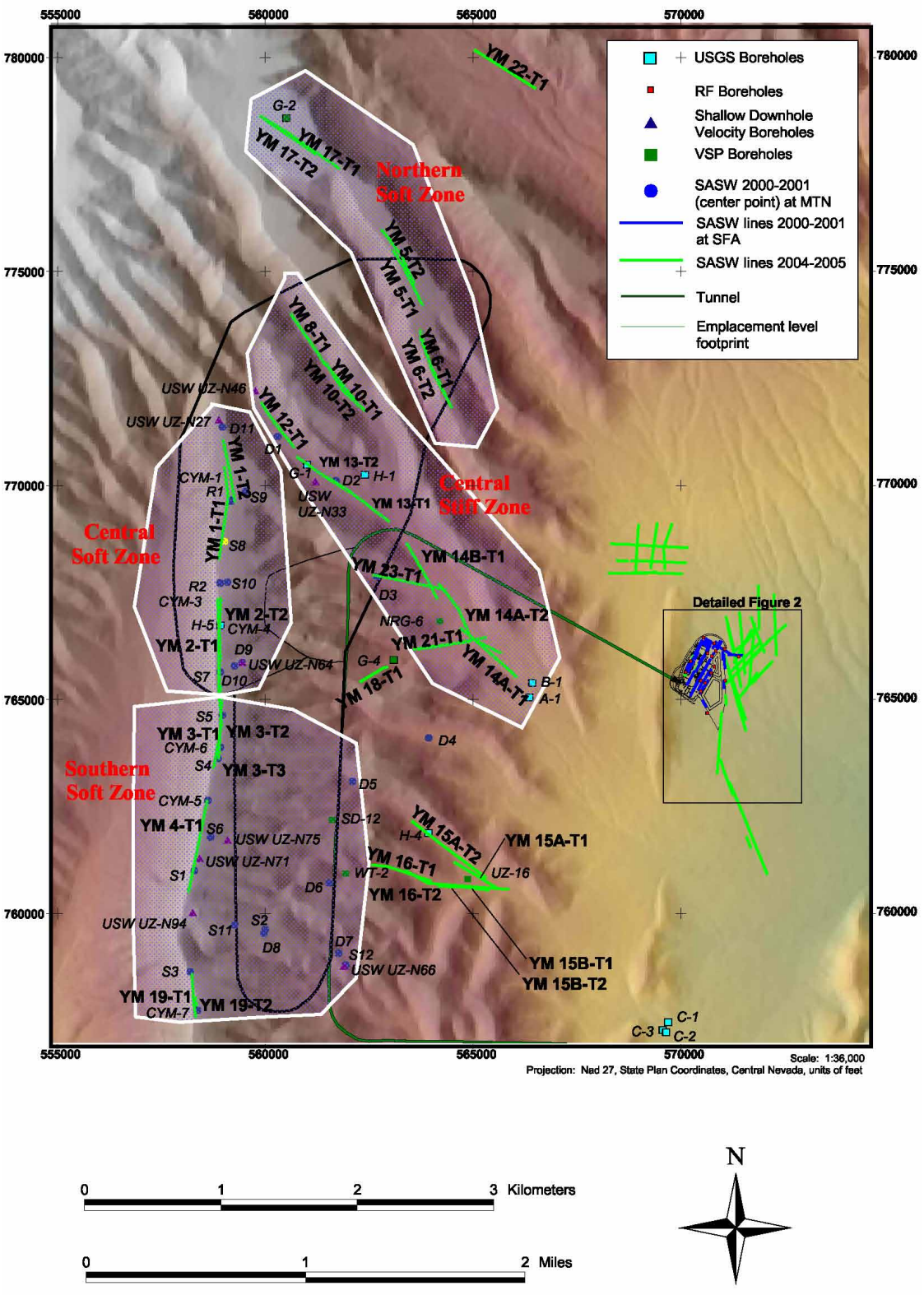

Source: BSC 2004 [DIRS 170027], Figure 6.2-90; Appendix C, Table C-1

Figure 6.4.2-6. Map of RB Showing all the Seismic Velocity Measurements

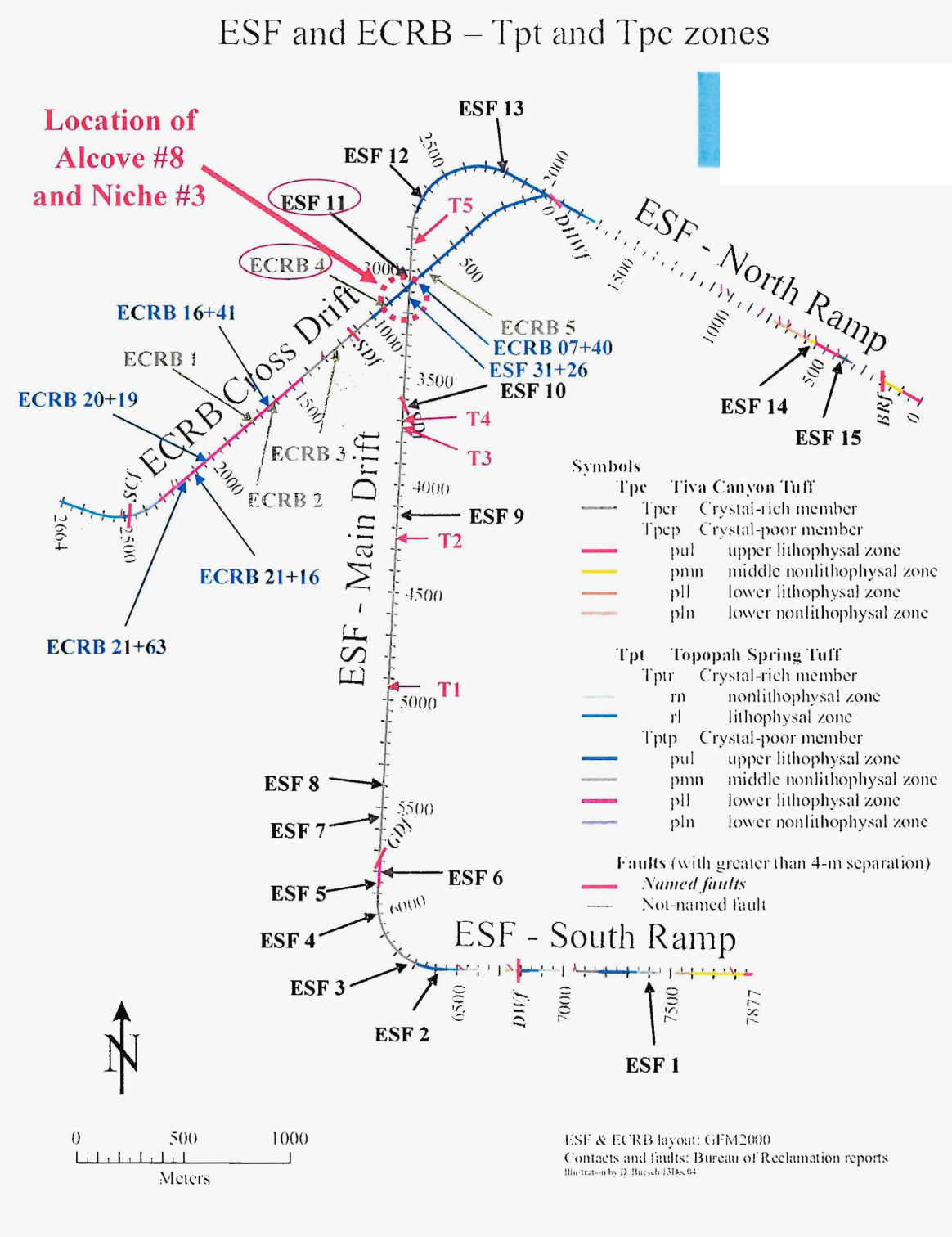

Source: Lin 2007 [DIRS 182739]

Figure 6.4.2-7. Locations of SASW Test Sites and NSA Engineering Inc. Test Site (2001) in the ESF and ECRB Tunnels

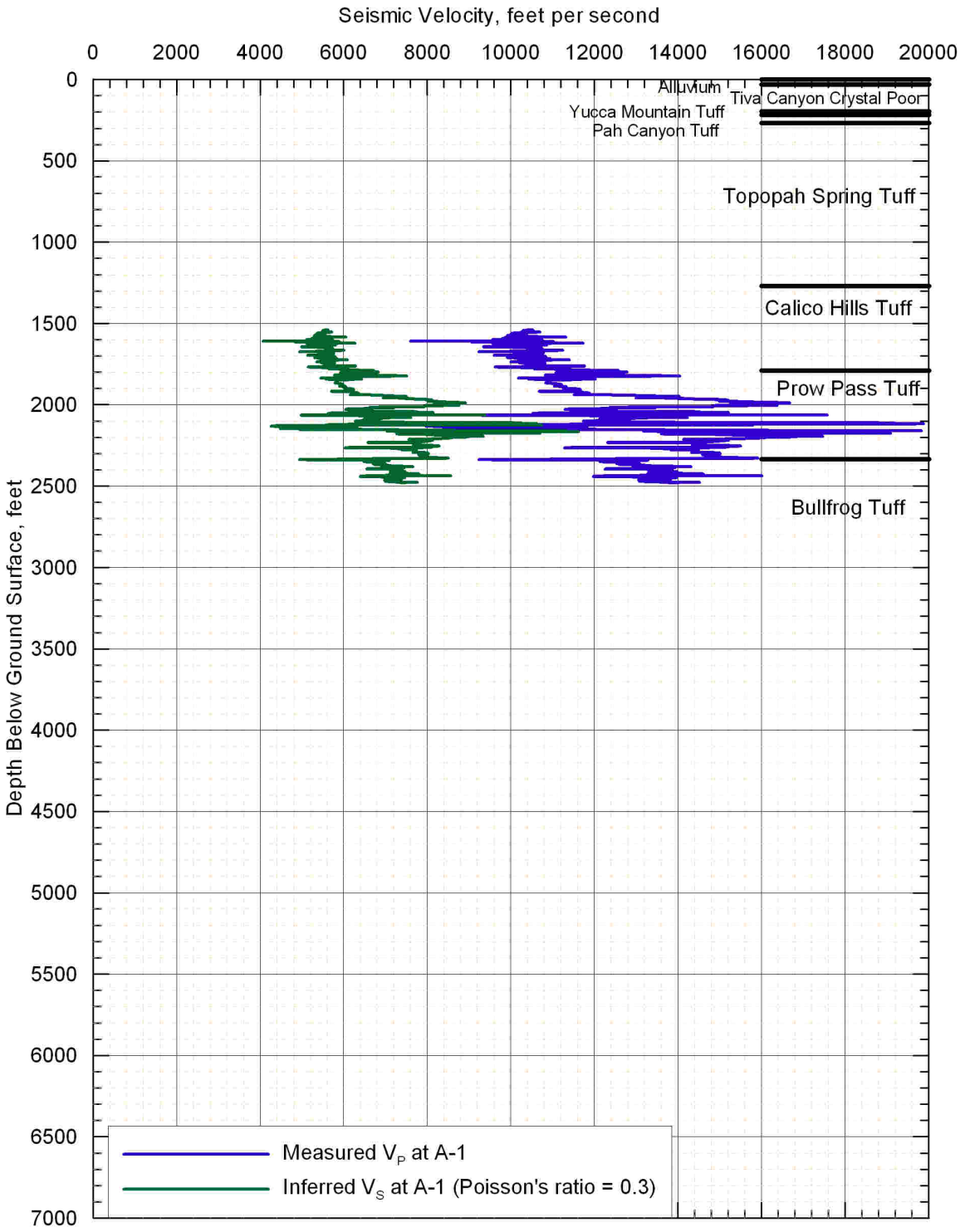

Source: Nelson et al 1991 [DIRS 101272]; Appendix C, Table C-1

Figure 6.4.2-8. Velocity Profiles from Sonic-Velocity Logging at Borehole UE-25 A-1

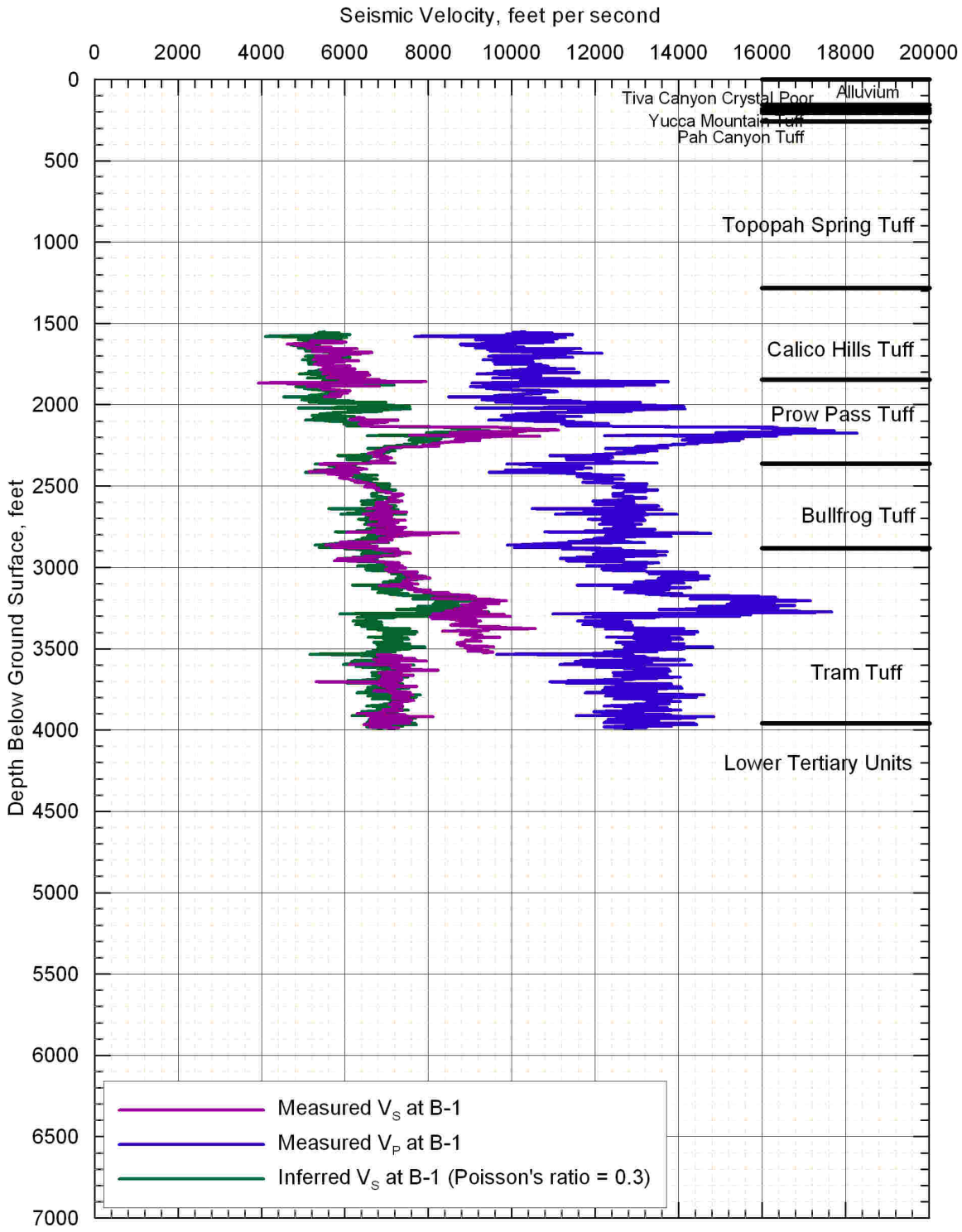

Source: Nelson et al 1991 [DIRS 101272]; Appendix C, Table C-1

Figure 6.4.2-9. Velocity Profiles from Sonic-Velocity Logging at Borehole UE-25 B-1

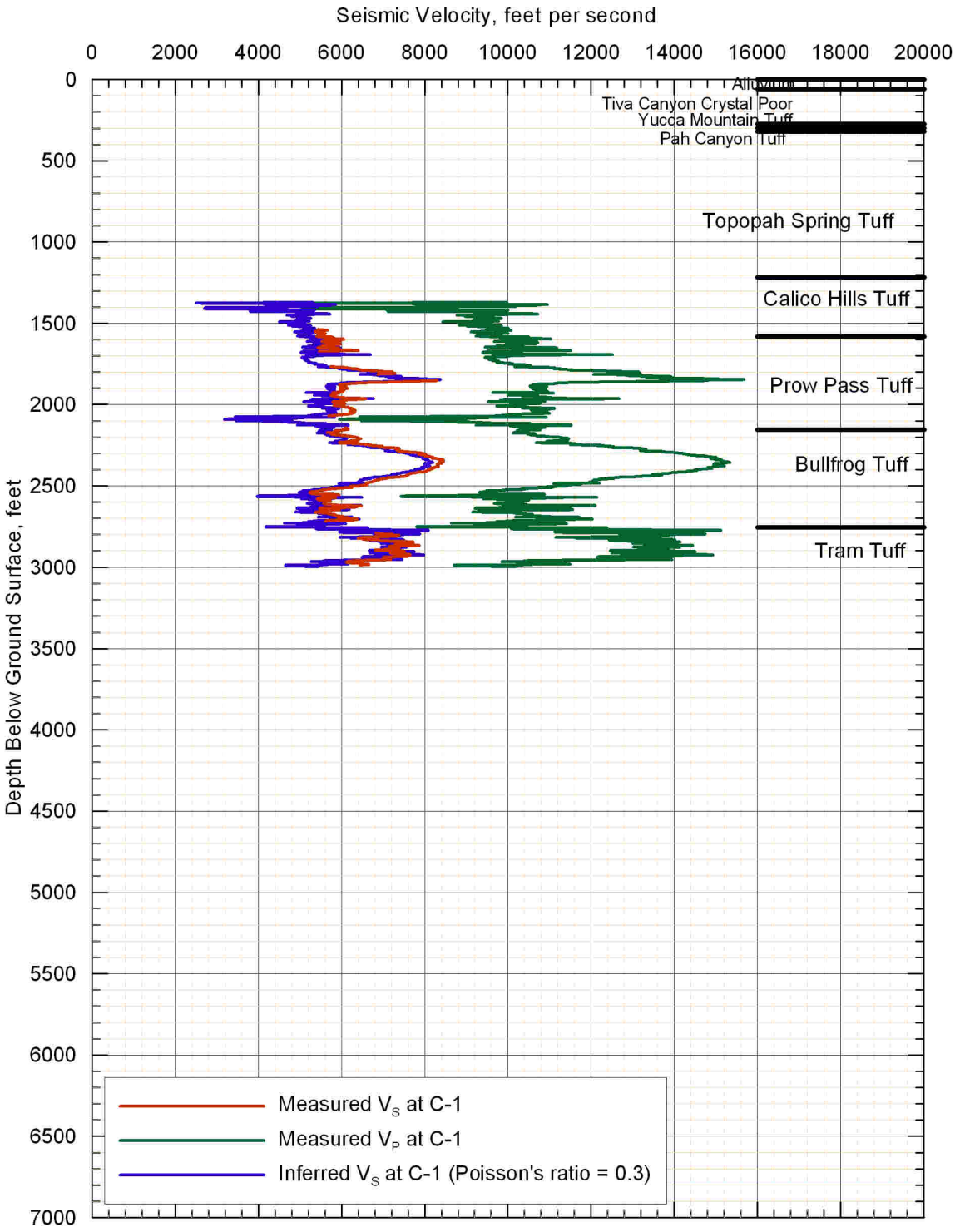

Source: Nelson et al 1991 [DIRS 101272]; Appendix C, Table C-1

Figure 6.4.2-10. Velocity Profiles from Sonic-Velocity Logging at Borehole UE-25 C-1

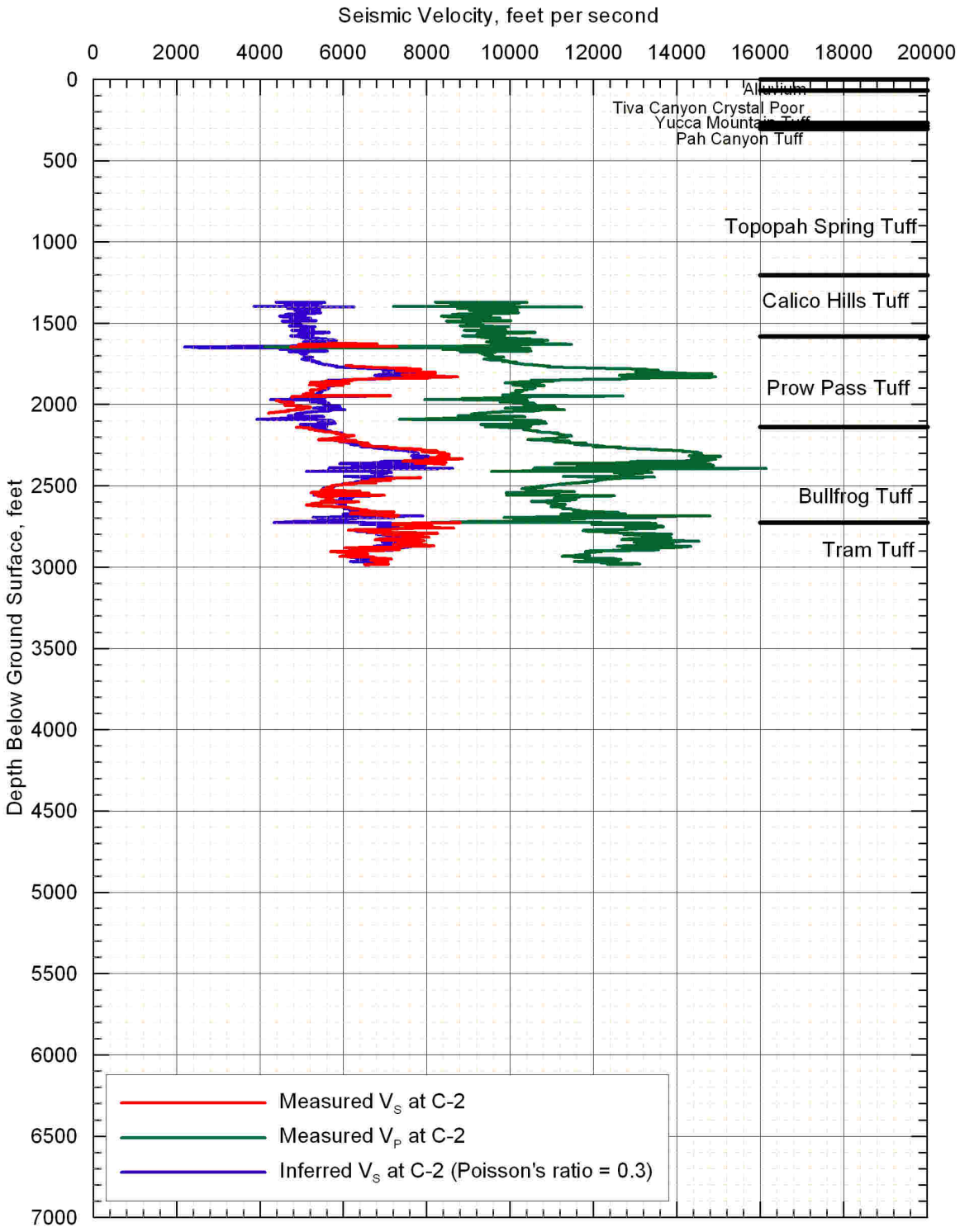

Source: Nelson et al 1991 [DIRS 101272]; Appendix C, Table C-1

Figure 6.4.2-11. Velocity Profiles from Sonic-Velocity Logging at Borehole UE-25 C-2

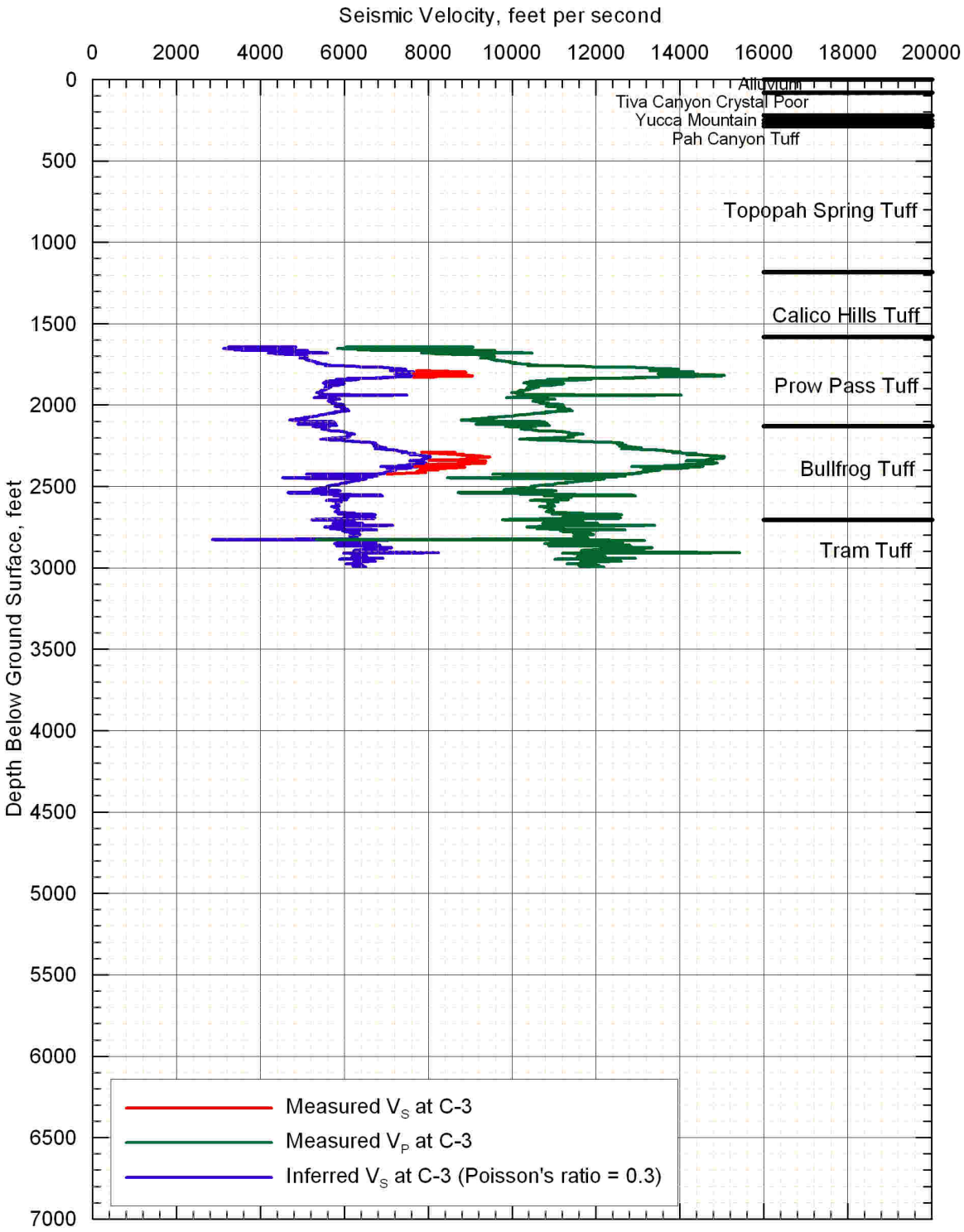

Source: Nelson et al 1991 [DIRS 101272]; Appendix C, Table C-1

Figure 6.4.2-12. Velocity Profiles from Sonic-Velocity Logging at Borehole UE-25 C-3

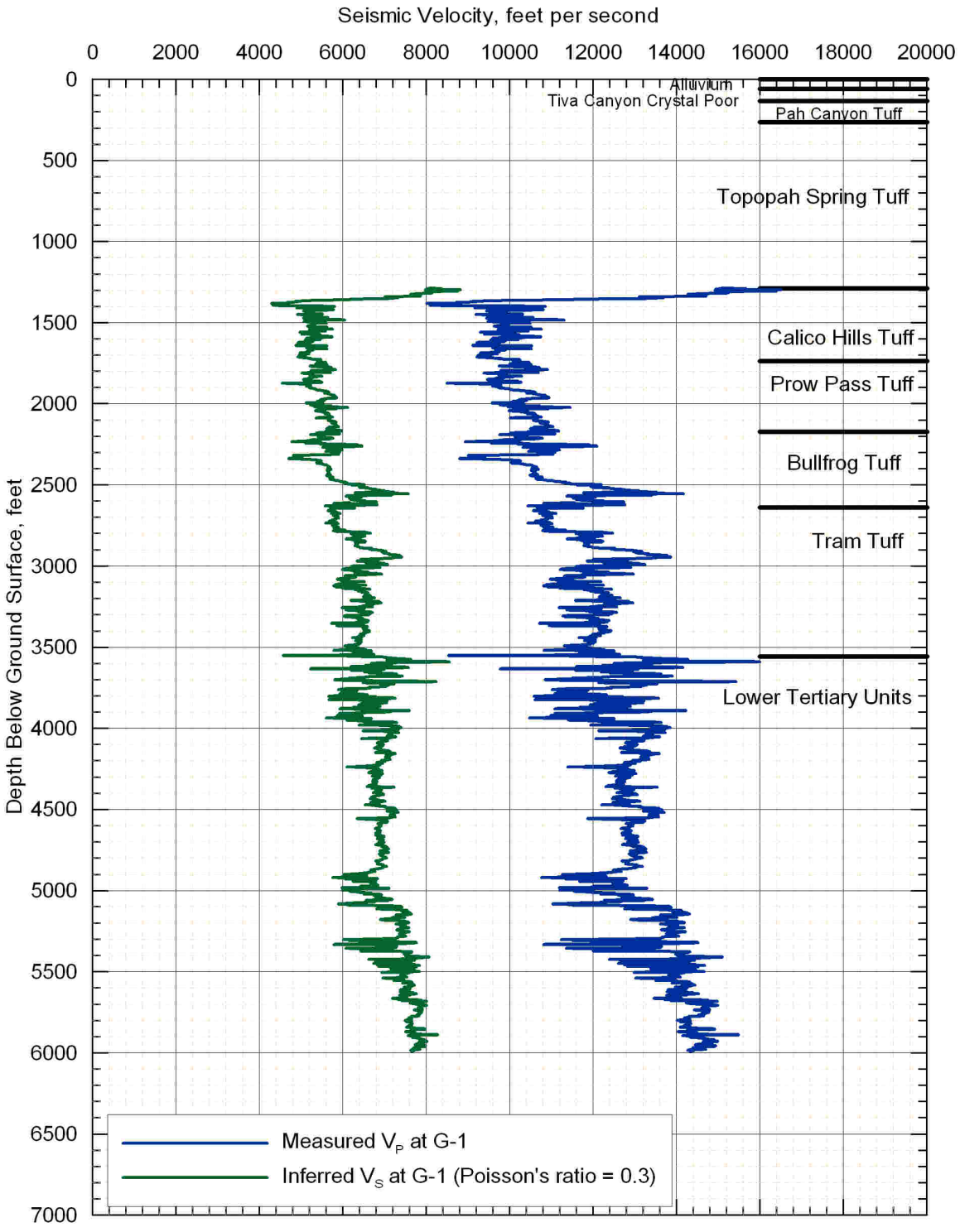

Source: Nelson et al 1991 [DIRS 101272]; Appendix C, Table C-1

Figure 6.4.2-13. Velocity Profiles from Sonic-Velocity Logging at Borehole USW G-1

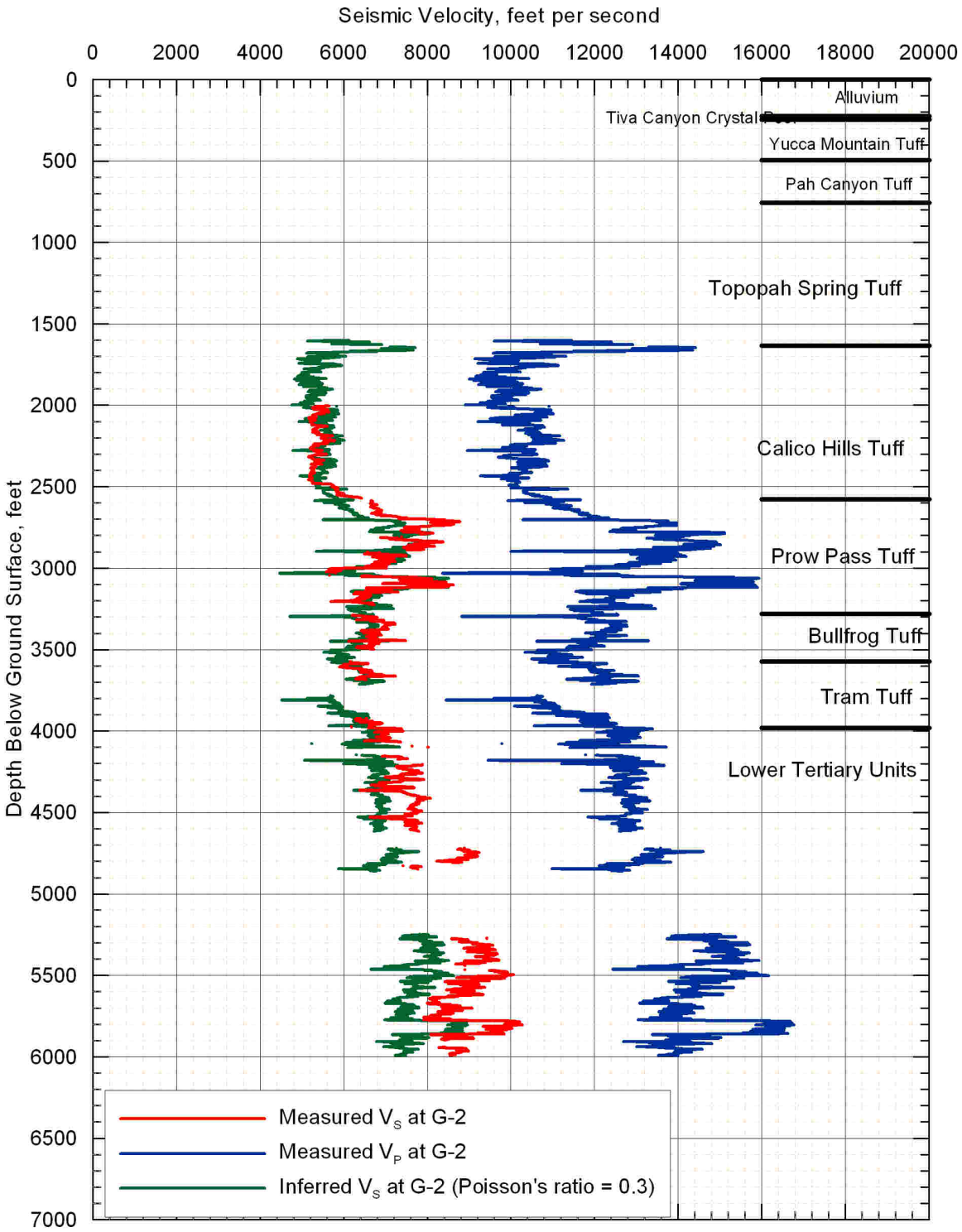

Source: Nelson et al 1991 [DIRS 101272]; Appendix C, Table C-1

Figure 6.4.2-14. Velocity Profiles from Sonic-Velocity Logging at Borehole USW G-2

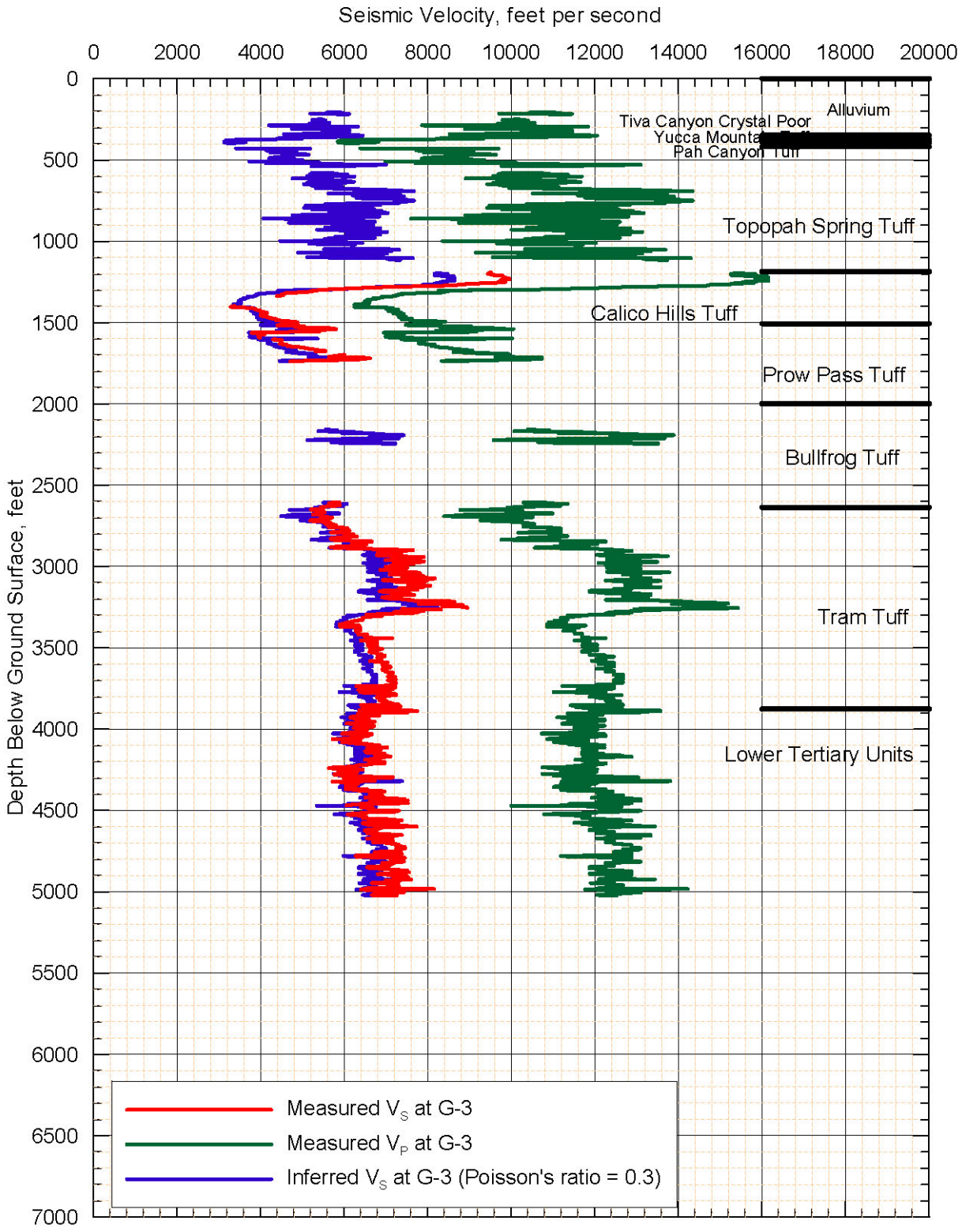

Source: Nelson et al 1991 [DIRS 101272]; Appendix C, Table C-1

Figure 6.4.2-15. Velocity Profiles from Sonic-Velocity Logging at Borehole USW G-3 and GU-3

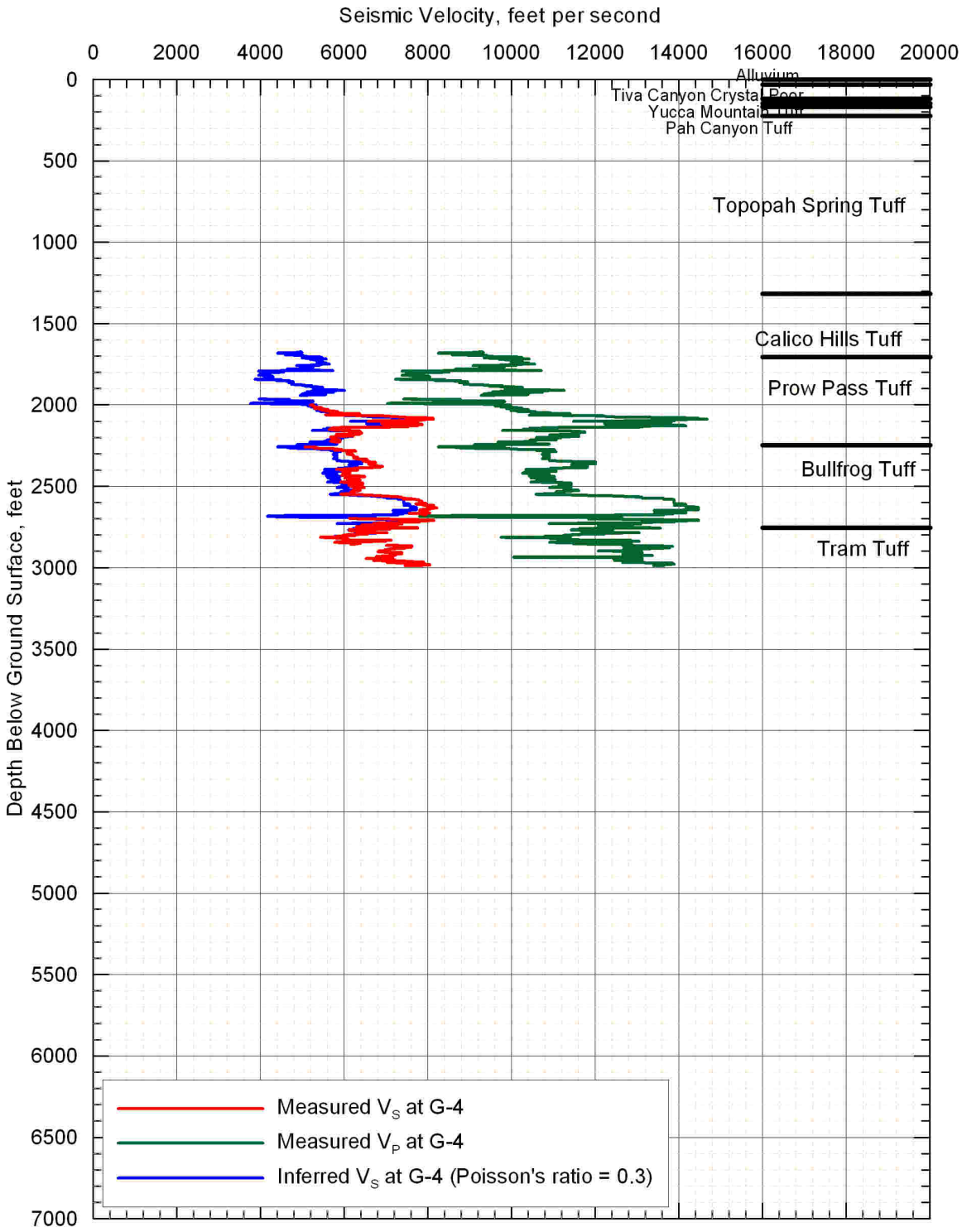

Source: Nelson et al 1991 [DIRS 101272]; Appendix C, Table C-1

Figure 6.4.2-16. Velocity Profiles from Sonic-Velocity Logging at Borehole USW G-4

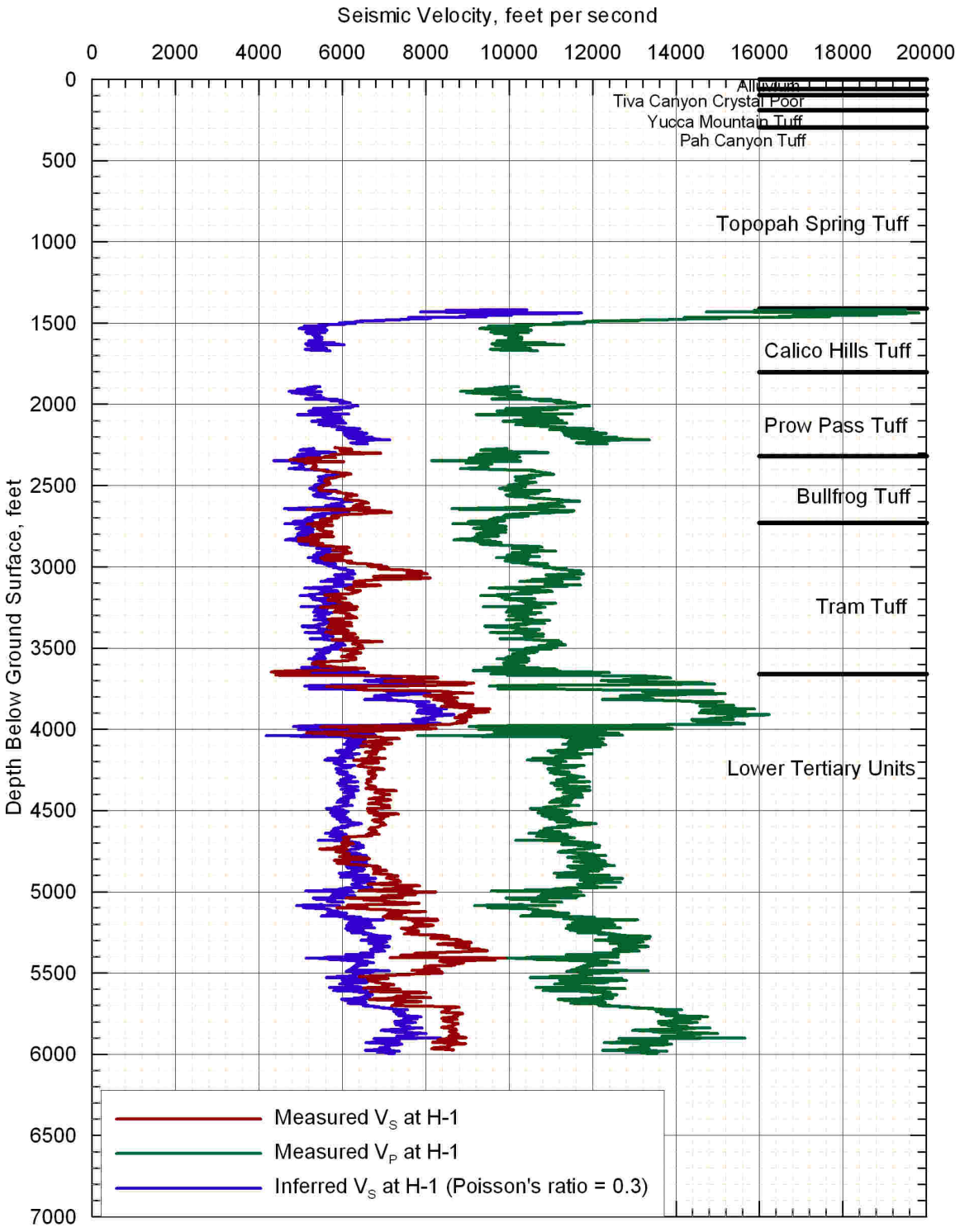

Source: Nelson et al 1991 [DIRS 101272]; Appendix C, Table C-1

Figure 6.4.2-17. Velocity Profiles from Sonic-Velocity Logging at Borehole USW H-1

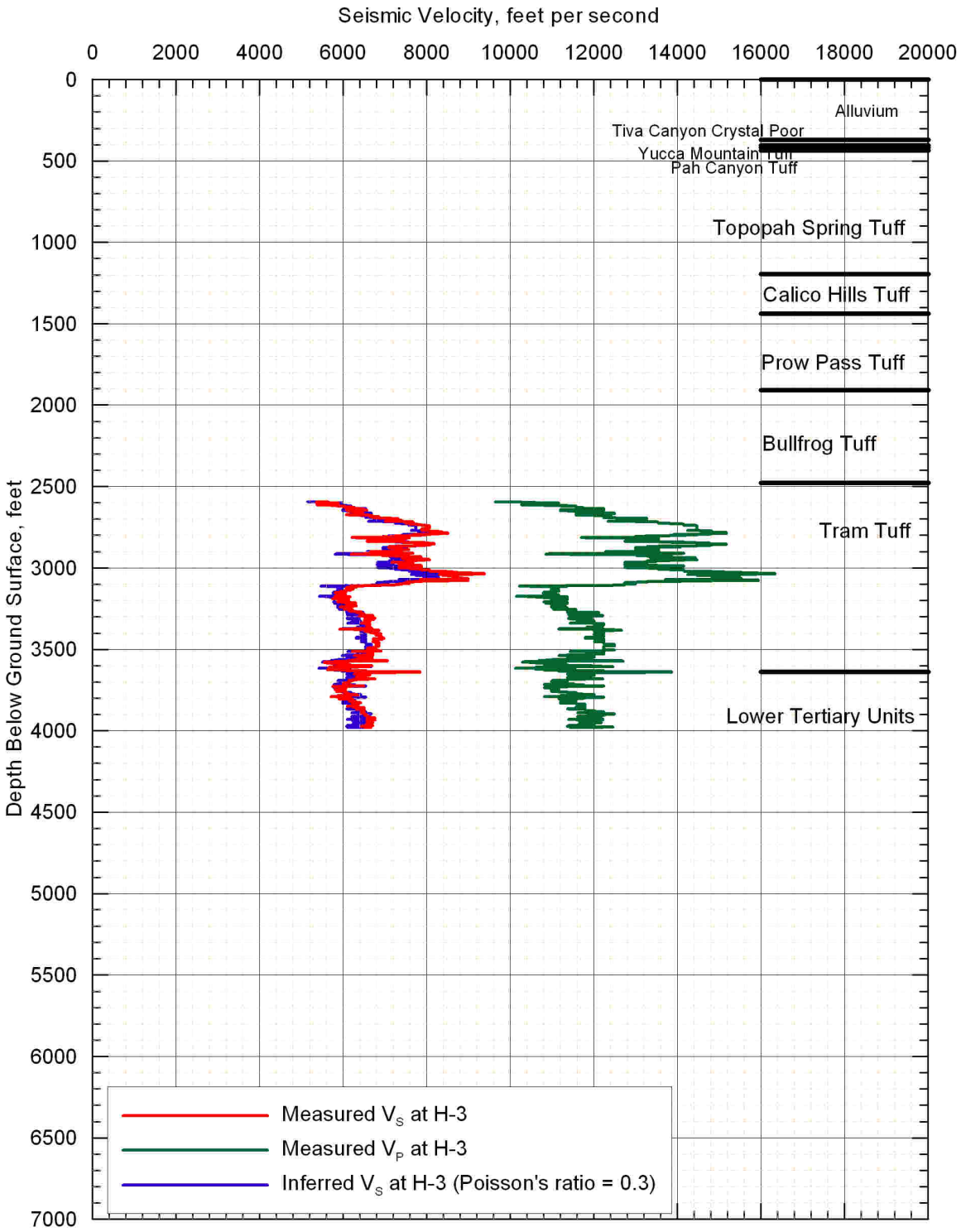

Source: Nelson et al 1991 [DIRS 101272]; Appendix C, Table C-1

Figure 6.4.2-18. Velocity Profiles from Sonic-Velocity Logging at Borehole USW H-3

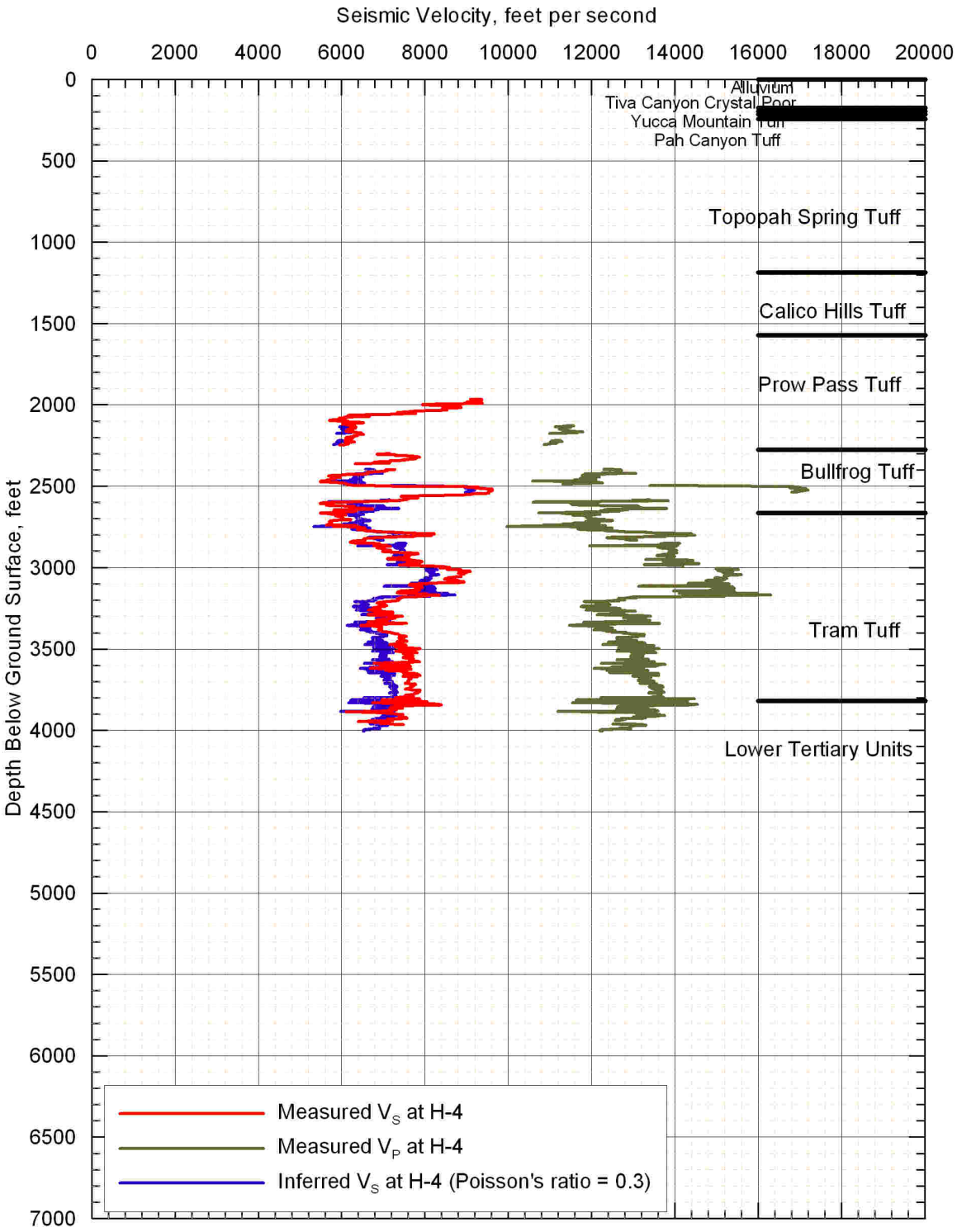

Source: Nelson et al 1991 [DIRS 101272]; Appendix C, Table C-1

Figure 6.4.2-19. Velocity Profiles from Sonic-Velocity Logging at Borehole USW H-4

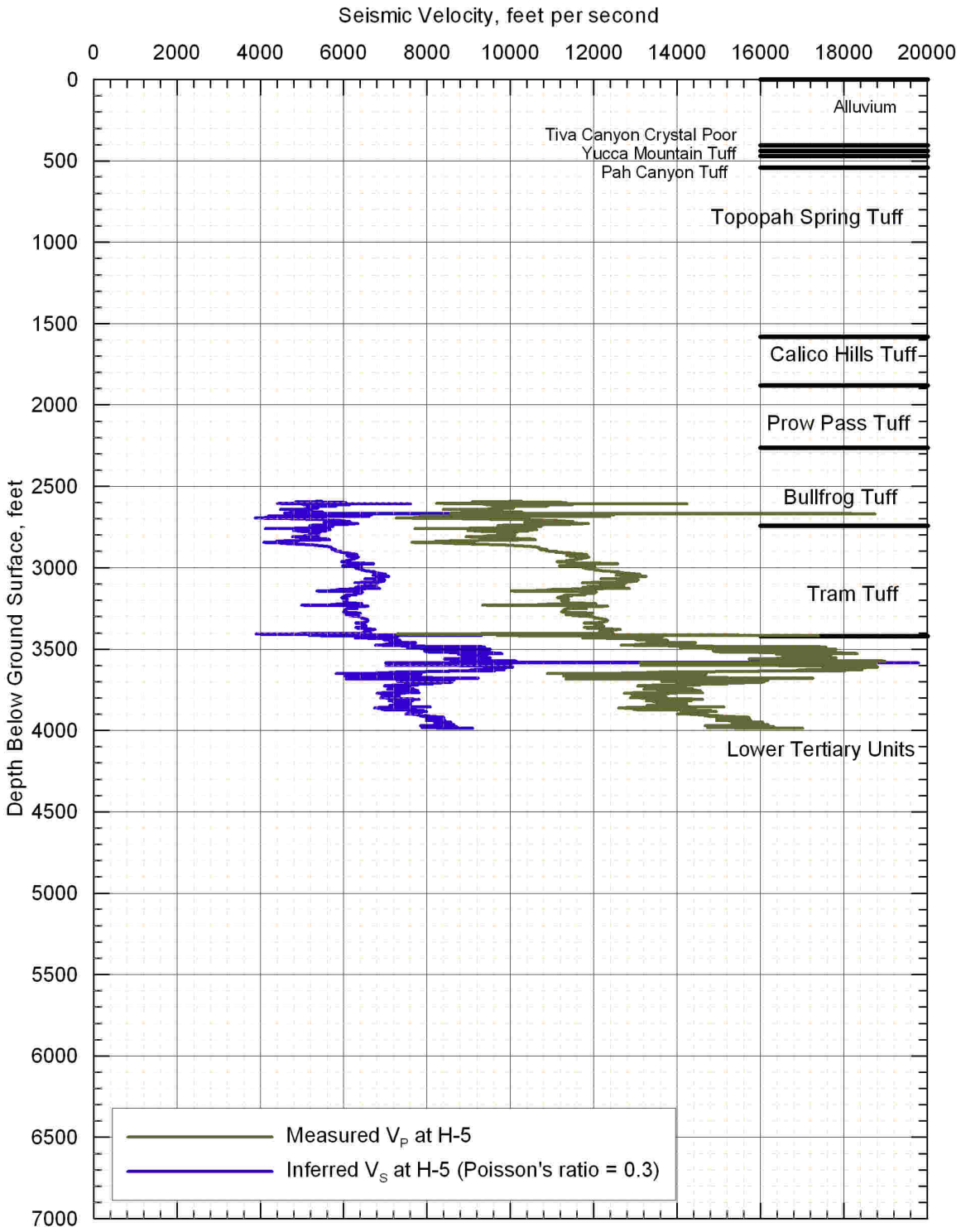

Source: Nelson et al 1991 [DIRS 101272]; Appendix C, Table C-1

Figure 6.4.2-20. Velocity Profiles from Sonic-Velocity Logging at Borehole USW H-5

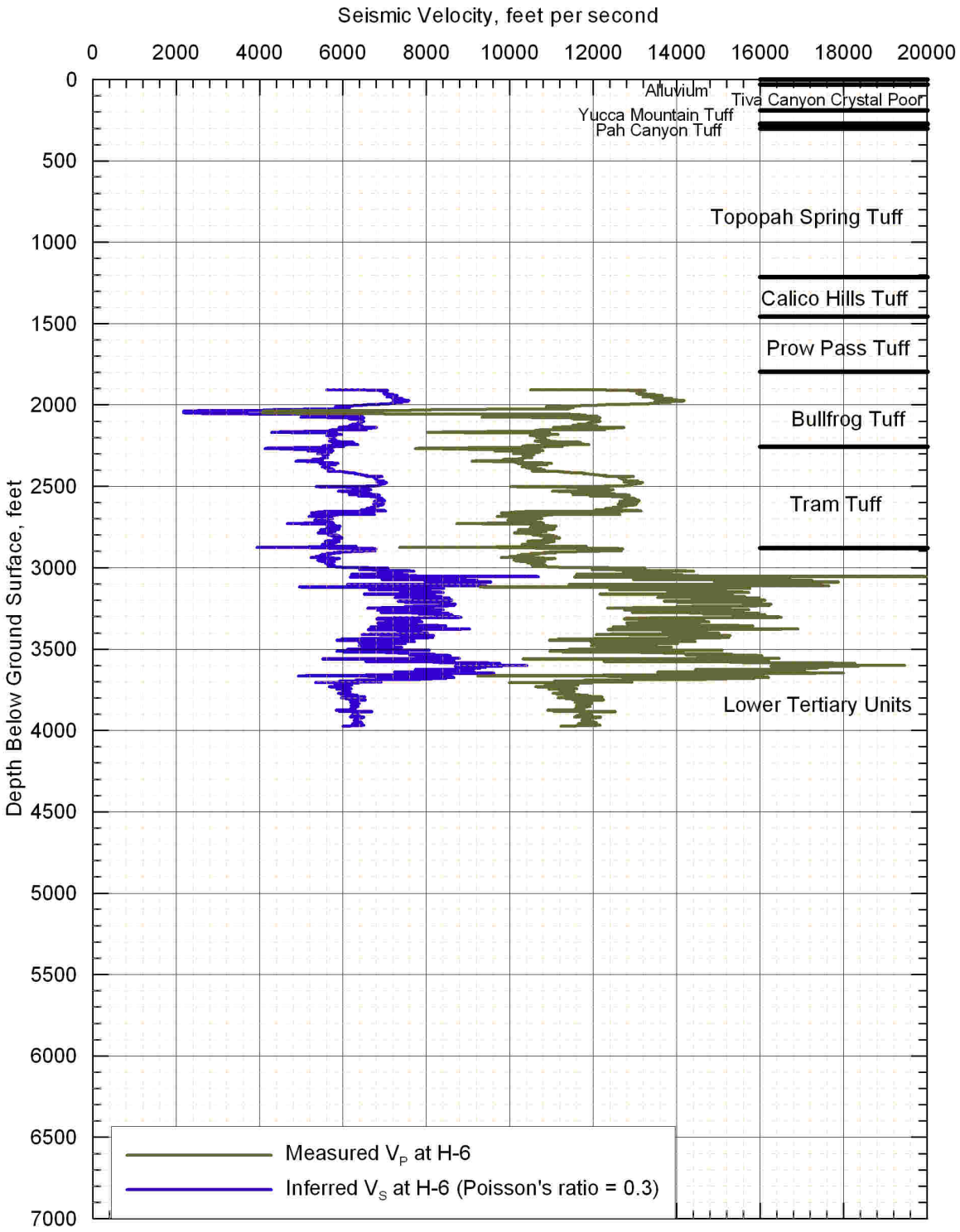

Source: Nelson et al 1991 [DIRS 101272]; Appendix C, Table C-1

Figure 6.4.2-21. Velocity Profiles from Sonic-Velocity Logging at Borehole USW H-6

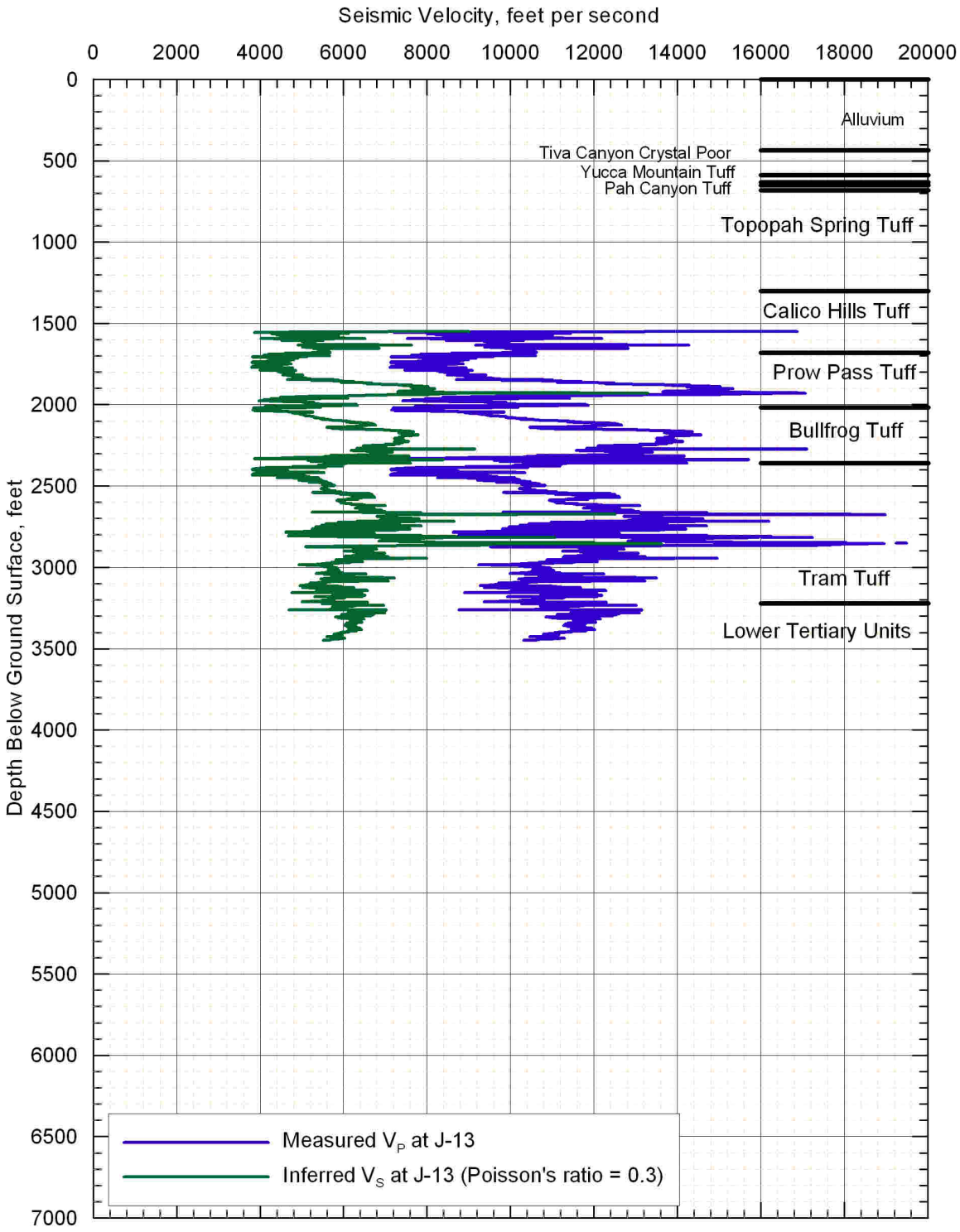

Source: Nelson et al 1991 [DIRS 101272]; Appendix C, Table C-1

Figure 6.4.2-22. Velocity Profiles from Sonic-Velocity Logging at Borehole USW J-13

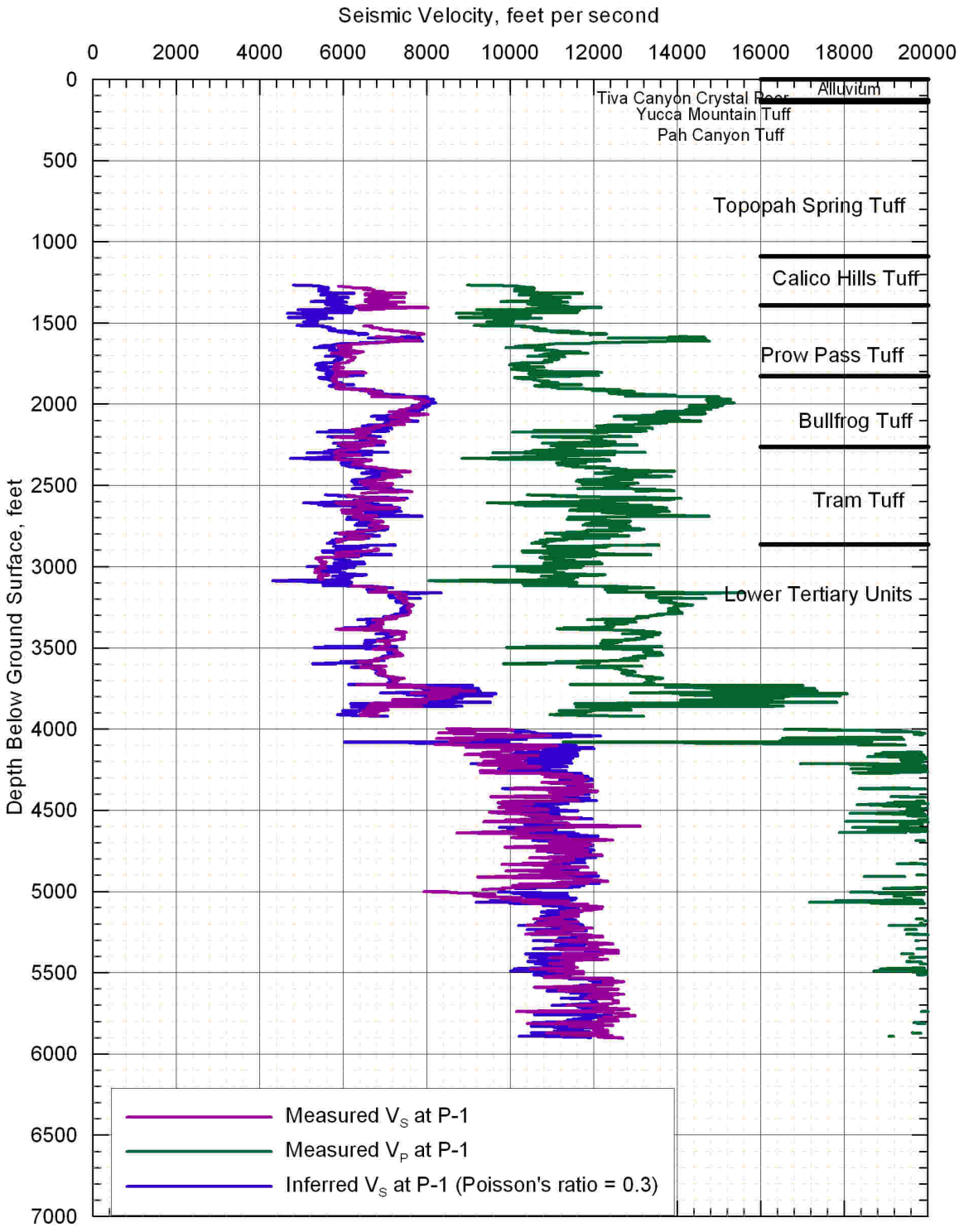

Source: Nelson et al 1991 [DIRS 101272]; Appendix C, Table C-1

Figure 6.4.2-23. Velocity Profiles from Sonic-Velocity Logging at Borehole UE-25 P-1

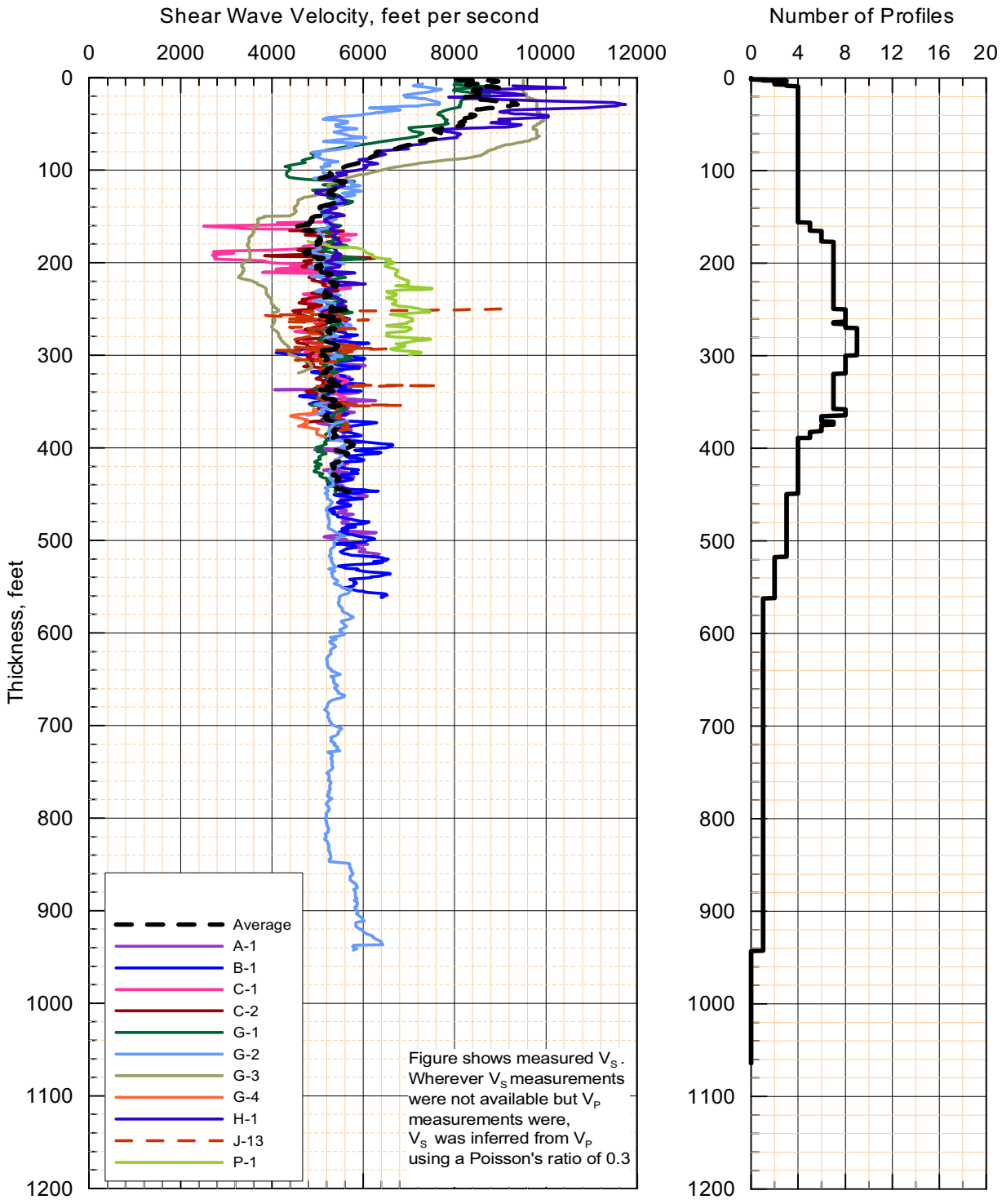

Source: Nelson et al 1991 [DIRS 101272]; Appendix C, Table C-1

Figure 6.4.2-24. Thickness and V_S Profiles for Calico Hills and Topopah Bottom Layer

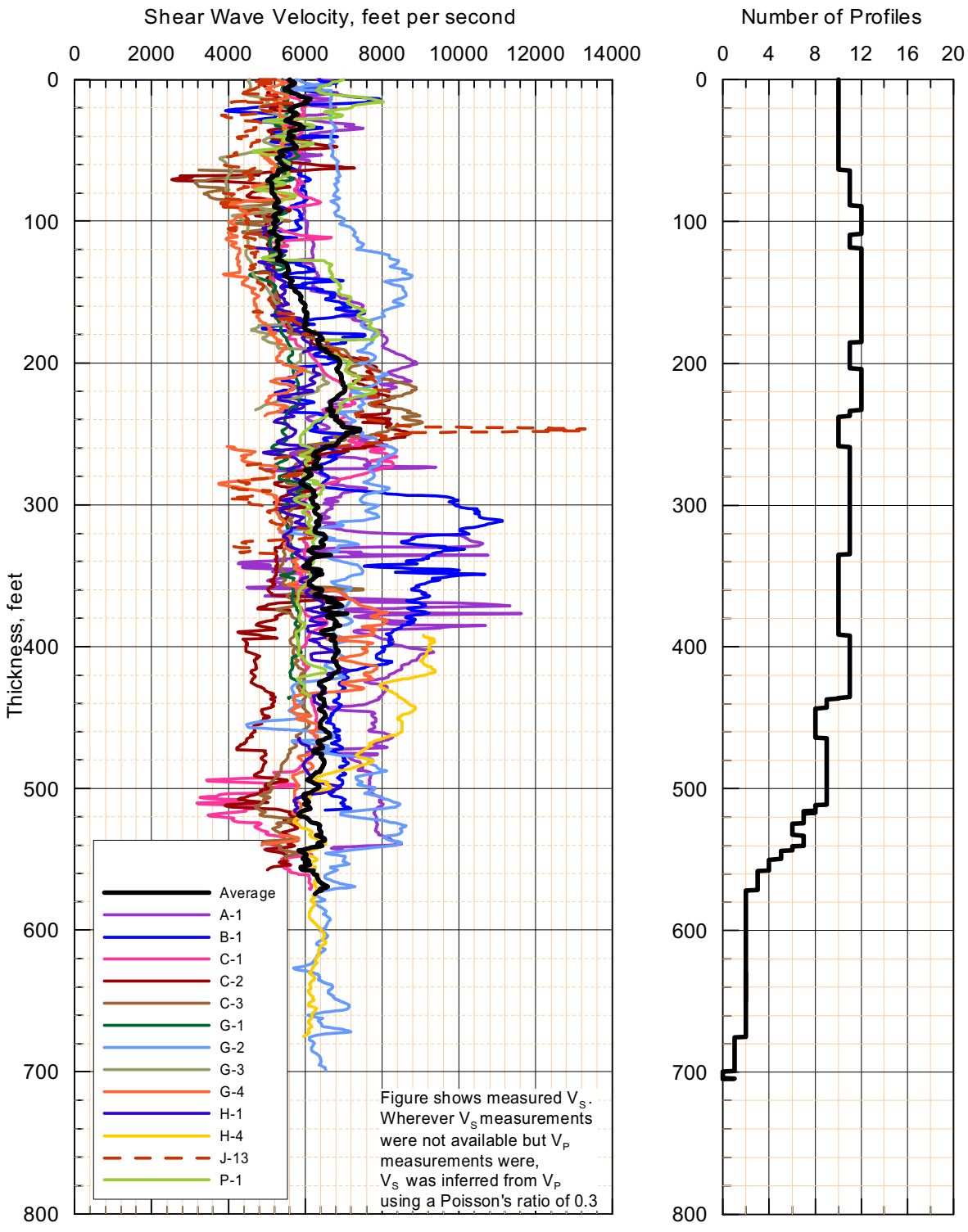

Source: Nelson et al 1991 [DIRS 101272]; Appendix C, Table C-1

Figure 6.4.2-25. Thickness and V_S Profiles for Prow Pass and Bottom of Calico Hills Layer

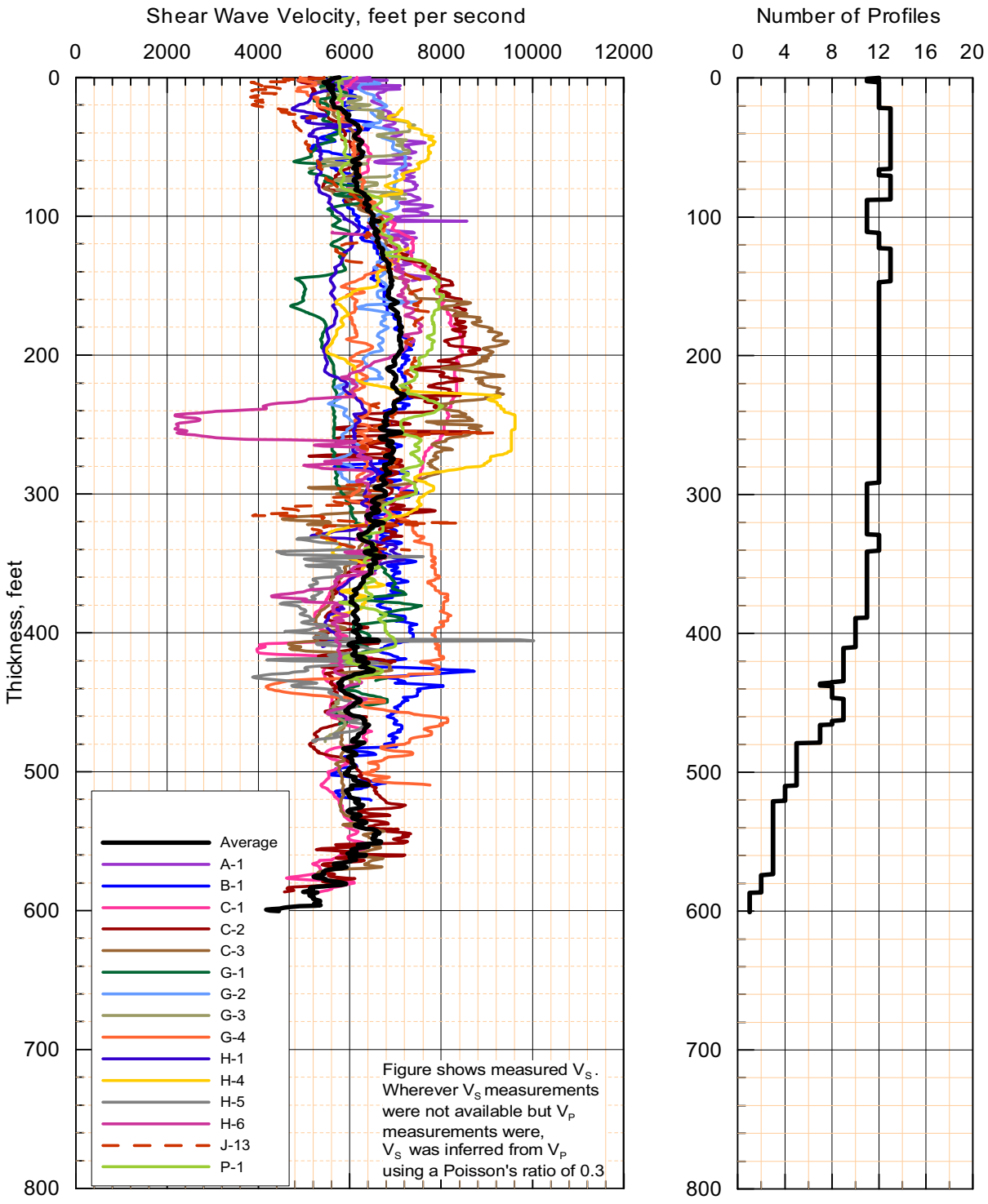

Source: Nelson et al 1991 [DIRS 101272]; Appendix C, Table C-1

Figure 6.4.2-26. Thickness and V_S Profiles for Bullfrog Layer